JAEA-Review
2015-027
DOI:10.11484/jaea-review-2015-027

JAEA-Review

The State of the Art of the Nondestructive Assay of Spent Nuclear Fuel Assemblies - A Critical Review of the Spent Fuel NDA Project of the U.S. Department of Energy's Next Generation Safeguards Initiative -

Alan Michael BOLIND and Michio SEYA

Integrated Support Center for Nuclear Nonproliferation and Nuclear Security

December 2015

Japan Atomic Energy Agency

日本原子力研究開発機構

本レポートは国立研究開発法人日本原子力研究開発機構が不定期に発行する成果報告書です。
本レポートの入手並びに著作権利用に関するお問い合わせは、下記あてにお問い合わせ下さい。
なお、本レポートの全文は日本原子力研究開発機構ホームページ（http://www.jaea.go.jp）
より発信されています。

国立研究開発法人日本原子力研究開発機構 研究連携成果展開部 研究成果管理課
〒319-1195 茨城県那珂郡東海村大字白方 2 番地4
電話 029-282-6387, Fax 029-282-5920, E-mail:ird-support@jaea.go.jp

This report is issued irregularly by Japan Atomic Energy Agency.
Inquiries about availability and/or copyright of this report should be addressed to
Institutional Repository Section,
Intellectual Resources Management and R&D Collaboration Department,
Japan Atomic Energy Agency.
2-4 Shirakata, Tokai-mura, Naka-gun, Ibaraki-ken 319-1195 Japan
Tel +81-29-282-6387, Fax +81-29-282-5920, E-mail:ird-support@jaea.go.jp

JAEA-Review 2015-027

The State of the Art of the Nondestructive Assay of Spent Nuclear Fuel Assemblies - A Critical Review of the Spent Fuel NDA Project of the U.S. Department of Energy's Next Generation Safeguards Initiative -

Alan Michael BOLIND※ and Michio SEYA

Integrated Support Center for Nuclear Nonproliferation and Nuclear Security
Japan Atomic Energy Agency
Tokai-mura, Naka-gun, Ibaraki-ken

(Received September 9, 2015)

The state of the art of the nondestructive assay of spent nuclear fuel assemblies is represented by the results of the Spent Fuel Nondestructive Assay Project of the Next Generation Safeguards Initiative (NGSI) of the U.S. Department of Energy / National Nuclear Security Administration. This report surveys the fourteen advanced nondestructive assay (NDA) techniques that were examined by the NGSI. For each technique, it explains how the technique operates, the NGSI's design of an instrument that uses the technique, how the data are analyzed, and the technique's chief limitations. After this survey of the NDA techniques, the report then discusses and critiques the current paradigm of the practice of NDA of spent fuel assemblies. It shows how the current main problem in the NDA of spent fuel assemblies—namely, an unacceptably large uncertainty in the assay results—is caused primarily by using too few independent NDA measurements. Because the physics of the NDA of spent fuel assemblies is three dimensional, at least three independent NDA measurements are required. Thus, NDA results should be able to be improved dramatically by combining the fourteen advanced NDA techniques plus other existing NDA techniques into appropriate combinations of three techniques. This report evaluates the NGSI's proposed NDA combinations according to these principles.

Keywords: Next Generation Safeguards Initiative, Spent Fuel Assembly, Nondestructive Assay, NDA, Safeguards, Material Accountancy

---

This report is based on research study of Alan Michael BOLIND on the NDA techniques in "NGSI Spent Fuel Nondestructive Assay Project" of U.S.DOE-NNSA, and also based on his submitted papers. This research study was performed in one of the subsidized projects for promotion of nuclear nonproliferation and nuclear security of MEXT (Ministry of Education, Culture, Sports, Science and Technology in Japan).

※Senior Post-Doctoral Fellow (September 2011 – March 2014).

JAEA-Review 2015-027

使用済み燃料集合体非破壊測定の最新技術状況 ー米国エネルギー省の次世代保障措置イニシアティブでの「使用済み燃料非破壊測定プロジェクト」に関する批判的レビューー

Alan Michael Bolind※、瀬谷 道夫

日本原子力研究開発機構
核不拡散・核セキュリティ総合支援センター

（2015 年 9 月 9 日受領）

使用済み燃料集合体非破壊測定の最新技術状況は、米国エネルギー省/国家核安全保障庁の次世代保障措置イニシアティブ（NGSI）での「使用済み燃料非破壊測定プロジェクト」における測定技術で代表される。この報告書は、NGSI において検討されている 14 の先進非破壊測定（NDA）技術について調査するものである。この報告書では、各技術について、どのように測定がなされるか、その技術を使う装置の NGSI での設計、測定データ分析方法、その技術の主たる制約について述べる。これらの NDA 技術の調査に引き続いて、（NGSI プロジェクトでの）使用済み燃料集合体 NDA 実施における現在の規範に関する議論と批判を行う。報告書では、現時点の（NGSI プロジェクトでの）使用済み燃料 NDA の主たる問題点、すなわち、受け入れ難い測定結果の大きな曖昧さ（誤差）が、第一義的には独立な測定手法の少なさから発生していることを示す。 使用済み燃料集合体の NDA の物理量は 3 次元構成となっているため、少なくとも 3 つの独立した NDA が必要である。そこで 14 の先進 NDA 手法と既存の NDA 手法を適切に組合せた 3 つの手法とすることで、NDA の結果が大きく改善される。この報告書では NGSI で現状提案されている NDA 手法の組合せについて評価を行う。

本報告書は、Alan Michael Bolind の研究期間における、米国エネルギー省・国家核安全保障庁の「NGSI・使用済み燃料非破壊測定プロジェクト」の NDA 技術に関する調査研究及び自身の論文をベースとするものである。なお、この調査研究は、文部科学省の核セキュリティ等強化推進補助事業の一環として実施したものである。

原子力科学研究所（駐在）：〒319-1195 茨城県那珂郡東海村大字白方 2-4

※任期付研究員（2011 年 9 月～2014 年 3 月）

Contents

目次

List of Tables

List of Figures

This is a blank page.

1. Introduction

This report describes and explains several advanced nondestructive assay (NDA) techniques for assaying spent nuclear fuel assemblies. The assaying of spent fuel assemblies is useful for safeguards material accountancy. Currently, NDA of spent fuel assemblies allows International Atomic Energy Agency (IAEA) inspectors and other inspectors to verify that spent fuel assemblies are indeed comprised mostly of spent fuel (i.e., the absence of gross defects). (See Reference [1] for the definitions of safeguards terminology.) It also acts to confirm roughly that the burnup values of spent fuel assemblies are the same as the values declared by the reactor operator; such confirmation assists with item-counting accountancy.

Ideally, if the accuracy of NDA techniques could be improved, the NDA of spent fuel assemblies would also allow inspectors to verify that no fuel pins have been diverted from assemblies (i.e., the absence of partial defects). Furthermore, it would allow both inspecting agencies and domestic materials-accountancy agencies to verify or even to reduce the shipper/receiver difference when spent fuel assemblies are reprocessed. A shipper/receiver difference arises when the calculated value of the plutonium of a spent fuel assembly (based on a burnup simulation of the assembly) is different from the value measured during the reprocessing. The accuracy of such burnup-simulation calculations is typically about 5% [2], so the accuracy on the plutonium or fissile content is also about 5% at best. NDA techniques that have a comparable accuracy could be used to confirm the shipper/receiver difference caused by these burnup calculations, while NDA techniques with better accuracy would reduce the shipper/receiver difference below that caused by these burnup calculations.

The framework of this report is the Spent Fuel Nondestructive Assay Project of the Next Generation Safeguards Initiative (NGSI) of the United States Department of Energy's (U.S. DOE) National Nuclear Security Administration (NNSA). (See Section 2.) This project surveyed fourteen advanced NDA techniques. This report describes these fourteen advanced techniques plus two current techniques and explains how they operate (Sections 4 and 5). This report then critiques the overall practice of NDA of spent fuel assemblies, to provide a context by which to understand how the NDA techniques should be applied (Section 6). In Section 7, the NGSI's proposed combinations of NDA techniques are evaluated according to this paradigm from Section 6. The report then concludes (Section 8).

2. The NGSI's Spent Fuel Nondestructive Assay Project

2.1 A description of the project

The United States Department of Energy's (U.S. DOE) National Nuclear Security Administration (NNSA) started the Next Generation Safeguards Initiative (NGSI) in 2008 [3]. The NGSI, in turn, began its Spent Fuel Nondestructive Assay Project in early 2009 [3-6]. The work of this project was distributed among several U.S. national laboratories and universities. The project was planned to last five years and to consist of three sequential phases [3, 6]:

- Phase I (Years 1-2): Simulations, preliminary findings, and peer review
- Phase II (Year 3): Prioritization for continued development (down-selection), integration, and prototype development
- Phase III (Years 4-5): Measurements for characterization and validations (field tests)

The project is now in Phase III.

The purpose of the Spent Fuel NDA Project is to develop one or more NDA instruments that are capable of performing the following two functions on spent fuel assemblies independently from information provided by the reactor operator [3, 6]:

(1) detecting the diversion of fuel pins from the assembly (i.e., a partial defect), and
(2) determining the mass of plutonium in the assembly with an uncertainty that is better than 5%.

The determination of the plutonium content is important because spent fuel assemblies contain much plutonium. Just two spent PWR assemblies can contain more than one significant quantity of plutonium (8 kg, [1]); see Section 3.3.

Note that the assay of the plutonium content is more important for safeguards than is the assay of the total fissile content, which includes the ^{235}U content. The fissile isotopic fraction of the uranium in spent fuel (i.e., $^{235}U/^{238}U$) is small. In contrast, the fissile isotopic fraction of the plutonium is relatively large, and the plutonium can be separated from the spent fuel chemically, which is generally easier to do than isotopic enrichment. Nonetheless, assaying the total fissile content is often an important step along the way to assaying the plutonium.

The intermediate goals of the project include the following list [3]:

(3) to develop libraries of simulation models of spent fuel assemblies that span a range of conditions of burning in a reactor,
(4) to evaluate each NDA technique by simulating the use of it to assay the models from the libraries,
(5) to prioritize specific combinations of NDA techniques as integrated NDA instruments for further study and testing, and
(6) to test these NDA instruments by measuring actual spent fuel assemblies with them, which would also validate the modeling approach.

A desired long-term outcome of this project is to provide improved NDA techniques, instruments, and methods for the International Atomic Energy Agency (IAEA) to use in their safeguards accountancy of nuclear material [3, 6, 7]. The execution of this project appears not to be predicated upon any endorsement or involvement of the IAEA, though.

Japan Atomic Energy Agency (JAEA) has at least two reasons for being interested in the progress and results of the NGSI's Spent Fuel NDA Project. The first reason is that JAEA and Los Alamos National Laboratory (LANL) signed Project Action Sheet Number 24 to collaborate in the testing of one of the NGSI's integrated NDA instruments. This testing occurred in June 2013. The second reason is JAEA's long-standing interest in improving and deploying safeguards technology both in Japan and around the world.

2.2 The NDA techniques that were investigated in Phases I and II

The NGSI investigated fourteen NDA techniques (Table 1) during Phase I of the project [5, 6, 8]. Relevant reports on the NGSI's research are referenced in Table 1. Two other passive NDA techniques—Total Neutron measurement (TN) and Total Gamma-ray measurement (TG)—were included in the project but were not specifically studied because they are already well developed and are in common use today as part of the Fork detector [7, 9, 10]. Thus, there were sixteen NDA techniques in total. The reader should note that in the literature, some lists of the fourteen techniques replace AIPN with TN. Some other NDA techniques that were not investigated by the NGSI are Prompt Gamma-ray Activation Analysis (PGAA), Neutron Resonance Capture Analysis (NRCA), and active X-Ray Fluorescence [11-14].

Table 1: The 16 NDA techniques (14 advanced NDA techniques, plus TN and TG)

NDA Technique		**Type**	**Detected Particles**	**NGSI References**
TN:	Total (gross) Neutron counting	Passive	Neutrons	[15]
PNAR:	Passive Neutron Albedo Reactivity	Passive	Neutrons	[16-18]
CIPN:	^{252}Cf Interrogation with Prompt Neutron detection	Active	Neutrons	[19]
AIPN:	Assembly Interrogation with Prompt Neutron detection	Passive	Neutrons	[20]
DDA:	Differential Die-Away	Active	Neutrons	[21-23]
DN:	Delayed Neutron counting	Active	Neutrons	[21, 24]
NM:	Neutron Multiplicity counting	Passive	Neutrons	[8, 25]
DDSI:	Differential Die-away Self Interrogation	Passive	Neutrons	[26-28]
NRTA:	Neutron Resonance Transmission Analysis	Active	Neutrons	[29-31]
LSDS:	Lead Slowing-Down Spectroscopy	Active	Neutrons	[32-36]
SINRD:	Self-Interrogation Neutron Resonance Densitometry	Passive	Neutrons	[37-39]
DG:	Delayed Gamma spectroscopy	Active	γ-rays	[40-49]
TG:	Total Gamma-ray counting	Passive	γ-rays	[15]
PG:	Passive Gamma spectroscopy	Passive	γ-rays	[50-53]
NRF:	Nuclear Resonance Fluorescence	Active	γ-rays	[54-57]
XRF:	X-Ray Fluorescence	Passive	X-rays	[58-68]

At the start of the Spent Fuel Nondestructive Assay Project, not all of these fourteen advanced techniques existed in forms that could measure spent fuel assemblies. Therefore, NGSI researchers had to invest a significant amount of effort to design practical NDA

instruments for many of the techniques. The NGSI's evaluation of the NDA techniques was therefore specifically of the NGSI's versions of the NDA instruments. For this reason, Phase I involved significant design spirals for several of the NDA techniques, as the NGSI researchers iterated between evaluation and re-design.

2.3 The computer simulations and the spent-fuel libraries

For Phases I and II, the NGSI used computer simulations to investigate various NDA techniques. The simulations of each NDA technique consisted of three parts: (1) making a computer model of the NDA instrument, (2) making a computer model of a spent fuel assembly, and finally (3) simulating the measurement of the spent fuel assembly by the NDA instrument. In fact, this third part was repeated many times with different spent fuel assemblies over a range of burnup (BU), initial enrichment (IE), and cooling time (CT). In this way, the NGSI was able to evaluate the performance of each NDA technique to quantify the fissile and elemental plutonium content in many different spent fuel assemblies.

For this second part of this simulation program, LANL, with the help of Oak Ridge National Laboratory (ORNL), has created seven libraries of computer simulations of spent fuel assemblies, as of July 2013 [53, 69-71]. The first library was used for most of the preliminary investigation of the NDA techniques. This library consists of sixty-four pressurized-water-reactor (PWR) fuel assemblies (17 pin x 17 pin). The sixty-four assemblies cover the following parameter values: IE equal to 2, 3, 4, and 5 wt.%; BU equal to 15, 30, 45, and 60 GWd/tU; and CT equal to 1, 5, 20, and 80 years. (The unit *GWd* stands for gigawatt-days, and the unit *tU* stands for metric tons of initial uranium metal in the fuel assembly.) The fifth library consists of 4x(5x5) boiling-water-reactor (BWR) assemblies and covers the following parameter values: three ranges of IE (low, medium, high); BU equal to 12, 24, 36, and 48 GWd/tU; and CT equal to 1, 5, 20, 40, 50, and 80 years. The other libraries improve upon these libraries in various ways, such as by investigating other factors that influence fuel assemblies during burning.

These libraries of spent-fuel-assembly models have been created using either the SCALE software package from ORNL or LANL's Monte Carlo code MCNP (typically version MCNPX) in combination with the burnup codes Monteburns and CINDER90 [71]. Precisely said, the first spent fuel library was created with the CINDER90 code that is built into the MCNPX code, rather than using Monteburns to access the CINDER90 code externally, as was done with the later libraries that were made from MCNPX. The importance of this distinction is that even though CINDER90 can keep track of 3400 isotopes, MCNPX can keep track only of the few hundred isotopes for which neutron cross-section data are available (390 isotopes for ENDF/B VII.0) [67, 68, 72]. By switching to accessing the CINDER90 code externally through Monteburns for the creation of the subsequent spent fuel libraries, the NGSI was able to avoid this limitation of MCNPX and make better use of the capability of CINDER90. Regardless of which code was used to create the models, the resulting models were all put into the MCNP format so that they could then be used with MCNP models of the NDA instruments to simulate NDA measurements. Therefore, the models in the libraries are now in the MCNP format.

In addition to the spent fuel assemblies in the libraries, special fuel assemblies were modeled as necessary. In particular, NGSI researchers sometimes altered the library fuel assemblies by replacing some fuel pins with dummy fuel pins made of unburnt, depleted-uranium oxide. Such

altered spent fuel assemblies were intended to represent fuel assemblies with partial defects. By simulating the measurement of such fuel assemblies by an NDA instrument, the NGSI could evaluate the NDA instrument's ability to detect partial defects.

2.4 The NGSI's evaluation of the NDA techniques in Phases I and II

The NGSI evaluated the NDA techniques according to several, simultaneous criteria in a systematic yet pragmatic way. As stated above in Section 2.1, the two ultimate goals of the project have been the detection of partial defects and the quantification of the elemental plutonium mass with an uncertainty better than 5%. Nevertheless, additional, intermediate performance criteria were also used. According to the literature, particularly the overviews by Tobin, Humphrey, and Charlton et al. [5, 6, 73], the evaluation of each technique seems to have consisted of answering the following main questions:

1. Does the technique produce a signal that can be interpreted in a reasonable way?
2. Will the NDA technique be expensive, require a large instrument to be built, or take more than five years to develop? If so, identify the causes of such weaknesses but do not try to solve them by further design iteration as part of this NGSI project.
3. How well can the NDA signal be correlated to the fissile and/or elemental-Pu content? Secondarily, how well can the NDA signal be correlated to the burnup, initial enrichment, and cooling time of the fuel assembly? This secondary correlation is useful only for verifying the truth of the reactor operator's declaration and for acting as a fingerprint to identify a fuel assembly after a loss of continuity of knowledge. The primary correlation is useful not only for these purposes but also for producing absolute values for various quantitative MC&A evaluations, such as of shipper-receiver differences between a reactor and a reprocessing facility. (MC&A is materials control and accountability.)
4. Is the NDA signal sensitive to specific Pu and U isotopes in the fuel assembly? If so, evaluate how well the signal can be correlated to the pertinent ratios of the isotopes, since such an ability is of equal or greater importance than the correlation to the absolute quantities of the isotopes. If not, determine the proportional contribution of each fissile isotope to the signal, and therewith define an effective ^{239}Pu content that is a weighted sum of the fissile isotopes. Since the weights depend on the NDA technique, the effective ^{239}Pu content changes from technique to technique. The hope is that these different equations with different weightings might present a way to separate the fissile isotopes from each other, if the data from different techniques are combined. (See Section 3.3.2.)
5. Can the technique detect a signal from the inner pins of the fuel assembly? If it cannot, focus only on the correlation of its signal with the fissile/Pu content. If it can, evaluate both the correlation of its signal with the fissile/Pu content and the effect that partial defects have on the signal. A good sensitivity of the technique to the presence of partial defects in the spent fuel assembly may make the technique to be useful even if its correlation to the fissile/Pu content is poor. The design spiral of such a technique should then prioritize the increasing of the sensitivity to partial defects.

2.5 The NGSI's selected combinations of techniques

During Phase II, the NGSI down-selected certain NDA techniques to continue to investigate through prototype fabrication and experimental testing. These NDA techniques

were PNAR, SINRD, CIPN, DDSI, DN, DDA, and DG. These techniques were then grouped together into five combinations that would each be designed and fabricated as a prototype instrument for further testing [15]. In addition to the NDA techniques already listed, TN was also considered and included in all the combinations, since it is essentially already part of the other neutron techniques in the combinations. TG as measured with ion chambers was also chosen to be incorporated into all but one of the prototype instruments, and for that one without TG, PG was planned. Note that although the NGSI's overview reports [5, 6, 73] identify only PG as one of the down-selected techniques, TG is the gamma-ray technique that they are actually pursuing for all but the one combination. The NGSI reports use the same acronym *PG* for both energy-spectroscopic gamma-ray measurements (PG) and energy-independent gamma-ray measurements (TG), but this report distinguishes between them.
The five combinations are described in Table 2.

. Note that these five combinations are different from the ones that were listed in at the end of Phase II (Table 2 in Humphrey et al. [6] and Table 4 in Charlton and Humphrey [5]). The main difference is that the SINRD technique has been separated out to be its own instrument in combination with TN and TG. The first combination is the one that has already been tested in Japan at the spent-fuel pool of the Fugen Advanced Thermal Reactor. The other combinations are being tested elsewhere. Section 7 and Table 19 evaluate the combinations.

Table 2: The five combinations of NDA techniques chosen for prototype design and testing (modified from Table 2 in Humphrey et al. [6] and Table 4 in Charlton and Humphrey [5], with permission from INMM), according to the order and updated information in Tobin et al. [15]

	Techniques	**Key Attributes**	**Potential Applications**	**Testing Location [15]**
1	PNAR, TN, TG	Passive, lightweight, relatively low cost, short measurement time, robust	Enhanced containment during shipment	Fugen Advanced Thermal Reactor, Tsuruga, Japan
2	CIPN, TN, TG	Active (source requires shielding), lightweight, relatively low cost, short measurement time, robust	Input accountability for a repository or reprocessing facility; Recovery from a loss continuity of knowledge	Post Irradiation Examination Facility (PIEF), Daejeon, Republic of Korea
3	SINRD, TN, TG	Passive, lightweight, relatively low cost, robust		PIEF, Daejeon, Republic of Korea
4	DN, DDA, TN, DG, PG	Active, relatively heavy, relatively high cost, longer measurement time, less robust, potential for high accuracy	Input accountability for a new reprocessing facility	Central Storage of Spent Nuclear Fuel (CLAB), Sweden
5	DDSI, TN, TG	Passive, relatively heavy, intermediate cost, longer measurement time, robust	Input accountability for a repository or reprocessing facility; Recovery from a loss continuity of knowledge	Location uncertain

3. A brief description of spent fuel assemblies

Since the objects to be assayed are spent fuel assemblies, it is appropriate to describe briefly here their important characteristics with regard to NDA. It is assumed, though, that the reader has a basic understanding of nuclear engineering, including types of reactors and the nuclear fuel cycle. For more detail, the reader can consult general reference texts, like Lamarsh and Baratta's *Introduction to Nuclear Engineering* [74] and the so-called "PaNDA manual" (by Reilly et al. [75, 76]), or specific references, such as sales literature [77] and study reports [78-80]. This topic of the important characteristics of spent fuel assemblies will also be revisited in Section 6.2.5.

3.1 Physical description of fuel assemblies

Table 3 and Figure 1 describe and illustrate the physical characteristics of typical light-water-reactor (LWR) fuel assemblies, such as their size and weight. PWR assemblies are larger than BWR assemblies, in terms of both size and weight. The smaller cross-sectional size of a BWR assembly means that the radiation signals (e.g., neutrons and gamma-rays) from its inner fuel pins can more easily escape the assembly to be detected by an NDA instrument, relative to the case of a PWR assembly. Note that PWR assemblies have smaller-diameter fuel pins but more of them, and some pin positions are not occupied by fuel pins but by guide tubes for the control rods to slide into and out of. The Partial Defect Tester, an NDA instrument, takes advantage of these guide tubes to insert detectors down them and into the spent fuel assembly [81, 82]. In contrast, a BWR assembly often has one or more central channels in which cooling water can flow, and four assemblies are arranged around a cruciform control blade to constitute a single fuel module. The fact that the control blade in a BWR module is only on two sides of each fuel assembly causes BWR fuel assemblies to burn unevenly across their transverse cross section [83], whereas the internally located control rods in a PWR fuel assembly permit a more even burning.

An important value to memorize is the amount of elemental uranium ("metal," excluding oxygen) in a fresh fuel assembly, which according to Table 3 is roughly 180 kg for a BWR assembly and 460 kg for a PWR assembly. Even more roughly, it is a fifth of a (metric) ton for a BWR assembly and half a (metric) ton for a PWR assembly. (A metric ton is 1000 kg.) These values are important because burnup is almost always quantified per metric ton of heavy metal in the assembly, which is practically equivalent to the uranium in the fresh assembly in most cases. Also, the isotopic composition of spent fuel is often given in weight percentages of the total heavy metal, so this knowledge of the total initial heavy metal (i.e., uranium) allows one to estimate the absolute masses of the isotopes in the spent fuel assembly.

Table 3: Physical characteristics of typical LWR nuclear fuel assemblies. Modified from Table 1.4. in Reference [84], which is also cited in References [85, 86].

Characteristics	**BWR** [a]	**PWR** [b]
Fuel rod array	8 x 8	17 x 17
Cross section, cm	13.9 x 13.9	21.4 x 21.4
Fuel rods per assembly	63	264
Fuel rod outer diameter, cm	1.252	0.950
Overall assembly length, m	4.470	4.059
Fuel rod length, m	4.064	3.851
Active fuel height, m	3.759	3.658
Nominal volume/assembly, m^3	0.0864 [c]	0.186 [c]
Assembly total weight, kg	319.9	657.9
UO_2/assembly, kg	208	523.4
Uranium/assembly, kg	183.3	461.4
Total metal/assembly, kg	111.9	134.5
Zircaloy/assembly, kg	103.3 [d]	108.4 [e]
Hardware/assembly, kg	8.6 [f]	26.1 [g]

[a] From General Electric Company, *General Electric Standard Safety Analysis Report*, BWR/6, Docket STN 50-447, San Jose, California (1973).

[b] From Westinghouse Nuclear Energy Systems, *Reference Safety Analysis Report*, RESAR-3, Docket STN 50-480, Pittsburgh, Pennsylvania (1972).

[c] Based on overall outside dimension. Includes spacing between the stacked fuel rods of an assembly.

[d] Includes Zircaloy fuel-rod spacers and fuel channel.

[e] Includes Zircaloy control-rod guide thimbles.

[f] Includes stainless steel tie-plates, Inconel springs, and plenum springs.

[g] Includes stainless steel nozzles and Inconel-718 grids.

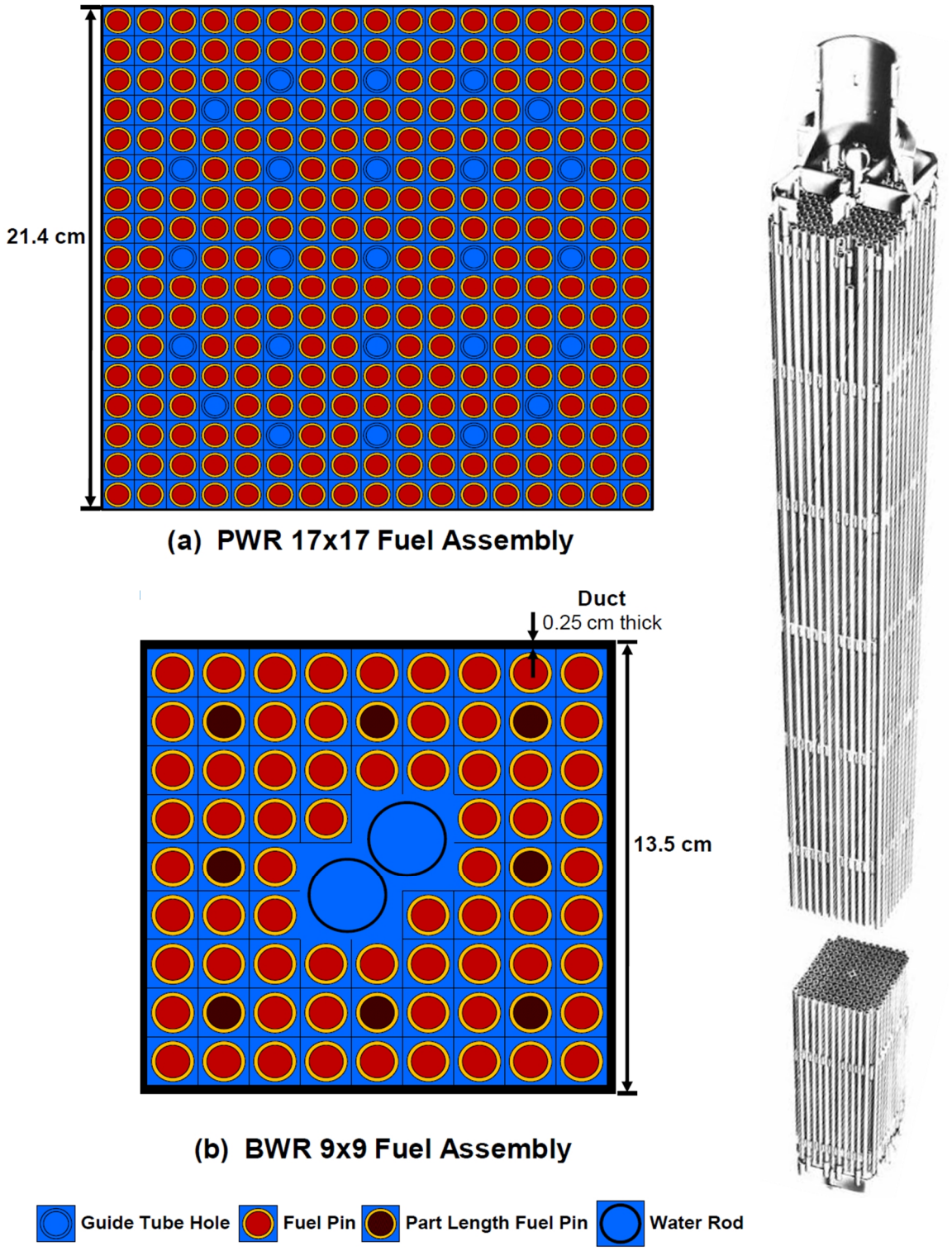

Figure 1: Left: Cross-sectional, schematic views of typical PWR and BWR fuel assemblies; copied from LaFleur [87] with permission. Right: Cut-away drawing of a PWR fuel assembly from the *N.S. Savannah*, a nuclear-powered, commercial ship; copied from the technical press information provided by the U.S. Maritime Administration [88].

3.2 Definition of the BIC set

Three parameters are usually used to describe spent fuel assemblies: burnup (BU), initial enrichment (IE), and cooling time (CT). This report will abbreviate this set of parameters as the "BIC" set (an acronym), for ease of reference.

In earlier literature, such as in Chapter 18 of the PaNDA manual [75], a distinction was made between *exposure*, which was defined as the energy that had been produced per initial metric ton of heavy metal, and *burnup*, which was defined as the fraction of the initial heavy atoms that had fissioned. (The heavy metal is uranium for UO_2 fuel and is uranium and plutonium for MOX fuel.) In this report and in much of the more recent literature, the term *burnup* refers to the energy produced per initial ton (i.e., it has the old definition of *exposure*), the fraction of fissioned atoms has no special name (or is also referred to as *burnup* but with the meaning indicated), and the term *exposure* is not used at all.

The quoted burnup of a given spent fuel assembly is usually an average or nominal value, since in fact, it varies both axially and transversely throughout the assembly. Parks [89 (p.24)], and Wagner, DeHart [90 (pp.1-2)] have described well the origins of the axial burnup profile in a spent PWR assembly:

> The dynamics of reactor operation result in non-uniform axial-burnup profiles in fuel with any significant burnup. At beginning of life in a PWR, a near-cosine axial flux shape will begin depleting fuel near the axial center of a fuel assembly at a faster rate than at the ends. As the reactor continues to operate, the cosine flux shape will flatten because of the fuel depletion and fission product poisoning that occurs near the center. However, because of the relatively high leakage near the end of the fuel, burnup will drop off rapidly near the ends. Partial length absorbers or non-uniform axial enrichment loadings can further complicate the burnup profile. In a BWR, the same phenomena occur, but the burnup profile is further complicated by the significantly varying moderator density profile and by non-uniform axial loadings of burnable poison rods and uranium enrichment.

Figure 2 illustrates a burnup profile for a typical spent BWR assembly, which, during burning, experiences the additional complications of the void fraction increasing from bottom to top and of the control blades being inserted from below. Two studies of the transverse variations in burnup are the study of PWR assemblies by Galloway et al. [53] and the study of BWR assemblies by Ezure [91].

The initial enrichment is the percentage of ^{235}U in the total uranium in the fresh fuel assembly. IE is typically in the range of 2% to 5% for commercial fuel; enrichments below 20% are considered low-enriched uranium (LEU) fuel, while enrichments above 20% are high-enriched uranium (HEU) fuel [1]. For MOX fuel made with depleted UO_2, the fraction of the elemental plutonium in the MOX is usually the quantity that is quoted; it is sometimes called the "plutonium loading." Sometimes, though, only the fissile plutonium isotopes (^{239}Pu and ^{241}Pu) are considered; the reader must be aware of the context.

Cooling time is the time that the assembly has been out of the reactor since it was permanently discharged. The burnup-credit community generally assumes a cooling time of five years for all of its studies, for historical reasons and because it is a bounding case for maximum residual reactivity (Section 4.3 of Parks et al. [89]). For safeguards NDA, though, CT is considered to be variable. The NGSI paper by Hu et al. [19] addresses the neutronic

effects of cooling time by considering the dominant influences, namely, the radioactive decay of ^{241}Pu and ^{155}Eu.

The use of the BIC set to characterize spent fuel assemblies is discussed in detail in Section 6.

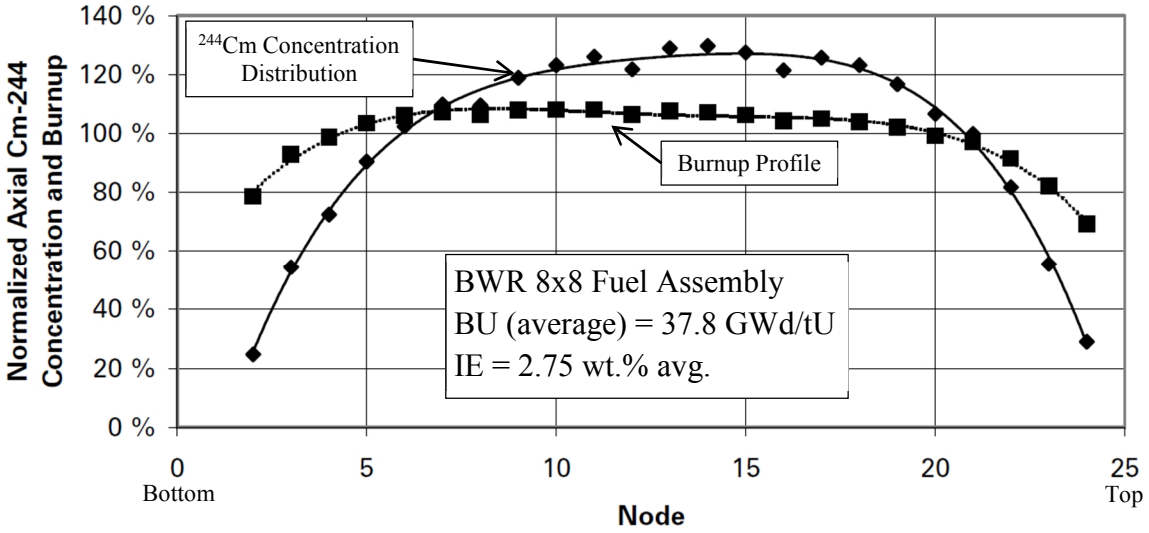

Figure 2: "The calculated axial distribution of the Cm-244 concentration and assumed discharge burnup." Modified from Figure 5 in Tanskanen [83], with permission from STUK.

3.3 Isotopic content and self-generated radiation

Finding references that list the isotopic composition of spent fuel assemblies can sometimes be difficult, for several reasons. Firstly, there can be many variables in how the fuel assembly is burned. Different reactors burn fuel differently; and even at the same reactor, the operational procedures and history can vary and thereby change the resulting characteristics of the spent fuel. Even within a single fuel assembly, the burnup varies axially and transversely, as mentioned above. All this variability makes it seem difficult to specify a representative set of spent fuel assemblies, regardless of whether all of these variables are truly important or not (see Section 6). Secondly, destructive assay of spent fuel is time consuming, complicated, and expensive, since it requires the use of hot cells to shield the chemists from the spent fuel's radiation. Burnup simulations are physically easier to do; but they require significant computational resources, and they must be benchmarked. Thirdly, the various studies have been performed for various purposes, and isotopes that were not immediately germane to those purposes have often been ignored. Such omissions often limit the usefulness of the data for the purposes of NDA, which is concerned not only with the U and Pu isotopes themselves but also with all the other isotopes that can produce or influence the signals that indicate the U and Pu isotopes. Fourthly, the data are sometimes reported only as relative quantities that indicate trends, possibly for the reason that governments may wish to restrict the public dissemination of information about absolute quantities of plutonium because of safeguards and security concerns. For all of these reasons and perhaps others, too, it can be difficult to find suitable data about isotopic composition in the literature.

Table 4: Selected literature references for the isotopic composition of spent fuel assemblies (1/2)

Name or Origin of Study	Year	Experiment/ Simulation	Type of Reactor	Ranges of BIC Variables									^{239}Pu – ^{242}Pu?	Trans-U to ^{244}Cm?	Fission Products?
				BU (GWd/tU)			IE (wt% HM)†			CT (years)					
Yankee [93-96]	1965-1969	Both	PWR	1.3	–	46			3.4	0			✓	✓	^{137}Cs, ^{90}Sr, ^{148}Nd
EUROCHEMIC [97]	1970	Both	CANDU	2.7	–	8			0.71	1	–	6	✓		
			BWR	13	–	22	2.33	–	2.60	0.2	–	2.1	✓		
			PWR	8	–	14	2.73	–	3.9			2.7	✓		
ENEL/EURATOM [98]	1971	Both	BWR			10			2.02	2.0	–	2.8	✓	✓	^{148}Nd, γ-ray, Noble
Saxton Pu Project [99]	1973	Both	PWR (MOX)										✓	✓	^{148}Nd
LANL, Japan, Europe [100]	1981	Experiment	PWR	9.9	–	26.7							✓		
			BWR	1.4	–	15.3							✓		
LANL, Bosler et al. [92]	1982	Both	PWR	0	–	50	2.2	–	4.5	0	–	10	✓	✓	^{148}Nd, γ-ray
JPDR-1 [101, 102]	1977-1982	Experiment	BWR	0.1	–	5.6			2.60	2.7	–	12.6	✓	✓	Nd, γ-ray
JPDR-1 [91]	1990	Simulation	BWR	0.1	–	5.6			2.60	7	–	13	✓	✓	^{148}Nd, γ-ray
U.S. DOE Fissile Materials Disposition Program [103-106]	1996-1998	Simulation	PWR (UOX)			47.8			4.2	0	–	$2.5\cdot10^5$	✓	✓	
			PWR (MOX)			42.2			6.7	0	–	$2.5\cdot10^5$	✓	✓	
			BWR (UOX)			37.6			3.25	0	–	$2.5\cdot10^5$	✓	✓	✓
			BWR (MOX)			37.6			3.0	0	–	$2.5\cdot10^5$	✓	✓	✓
			PWR (MOX)	35	&	52.5			4.56	0	–	$2.5\cdot10^5$	✓	✓	✓
			PWR (MOX)	21.5	&	64.7	4.25	&	4.80	0	–	$2.5\cdot10^5$	✓	✓	✓
JAERI [107, 108]	1999	Simulation	PWR (UOX)	33	–	60	3.2	–	5.0	0	–	30	✓	✓	✓
			PWR (MOX)	33	–	60	5.3	–	7.9	0	–	30	✓	✓	✓
			BWR (UOX)	33	–	60	3.0	–	4.7	0	–	30	✓	✓	✓
			BWR (MOX)	33	–	60	4.7	–	7.2	0	–	30	✓	✓	✓

Table 4: Selected literature references for the isotopic composition of spent fuel assemblies (2/2)

Name or Origin of Study		Year	Experiment/ Simulation	Type of Reactor	Ranges of BIC Variables									^{239}Pu – ^{242}Pu?	Trans-U to ^{244}Cm?	Fission Products?
					BU (GWd/tU)			IE (wt% HM) †			CT (years)					
STUK [83]		2000	Simulation	BWR			37.8			2.75	0	–	13.4	✓	✓	✓
				VVER-440			36			3.6	0	–	1	✓	✓	✓
JAERI [80]		2002	Experiment	PWR	7.8	–	47.3	2.6	&	4.1	3.6	–	4.2	✓	✓	Many
				BWR	4.2	–	44.0	3.41	&	3.91	5.5	–	6.5	✓	✓	Many
OECD / NEA Burnup Credit Criticality Benchmark [109]	I-A [110]	1996	Simulation	PWR (UOX)	30	&	40			3.6	1	&	5	✓		Poisons ‡
	I-B [111]	1994	Simulation	PWR (UOX)	27.4	–	44.3			3		?		✓		Poisons
	II-A [112]	1996	Simulation	PWR (UOX)	10	–	50	3.6	&	4.5	1	&	5	✓		Poisons
	II-C [113]	2008	Simulation	PWR (UOX)	32	&	50			4			5	✓		Poisons
	II-D [114]	2006	Simulation	PWR (UOX)	30	&	45			4	0	&	5	✓		Poisons
	III-A [115]	2000	Simulation	BWR (UOX)	20	–	40			3.8	1	&	5	✓		Poisons
	III-B [116]	2002	Simulation	BWR (UOX)			40	2.3	–	4.9			5	✓		Poisons + 5
	IV-A [117]	2003	Simulation	PWR (MOX)	20	–	60	4.0	–	8.0	1	&	5	✓	✓	Poisons
	IV-B [118]	2003	Simulation	PWR (MOX)	16	–	48	4	–	8	0	–	5	✓	✓	Poisons
	VII [119]	2012	Simulation	PWR (UOX)			50			4.5	0	–	$1 \cdot 10^6$	✓	✓	Poisons+
LaFleur [87]		2011	Simulation	PWR (UOX)	10	–	50			4			5	✓	✓	Most
				PWR (MOX)	10	–	50			6			5	✓	✓	Most
				BWR (UOX)	10	–	50			3			5	✓	✓	Most
				BWR (MOX)	10	–	50			6			5	✓	✓	Most
SFCOMPO Database [120]			Experiment	At this time of writing, it contains data from fourteen reactors, BWR and PWR, all UOX.												

† Here, IE for MOX fuel is the weight percentage of Pu loaded (all Pu isotopes).
‡ These neutron poisons are the set of 15 fission products that have the strongest neutron-capturing effect in spent fuel; see Sections 3.3.3 & 6.2.5

For this reason, a list of data references has been compiled in Table 4 as an aid to the reader. For each entry, the table states the type of fuel assembly, the type of fuel if the study examined more than UO_2 (UOX) fuel, the range of BIC-set values, and the categories of isotopes that the study covered. The quality of the data and their ease of use vary widely among the studies, yet they can serve as a starting point for further investigation of the literature. Some of the data from the study by Nakahara et al. [80] are repeated in Table 5 as example values for absolute quantities of isotopes in spent fuel assemblies.

One study that is highly recommended for newcomers to the NDA of spent fuel assemblies is the work by Bosler et al. [92]. Although it does not significantly address fission products, its systematic approach and many figures illustrate well how all the important uranium and transuranic isotopes vary greatly with the BIC set and do not vary much with fuel-pellet density, reactor power level, and irradiation history.

Table 5: Destructive analytical data on the isotopic content of typical spent PWR and BWR assemblies; data are from Tables XX and XXI in Nakahara et al. [80].

Type	PWR	BWR
Fuel type	UO_2	UO_2
Sample identification number	SF97-6	SF98-6
Fuel rod average burnup (GWd/tU)	44	36
Local burnup at sample position (GWd/tU)	40.79	39.92
Initial enrichment (wt%)	4.11	3.91
Cooling time (years)	3.96	5.489
Void fraction at sample position	NA	0.545

	PWR	BWR			PWR	BWR
Nuclide (kg/metric ton initial U)				Nuclide (kg/metric ton initial U)		
^{234}U	0.206	0.186		^{143}Nd	0.974	0.920
^{235}U	10.160	9.062		^{144}Nd	1.311	1.284
^{236}U	5.272	5.140		^{145}Nd	0.825	0.795
^{238}U	931.000	933.400		^{146}Nd	0.859	0.843
^{237}Np	0.557	0.516		^{148}Nd	0.450	0.447
^{238}Pu	0.218	0.169		^{150}Nd	0.213	0.210
^{239}Pu	5.677	5.305		^{137}Cs	1.531	1.508
^{240}Pu	2.326	2.630		^{134}Cs	0.163	0.151
^{241}Pu	1.494	1.292		^{154}Eu	0.029	0.029
^{242}Pu	0.598	0.543		^{144}Ce	0.371	0.352
^{241}Am	0.043	0.041		^{125}Sb	0.005	0.005
^{242m}Am	0.001	0.001		^{106}Ru	0.196	0.111
^{243}Am	0.117	0.112		^{147}Sm	0.237	0.289
^{242}Cm	0.016	0.059		^{148}Sm	0.181	0.186
^{243}Cm	0.001	0.001		^{149}Sm	0.004	0.003
^{244}Cm	0.042	0.042		^{150}Sm	0.341	0.354
^{245}Cm	0.002	0.002		^{151}Sm	0.013	0.013
^{246}Cm	0.000	0.000		^{152}Sm	0.121	0.123
^{247}Cm	0.000	0.000		^{154}Sm	0.042	0.044

As will be discussed in more detail in Section 6.2, four main groups of isotopes can be identified: (1) those actinides that spontaneously generate neutrons, (2) those actinides that produce neutrons by induced fission (i.e., the fissile isotopes), (3) those actinides and fission products that capture neutrons, and (4) those fission products that do not have significant neutronic properties but do emit gamma-rays. These groups and their associated radiations will now be described briefly in turn.

3.3.1 Primary-neutron sources

Neutrons that are spontaneously generated in the fuel assembly are called primary neutrons, so the isotopes that generate them are the primary-neutron sources. There are three main ways that primary neutrons can be created—by spontaneous fission, by (α,n) reactions, and by photo-reactions—but only the first two are significant after several days of cooling. The reason is that unless the fuel assembly is in heavy water, only high-energy gamma-rays (more than 5 MeV, roughly) can induce significant neutron-emitting photo-reactions, and the fission products that emit high-energy gamma-rays decay away quickly after the fuel assembly is discharged from the reactor (see Figures 57 and 62). Thus, only spontaneous fission and (α,n) reactions are important to spent-fuel-assembly NDA, and of these two, spontaneous fission is by far the dominant source, being greater by an order of magnitude or more. See Figure 3 below; and also see Table 1.1 in LaFleur [87], Table 18-5 in Reilly et al. [75], and the works by Bosler et al. [92] and Richard et al. [121].

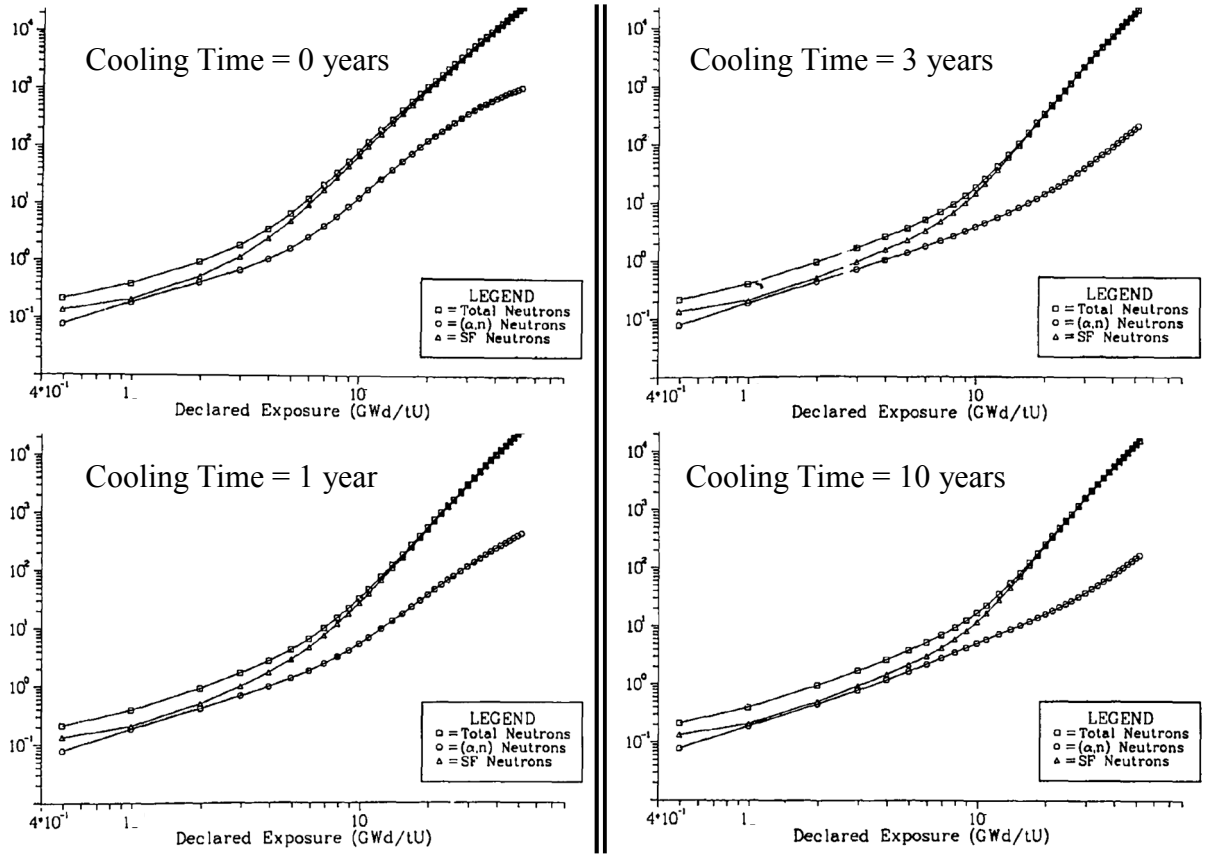

Figure 3: Comparison of primary-neutron production rates (arbitrary, logarithmic ordinate) from spontaneous fission and (α,n) reactions (all isotopes). Modified from Bosler et al. [92]

The chief (α,n) reactions in spent fuel assemblies are those between the alpha particles emitted by the actinides, on the one hand, and the ^{17}O and ^{18}O atoms in the UO_2, on the other hand. Metaphorically speaking, in an (α,n) reaction, the energetic alpha particle knocks loose one of the "extra" neutrons in an ^{17}O or ^{18}O atom. ^{17}O and ^{18}O are present in natural oxygen at 0.038 and 0.204 atom percent abundances, respectively, and the production by ^{18}O dominates [122]. Since the (α,n) reaction depends on the energy with which the alpha particle hits the oxygen atom, the (α,n) neutron production rate has much variability with the physical and chemical form of the fuel. Chapter 11 of Reilly et al. [75], and the works by Perry and Wilson [122] and by Jacobs and Liskien [123] are useful references for neutron production by (α,n) reactions.

Table 6: Selected actinide sources of primary neutrons [75, 76, 122, 124, 125]. The red boxes indicate the three most important neutron sources in spent nuclear fuel: ^{240}Pu, ^{242}Cm, and ^{244}Cm.

		Spontaneous Fission			(α,n) Reaction †		
Isotope	**Total Half-Life**	**Spontaneous Fission Branching Ratio**	**Spontaneous Fission Yield (n/s·g)**	**Spontaneous / Thermal Fission Multiplicity, ν**	**α-Yield (α/s·g)**	**Mean α Energy (MeV)**	**(α,n) Yield in Oxide (n/s·g)**
^{232}Th	$1.41 \cdot 10^{10}$ y	$1.41 \cdot 10^{-11}$	$> 6 \cdot 10^{-8}$	2.14 / 1.9	$4.1 \cdot 10^{3}$	4.00	$2.2 \cdot 10^{-5}$
^{232}U	71.7 y	$8.96 \cdot 10^{-13}$	1.3	1.71 / 3.13	$8.0 \cdot 10^{11}$	5.30	$1.49 \cdot 10^{4}$
^{233}U	$1.59 \cdot 10^{5}$ y	$1.33 \cdot 10^{-12}$	$8.6 \cdot 10^{-4}$	1.76 / 2.4	$3.5 \cdot 10^{8}$	4.82	4.8
^{234}U	$2.45 \cdot 10^{5}$ y	$1.17 \cdot 10^{-11}$	$5.02 \cdot 10^{-3}$	1.81 / 2.4	$2.3 \cdot 10^{8}$	4.76	3.0
^{235}U	$7.04 \cdot 10^{8}$ y	$2.01 \cdot 10^{-9}$	$2.99 \cdot 10^{-4}$	1.86 / 2.41	$7.9 \cdot 10^{4}$	4.40	$7.1 \cdot 10^{-4}$
^{236}U	$2.34 \cdot 10^{7}$ y	$1.20 \cdot 10^{-9}$	$5.49 \cdot 10^{-3}$	1.91 / 2.2	$2.3 \cdot 10^{6}$	4.48	$2.4 \cdot 10^{-2}$
^{238}U	$4.47 \cdot 10^{9}$ y	$5.45 \cdot 10^{-7}$	$1.36 \cdot 10^{-2}$	2.01 / 2.3	$1.2 \cdot 10^{4}$	4.19	$8.3 \cdot 10^{-5}$
^{237}Np	$2.14 \cdot 10^{6}$ y	$2.14 \cdot 10^{-12}$	$1.14 \cdot 10^{-4}$	2.05 / 2.70	$2.6 \cdot 10^{7}$	4.77	$3.4 \cdot 10^{-1}$
^{238}Pu	87.74 y	$1.84 \cdot 10^{-9}$	$2.59 \cdot 10^{3}$	2.21 / 2.9	$6.4 \cdot 10^{11}$	5.49	$1.34 \cdot 10^{4}$
^{239}Pu	$2.41 \cdot 10^{4}$ y	$4.40 \cdot 10^{-12}$	$2.18 \cdot 10^{-2}$	2.16 / 2.88	$2.3 \cdot 10^{9}$	5.15	$3.81 \cdot 10^{1}$
^{240}Pu	$6.56 \cdot 10^{3}$ y	$5.66 \cdot 10^{-8}$	$1.02 \cdot 10^{3}$	2.16 / 2.8	$8.4 \cdot 10^{9}$	5.15	$1.41 \cdot 10^{2}$
^{241}Pu	14.35 y	$5.74 \cdot 10^{-15}$	$5 \cdot 10^{-2}$	2.25 / 2.8	$9.4 \cdot 10^{7}$	4.89	1.3
^{242}Pu	$3.76 \cdot 10^{5}$ y	$5.50 \cdot 10^{-6}$	$1.72 \cdot 10^{3}$	2.15 / 2.81	$1.4 \cdot 10^{8}$	4.90	2.0
^{241}Am	433.6 y	$4.13 \cdot 10^{-12}$	1.18	3.22 / 3.09	$1.3 \cdot 10^{11}$	5.48	$2.69 \cdot 10^{3}$
^{242}Cm	163 d	$6.81 \cdot 10^{-8}$	$2.10 \cdot 10^{7}$	2.54 / 3.44	$1.2 \cdot 10^{14}$	6.10	$3.76 \cdot 10^{6}$
^{244}Cm	18.1 y	$1.34 \cdot 10^{-6}$	$1.08 \cdot 10^{7}$	2.72 / 3.46	$3.0 \cdot 10^{12}$	5.80	$7.73 \cdot 10^{4}$
^{246}Cm	4706 y	$2.94 \cdot 10^{-4}$	$1.01 \cdot 10^{7}$	2.948 / –	$1.1 \cdot 10^{10}$	–	–
^{249}Bk	320 d	$4.61 \cdot 10^{-10}$	$1.0 \cdot 10^{5}$	3.40 / 3.7	$8.8 \cdot 10^{8}$	5.40	$1.8 \cdot 10^{1}$
^{252}Cf	2.646 y	$3.09 \cdot 10^{-2}$	$2.34 \cdot 10^{12}$	3.757 / 4.06	$1.9 \cdot 10^{13}$	6.11	$6.0 \cdot 10^{5}$

† The errors in the (α,n) yields are at least 10%, because they depend upon the chemical and physical composition of the material.

Table 6 lists the primary-neutron production rates of the relevant actinide isotopes, *per gram*, so the absolute production rates are these rates multiplied by the quantities of the isotopes in the spent fuel. The three isotopes that produce the most primary neutrons in spent

fuel assemblies (by spontaneous fission) are ^{240}Pu, ^{242}Cm, and ^{244}Cm (see Figure 4), because they not only have a high production rate per gram but also are present in significant quantities in the spent fuel. These isotopes are created from ^{238}U (primarily) by successive neutron capture in the nuclear reactor; see Figure 5. Table 7 ranks these three isotopes and ^{246}Cm according to their relative importance. It shows that after more than a century of cooling time, the ^{240}Pu and ^{246}Cm eventually overtake the ^{244}Cm as the chief producers of primary neutrons, because they have longer half-lives than ^{244}Cm does. Also, this table plus Table 6 and Figure 4 together explain the comparative neutron-production rates of ^{242}Cm and ^{244}Cm in spent fuel. Even though the branching ratio for the spontaneous fission of ^{242}Cm is much smaller than that for ^{244}Cm, the shorter half-life of ^{242}Cm causes it to produce effectively double the amount of neutrons as an equivalent amount of ^{244}Cm. Thus, even though there is less ^{242}Cm than ^{244}Cm in all but the lowest burnup fuels, the primary-neutron production rate of ^{242}Cm competes well with that of ^{244}Cm until two years after discharge, by which time most of the ^{242}Cm has decayed away.

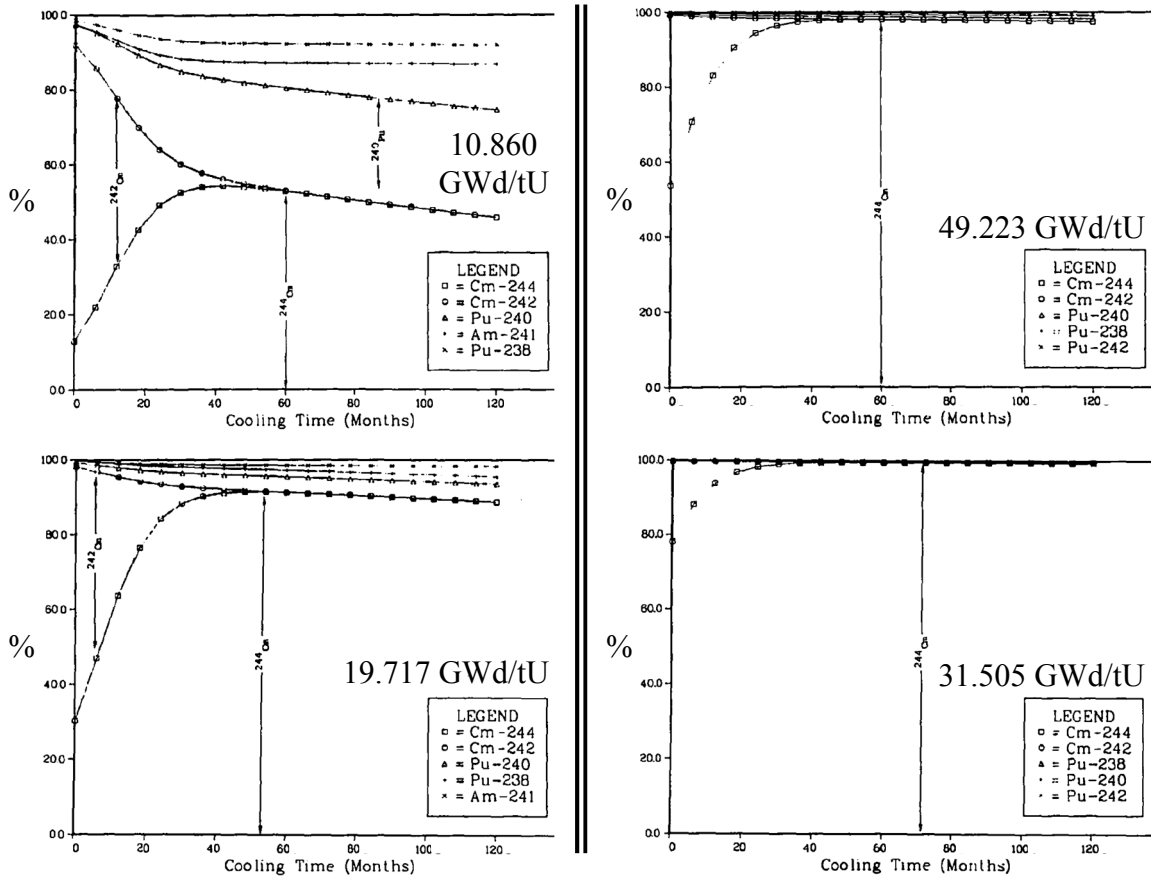

Figure 4: Fractional breakdown (sum = 100%) of the primary-neutron production of the five most prolific isotopes in typical spent fuel assemblies. Modified from Bosler et al. [92].

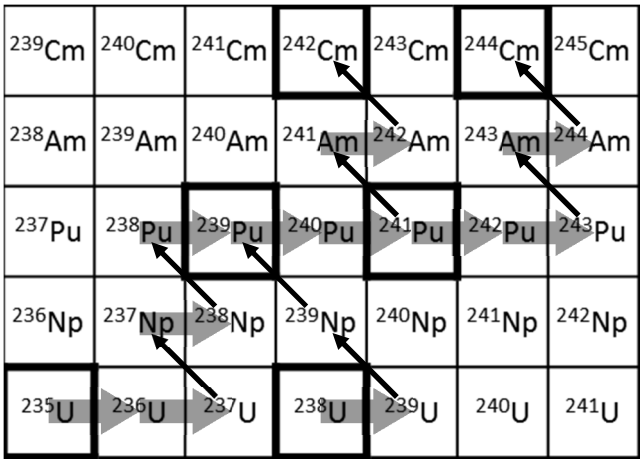

Figure 5: Main nucleosynthesis pathways for ^{242}Cm and ^{244}Cm [126-128]. Broad arrows represent neutron capture; narrow arrows represent β-decay. Reprinted with permission from Elsevier.

Table 7: Ranking of the isotopes that produce the most primary neutrons in spent nuclear fuel. The values are from various computer simulations and are intended for rough comparisons only [83, 87, 124, 129]. Modified from Bolind [130], with permission from INMM.

Rank	At Discharge			After Cooling 3 Years			After Cooling 140 Years		
	Isotope	Conc.	N. Prod.	Isotope	Conc.	N. Prod.	Isotope	Conc.	N. Prod.
1	Cm-244	1	1	Cm-244	1	1	Pu-240	21000	2
2	Cm-242	1/4	1/2	Pu-240	112	1/90	Cm-246	1.2	1.2
3	Pu-240	100 *	1/100	Cm-246	1/150	1/150	Cm-244	1	1
4	Cm-246	1/170	1/170						

"Conc." is the concentration in the spent fuel, as a fraction or multiple of that of Cm-244. The concentration of Cm-244 in spent fuel is typically between 0.001 and 100 parts per million, by weight [83, 87]. See also the references listed in Table 4.
"N. Prod." is the neutron production rate relative to that of Cm-244. See Table 6.
* 100 is a rough, middle value for medium burnup LEU (about 30 GWd/tU) and low burnup MOX. The range of relative concentration is about 10 to 10000, so that the neutron production by Cm-246 might be greater than that by Pu-240 [87].

Tables 8 and 9 and Figures 6 through 8 provide more absolute numbers of the primary-neutron and gamma radiations that are generated by spent fuel assemblies. The report by Tanskanen [83] is associated with Figures 6 and 7 and contains additional useful data and figures that complement Figure 4. The data in Figure 6 for VVER-440 fuel assemblies can be considered as representing small-sized PWR fuel assemblies, since the VVER-440 reactor is a kind of pressurized-water reactor [131].

It must be noted that in all these figures and tables, the neutron rates are for the *generation of primary neutrons only*, since they are calculated from the amounts of ^{244}Cm and other isotopes in the spent fuel assemblies as determined by burnup simulations. To calculate the number of neutrons emitted from a fuel assembly, one must also take into account neutron absorption and neutron multiplication by induced fission. Alternatively, to determine experimentally the emitted neutron intensity, one must account for the efficiency and

geometric arrangement of the neutron detectors, which historically has not usually been done; the common NDA practice has been to calibrate the NDA instrument's measured signal directly to the fuel assembly's quantity of interest, rather than to make the extra effort to determine an absolute value for a physical property of the assembly (see Section 6.2.1). Furthermore, the numbers in these figures and tables are for entire fuel assemblies and therefore do not reflect the variations in the neutron and gamma radiations caused by the axial burnup profiles of the assemblies. Nevertheless, these numbers provide a rough sense of the quantities of radiation with which spent-fuel NDA deals.

Table 8: Rough magnitudes of types of radiation generated by spent LWR fuel (type not specified) per metric ton of uranium; from Table XVII in Reilly [132].

Burnup	GWd/tU	20	30	40
Initial enrichment	weight%	~2 to 3%	~2 to 3%	~2 to 3%
Cooling time	years	1	1	1
Primary-neutron intensity	neutrons/(s·tU)	—	$2.8 \cdot 10^{8}$	$9.5 \cdot 10^{8}$
Secondary-neutron intensity	neutrons/(s·tU)	Not determined		
Total fission-product activity	Bq/tU	$4.3 \cdot 10^{16}$	$8.5 \cdot 10^{16}$	$10.8 \cdot 10^{16}$
Fission-product gamma-ray intensity	photons/(s·tU)	$1.2 \cdot 10^{16}$	$2.2 \cdot 10^{16}$	$2.4 \cdot 10^{16}$
Total cladding and hardware activity	Bq/tU	$3.8 \cdot 10^{14}$	$7.3 \cdot 10^{14}$	$11.5 \cdot 10^{14}$
Cladding gamma-ray intensity	photons/(s·tU)	$2.5 \cdot 10^{14}$	$6.6 \cdot 10^{14}$	$9.9 \cdot 10^{14}$

Table 9: Rough magnitudes of types of radiation generated by spent LWR UOX and MOX fuel assemblies, per assembly; from Table 1.1 in LaFleur [87], with permission from the author.

		BWR (9 x 9)		PWR (17 x 17)	
		UOX	MOX	UOX	MOX
Burnup	GWd/tU	30	30	30	30
Initial enrichment	weight%	3% ^{235}U	6% Pu	4% ^{235}U	6% Pu
Cooling time	years	5	5	5	5
Total primary-neutron intensity	neutrons/s	$1.28 \cdot 10^{8}$	$41.9 \cdot 10^{8}$	$1.13 \cdot 10^{8}$	$49.8 \cdot 10^{8}$
From spontaneous fission	neutrons/s	$1.25 \cdot 10^{8}$	$41.3 \cdot 10^{8}$	$1.10 \cdot 10^{8}$	$49.2 \cdot 10^{8}$
From (α,n) reactions	neutrons/s	$0.03 \cdot 10^{8}$	$0.6 \cdot 10^{8}$	$0.03 \cdot 10^{8}$	$0.6 \cdot 10^{8}$
Secondary-neutron intensity	neutrons/s	Not determined			
Gamma-ray intensity	photons/s	$8.2 \cdot 10^{15}$	$8.3 \cdot 10^{15}$	$8.7 \cdot 10^{15}$	$9.1 \cdot 10^{15}$

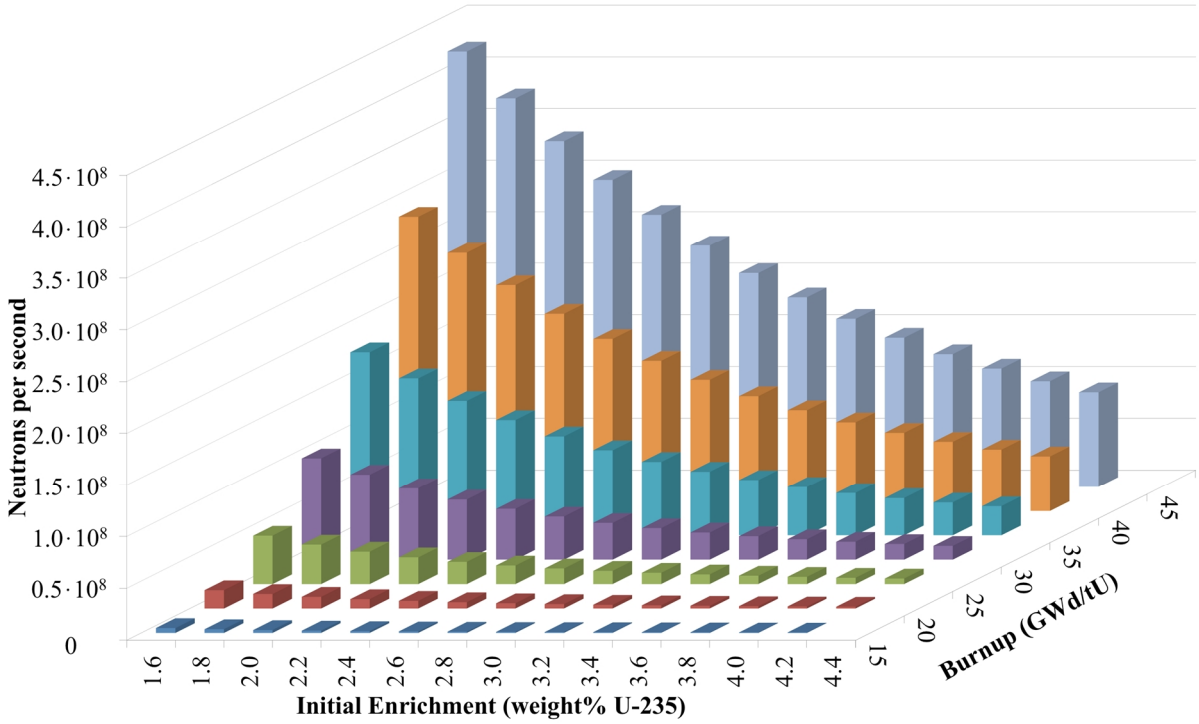

Figure 6: Calculated production rate of primary neutrons from ^{244}Cm in a spent VVER-440 fuel assembly (~120 kg of initial U) at discharge. Data from Tiitta and Hautamäki [79].

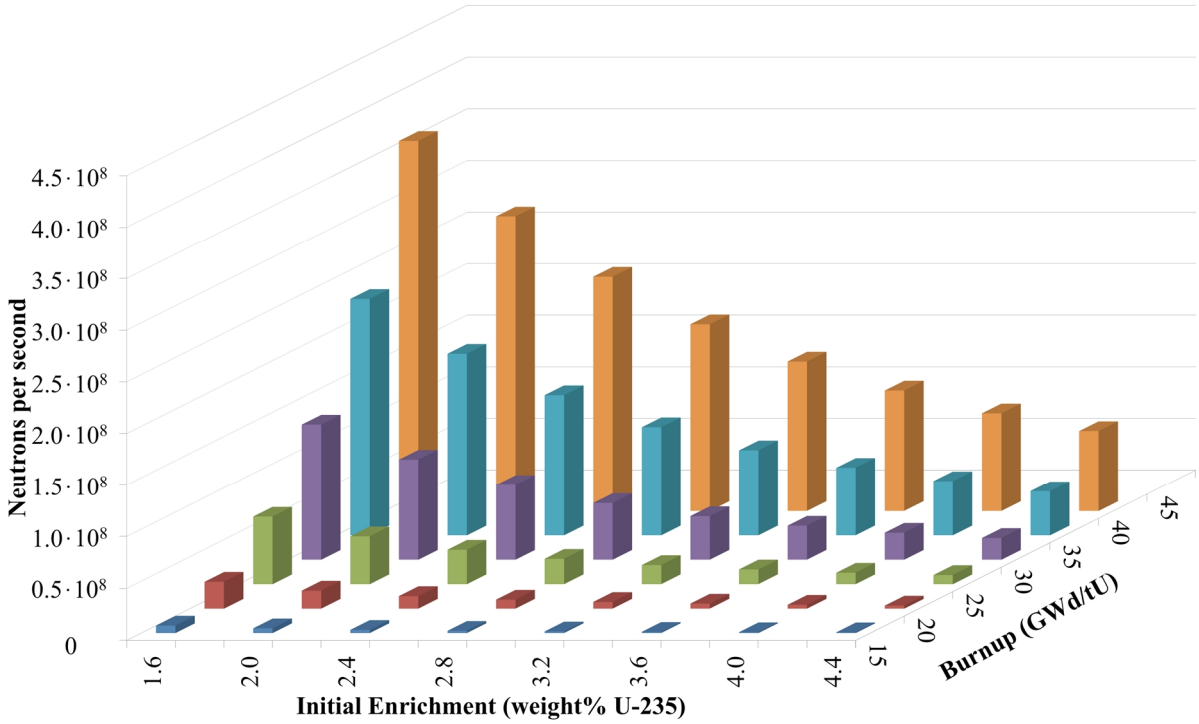

Figure 7: Calculated production rate of primary neutrons from ^{244}Cm in a spent BWR fuel assembly (~178 kg U; burned at 0.5 void fraction) at discharge. Data from Tiitta et al. [78].

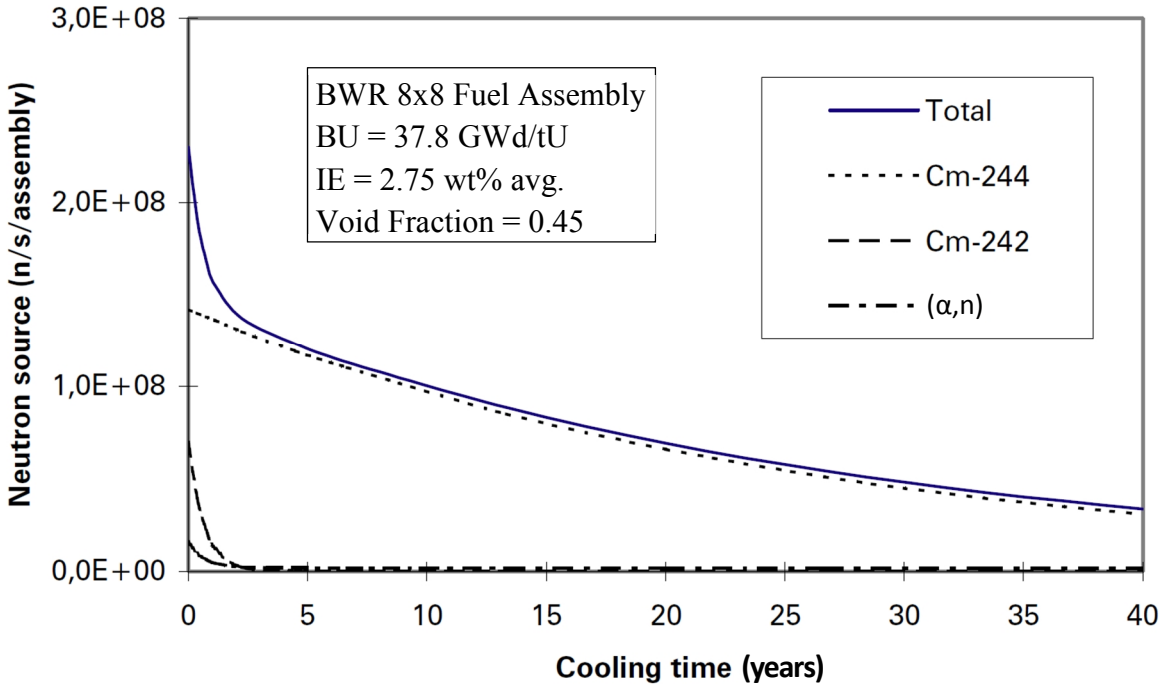

Figure 8: Total neutron source strength and its major components as a function of cooling time, for the indicated conditions. Modified from Figure 1 in Tanskanen [83], with permission from STUK.

3.3.2 Secondary-neutron sources and effective Pu-239

Neutrons that are created from fission events that are induced by other neutrons are called secondary neutrons. Almost all of the neutrons in an operating nuclear reactor are secondary neutrons, since they come from fission chain reactions, so this terminology is not often used in the context of nuclear-reactor engineering. In the context of spent-fuel NDA, though, the distinction between primary and secondary neutrons is very useful because the fuel assembly is not close to criticality and so the primary-neutron sources are relatively strong.

Although fast fission of ^{238}U and other non-fissile isotopes does occur, secondary neutrons are chiefly associated with the fission of the three main fissile isotopes, namely, ^{235}U, ^{239}Pu, and ^{241}Pu. (^{245}Cm is another fissile isotope that might be important for high-burnup spent MOX fuel [133], but it will be ignored in this report.) These three isotopes all have large thermal and epithermal fission cross sections (Figure 9), by the definition of *fissile*. It is convenient to treat these fissile isotopes together as group, but since they have different cross sections, their quantities in the fuel must be weighted somehow in the summation. This situation has led the NGSI to develop the concept of *effective ^{239}Pu* (^{239}Pu$_{\text{effective}}$), which treats the ^{235}U and the ^{241}Pu in the fuel as effective quantities of ^{239}Pu according to how they affect the NDA results. (See Section 2.4.) With the nuclides' notations standing for their quantities, the expression is as follows [73]:

$$^{239}\text{Pu}_{\text{effective}} = C_1 \cdot {}^{235}\text{U} + {}^{239}\text{Pu} + C_2 \cdot {}^{241}\text{Pu} \qquad \text{Equation 1}$$

This concept is akin to the earlier concept of effective ^{240}Pu, which comes from neutron coincidence counting (Equation 16-1 in Reilly et al. [75]). In that application, the ^{238}Pu, ^{240}Pu, and ^{242}Pu all produce neutron pairs and triplets slightly differently, according to "(a) the

relative spontaneous fission half-lives of each isotope [and] (b) the relative neutron multiplicity distributions of each isotope." [75] The quantities of ^{238}Pu and ^{242}Pu are therefore weighted such that they contribute the same signal as an equivalent quantity of ^{240}Pu in the sample being assayed. Caldwell, Kunz, and Atencio's 1984 patent for a differential die-away instrument presents definitions for both ^{239}Pu$_{effective}$ and ^{240}Pu$_{effective}$ [134].

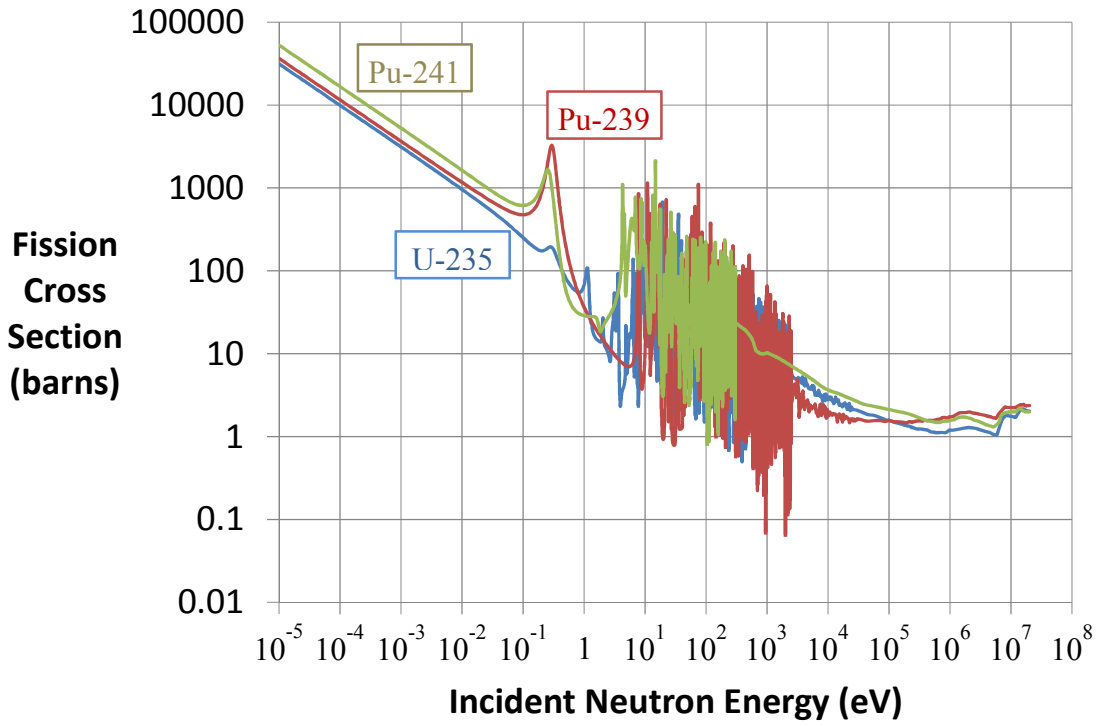

Figure 9: Energy-dependent fission cross sections for ^{235}U, ^{239}Pu, ^{241}Pu; data are from ENDF/B-VII.1 [125].

As mentioned in Section 2.4, the weighting coefficients C_1 and C_2 can be determined in a variety of ways, depending on which signal is being analyzed. For instance, if the prompt neutron multiplication is being considered, then the coefficients depend on the isotopes' fission cross sections (σ_f), on their average neutron multiplicity from fission ($\bar{\nu}$), and on the energy spectrum of the neutron flux inside the fuel assembly (ϕ) [19]:

$$C_i = \frac{\iiint_{Volume} \int_{Energy} \sigma_{f,i}(E)\bar{\nu}_i(E)\phi(E,\vec{\boldsymbol{r}})dE\, d\vec{\boldsymbol{r}}}{\iiint_{Volume} \int_{Energy} \sigma_{f,\,\text{Pu-239}}(E)\bar{\nu}_{\text{Pu-239}}(E)\phi(E,\vec{r})dE\, d\vec{\boldsymbol{r}}} \qquad \text{Equation 2}$$

(Fortunately, the energy spectrum does not change much with the BIC set; see Section 6.2.3.) Alternatively, if the delayed neutron multiplication is being considered, then the delayed-neutron yield ($\beta\bar{\nu}$) replaces the neutron multiplicity. For delayed gamma-ray measurements (Section 5.1.1), this variable is replaced yet again by the fissile isotopes' different production rates of the various fission products that emit the characteristic gamma-rays. Therefore, there can be many versions of ^{239}Pu$_{effective}$; the NGSI reports typically append the name of the NDA technique to the subscript to indicate which version is being considered.

This idea that different NDA techniques use different coefficients and so have different equations for $^{239}Pu_{effective}$ has led to the idea of using three equations from three NDA techniques to solve simultaneously for the quantities of the three fissile isotopes. As mentioned in Section 2.4, this concept has guided much of the NGSI's Spent Fuel NDA Project. This concept presumes, though, that the NDA techniques are measuring signals directly from the fissile isotopes, similar to the way that neutron-coincidence counters practically analyze directly the spontaneously fissioning isotopes (^{238}Pu, ^{240}Pu, and ^{242}Pu) when assaying purified nuclear materials or slightly contaminated waste. (See the introduction to Section 4.2.) As will be demonstrated in Section 6, the NDA of spent fuel assemblies is fundamentally a three-dimensional problem, at minimum, and the production of neutrons and gamma-rays from the induced fission of the fissile isotopes is merely one of those dimensions. Therefore, the NDA techniques are most certainly not directly measuring the fissile isotopes but rather are detecting them indirectly. The NGSI partially recognized this problem when they identified neutron absorbers as being particularly responsible for uncertainty in assay results (e.g., in References [73] and [135]), but a more complete picture of the problem is provided by the paradigm that is presented in Section 6. In general, then, this usage of multiple versions of $^{239}Pu_{effective}$ to separate out the three fissile isotopes is not a viable approach because other factors dominate the assay to first order. Nonetheless, $^{239}Pu_{effective}$ is often a convenient shorthand for "*fissile content*" and can be useful conceptually.

3.3.3 Neutron absorbers

The burning and cooling of fuel assemblies produces neutron-capturing isotopes, also known as neutron absorbers and as neutron poisons, in the fuel. These isotopes are those that capture the incident neutron without fissioning. These neutron absorbers can be divided into two groups—the transuranic absorbers and the fission-product absorbers.

All of the transuranic isotopes have greater neutron-capture cross sections than ^{238}U, so they can all be considered to be neutron absorbers, but the ^{241}Am is noteworthy. The ^{241}Am has the largest capture cross section of all the long-lived isotopes on the nucleosynthesis pathways to ^{244}Cm and ^{242}Cm (Figure 5), and it is created from the radioactive β-decay of the ^{241}Pu.

As for the fission products, the burnup-credit community has recognized that a mere sixteen isotopes are responsible for about 80% of the neutron capturing in fission products [89, 133, 136]. These sixteen isotopes are ^{95}Mo, ^{99}Tc, ^{101}Ru, ^{103}Rh, ^{109}Ag, ^{133}Cs, ^{143}Nd, ^{145}Nd, ^{147}Sm, ^{149}Sm, ^{150}Sm, ^{151}Sm, ^{151}Eu, ^{152}Sm, ^{153}Eu, and ^{155}Gd [89]. These isotopes are either stable or relatively long-lived. For safeguards, ^{155}Eu should also be included in the list because it decays to ^{155}Gd; it is not included in the burnup-credit list because the burnup-credit community always assumes a five-year cooling time. Thus, the fission-product neutron absorbers can be represented by this set of 16+1 isotopes.

3.3.4 Gamma-ray emitting isotopes

The gamma-ray emitting isotopes that are the most important for NDA of spent fuel assemblies are listed in Table 15 and discussed in Sections 5.1.2 (TG) and 5.1.3 (PG). For passive NDA of spent fuel after the first year of cooling, the three main isotopes are ^{134}Cs,

^{137}Cs, and ^{154}Eu. Tables 8 and 9 indicate that the gamma-ray flux that is generated by a spent fuel assembly can be of the order of 10^{15} to 10^{16} photons per second at early cooling times. Note, though, that the data from these tables do not account for the self-shielding of the gamma-rays, neither the self-shielding that occurs within each fuel pin nor the outer fuel pins' shielding of the gamma-rays from the inner pins. Thus, the photon flux that is actually emitted from the fuel assembly must be less than the values from these tables.

4. The neutron-based NDA techniques

In this section, the eleven neutron-based NDA techniques of the NGSI (Table 1) are described and discussed. At the beginning of the subsection of each NDA technique, a short summary table is given that lists the prominent characteristics of that technique. Afterward, the principle of operation, the design of the NGSI's version of the NDA instrument, the method by which the data are analyzed, and the limitations of the technique are described.

The eleven techniques (ten advanced techniques plus TN) are categorized in Table 10 according to their principle of operation: (1) measuring neutron multiplication, (2) measuring neutron coincidence, and (3) measuring neutron energy. This categorization is a good way to highlight the similarities and the differences among all the techniques. The rest of this section will follow this categorization.

Table 10: The eleven neutron-based NDA techniques, categorized according to their principle of operation. Modified from Bolind [130], with permission from INMM.

The Attribute That Is Analyzed	The Neutron-Based NDA Techniques	
Neutron Multiplication	TN:	Total (gross) Neutron counting
	PNAR:	Passive Neutron Albedo Reactivity
	CIPN:	^{252}Cf Interrogation with Prompt Neutron detection
	AIPN:	Assembly Interrogation with Prompt Neutron detection
	DDA:	Differential Die-Away analysis
	DN:	Delayed Neutron counting
Neutron Coincidence	NM:	Neutron Multiplicity counting
	DDSI:	Differential Die-away Self Interrogation
Neutron Energy	NRTA:	Neutron Resonance Transmission Analysis
	LSDS:	Lead Slowing-Down Spectroscopy
	SINRD:	Self-Interrogation Neutron Resonance Densitometry

This categorization can be understood by reference to the one-speed neutron diffusion equation (see also Section 6.2.3):

$$S + (\bar{\nu} - 1)\Sigma_{\mathrm{f}}\phi - \Sigma_{\mathrm{a,capture}}\phi - (-D\nabla^2\phi) = \frac{1}{v}\frac{\partial\phi}{\partial t} \qquad \text{Equation 3}$$

Here, ϕ is the neutron flux (in units of neutrons/(cm^2·s)), v is the neutron velocity (cm/s), t is time (s), D is the neutron diffusion coefficient (cm), $\Sigma_{\mathrm{a,capture}}$ is the macroscopic absorption cross section for non-fission-inducing absorption (cm^{-1}), Σ_{f} is the macroscopic fission cross section (cm^{-1}), $\bar{\nu}$ is the average number of neutrons emitted per fission, and S is the source of neutrons. In this equation, the first term often corresponds to the production of primary neutrons (N_{PRI}; e.g., neutrons from spontaneous fission), the second term corresponds to the production of secondary neutrons by induced fission, the third term corresponds to the capture of neutrons, the fourth term corresponds to the diffusion of neutrons and ultimately to their leakage out of the fuel assembly, and the last term (on the right-hand side) is the change in the

neutron flux with time. The fourth term—the diffusion term—does not change significantly with the burning, enrichment, or cooling of the fuel assembly; see the discussion of this assertion in Section 6.2.3. The right-hand-side term either is zero for a steady-state NDA measurement or is represented by a die-away time for a time-dependent NDA measurement.

Therefore, neutron multiplication techniques are those that analyze the second and third terms together. (DN emphasizes the second term; see Section 4.1.6.) Neutron coincidence techniques look for die-away times corresponding to the first term and/or the pair of the second and third terms. Neutron energy techniques examine energy-resonance processes that are described not by this one-speed neutron diffusion equation only but rather by an energy-dependent treatment, such as by multi-group transport equations.

The emphasis of this report is on the description of how the NDA techniques can assay spent fuel assemblies. It is assumed that the reader has a basic knowledge of neutron production, transport, and interactions with nuclei. If not, the reader is advised to read first the following works: Chapters 11–18 of the report by Reilly et al. [75] and an introductory nuclear-engineering text, such as the book by Lamarsh and Baratta [74] or the course notes from the U.S. Department of Energy [137, 138] or the Canadian Nuclear Safety Commission [139]. A conference paper by one of the authors may also be a quick introduction [130].

The type of neutron detectors that are used for a particular neutron NDA technique depends primarily on whether or not a high detection efficiency is required (see Chapter 13 of Reilly et al. [75]). Neutron-coincidence NDA techniques require a high efficiency; their figure of merit is the ratio of the square of the detection efficiency to the detector die-away time (ε^2/τ) (page 26 of Smith and Jaramillo [140], and Evans et al. [141]). Therefore, these techniques require the use of ^{3}He-gas proportional detectors, which can detect about 77% of the neutron flux that is perpendicularly incident to the detector (Table 13-3 in Reilly et al. [75]). However, ^{3}He detectors are also sensitive to the spurious detection of gamma-rays; the gamma-radiation must be less than 1 R/hr. This fact necessitates the use of heavy lead shielding between the ^{3}He detectors and the spent fuel assembly. In contrast, neutron-multiplication and neutron-energy NDA techniques do not require detection efficiency that is as high. They can use fission chambers, which have a much lower detection efficiency (0.5%) but do not need lead shielding because they are very insensitive to gamma-rays (up to 10^6 R/hr) (Table 13-3 in Reilly et al. [75]). Furthermore, the worldwide shortage of ^{3}He gas is causing fission chambers to become comparatively less expensive.

4.1 Distinguishing fissile material by neutron multiplication

The NDA techniques that detect fissile material by neutron multiplication can be further split into two subcategories: (1) those that measure the effects of a continuous neutron flux and (2) those that measure the effects of pulses of neutrons. The NDA techniques in the first subcategory make measurements that are independent of time, while those in the second subcategory depend on the timing of the pulses. The time-independent, neutron-multiplication techniques are TN, PNAR, CIPN, and AIPN. The time-dependent, neutron-multiplication techniques are DDA and DN. These NDA techniques will be discussed in this order.

The first subcategory (continuous flux) contains both passive and active techniques. The passive, time-independent techniques use the continuous neutron flux that is self-generated by the spent fuel assembly, from spontaneous fission, (α,n) reactions, and induced fission. The active, time-independent techniques use a continuous neutron source such as ^{252}Cf, which produces neutrons by spontaneous fission. The second subcategory (pulsed flux) contains only active techniques, since the passive neutron flux is continuous. The pulsing can be made by moving quickly a continuous source (such as ^{252}Cf) to and from the spent fuel assembly; this method is known as “shuffling.” The pulsing can also be made by turning a neutron generator on and off. Such cycling is easy to do if the neutrons are generated with a particle accelerator, since the accelerator can generate a pulsed beam of particles or can be cycled on and off.

4.1.1 Total Neutron counting (TN)

Name	Total Neutron counting (TN) (also known as gross neutron counting)
References	NGSI: [121] Other: [9, 75, 142-145]
Measurement environment	In water (in air or other gas is also possible)
Passive vs. Active	Passive
Time dependency	Time-independent (continuous)
Particles detected	Neutrons
The type of detectors	Fission chambers
Particles' detected attribute	Existence (quantity): the production of primary neutrons and their multiplication
Governing physical properties of the fuel assembly	The number of primary neutrons (N_{PRI}) The leakage multiplication of primary neutrons (M_L)
Governing isotopes	Primary-neutron sources (^{244}Cm, ^{242}Cm, ^{240}Pu, (α,n) reaction isotopes); fissile isotopes; neutron absorbers
Maturity	Currently in use
Limitations	Cannot distinguish among primary-neutron production, secondary-neutron production (induced fission), and neutron absorption
Selected by the NGSI for prototype testing?	Yes

4.1.1.1 Principle of operation

Total neutron counting is the most basic neutron NDA technique. It is merely the measurement of the self-generated neutron flux that is emitted from the fuel assembly. Therefore, it is a passive and time-independent technique. The self-generated neutron flux originates with the production of primary neutrons. These neutrons are then multiplied by inducing fission in the fissile isotopes (along with a minor amount of fast fission in ^{238}U). Both primary and secondary neutrons are emitted from the fuel assembly. Neutron-absorbing isotopes (poisons) in the fuel assembly reduce the number of neutrons multiplied and emitted.

In terms of the neutron diffusion equation (Equation 3), the TN technique analyzes the strength of the primary-neutron source term, *S*, but these neutrons are also multiplied by the difference between the fission and capture terms. The $\partial\phi/\partial t$ term is zero since TN is a steady-state measurement.

$$S + (\bar{\nu} - 1)\Sigma_{\mathrm{f}}\phi - \Sigma_{\mathrm{a,capture}}\phi - (-D\nabla^2\phi) = \frac{1}{v}\frac{\partial\phi}{\partial t} \qquad \text{Equation 3}$$

Total neutron counting is currently used in IAEA safeguards, such as in the Fork detector (FDET) and the Safeguards MOX Python (SMOPY) detector [7, 9, 75, 143, 146]. The fuel assembly is raised out of its rack in the spent fuel pool, the detector is placed next to the assembly (usually near the midplane), and the measurement is made. (See Figure 10.) The Fork and SMOPY detectors also include gamma-ray detectors besides the neutron detectors.

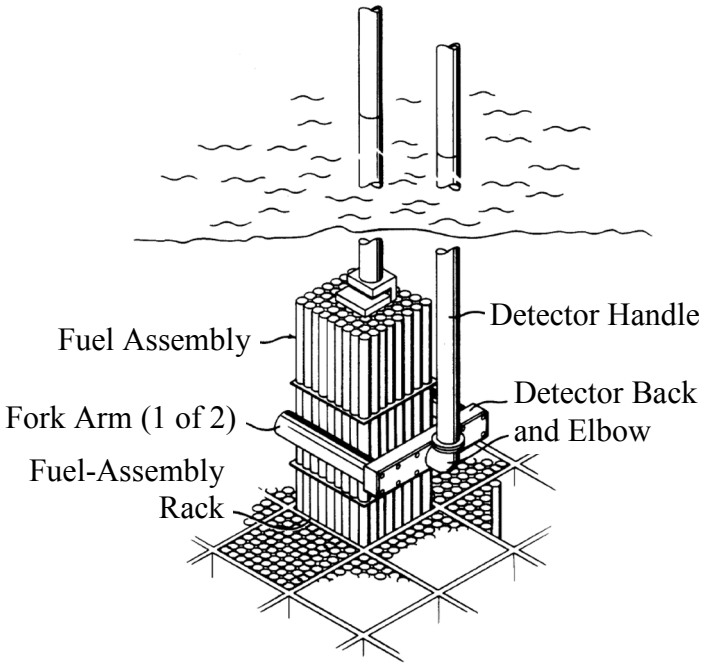

Figure 10: Measurement of a spent fuel assembly with the Fork detector; modified from the patent drawing [147].

4.1.1.2 The NGSI's design

The NGSI did not specifically investigate TN, since it is already a well-developed technique. TN is inherently incorporated into all of the neutron-based NDA techniques because all of these techniques use neutron detectors. A TN measurement can thus be made by removing any active neutron sources for a sufficiently long period of time. Of course, the TN signal will be different for different configurations of the neutron detectors with respect to each other and to the position of the spent fuel assembly. Therefore, the TN signal as measured by one NDA instrument can be compared with that from another NDA instrument (such as the Fork detector) only through proper calibration.

4.1.1.3 Data analysis

In the past, TN has been used primarily to indicate the burnup (BU) of the fuel. The BU can be compared with the reactor operator's declaration to verify it. If a discrepancy is found, the inspecting agency then asks the reactor operator to justify the discrepancy, because the discrepancy may be caused by a partial defect.

The TN count rate scales as a power function with BU (Equation 5 in Rinard and Bosler [9] and Equation 18-4 in Reilly et al. [75]):

$$\mathrm{TN} = \alpha(\mathrm{BU})^{\beta} \qquad \text{Equation 4}$$

The value of β is between 3 and 4 [75, 145, 148]. The values of the α and β parameters are determined uniquely for each set of spent fuel assemblies being measured, such as all of the spent fuel assemblies in a given spent fuel pool. The parameters are determined by calibration: The set of assemblies is measured; a curve is drawn through the data; and the parameters are found from the curve. Outlying fuel assemblies are thus revealed and can be investigated further. Figure 11 illustrates part of this methodology.

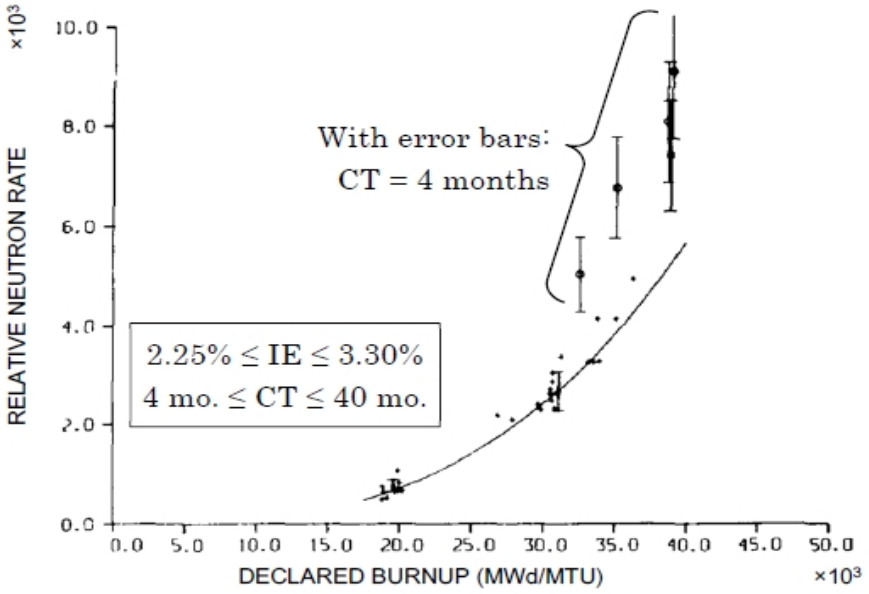

Figure 11: Total neutron count rates from 36 LEU PWR assemblies. Modified from Figure 28 in Phillips et al. [127].

Figure 11 also exhibits the uncertainty of the TN technique, which was mentioned earlier. The scatter in the data is significant; even after excluding the four-month cooling times, it is still about ±3 GWd/tU. Furthermore, these particular data have been drawn from a narrow set. The fuel assemblies with the lowest BU also had the lowest IE and the longest CT; and as the BU increased among the set of fuel assemblies, IE increased, and CT decreased. Therefore, the scatter of a set of fuel assemblies that truly spanned the whole domain of the BIC set would be much greater.

The reason that the TN count rate scales with BU (Equation 4) is that the quantity of primary-neutron-producing isotopes in the fuel assembly scales with BU. More specifically, the quantity of ^{244}Cm scales with BU, since this isotope dominates the production of primary neutrons after the ^{242}Cm has decayed away, after two to three years of cooling [92]. (See also Figures 6 through 8.) Therefore, it is more correct to say that the TN count rate scales with ^{244}Cm than it is to say that it scales with BU. This rationale is important because the physical processes at work in the production of ^{244}Cm and in the definition of BU are different. ^{244}Cm is created by successive neutron capture in ^{238}U, but BU is defined with respect to fission, mostly of fissile isotopes. Thus, two correlations are actually at work here: one between the TN count rate and the quantity of ^{244}Cm, and another between the quantity of ^{244}Cm and BU. Unfortunately, most of the literature on TN skip the correlation through ^{244}Cm and instead jump straight from the TN count rate to BU.

A formula that connects the TN count rate with the production of primary neutrons (i.e., Equation 7) will be developed in the discussion of the PNAR technique, in Section 4.1.2.3.

4.1.1.4 Limitations

Total neutron counting reveals that a fuel assembly is emitting neutrons, but it does not indicate the origins of the neutrons. For example, a fuel assembly with a high concentration of primary neutron sources but with a low concentration of fissile material could produce the same total number of neutrons as another fuel assembly that has a lower concentration of primary neutron sources but a higher concentration of fissile material that multiplies its primary neutron flux. Furthermore, TN does not account for the neutron absorbers (poisons) in the fuel assembly, which also change the number of neutrons emitted. In other words, TN cannot separate the amount of primary neutrons (N_{PRI}) from the leakage multiplication of those neutrons (M_L). (See Equation 7 in the PNAR section, below.) Therefore, total neutron counting can give only a limited amount of information about the spent fuel assembly. For this reason, it can be used only in a relative way to check for outlying fuel assemblies (see the previous paragraphs).

4.1.2 Passive Neutron Albedo Reactivity (PNAR)

Name	Passive Neutron Albedo Reactivity (PNAR)
References	NGSI: [15-18, 135, 149-151] Other: [152-160]
Measurement environment	In water
Passive vs. Active	Passive
Time dependency	Time-independent (continuous)
Particles detected	Neutrons
Type of detectors	Fission chambers
Particles' detected attribute	Multiplication, of reflected neutrons
Governing physical properties of the fuel assembly	The number of primary neutrons (N_{PRI}) The leakage multiplication of primary neutrons without reflection (M_L) The leakage multiplication of reflected neutrons ($M_{L,refl}$)
Governing isotopes	Primary-neutron sources; fissile isotopes; neutron absorbers
Maturity	Being tried for the first time, by the NGSI
Limitations	Cannot distinguish among primary-neutron production, secondary-neutron production (induced fission), and neutron absorption Large uncertainty or long measurement time, for low BU and a small quantity of primary-neutron sources, because the signal is weak Greatly affected by any water-filled gap (annulus) between the fuel assembly and the PNAR instrument during the measurement without albedo
Selected by the NGSI for prototype testing?	Yes, at the Fugen Advanced Thermal Reactor, Tsuruga, Japan [15]

4.1.2.1 Principle of operation

The technique of Passive Neutron Albedo Reactivity (PNAR) is time-independent and passive.[1] PNAR makes two measurements: one in which the neutrons are reflected back into the fuel assembly by the surrounding cooling water and one in which they are not. PNAR analyzes the difference between these count rates; the reflected neutrons induce more fission in the fuel assembly and boost the count rate. In other words, the PNAR technique uses the fuel assembly's own, emitted neutrons to interrogate it.

The reflection of neutrons by the surrounding cooling water (albedo) is the standard case; it is the same as a TN measurement. The removal of the albedo is the more difficult case and is what makes PNAR to be a unique NDA technique.

To remove the albedo completely, the spent fuel assembly would have to be suspended in an infinite vacuum (as in outer space)—but with the cooling water still inside the fuel assembly, between the fuel pins, just as if it would still be immersed. Any neutron that would

[1] *Albedo* is a noun that means *reflective power*; it is defined as the ratio of the amount of radiation that is reflected by a surface to the amount that is incident upon it.

leave the exterior boundary of the fuel assembly would therefore never come back to the fuel assembly; it would permanently leak away into the infinite vacuum.

Of course, it is impossible to suspend the fuel assembly in an infinite vacuum, so the next best option is to surround the fuel assembly with a strongly neutron absorbing substance, such as cadmium. This option is what PNAR does. Unfortunately, no neutron-absorbing liner can perfectly absorb all the neutrons that touch it; it does reflect some of them. Furthermore, the fuel assembly must be moved into and out of the measurement instrument, or else the instrument must be moved up and down along the assembly. Therefore, there must be a clearance between the fuel assembly and the neutron-absorbing liner, and this clearance will be filled with water, which will partially reflect the emitted neutrons. Therefore, the real no-reflection count rate cannot equal the idealized vacuum count rate but rather merely approximates it.

In terms of the neutron diffusion equation (Equation 3), the PNAR technique analyzes both the strength of the primary-neutron source term, *S*, and the multiplication expressed by the difference between the fission and capture terms. The $\partial\phi/\partial t$ term is zero since both PNAR measurements are steady-state.

$$S + (\bar{\nu} - 1)\Sigma_{\mathrm{f}}\phi - \Sigma_{\mathrm{a,capture}}\phi - (-D\nabla^2\phi) = \frac{1}{v}\frac{\partial\phi}{\partial t} \qquad \text{Equation 3}$$

4.1.2.2 The NGSI's design

The NGSI's implementation of PNAR uses fission-chamber neutron detectors and uses a sheet of cadmium to absorb the neutrons for the no-reflection measurement [16, 17, 153, 154, 161]. The sheet surrounds the circumference of the fuel assembly, but a small gap remains between the sheet and the fuel assembly to provide sufficient clearance for moving the fuel assembly into and out of the detector. (Cooling of the assembly during this measurement is provided primarily by the water that is inside the fuel assembly, between the individual fuel pins.) The fission chambers are embedded in polyethylene to thermalize the neutrons and thereby increase their probability to be detected.

An early version of the NGSI's PNAR instrument is shown in Figure 12; it has not yet been built. This instrument is rectangular, to accommodate rectangular LWR fuel assemblies, and it has a removable Cd sleeve, which must be inserted to make the no-reflection measurement. The PNAR instrument that has been used to measure spent fuel assemblies in the spent fuel pool of the Fugen Advanced Thermal Reactor in Tsuruga, Japan, is shown in Figure 13. This instrument has a cylindrical exterior and a cylindrical hole along its centerline, through which a cylindrical Fugen fuel assembly can pass. The instrument has a Cd liner that extends over only the bottom portion of the center hole. The instrument is thus divided into two sections: the bottom section that has the Cd liner and the upper section that does not. When a fuel assembly is in the PNAR instrument, the portion in the lower section does not have albedo, while the portion in the upper section does have albedo. In this way, both measurements, with and without albedo, are made simultaneously, although at different axial positions along the spent fuel assembly.

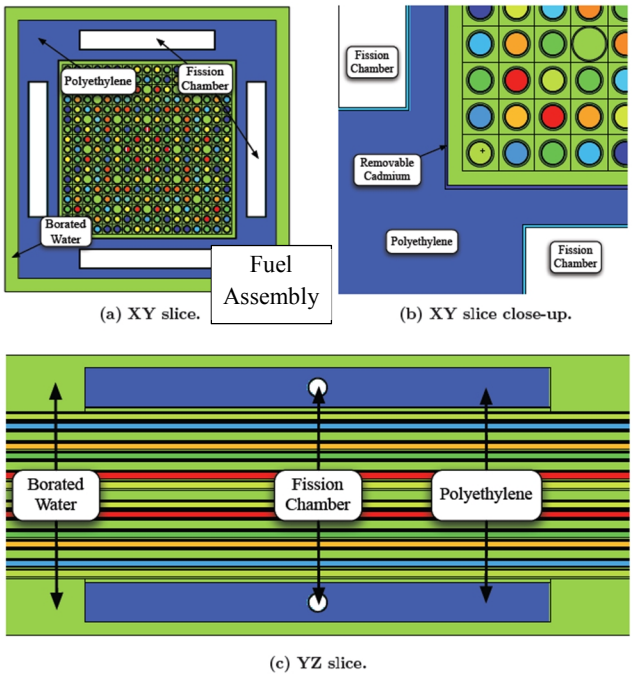

Figure 12: An early version of the NGSI's PNAR instrument. The three figures are not to scale. Copied from Conlin et al. [16] with permission from INMM.

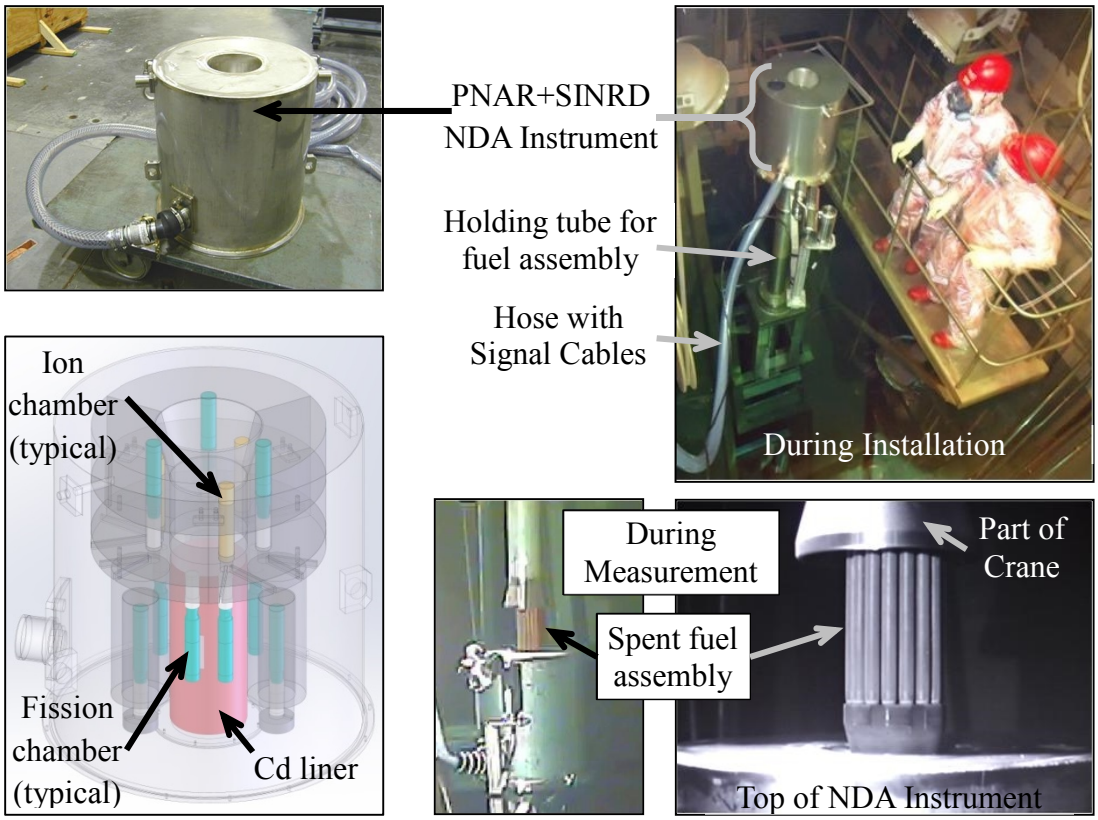

Figure 13: The NGSI's PNAR instrument that was used to measure spent fuel assemblies at the Fugen Advanced Thermal Reactor. In the bottom-left schematic, which was created by LANL researchers, the green tubes are fission chambers, the yellow tubes are ion chambers, and the red part is a Cd liner (which extends only partway up the central hole).

Some other, related PNAR work has been done outside the main NGSI effort. The first description of PNAR may have been the one by Lee and Lindquist in 1982 [152], though they used ^{3}He neutron detectors instead of fission chambers. Later, in 1997, Menlove and Beddingfield [153] suggested also performing neutron coincidence counting with the ^{3}He detectors to improve the PNAR signal, and this version of PNAR was the one that was initially examined by the NGSI [154]. Eventually though, the NGSI chose to abandon the neutron-coincidence-counting aspect so that they could use fission-chamber neutron detectors instead of ^{3}He detectors [5, 16]. The reason was that fission chambers are cheaper and simpler and do not require lead shielding to reduce the number of spurious detections caused by gamma-rays, so that a PNAR instrument with fission chambers is much lighter (Figure 1 in Menlove et al. [161]). Lastly, some study has been made in Korea of the use of PNAR to assay ingots of uranium and trans-uranium isotopes [155-157].

4.1.2.3 Data analysis

The PNAR metric that the NGSI chiefly uses for data analysis is the so-called "cadmium ratio," which is the ratio of the count rate with reflection (C_{REF}) to the count rate without reflection (C_{NOREF}) [18, 135]:

$$\mathrm{ARR} = \frac{C_{REF}}{C_{NOREF}} \qquad \text{Equation 5}$$

This ratio is equal to one if there is no fissile material in the fuel assembly and is greater than one if there is fissile material. This report recommends that the name "albedo reactivity ratio," abbreviated as *ARR*, be used instead of "cadmium ratio." The name "cadmium ratio" is ambiguous and is a misnomer if any material other than Cd is used for the neutron-absorbing liner. In contrast, the name "albedo reactivity ratio" accurately describes the physical process being measured, is applicable regardless of the liner material, and is taken from the name of the technique, Passive Neutron Albedo Reactivity.

By simulating PNAR measurements of the spent fuel assembly models in the Monte Carlo libraries (Section 2.3), the NGSI has tried to correlate the ARR with the fissile content in the spent fuel assembly [16-18, 135, 149]; see Figure 14. However, the uncertainty in the correlation is quite large, as can be seen in this figure. Burr et al. [135] have estimated that, without additional knowledge of a fuel assembly's BU or IE or CT, the relative error standard deviation of a PNAR measurement is 15% at least. Therefore, the NGSI is hoping that including other NDA techniques along with the PNAR technique will provide such additional knowledge in order to reduce this uncertainty.

A recent publication by one of the authors has provided more insight into how to analyze the PNAR data (reprinted here from [160] with permission from Elsevier). The count rates in the no-reflection and with-reflection measurements can be expressed, respectively, by the following equations:

$$C_{NOREF} = \varepsilon M_L N_{PRI} \qquad \text{Equation 6}$$

$$C_{REF} = \varepsilon \frac{M_L N_{PRI}}{1 - M_{L,refl}\,\bar{\nu} p_{f,emit}} \qquad \text{Equation 7}$$

Here, N_{PRI} is the number of primary neutrons in the spent fuel assembly, M_L is the leakage multiplication of those neutrons in the ideal no-reflection case, ε is the efficiency with which the fission chambers can detect the neutrons that are outside the fuel assembly, $p_{f,emit}$ is the probability that an emitted neutron will be reflected back into the fuel assembly and induce fission, $\bar{\nu}$ is the average number of neutrons born in an induced fission event, and $M_{L,refl}$ is the leakage multiplication of neutrons that are born from fission events that have been induced by reflected neutrons. (Note that Equation 7 is the equation for a TN measurement and is similar to Equation 14.1 of Reilly et al. [75] and to Equation 17 of Henzl et al. [23].) From these equations, an expression for the ARR can be obtained:

$$\mathrm{ARR} = \frac{C_{REF}}{C_{NOREF}} = \frac{1}{1 - M_{L,refl}\,\bar{\nu} p_{f,emit}} \qquad \text{Equation 8}$$

This equation shows that the ARR is governed by the fission induced by the neutron albedo, as expected. The quantity $\bar{\nu} p_{f,emit}$ is the number of interrogating neutrons from the albedo, per emitted neutron, and $M_{L,refl}$ is the leakage multiplication of those interrogating neutrons.

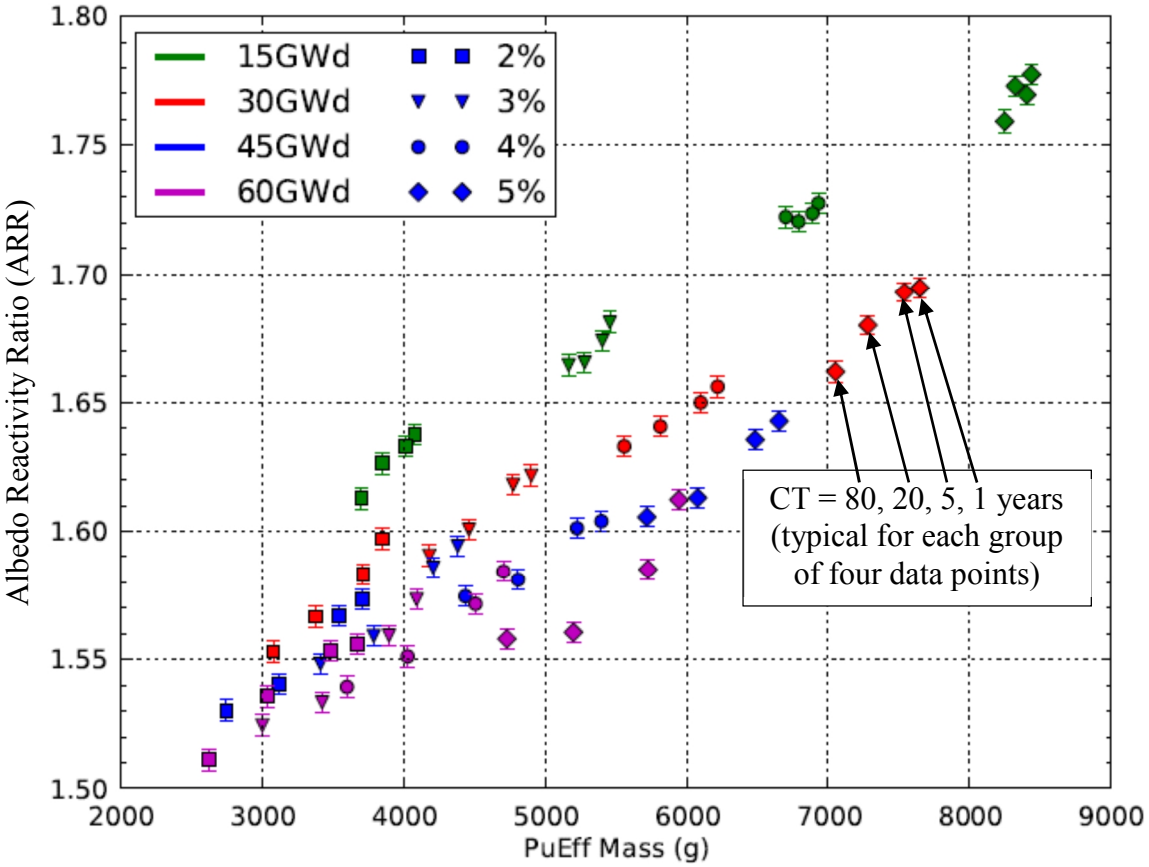

Figure 14: The change in the Albedo Reactivity Ratio (ARR) as a function of the fissile content of the fuel assembly. Modified from Figure 3 in Conlin et al. [17].

Equations 6 and 8 show that the no-reflection count rate (C_{NOREF}) and the ARR are independent quantities. This result corresponds directly to the fact that the PNAR technique consists of two measurements, namely, a TN measurement and a measurement with less multiplication because of the removal of the albedo. Therefore, the PNAR technique should be expected to produce two independent pieces of information, not just one. These two quantities—C_{NOREF} and the ARR—can therefore be used in a two-parameter correlation to the fissile content, in contrast to the one-parameter correlation of the NGSI (Figure 14). Because it would use more independent information, such a two-parameter correlation would have less uncertainty than the one-parameter correlation shown in Figure 14. In the NGSI's terminology, the TN technique and the PNAR technique can be integrated together to reduce the overall uncertainty, although since the TN technique is inherently part of the PNAR technique, such an integration would really be just the use of all of the information that is available from the PNAR technique. As Section 6 will show, though, a three-parameter correlation is actually necessary for a full characterization of the spent fuel assembly.

See Section 4.1.3.3 for a comparison of the PNAR technique with the CIPN technique.

4.1.2.4 Limitations

The PNAR technique cannot completely distinguish among primary-neutron production, secondary-neutron production (induced fission), and neutron absorption. The fact that PNAR produces two independent quantities helps to distinguish these three physical properties somewhat, certainly more so than the TN technique can do alone. Nevertheless, some of this uncertainty remains.

Since PNAR is a passive technique, the uncertainties in the measured count rates themselves can also be large if the neutron flux that is emitted from the fuel assembly is weak, or alternatively, the measurement times become very long in such a case. A weak neutron flux is nearly always attributable to an insufficient amount of primary-neutron-emitting isotopes in the spent fuel assembly, and the lack of such isotopes is attributable, in turn, to an insufficient amount of burnup. Therefore, PNAR may be impractical for fresh or slightly burned fuel assemblies. For example, the NGSI plans to put a ^{252}Cf source in the middle of their fresh fuel assembly to provide sufficient primary neutrons for their PNAR tests [151].

The sensitivity of PNAR is also reduced by the presence of a water-filled gap (annulus) between the fuel assembly and the neutron-absorbing liner in the no-reflection measurement (Section 4.1.2.1). Such a gap reflects many neutrons; about 97% of the neutrons that try to cross a 1 cm gap will experience at least one scattering collision along the way [130]. Other than minimizing the gap width, the only thing that can be done is to try to correct for the effect of this reflection. The author's paper that was mentioned above [160] suggests such an algorithm to correct the non-ideal no-reflection count rate.

4.1.3 ^{252}Cf Interrogation with Prompt Neutron detection (CIPN)

Name	^{252}Cf Interrogation with Prompt Neutron detection (CIPN)
References	NGSI: [15, 19, 162-164] Other: [144, 165, 166]
Measurement environment	In water (in air or other gas is also possible)
Passive vs. Active	Active; minimum source = $1.17 \cdot 10^8$ neutrons/s (50 μg of ^{252}Cf) [19]
Time dependency	Time-independent (continuous)
Particles detected	Neutrons
Type of detectors	Fission chambers
Particles' detected attribute	Multiplication, of external-source neutrons
Governing physical properties of the fuel assembly	The number of primary neutrons (N_{PRI}) The leakage multiplication of primary neutrons without reflection (M_L) The leakage multiplication of external-source neutrons ($M_{L,ext}$)
Governing isotopes	Primary-neutron sources; fissile isotopes; neutron absorbers
Maturity	Has been tested by others besides the NGSI
Limitations	Requires a ^{252}Cf neutron source, resulting in higher cost and the difficulties of shielding and transportation Cannot distinguish between secondary-neutron production (induced fission) and neutron absorption
Selected by the NGSI for prototype testing?	Yes, in the Post Irradiation Examination Facility (PIEF), Daejeon, Republic of Korea [15]

4.1.3.1 Principle of operation

^{252}Cf Interrogation with Prompt Neutron Detection (CIPN) is an active technique that uses the spontaneous-fission neutrons from an external, ^{252}Cf source to induce fission in the fissile material in the spent fuel assembly. Two measurements are made: one with the ^{252}Cf source beside to the fuel assembly and one without the source. The measurement without the source is identical to a TN measurement.

In terms of the neutron diffusion equation (Equation 3), the CIPN technique analyzes both the strength of the primary-neutron source term, *S*, and the multiplication expressed by the difference between the fission and capture terms. The $\partial\phi/\partial t$ term is zero since both CIPN measurements are steady-state.

$$S + (\bar{\nu} - 1)\Sigma_{\mathrm{f}}\phi - \Sigma_{\mathrm{a,capture}}\phi - (-D\nabla^2\phi) = \frac{1}{v}\frac{\partial\phi}{\partial t} \qquad \text{Equation 3}$$

The typical approach to CIPN has two main goals: (1) to minimize the contribution of the ^{252}Cf neutrons to the count rate of the active measurement and (2) to minimize the contribution of the self-generated neutron flux (from the primary neutrons) to the count rate of the active measurement. If neither the ^{252}Cf neutrons nor the self-generated neutrons are detected, then the count rate can be attributed solely to the detection of neutrons from induced

fission, and since almost all of the induced fission occurs in the fissile isotopes, the count rate is then mostly a function of the quantity of fissile material in the spent fuel assembly. The only remaining isotopic variable in the active measurement is the quantity of neutron absorbers in the fuel assembly.

The first goal can be achieved by moderating the ^{252}Cf neutrons before they enter the fuel assembly and by placing the neutron detectors toward the side of the fuel assembly that is opposite the side on which the ^{252}Cf source is located. Since the average distance that thermal neutrons can travel in a uranium-water lattice without being absorbed is only 3 cm approximately [130], the moderation of the ^{252}Cf drastically reduces the likelihood that any of them will survive the journey across the fuel assembly to the detectors on the other side. (In contrast, the corresponding, average distance that fast neutrons (with a fission energy spectrum) can travel in a uranium-water lattice is approximately 15 cm, which is more than two thirds of the width of a PWR fuel assembly.) The second goal can be achieved by making the ^{252}Cf source to be so strong that the production of secondary neutrons by induced fission in the fuel assembly overwhelms the production of primary neutrons by spontaneous fission.

4.1.3.2 The NGSI's design

Figure 15 is a schematic of the NGSI's design of a CIPN instrument [19, 163]. The Cf source is on the right (in each picture) of the fuel assembly, and the fission chambers, which are the neutron detectors, are on the left and front and back sides. In accordance with the first goal mentioned in the previous paragraph, the ^{252}Cf source is embedded in polyethylene to moderate its neutrons. The one-millimeter-thick Cd sheet between the ^{252}Cf source and the spent fuel assembly is intended to smooth out the flux of ^{252}Cf neutrons along the vertical axis of the fuel assembly. The fission chambers are arranged with their long axes to be perpendicular to the vertical axis of the fuel assembly, so that they will more equally detect the neutrons coming from the sides and corners of the assembly as they will detect the neutrons coming from the middle. The fission chambers are embedded in polyethylene to thermalize the neutrons and thereby increase their probability to be detected. There is no Cd sheet between the fuel assembly and the fission chambers, which allows the fission chambers to detect neutrons from the entire neutron-energy spectrum.

The ^{252}Cf source must be moved away from the spent fuel assembly during the passive, TN measurement. Therefore, the NGSI has investigated locating the ^{252}Cf inside a removable "door"; that is, they have designed as detachable the right-hand portion of the CIPN instrument illustrated in Figure 15(a) [163].

To meet the second design goal mentioned in the previous subsection, the NGSI calculated that an initial source of 200 μg of ^{252}Cf would still have sufficient strength at the end of a five-year lifetime, namely, 50 μg, to override the self-generated flux of a spent PWR fuel assembly that had been burned to 45 GWd/tU [19]. This 50 μg would be about 2.5 times stronger than the self-generated flux. The cost and availability of a 200 μg ^{252}Cf source were deemed to be reasonable.

In addition to the two goals mentioned in the previous subsection, the NGSI also designed the CIPN instrument such that all of the fuel pins in the assembly would contribute roughly equal numbers of neutrons to the count rate, after accounting for the multiplication of the

neutrons from each pin by induced fission in the other pins [19]. By this design, the diversion of fuel pins from various regions of the fuel assembly would reduce the count rate by roughly equal amounts (Figure 16).

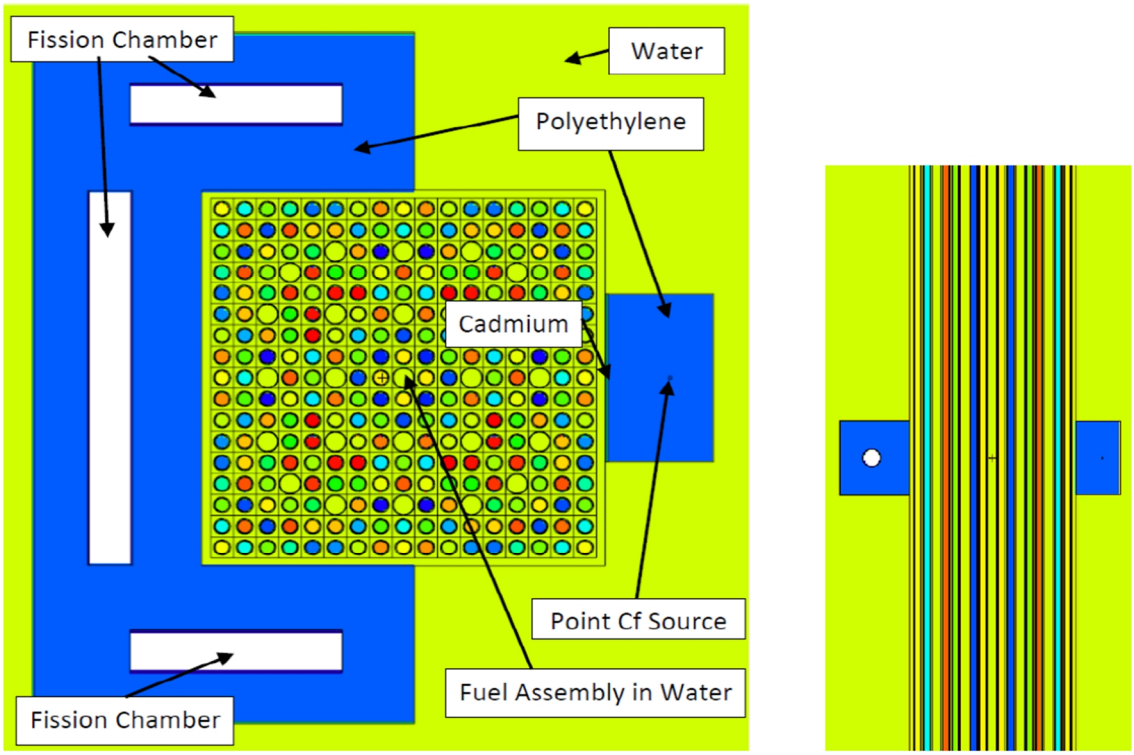

Figure 15: A schematic of the NGSI's CIPN instrument: (a) cross section, as viewed from the top; (b) side view (different scale). Copied from Hu et al. [163] with permission of authors.

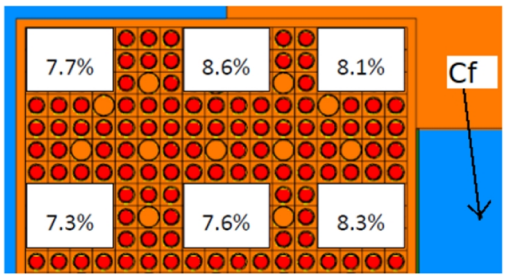

Figure 16: Percentage reduction in the CIPN count rate caused by the replacement of 11 or 12 fuel pins with dummy, depleted-uranium pins in various regions of a fresh PWR fuel assembly (2% initial enrichment). Copied from Hu et al. [163] with permission of authors.

4.1.3.3 Data analysis

The NGSI's main metric for CIPN is the normalized net count rate, which is the normalized difference between the active count rate (C_{REFEX}) and the passive count rate (C_{REF}). The difference is normalized by dividing it by the strength of the ^{252}Cf source (N_{EXT}). This metric is expressed in symbols (this report's symbols, not the NGSI's) as follows:

$$\text{CIPN Normalized Net Count Rate} = \frac{C_{REFEX} - C_{REF}}{N_{EXT}} \qquad \text{Equation 9}$$

The NGSI has tried to correlate this metric directly with the effective fissile content of the spent fuel assemblies, as illustrated in Figure 17. The difficulty is that the count rate is not a bijective (one-to-one) function of the fissile content; rather, it depends also on the BU, IE, and CT of the spent fuel assembly. In other words, one value of the count rate can correspond to a fairly wide range of possible fissile content. This type of uncertainty in the fissile content has been examined by Burr et al. [135], who found that for CIPN, the relative error standard deviation is at least 13%.

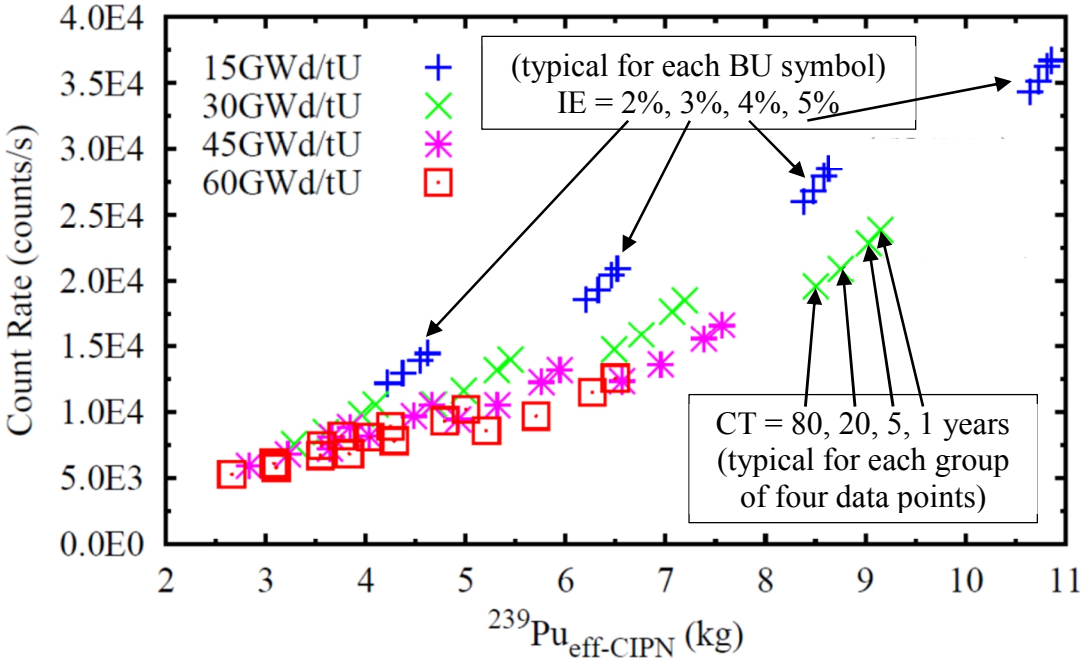

Figure 17: The CIPN normalized net count rates for all 64 spent fuel assemblies from the NGSI Library No. 1, as a function of the effective fissile content. The count rate has been normalized with the count rate from a 100-μg ^{252}Cf source, which releases $2.34 \cdot 10^8$ neutrons/s. Modified from Figure 9 of Hu et al. [163].

To improve the correlation, the NGSI proceeded to include additional information about the BU and CT, which would come either from the reactor operator's declaration or from some other NDA measurements. The NGSI concluded that the physical cause of the scatter in the data of Figure 17 was a failure to account for the quantities of neutron-absorbing isotopes (neutron poisons) in the spent fuel assemblies. These absorbers are either fission products or transuranic isotopes; in both cases, their creation is a function of BU. Two absorbers also depend on CT: ^{155}Gd (which is the decay product of ^{155}Eu) and ^{241}Am (which is the decay product of ^{241}Pu). Therefore, the NGSI defined a so-called "corrected" effective fissile content that includes not only the fissile isotopes but also these neutron absorbers. (To avoid confusion between this "corrected" effective fissile content and the actual effective fissile content, which could be considered to be the correct fissile content, this report will used the term "modified effective fissile content" instead of "corrected effective fissile content.") The NGSI found that the correlation between this modified effective fissile content and the normalized net count rate is almost a bijection (Figure 18). Therefore, the measured count rate from an unknown spent fuel assembly would reveal the assembly's modified effective fissile content, and the actual effective fissile content could then be found by using the knowledge of

the assembly's BU and CT to calculate the amounts of neutron absorbers and remove them from the modified effective fissile content.

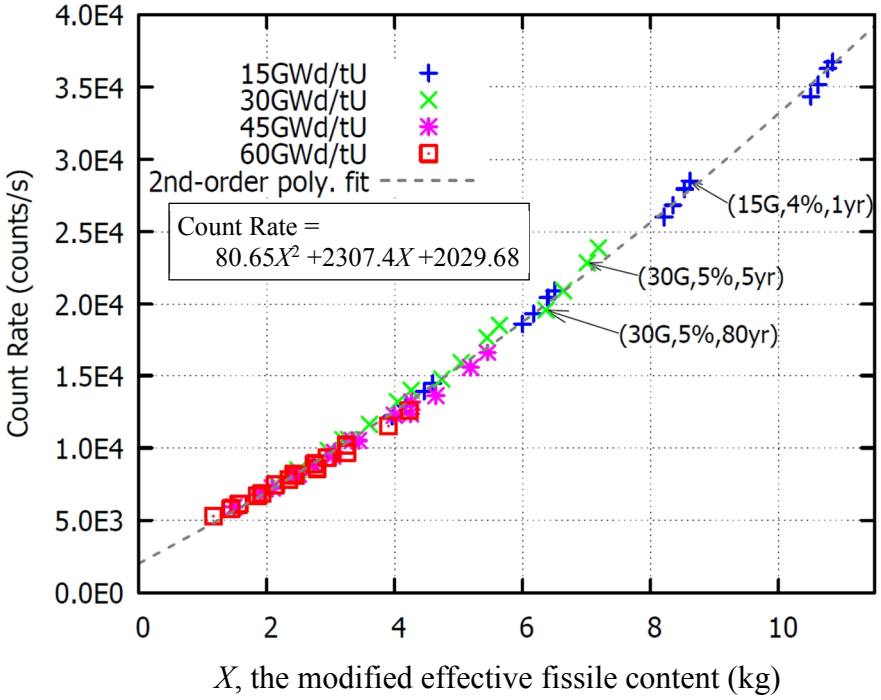

Figure 18: The correlation between the normalized net count rate and the modified effective fissile content, *X*. Modified from Figure 10 in Hu et al. [163].

The NGSI defined the modified effective fissile content, *X*, as follows:

$$X = \left[{}^{239}\mathrm{Pu}_{\text{eff-CIPN}} - \left(\frac{48.97\ \text{kg fissile}}{\text{kg of } {}^{155}\mathrm{Gd}}\right){}^{155}\mathrm{Gd} - \left(\frac{0.66\ \text{kg fissile}}{\text{kg of } {}^{241}\mathrm{Am}}\right){}^{241}\mathrm{Am}\right] \cdot \left(\frac{\mathrm{BU}}{15\ \text{GWd/tU}}\right)^{-0.302} \qquad \text{Equation 10}$$

Here, the isotopic symbols for ^{155}Gd and ^{241}Am stand for the masses of these isotopes. These quantities of ^{155}Gd and ^{241}Am as functions of BU and CT were determined empirically from the NGSI's spent-fuel-assembly Monte Carlo library. (See Hu et al. [19] for details.) The coefficients on the masses of ^{155}Gd and ^{241}Am in Equation 10 represent the apparent loss of fissile material caused by the absorption of neutrons in these isotopes. The coefficient (BU / 15 GWd/tU)$^{-0.302}$ is supposed to represent the loss of fissile material by the other neutron absorbers besides ^{155}Gd and ^{241}Am.

This form of equation for *X* may have one small issue, though; namely, the coefficient (BU / 15 GWd/tU)$^{-0.302}$ multiplies the ^{155}Gd and ^{241}Am terms, which have already accounted for the BU dependence of those two isotopes. A better formalism might be to treat the other absorbers in the same way as the ^{155}Gd and ^{241}Am have been treated:

$$\text{"}X\text{"} = {}^{239}\mathrm{Pu}_{\text{eff-CIPN}} - \left(\frac{48.97\ \text{kg fissile}}{\text{kg of } {}^{155}\mathrm{Gd}}\right){}^{155}\mathrm{Gd} - \left(\frac{0.66\ \text{kg fissile}}{\text{kg of } {}^{241}\mathrm{Am}}\right){}^{241}\mathrm{Am} - \left(\frac{B\ \text{kg fissile}}{\text{kg of } A}\right)A \qquad \text{Equation 11}$$

Here, *A* would stand for the mass of the other neutron absorbers, and *B* would stand for the apparent loss of fissile material cause by the absorption of neutrons in these other isotopes.

Unlike the masses of ^{155}Gd and ^{241}Am, which are functions of both BU and CT, *A* would be a function of BU only. It is not clear yet if this other form would be significantly better.

The effect of including the neutron absorbers into the effective fissile content can be seen in Figure 19, which is an overlay of Figure 18 onto Figure 17. The data points have shifted to the left, because the neutron absorbers act like negative fissile material. Notice that the data points for the lowest burnup (15 GWd/tU, marked by blue crosses) have hardly moved, which is consistent with the fact that such slightly burned fuel contains only a little amount of neutron absorbers.

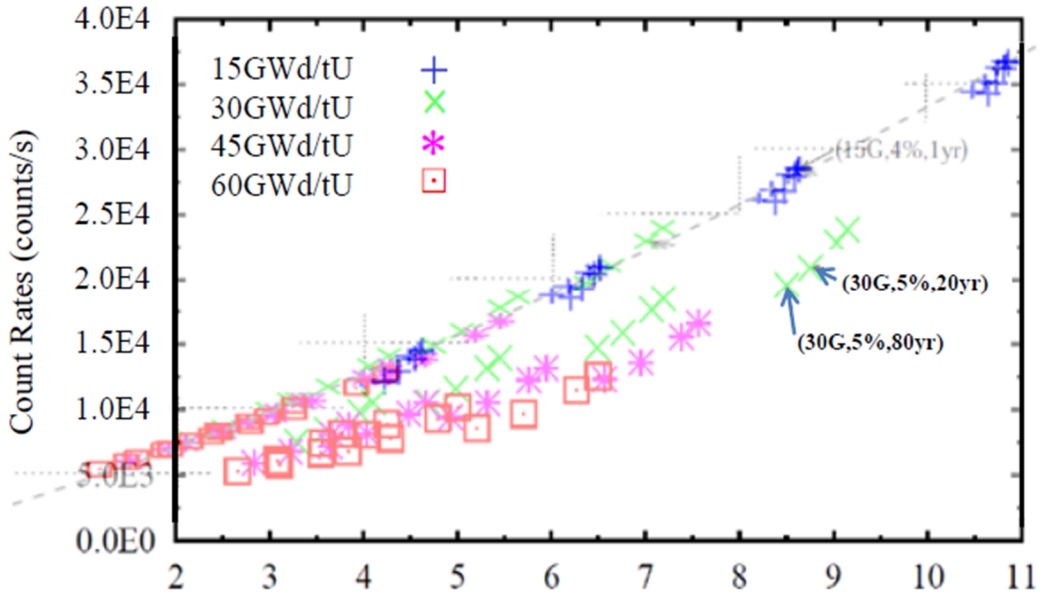

Figure 19: Figure 18 has been stretched to match the scale of Figure 17 and then has been laid over it.

The recent publication by one of the authors, which was mentioned previously in the discussion of the PNAR technique (Section 4.1.2.3), provides an analysis of the CIPN technique, as well [160]. The passive count rate in CIPN is the same as the no-reflection count rate in PNAR and as the TN count rate. The expression for it is repeated here:

$$C_{REF} = \varepsilon \frac{M_L N_{PRI}}{1 - M_{L,refl}\,\bar{\nu}p_{f,emit}} \qquad \text{Equation 7}$$

The active count rate in CIPN (C_{REFEX}, i.e., the count rate with reflection and with an external source) can be expressed as follows:

$$C_{REFEX} = \varepsilon \frac{M_L N_{PRI} + M_{L,ext} N_{EXT}}{1 - M_{L,refl}\,\bar{\nu}p_{f,emit}} \qquad \text{Equation 12}$$

Here, $M_{L,ext}$ is the leakage multiplication of the neutrons from the external, ^{252}Cf source; the other quantities are as defined above. The detection efficiency, ε, in this case accounts for the asymmetry in the emission of neutrons from the spent fuel assembly. C_{REFEX} is therefore an average count rate of the neutrons emitted from the fuel assembly around the circumference of the assembly.

With these two equations, the normalized net count rate of CIPN (Equation 9) can be expressed as follows:

$$\frac{C_{REFEX} - C_{REF}}{N_{EXT}} = \varepsilon \left(\frac{M_{L,ext}}{1 - M_{L,refl}\,\bar{\nu}p_{f,emit}} \right) \qquad \text{Equation 13}$$

"The quantity in parentheses is the multiplication of external-source neutrons when reflection is present, which is typical for the active neutron measurement. [Equation 13] thus verifies that the CIPN metric correlates with neutron multiplication [19]. Furthermore, the absence of any quantities related to N_{PRI} on the right-hand side and the subtraction in the numerator of the left-hand side together explain in part why a strong ^{252}Cf source reduces the statistical uncertainty of the CIPN metric [19]." (Reprinted from [160] with permission from Elsevier.)

Like the PNAR technique, the CIPN technique should produce two independent quantities, not just the one metric of the normalized net count rate. These two quantities could be chosen to be the TN count rate (C_{NOREF}) and the normalized net count rate, but the interpretation of these quantities is complicated in terms of the isotopic content of the spent fuel assembly or of its physical properties, as the right-hand sides of Equations 7 and 13 show. A better approach is to determine the number of primary neutrons (N_{PRI}) and their leakage multiplication when albedo is present (ARR·M_L), since these quantities are inherent to the spent fuel assembly and are therefore independent of the NDA technique used to find them.

These two alternative CIPN metrics can be found by solving Equations 7 and 12 simultaneously. "These two equations contain three unknowns: the two new metrics and $M_{L,ext}/\left(1 - M_{L,refl}\bar{\nu}p_{f,emit}\right)$. Since there are more unknowns than equations, it is impossible to solve for the two new metrics without some additional information. This additional information is the recognition that the multiplication of primary neutrons and the multiplication of external-source neutrons are basically the same physical process. It is well known that M_L and $M_{L,ext}$ are significantly different from each other for all spent fuel assemblies in practically all measurement scenarios [23, 167-169]. However, this difference is caused mainly by the differences in the spatial distributions of the external-source and primary neutrons, and these spatial distributions are dominated, in turn, by the geometry of the external source and the fuel assembly. Since this geometry does not change with the burning, enrichment, and cooling of the fuel (i.e., with the BIC variables), it can be expected that changes in the BIC set of variables should change both multiplications approximately by the same proportion. Therefore, a *ratio* of the two multiplications should stay almost constant, regardless of the burning, enrichment, and cooling of the fuel (i.e., over the whole domain of the BIC set). Figure 5 in Schulze et al. [165] and Figure 3 in Würz et al. [166] support this hypothesis (though these authors do not state the sources of their figures). If true, the constancy of this ratio would allow it to be estimated *a priori* to the NDA measurements, such as by conducting Monte Carlo simulations of similar measurements. The knowledge of this ratio would thus constitute the additional information that would allow the system of simultaneous equations to be solved.

"The key to the solution algorithm, therefore, is to rearrange Equations 7 and 12 to form a ratio of the two neutron multiplications:

$$\frac{C_{REFEX} - C_{REF}}{C_{REF}} = \left[\frac{\left(\frac{M_{L,ext}}{1 - M_{L,\mathrm{refl}}\,\bar{\nu}p_{f,emit}}\right)}{\left(\frac{M_L}{1 - M_{L,\mathrm{refl}}\,\bar{\nu}p_{f,emit}}\right)}\right]\left(\frac{N_{EXT}}{N_{PRI}}\right) \qquad \text{Equation 14}$$

(Of course, the ratio in the brackets can be simplified by cancelling the denominators in the parentheses, but since both CIPN measurements contain reflection (albedo), it is better to include the ARR with each leakage multiplication.) With the ratio in the brackets being estimated *a priori*, this equation can be solved for the only remaining unknown, N_{PRI}. This value of N_{PRI} can then be put into Equation 7 to find $M_L/\left(1 - M_{L,refl}\bar{\nu}p_{f,emit}\right)$." (Reprinted from [160] with permission from Elsevier.) The two alternative metrics are thereby determined.

As with PNAR, the two alternative metrics can be used in a two-parameter correlation to the effective fissile content. Since such a two-parameter correlation would contain more independent information, it would have less scatter than is exhibited in the one-parameter correlation (Figure 17). Of course, the modification of the effective fissile content to obtain the one-parameter bijective correlation in Figure 18 could not be applied directly to the two-parameter correlation; it would have to be adapted for the two-parameter correlation. Nevertheless, the modification in Figure 18 relies on additional information about BU and CT from the reactor operator (or some other NDA techniques that are as yet unnamed), and furthermore, it is almost completely empirical. Therefore, a two-parameter correlation from the two alternative CIPN metrics would still be an improvement over the NGSI's current practice. As mentioned before for the PNAR technique, a three-parameter correlation is actually necessary, as Section 6 will show.

Both PNAR and CIPN analyze the passive neutron flux and the multiplication of neutrons. It is instructive therefore to use Equations 8 and 13 to elucidate the main difference between them. The ARR from PNAR (Equation 8) can be rearranged as follows:

$$1 - \frac{1}{\mathrm{ARR}} = \frac{C_{REF} - C_{NOREF}}{C_{REF}} = \left(M_{L,refl}\right)\bar{\nu}p_{f,emit} \qquad \text{Equation 15}$$

The normalized net count rate from CIPN (Equation 13) can be similarly rearranged:

$$\frac{C_{REFEX} - C_{REF}}{\varepsilon} = \left(\frac{M_{L,ext}}{1 - M_{L,refl}\,\bar{\nu}p_{f,emit}}\right)N_{EXT} \qquad \text{Equation 16}$$

On the right-hand sides of these two equations, the quantities outside the parentheses are the so-called interrogating neutrons: $\bar{\nu}p_{f,emit}$ is the number of interrogating neutrons from the albedo, per emitted neutron, and N_{EXT} is the number of interrogating neutrons from the external, ^{252}Cf source. The quantities in parentheses are the respective leakage multiplications of these interrogating neutrons. The difference between PNAR and CIPN is thus revealed: N_{EXT} is a known number of interrogating neutrons, but $\bar{\nu}p_{f,emit}$ is an unknown number of interrogating neutrons, since it depends on the unknown number of emitted neutrons. PNAR thus contains one more unknown variable than does CIPN, so that it is impossible to separate the leakage multiplication from the interrogating neutrons in the PNAR technique as can be

done in the CIPN technique (Equation 14). This ability of the CIPN technique is one of its main advantages.

4.1.3.4 Limitations

The CIPN technique suffers a similar fundamental limitation as does the PNAR technique, in that it cannot distinguish between secondary-neutron production (induced fission) and neutron absorption. The improvement over PNAR is that the knowledge of the strength of the interrogating neutron source in CIPN enables CIPN to isolate the number of primary neutrons in the spent fuel assembly, as explained in the previous subsection. Furthermore, the active source enables CIPN to analyze fresh and slightly burned fuel assemblies as equally well as it can analyze fully burned assemblies.

CIPN has limitations associated with the ^{252}Cf source. This source needs to be shielded from personnel at all times, making it difficult to transport and to handle. It also decays over time, so that it must be replaced at the end of its lifetime (about 5 years).

4.1.4 Assembly Interrogation with Prompt Neutron Detection (AIPN)

Name	Assembly Interrogation with Prompt Neutron detection (AIPN)
References	[20]
Measurement environment	In water (in air or other gas is also possible)
Passive vs. Active	Active
Time dependency	Time-independent (continuous)
Particles detected	Neutrons
Type of detectors	Fission chambers
Particles' detected attribute	Multiplication, of external-source neutrons
Governing physical properties of the fuel assembly	The number of primary neutrons (N_{PRI}) The leakage multiplication of primary neutrons without reflection (M_L) The leakage multiplication of external-source neutrons ($M_{L,ext}$)
Governing isotopes	Primary-neutron sources; fissile isotopes; neutron absorbers
Maturity	Has never been tested
Limitations	Cannot distinguish between neutron multiplication in the target fuel assembly and multiplication in the interrogating fuel assembly Cannot distinguish between secondary-neutron production (induced fission) and neutron absorption
Selected by the NGSI for prototype testing?	No

Assembly Interrogation with Prompt Neutron Detection (AIPN) is an active technique that is almost identical to CIPN except that the ^{252}Cf source is replaced by another used fuel assembly. The advantage is that, while a ^{252}Cf source is difficult to handle and to transport to a spent fuel pool, a spent fuel pool already contains many spent fuel assemblies, each of which is emitting many neutrons. Therefore, AIPN tries to use the self-generated neutron flux of one spent fuel assembly to interrogate a neighboring assembly.

AIPN has a critical flaw, though, which is that the interrogating spent fuel assembly (the one *not* being measured) not only emits neutrons but also multiplies neutrons that come into it. Unlike a ^{252}Cf source that cannot undergo significant induced fission, an interrogating spent fuel assembly contains fissile material and can therefore experience a significant amount of induced fission. Therefore, when the interrogating fuel assembly is put next to the unknown fuel assembly to be measured, the neutrons emitted by the unknown fuel assembly go into the interrogating fuel assembly, induce fission in it, and change the number of neutrons that it emits. Therefore, the source strength of the interrogating spent fuel assembly during the measurement is not constant and is unknown.

Unfortunately, the NGSI did not address this flaw of AIPN in Phase I. The NGSI's AIPN report [20] states that the strength of the interrogating spent fuel assembly during the active

measurement was predetermined by simulating its passive neutron emission in isolation. Therefore, this strength was taken as constant during the simulation of the active measurement of the unknown spent fuel assembly. The results and conclusions of this AIPN report are therefore incomplete and not yet applicable. For this reason and because AIPN is otherwise similar to CIPN, the AIPN technique will not be discussed further in this report. Nevertheless, the NGSI's work is a significant step toward the development of AIPN, and AIPN may be useful if a way can be found to take into account the multiplication in the interrogating spent fuel assembly.

4.1.5 Differential Die-Away analysis (DDA)

Name	Differential Die-Away analysis (DDA)
References	NGSI: [15, 21-175] Other: [134, 176-180]
Measurement environment	In water (in air or other gas is also possible)
Passive vs. Active	Active; minimum source = $1 \cdot 10^9$ neutrons/s [21, 170]
Time dependency	Time-dependent (pulsed)
Particles detected	Neutrons
Type of detectors	^{3}He detectors
Particles' detected attribute	Multiplication, of external-source neutrons
Governing physical properties of the fuel assembly	The die-away time, which is proportional to the leakage multiplication of external-source neutrons with reflection (ARR$\cdot M_{L,ext}$)
Governing isotopes	Fissile isotopes; neutron absorbers
Maturity	Has been used for many years to assay waste that contains tens of grams of plutonium; has not yet been tested on spent fuel assemblies
Limitations	Cannot distinguish between secondary-neutron production (induced fission) and neutron absorption
Selected by the NGSI for prototype testing?	Yes, at the Central Storage of Spent Nuclear Fuel (CLAB), Sweden [15]

4.1.5.1 Principle of operation

Differential Die-Away analysis (DDA) is an active technique that uses pulses of neutrons from a neutron-generator machine to initiate fission chains in the spent fuel assembly. Because the spent fuel assembly is subcritical, the fission chains die away (decline) with time after each pulse (see Figure 20). The rate at which they die away is a function of the neutron multiplication in the fuel assembly and is therefore also a function of the fissile content and the neutron-absorber content. DDA monitors the neutron flux being emitted from the fuel assembly as a function of the time after each pulse and associates changes in the flux's characteristic die-away time with changes in the multiplication and fissile content.

In terms of the neutron diffusion equation (Equation 3), the DDA technique analyzes the multiplication expressed by the difference between the fission and capture terms. This multiplication is expressed through the $\partial\phi/\partial t$ term as a die-away time.

$$S + (\bar{\nu} - 1)\Sigma_{\mathrm{f}}\phi - \Sigma_{\mathrm{a,capture}}\phi - (-D\nabla^2\phi) = \frac{1}{v}\frac{\partial\phi}{\partial t} \qquad \text{Equation 3}$$

There are at least two different purported meanings of the adjective *differential* in the name of DDA. Caldwell et al. claim, on page 3 of their work [176], that *differential* refers to the much faster die-away time of neutrons in the neutron-detector units (the neutron detector plus the surrounding polyethylene moderator) versus the die-away time of neutrons in the sample being assayed (0.015 ms vs. 0.5 ms, respectively, for their particular application). The neutron-detector units thus have sufficient time resolution to monitor the decline of the

neutron flux in the sample. Henzl et al. claim [22, 175] that *differential* refers to the difference between the shorter die-away time in a sample (spent fuel assembly) that has no fissile material and the longer die-away time in one that does. Regardless of the originally intended meaning of *differential*, both facts are true.

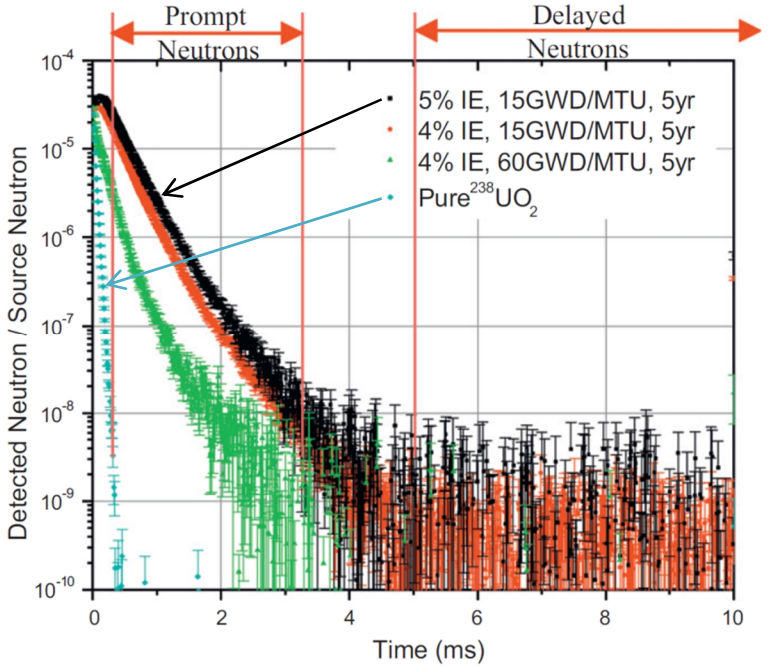

Figure 20: A simulated example of the DDA signal (counts as a function of the time after the neutron pulse), including error bars on the data points; modified from Lee et al. [170, 171] with permission from INMM and Elsevier. The neutron detectors that were used to create this figure were covered in Cd and so detected only fast neutrons.

A modification to DDA is to design the DDA instrument to be sensitive only to neutrons produced by fission in the spent fuel assembly and not to the interrogating neutrons from the neutron generator [175]. This distinction can be made in two steps: (1) by detecting only fast neutrons and (2) by waiting to begin counting after each pulse until almost all of the interrogating neutrons have been moderated to less than 1 eV in the spent fuel assembly. The fast neutrons that are detected after this time can then be attributed to fission only. Henzl et al. [175] found that the waiting time is on the order of 10 μs. They also found, though, that this second step of waiting may not be necessary in practice, since the number of fast interrogating neutrons that are detected at early times before they are moderated is practically constant with the burning, enrichment, and cooling of the spent fuel assembly [22, 175]. (This finding accords with the assertion made in Section 6.2.3 that neutron scattering—which is the same as neutron moderation—is not a function of the BIC set.)

Figure 20 provides an example of making this distinction between interrogating and fission neutrons. The neutron detectors that were used to create this figure were wrapped in cadmium, so as to prevent them from detecting thermal neutrons, since the cutoff-energy for Cd is about 1 eV. The die-away curve that corresponds to pure $^{238}UO_2$—which cannot undergo significant thermal fission—appears to decline by an order of magnitude within tens of microseconds after the pulse. This die-away time corresponds well with the waiting period of approximately 10 μs that has been suggested by Henzl et al. [175]. It also corresponds with the average

slowing-down time of neutrons from 1 MeV to 1 eV by moderation in water, which is about 2 μs, since the water between the fuel pins of the spent fuel assembly dominates the moderation of the neutrons. (See Fig. 9 in Chabod [181], scaled for density.) The lengthening of the die-away times of the other fuel assemblies in Figure 20 can thus be attributed to induced fission in their fissile isotopes.

4.1.5.2 The NGSI's design

Figure 21 illustrates the DDA instrument that the NGSI has examined by computer modeling; the design is from 2012. The NGSI has proposed to use the same instrument to perform both a DDA measurement and a DN measurement. The deuterium-tritium (D-T) neutron generator at the left emits pulses of high-energy neutrons (14 MeV, $1 \cdot 10^9$ neutrons/s [21]). (See Reference [182] for a survey of deuterium-deuterium (D-D) and D-T neutron-generator technology.) These neutrons are slowed down below 1 MeV by inelastic scattering in the block of tungsten that surrounds the neutron generator. This slowing down is called "spectrum tailoring" and inhibits the inducing of fission in ^{238}U, since the threshold energy for inducing fission in ^{238}U is 1 MeV. The minimization of induced fission in ^{238}U is necessary primarily for the DN measurement (see Section 4.1.6.1), since the fast fission of ^{238}U by the D-T generator's interrogating neutrons should occur fast enough (within the first 10 μs after the pulse) that the DDA measurement would not misinterpret it as fission in fissile material. The stainless steel around the back of the tungsten block reflects neutrons back toward the fuel assembly. The lead around the other three sides of the fuel assembly shields the ^{3}He neutron detectors from the intense gamma-rays that are generated by the radioactive decay of the spent fuel assembly; this shielding inhibits the accidental detection of the gamma-rays by the ^{3}He detectors. The ^{3}He neutron detectors are embedded in polyethylene blocks that slow down the neutrons so that the detectors can detect them more readily. The polyethylene blocks surrounding the neutron detectors that are used for the DDA measurement are covered with sheets of cadmium, which filter out almost all of the thermal neutrons that would otherwise go to the detectors. (No cadmium is placed on the detectors that are used for the DN measurement.) ^{3}He neutron detectors were chosen for the NGSI design for various reasons, including their higher detection efficiency, but fission-chamber neutron detectors could also be used instead.

The proposed DDA/DN instrument is not portable, in general. The lead, tungsten, and stainless steel are too heavy (over 100 kg), not to mention the weight, volume, complexity, and electrical-power requirements of the neutron generator and ^{3}He detectors and associated equipment. Therefore, this instrument would have to be installed in the same facility (e.g., spent fuel pool) as the spent fuel assemblies to be measured.

The NGSI has assumed that the DDA measurement and the DN measurement would be made separately, using different duty cycles of pulses and counting periods. For the DDA/DN instrument shown in Figure 21, the DDA duty cycle would be a 10 μs long neutron pulse from the D-T neutron generator, followed by a 10 μs waiting period, followed by about 1000 μs of counting [21]. This cycle would be repeated until the desired counting statistics would be achieved.

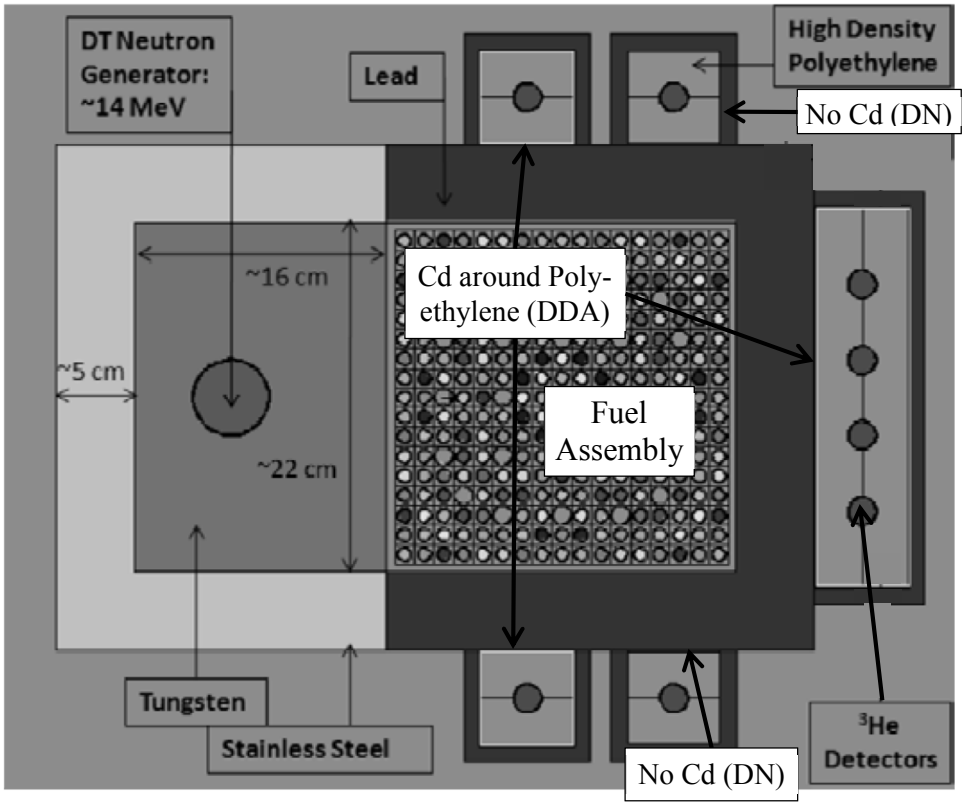

Figure 21: Computer model of a proposed NGSI DDA/DN system, modified from Blanc et al. [21] with permission from INMM.

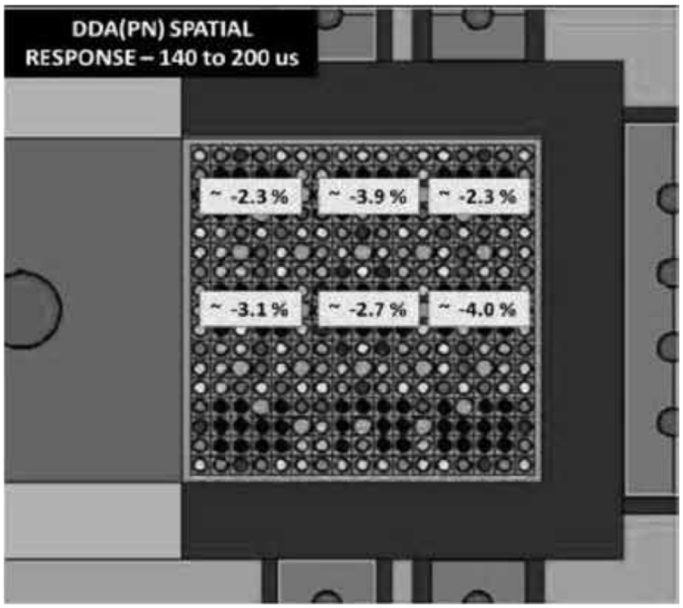

Figure 22: Percentage reduction in the DDA count rate between 140 μs and 200 μs (after the pulse) caused by the replacement of 11 or 12 fuel pins with dummy, depleted-uranium pins in various regions of a spent PWR fuel assembly (4% initial enrichment, burned to 45 GWd/tU, and cooled for 5 years). Copied from Blanc et al. [21] with permission from INMM.

The dominating factor that determines this DDA duty cycle is the relatively short duration of the dying away process—only 1 ms. The pulse length (10 μs) and repetition (980 Hz) are

achievable by the neutron generator and neutron detectors. Therefore, the duty cycle is repeated as soon as there are no more neutrons to be counted (i.e., when they have died away). It is presumably because of this fact that the NGSI has chosen to perform DDA with a D-T neutron generator rather than by shuffling a ^{252}Cf source (see Section 4.1.6.2), since the minimum time to move a ^{252}Cf source into or away from the irradiating position (about 1.5 m) is practically about 750 ms [183].

As with the NGSI's analysis of CIPN (Section 4.1.3.2), the NGSI determined that a DDA measurement would be sensitive to the diversion of fuel pins (i.e., to partial defects). The percentage changes in the DDA signal caused by the substitution of fuel pins with depleted-uranium fuel pins in various regions of the spent fuel assembly are indicated in Figure 22.

4.1.5.3 Data analysis

The data from a DDA measurement can be expressed in several ways. Perhaps the most intuitive way is to plot the number of counts (detected neutrons) as a function of the time after each neutron pulse, as Figure 20 illustrates. This figure has normalized the number of counts by the strength of the neutron pulses from the D-T generator. Note that this figure is actually a histogram, in which the time axis has been discretized into many time bins of finite time width. The time resolution of Figure 20 has not been specified but it appears to be about 10 μs. The error bar on each datum point represents the error in the number of counts in that time bin. This figure shows that the number of neutrons being detected from the spent fuel assembly decreases with time. The die-away process is shown to be roughly exponential, since the curves up to 2 ms are roughly straight lines on this log-linear plot. Furthermore, the die-away time increases as the amount of fissile material increases from zero in pure $^{238}UO_2$ to the amount in lightly burned fuel (5% IE, 15 GWd/tU). The flat, small number of neutrons after about 4 ms in Figure 20 has been attributed only to delayed neutrons. The raw data of a real measurement would also include the passive neutron flux that is self-generated inside the spent fuel assembly, but presumably this constant, passive flux has been subtracted from the data in Figure 20.

Rather than plot the data for every DDA measurement, it is more convenient to represent the DDA signal by a single number. There are at least two such representations: the die-away time constant (τ) and the normalized number of counts within a certain time window. The NGSI has used both. The die-away time can be found by fitting the data in the histogram with an exponential curve, since τ is inversely proportional to the slope of the straight line on a log-linear plot: $\log_{10}(\text{Counts}) = (-1/\tau)\cdot\log_{10}(e)\cdot t + \log_{10}(\text{Pulse Strength})$. The normalized number of counts in a time window is simply the summation of the histogram within the time window, which is similar to "integrating under the curve" if the histogram would be a continuous function. In the extreme case, the entire histogram can be summed, which would be the total normalized number of counts following pulses; this quantity will be called the "total normalized counts" in the following discussion. The original practitioners of DDA (not on spent fuel assemblies but on contaminated waste) appear to have used the total normalized counts as their representative DDA metric [176].

With either representation, it is useful to reject the data points at the earliest times because they represent the detection of neutrons from the D-T generator, as mentioned earlier in

Section 4.1.5.1. This fact can be seen by a de-convolution of the die-away curve into its two components, neutrons from the generator and neutrons from induced fission, as illustrated in Figure 23. However, this figure was created from Monte Carlo simulations by tracking the origins of the neutrons, which is impossible to do in real life, of course. Therefore, such a clean separation of components may be impossible to make from real data. Nevertheless, the figure illustrates the physics of the DDA measurement.

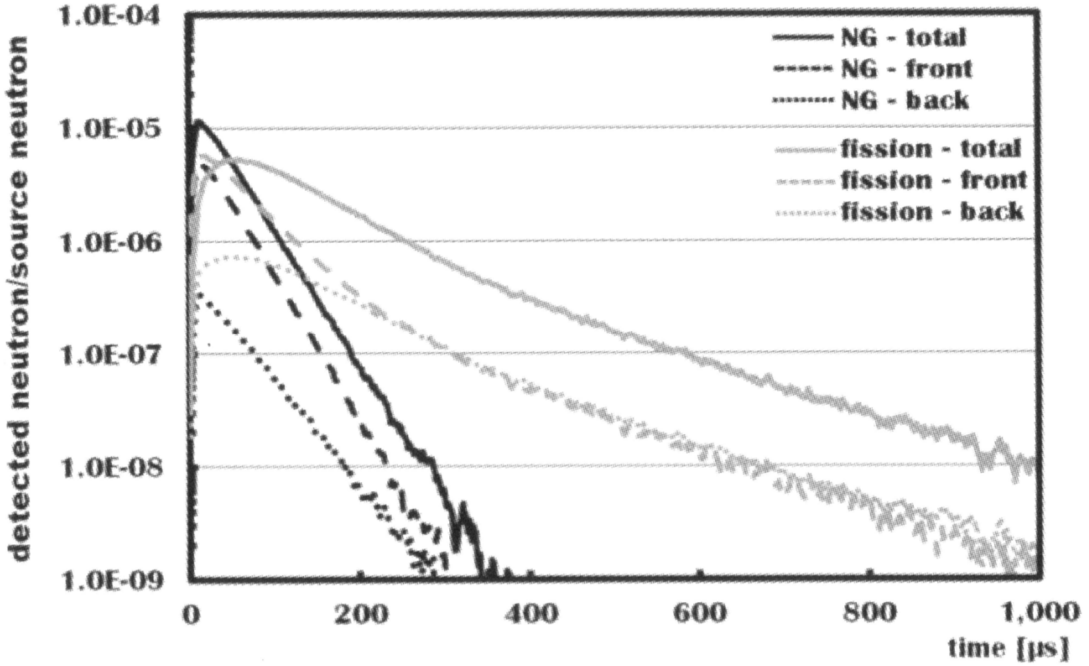

Figure 23: Separation of the DDA signal into two components: neutrons from the D-T generator and neutrons from fission; “front” and “back” refer to the detectors closest to the generator and those farthest from the generator, respectively (Figure 21). Copied from Henzl et al. [22] with permission from INMM.

The fact that the measured, total die-away curve (e.g., Figure 20) is a summation of components with different die-away times requires that DDA practitioners must be careful about relating die-away times to neutron counts within time windows. With the neutron counts being normalized, such a relationship is effectively a function of the shape of the die-away curve, so that curves with longer die-away times are “flatter” and thus contain more “area” underneath them (i.e., counts) than curves with shorter die-away times. Such a relationship is able to be interpreted if the curve has a single die-away time within the time window. For example, the die-away time due to the neutron-generator’s neutrons in Figure 23 is negligible after 200 μs. If the curve is a summation of multiple curves with multiple die-away times from multiple processes, though, then the interpretation of the relationship between the apparent die-away time in the window and the number of neutron counts in the widow becomes complicated.

Henzl et al. [22] have investigated the die-away times and normalized counts within various time windows. The paper did not specify how the die-away times were obtained for each window, but it can be presumed that they came from a form of least-squares regression of the histogram data within each window; the quality of each fit was also not reported. They found that the die-away time constant as calculated from the later-time data (between 500 μs

and 1000 μs after the pulse) and the normalized counts summed over the entire 1000 μs after the pulse (i.e., the total normalized counts) are both linear functions of the multiplication of the interrogating neutrons (see Figure 24). These relationships are not surprising, given the single die-away constant that is exhibited at later times as shown by Figure 23. Since these two relationships are not independent of each other, either one can be used to determine the multiplication of external neutrons by the fuel assembly. This determination is the main result or output of a DDA measurement.

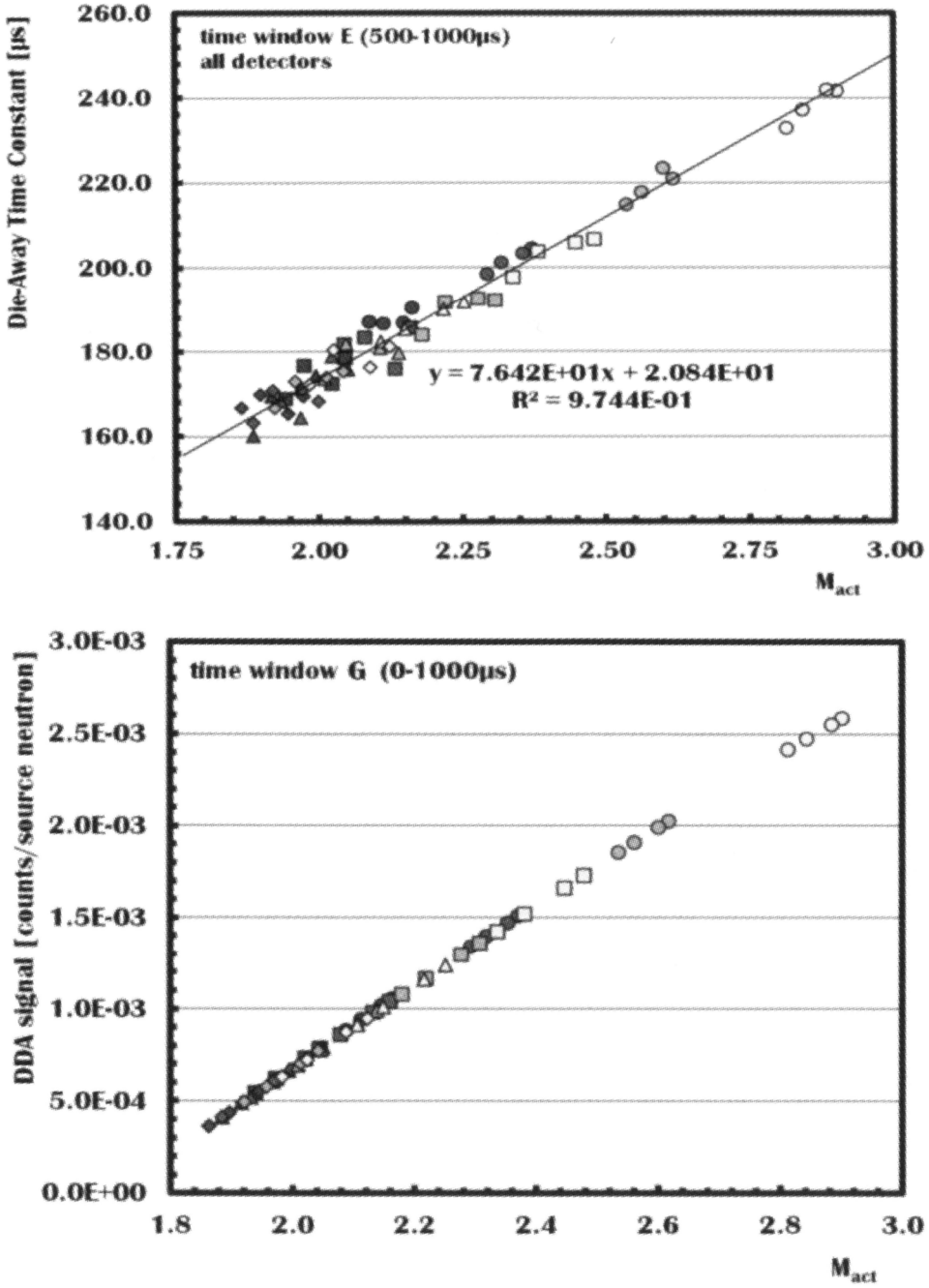

Figure 24: The linear relationships between neutron multiplication (M_{act}) and the die-away time constant at later times (top figure) and between M_{act} and the total normalized neutron counts after the pulse (bottom figure). The 64 data points represent the 64 fuel assemblies from the first spent-fuel library (Section 2.3). Copied from Henzl et al. [22] with permission from INMM.

Even though the relationship between neutron multiplication and the total normalized counts may be bijective (Figure 24, bottom), the relationship between the neutron multiplication and the effective fissile content is not, as shown by Figure 25. (The DDA "count rate" in this figure is presumably either the total normalized counts divided by the counting period, or the normalized counts within some specific, later time window.) This multivariate problem is basically the same problem that the PNAR and CIPN techniques have (Figures 14 and 17). Therefore, to properly interpret the DDA signal, it is necessary to obtain some other information about the BIC variables, such as from the reactor operator or another NDA technique. For this reason, the NGSI is proposing to integrate the DDA and DN techniques; the integration will be discussed in the section on the DN technique (Section 4.1.6).

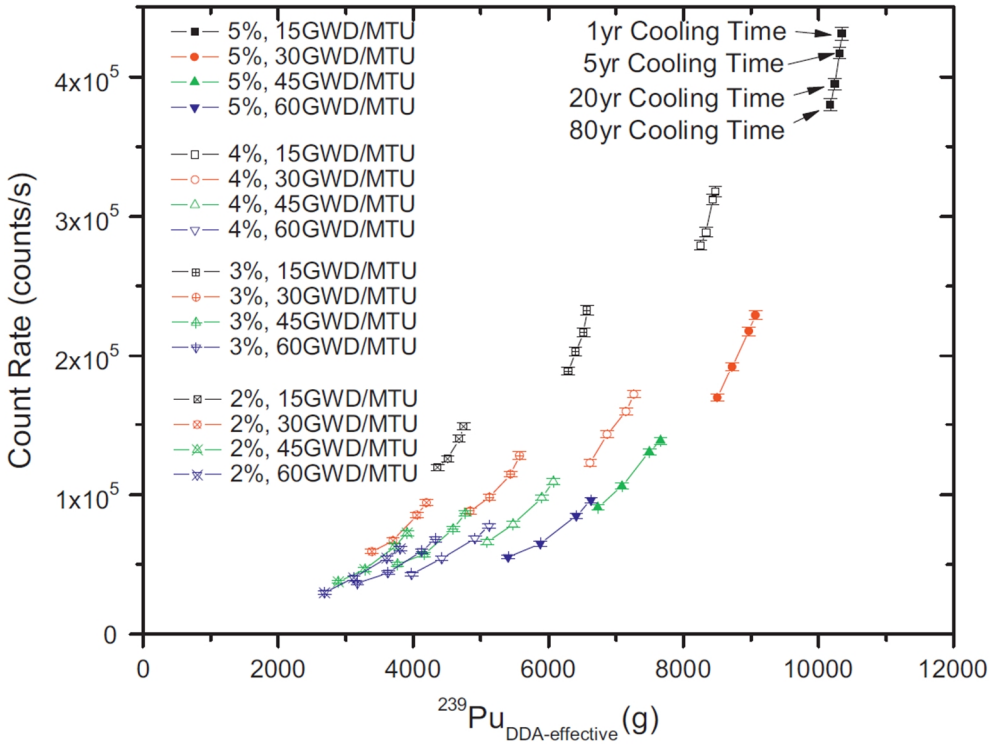

Figure 25: The DDA signal of the 64 spent fuel assemblies from the first spent-fuel library (Section 2.3), plotted against their fissile content. Reprinted from Lee et al. [171] with permission from Elsevier.

Henzl et al. [22] have also claimed that more information can be extracted by measuring the die-away time or normalized counts in other time windows. For example, their simulations indicate that the time constant or normalized counts in the time window from 100 μs to 200 μs, as measured by the detectors farthest from the neutron generator, is independent of IE [22, 175]. At this point, since there is not yet a clear explanation for why such behavior should occur, such indications cannot yet be taken as conclusive; there is a chance that they might be an artifact of the simulation. Further work by this group or by others may clarify the physics and confirm such additional claims.

The total normalized counts can be compared meaningfully with the results of the CIPN technique. By summing all of the counts over the entire counting period after the pulse, all of the time dependency of the data is lost. The only difference, then, between the total

normalized counts of the DDA technique and the count rate as measured by the CIPN technique is that the DDA technique can better exclude the interrogating neutrons from the analysis by excluding the initial pulse from the counting period. If the pulse is included in the counting period as suggested by Henzl et al. [22] (page 63), though, then there is practically no difference between the total normalized counts of DDA and the results of CIPN. Therefore, the observation that the total normalized counts is a clean linear function of the multiplication of external neutrons (Figure 24, bottom) is the same as the observation that the normalized net CIPN count rate is a linear function of that same multiplication (Equations 9 and 13). It is correspondingly not surprising that Figures 25 (DDA) and 17 (CIPN) exhibit a similar dependency on the BIC set.

4.1.5.4 Limitations

The DDA technique suffers the same limitation as the CIPN and PNAR techniques, in that it cannot distinguish between neutron absorption and production, so that its results depend on the BIC set (Figure 25). Furthermore, the NGSI's DDA/DN instrument is heavy and can be expensive because of the cost of the ^{3}He detectors and the D-T neutron generator.

On the other hand, Henzl et al. may have found ways to extract more information from the DDA technique, as mentioned above. Furthermore, the DDA and DN techniques are relatively easy to combine to obtain more independent information and thereby resolve this problem of distinguishing between neutron absorption and production.

4.1.6 Delayed Neutron counting (DN)

Name	Delayed Neutron counting (DN)
References	NGSI: [21, 24, 173, 184] Other: [185]
Measurement environment	In water (in air or other gas is also possible)
Passive vs. Active	Active; minimum source = $5 \cdot 10^{10}$ neutrons/s [21, 173]
Time dependency	Time-dependent (pulsed)
Particles detected	Neutrons
Type of detectors	^{3}He detectors
Particles' detected attribute	Multiplication, of external-source neutrons, but specifically the production of delayed neutrons
Governing physical properties of the fuel assembly	The leakage multiplication of external-source neutrons with reflection (ARR$\cdot M_{L,ext}$), but specifically isolating the amount of induced fission from the amount of neutron absorption
Governing isotopes	Fissile isotopes; neutron absorbers
Maturity	Has been used for many years to assay uranium materials, contaminated waste, and even naval spent fuel assemblies; has not yet been tested on commercial spent fuel assemblies
Limitations	Cannot distinguish between secondary-neutron production (induced fission) and neutron absorption when used alone Requires a strong neutron source to overcome the passive neutron flux from the spent fuel assembly
Selected by the NGSI for prototype testing?	Yes, probably at the Central Storage of Spent Nuclear Fuel (CLAB), Sweden [15]

4.1.6.1 Principle of operation

Delayed Neutron counting (DN) is an active technique that uses pulses of neutrons from a neutron-generator machine to induce fission in the fissile isotopes in the spent fuel assembly. Roughly 99% of the neutrons that are emitted from the fission events are prompt neutrons, meaning that they are emitted instantaneously. The remaining 1% of the neutrons are emitted during the radioactive decay of certain fission products, which can occur significantly over a period of minutes [186]. (See Table 11 and Equation 17.) For example, the fission product ^{87}Br decays with a half-life of 55.65 seconds to ^{87}Kr by β-ray emission, and sometimes (2.6% of the time) this β-decay is also accompanied by the emission of a neutron, thus forming ^{86}Kr [74, 187]. The DN technique involves irradiating the spent fuel assembly for a certain amount of time and then turning off or removing the irradiating neutron source so as to remove all of the prompt neutrons and leave only the delayed neutrons to be detected. Since the delayed neutrons are produced only in fission, the delayed-neutron count rate can be associated more or less directly with the amount of fission induced during the irradiation period and therefore with the amount of fissile material in the spent fuel assembly.

Table 11: Delayed-neutron-precursor half-lives, decay constants (λ), delayed-neutron yields (βν̄), and delayed-neutron-production coefficients (λβν̄) for ^{238}U and the fissile isotopes. (See Equation 17.) The delayed neutron data are from Waldo et al. [188], as quoted by Rinard [185]. The ν̄ values are from Chadwick et al. [125].

	U-235 (thermal fission)				U-238 (fast fission)				Pu-239 (thermal fission)				Pu-241 (thermal fission)			
$\bar{\nu}$	2.44 (n/fission)				2.7 (n/fission)				2.86 (n/fission)				2.95 (n/fission)			
Group	$T_{1/2}$ (s)	λ (1/s)	1000·βν̄ (n/fis)	λβν̄ (n/fis·μs)	$T_{1/2}$ (s)	λ (1/s)	1000·βν̄ (n/fis)	λβν̄ (n/fis·μs)	$T_{1/2}$ (s)	λ (1/s)	1000·βν̄ (n/fis)	λβν̄ (n/fis·μs)	$T_{1/2}$ (s)	λ (1/s)	1000·βν̄ (n/fis)	λβν̄ (n/fis·μs)
1	54.58	0.0127	0.55	7	52.51	0.0132	0.577	8	54.15	0.0128	0.22	3	54.15	0.0128	0.156	2
2	21.87	0.0317	3.66	116	21.59	0.0321	6.08	195	23.03	0.0301	1.92	58	23.18	0.0299	3.57	107
3	6.03	0.115	3.28	377	4.99	0.139	7.19	999	5.59	0.124	1.36	169	5.59	0.124	2.79	346
4	2.23	0.311	6.60	2053	1.94	0.358	17.2	6158	2.13	0.325	2.10	683	1.97	0.352	6.08	2140
5	0.495	1.40	1.92	2688	0.492	1.41	10.0	14100	0.619	1.12	0.55	616	0.431	1.61	2.84	4572
6	0.179	3.87	0.70	2709	0.172	4.02	3.3	13266	0.258	2.69	0.29	780	0.200	3.47	0.25	868
Sums			16.7				44.4				6.45				15.7	
(βν̄) of Isotope / (βν̄) of U-235 =							2.66				0.39				0.94	

$$N_{DN}(t) = \sum_{i=1}^{6} \lambda_i \beta_i \bar{\nu} e^{-\lambda_i t} = \text{delayed-neutrons/s, per fission event} \qquad \text{Equation 17}$$

In terms of the neutron diffusion equation (Equation 3), the DN technique is somewhat similar to the TN technique, in that it makes use of the neutron source term, *S*. But unlike in the TN technique, the *S* term in the DN technique corresponds chiefly to the delayed-neutron precursors that are generated during the irradiation periods, not to the primary-neutron sources. This correspondence can be seen by applying Equation 3 twice, firstly to the flux during the irradiation period (ϕ_{irr}; Equation 18) and secondly to the flux during the delayed-neutron counting period (ϕ_{DN}; Equation 19).

$$S_{PRI} + (\bar{\nu} - 1)\Sigma_{\mathrm{f}}\phi_{irr} - \Sigma_{\mathrm{a,capture}}\phi_{irr} - (-D\nabla^2\phi_{irr}) = \frac{1}{v}\frac{\partial \phi_{irr}}{\partial t} \qquad \text{Equation 18}$$

$$N_{DN}\left[\int_{\mathrm{Irradiation}} \Sigma_f \phi_{irr} dt'\right] + S_{PRI} + (\bar{\nu} - 1)\Sigma_{\mathrm{f}}\phi_{DN} - \Sigma_{\mathrm{a,capture}}\phi_{DN} - (-D\nabla^2\phi_{DN}) = \frac{1}{v}\frac{\partial \phi_{DN}}{\partial t} \qquad \text{Equation 19}$$

The $\partial\phi/\partial t$ term can be taken as corresponding to the generation or decay of the delayed-neutron population, S_{PRI} corresponds to the generation of primary neutrons (i.e., to N_{PRI}), and N_{DN} is from Equation 17. Note that the decay of the delayed-neutron precursors during the irradiation period has been neglected in the integral in Equation 19 for simplicity.

If the primary-neutron flux can be neglected or subtracted as background, then the only source term in Equation 19 is the delayed-neutron source term. Of course, these delayed neutrons are multiplied through the pair of fission and absorption terms in Equation 19. Of

essential importance, however, is the fact that the delayed-neutron source term *is independent of the neutron flux during the DN measurement* (i.e., is independent of ϕ_{DN}). Instead, this source term is proportional to the integration of the fission term during the irradiation period. Moreover, this source term is *not* dependent on the absorption term during the irradiation period. By this fact, the DN technique practically isolates the fission term during the irradiation period, in contrast with the PNAR, CIPN, and DDA techniques that can observe only neutron multiplication—that is, the pair of fission and absorption terms together. Thus, the DN technique produces information that is significantly independent of the information provided by these other techniques. It is for this reason that a combination of DN with any of these other techniques is powerful and desirable. (See also Section 4.1.6.3, below.)

The association of the delayed neutrons with fissile material is predicated upon the absence of a significant amount of fast fission of ^{238}U. Even though the fission cross section of ^{238}U is only about 1 barn above 1 MeV (and it is negligible below this energy), its fast fission can still make a relatively significant contribution to the delayed-neutron population because of two factors. Firstly, the amount of ^{238}U in a spent fuel assembly is almost two orders of magnitude greater than the amount of fissile material, which partially compensates for its small fission cross section. Secondly, the fast fission of ^{238}U produces more than 2.6 times the number of delayed neutrons than the thermal fission of the fissile isotopes produces, on a per-fission basis. (See Table 11.)

Therefore, the fast fission of ^{238}U must be minimized in the DN technique. This minimization consists only of minimizing the fast fission by the irradiating neutrons, by moderating them to below 1 MeV before introducing them to the spent fuel assembly. Nothing can be done to minimize the fast fission of ^{238}U by the fast neutrons that are born by induced fission in the fissile isotopes.

It is essential to recognize that although the DN technique is time-dependent because of the pulsing of the irradiating neutron source, it is like a steady-state, time-independent active technique in other respects. Specifically, the decay curves of the delayed-neutron emitters are *not* measured; only the total flux of the delayed neutrons (including any prompt multiplication of them) is measured. In fact, the cycle of irradiation and delayed-neutron counting is ideally kept as short as possible so as to maintain a consistent, maximum, asymptotic value of the delayed-neutron population during the counting periods. In this way, a DN measurement is somewhat similar to a DDA measurement of the "total normalized counts" and is therefore also similar to a CIPN measurement (see Section 4.1.5.3). The difference is that the external-source neutrons in the DDA and CIPN techniques originate outside the fuel assembly but the delayed neutrons in the DN technique originate inside the fuel assembly.

4.1.6.2 The NGSI's design

The traditional application of delayed-neutron counting is the use of the ^{252}Cf shuffler instrument to assay uranium oxide or scrap or drums of contaminated waste [183, 185, 189, 190]. Spent highly-enriched-uranium naval fuel has also been assayed with a ^{252}Cf shuffler [183]. In this instrument, ^{252}Cf is used as a neutron source, in amounts ranging from a few micrograms to several grams, depending on the application. The ^{252}Cf source is attached to a cable that can move it quickly back and forth between a shielded storage chamber and the

sample chamber that contains the sample item to be assayed. In this way, the assay sample can be irradiated for a certain period of time, following which the ^{252}Cf source can be quickly removed to the storage chamber and the delayed neutrons can be counted. The cycle of irradiation and counting—the "shuffling" of the ^{252}Cf source—can be repeated as many times as necessary to achieve the desired counting statistics.

The neutron energy spectrum inside the sample chamber is kept as fast as possible, by removing as much moderating material (light elements) as possible and by lining the sample chamber with cadmium. Only whatever moderating material is inside the assay sample contributes to moderating the neutron energy spectrum. The reason to keep the spectrum fast is to minimize the neutron cross sections of all of the materials in the assay sample and thereby to maximize the ability of the irradiating, ^{252}Cf neutrons to penetrate through to the center of the assay sample. Such penetration is important because a drum of contaminated waste can be large; a typical 55-gallon drum has a diameter of approximately 57 cm and a height of approximately 85 cm.

The NGSI's design of a DN instrument is different from the ^{252}Cf shuffler for four reasons. The first reason is that the spent fuel assemblies to be assayed with the DN instrument have a different geometry than do the drums that are assayed with the ^{252}Cf shuffler. They are much taller (PWR assemblies are about 4 m tall), but they also have a much smaller "diameter" (PWR assemblies are only about 21 cm wide on a side). The smaller width improves the ability of the irradiating neutrons to penetrate the spent fuel assembly. The second reason is that spent fuel assemblies are immersed in water, so that it is futile to try to keep the neutron spectrum fast. The third reason is that the NGSI wishes to combine the DN instrument with the DDA instrument, and the DDA instrument needs to use a D-T neutron generator instead of a ^{252}Cf source, as explained in Section 4.1.5.2. The fourth reason is that the ^{252}Cf shuffler has never been applied to spent *commercial-reactor* fuel assemblies, which have much greater amounts of ^{244}Cm and therefore much larger passive neutron fluxes than do spent naval fuel assemblies [183]. The greater amount of ^{244}Cm comes from the much greater amount of ^{238}U in fresh commercial fuel assemblies. The spent-naval-fuel ^{252}Cf shuffler could operate with a 3000 μg ^{252}Cf source ($7 \cdot 10^9$ neutrons/s) to produce enough delayed neutrons to overcome the passive neutron flux in that fuel. In contrast, the NGSI's design needs more than $5 \cdot 10^{10}$ neutrons/s to produce enough delayed neutrons to overcome the passive neutron flux in commercial fuel, i.e., to produce a signal-to-background ratio of at least 20% [21, 173]. The cost of a corresponding amount of ^{252}Cf would be prohibitively high [24]. (Note that the CIPN technique (Section 4.1.3) can use a smaller ^{252}Cf source because it detects the more copious prompt neutrons in addition to the delayed neutrons.)

The design of the NGSI's integrated DDA/DN instrument has already been described in Section 4.1.5.2 for the DDA technique. It was mentioned there that the tungsten and stainless steel are included around the D-T neutron generator in order to tailor the neutron energy spectrum to be below 1 MeV. The purpose of this spectrum tailoring is to minimize the induced fission in ^{238}U for the DN measurement, as explained in the previous subsection (Section 4.1.6.1). Apart from this spectrum tailoring, which occurs for both the DDA measurement and the DN measurement, there are two other main aspects of the instrument that are unique to the DN measurement.

The first unique aspect of the DN instrument is that it uses the ^{3}He neutron detectors that are *not* shielded by Cd (see Figure 21). The DDA technique distinguishes the interrogating neutrons from the induced-fission neutrons both by time and by neutron energy, since it waits until the interrogating neutrons have been moderated and then detects only fast neutrons. In contrast, the DN technique waits until the interrogating neutrons have not only been moderated but have also been absorbed or leaked away; in fact, it even waits until all of the fission chains initiated by the interrogating neutrons have also died away. Therefore, since the DN technique uses only time to distinguish the interrogating neutrons from the delayed neutrons, it does not need also to use Cd filters to separate fast neutrons from thermal neutrons. Neutrons with any energy are meaningful to the DN technique.

The second unique aspect of the DN instrument is its duty cycle. The NGSI is planning to perform 900 ms of irradiation with the D-T generator, followed by 100 ms of waiting, followed by 1000 ms of counting the delayed neutrons. The total duration of the duty cycle is thus 2 seconds. The DN measurement, with this duty cycle, would be performed separately from the DDA measurement. The reason to separate the measurements, rather than to perform both a DDA measurement and a DN measurement after each DDA pulse, is that it increases the strength of the delayed-neutron flux that is measured by the DN measurement. The ratio of the DN counting period to the irradiation period could easily be made to be the same in a combined DDA and DN duty cycle (value = 1.11), but the ratio of the waiting period to the irradiation period for the DN measurement of this combined duty cycle would be 11.1, instead of the 0.111 value for the separate DN duty cycle that the NGSI is proposing. This is to say that the time spent on making a DDA measurement in each cycle would be better spent on longer irradiation, as far as the DN measurement is concerned. Therefore, a separation of the DDA and DN duty cycles optimizes the signal strength and measurement time for each type of measurement.

The two-second duty cycle of the NGSI's DN measurement is much shorter than a typical duty cycle of a ^{252}Cf shuffler. The reason is the ability of the D-T generator to cycle at a higher frequency than the maximum frequency with which the ^{252}Cf source can be shuffled (see Section 4.1.5.2). With a shorter duty cycle, the delayed-neutron precursors with the shorter half-lives (Table 11) do not decay away as much during the counting periods, leading to a larger delayed-neutron population and a greater DN signal.

4.1.6.3 Data Analysis

The NGSI's initial method of analyzing DN data is to correlate it with the effective fissile content, with the fissile isotopes being weighted according to their production of delayed neutrons rather than of all neutrons. This correlation for the 64 spent fuel assemblies in the first spent-fuel library (Section 2.3) is shown in Figure 26. It is seen that the correlation depends on the BIC set, just like the correlations of the TN, PNAR, CIPN, and DDA techniques do. The count rate in this figure is the count rate after subtracting off the passive count rate, which is essentially the same as subtracting off a TN measurement.

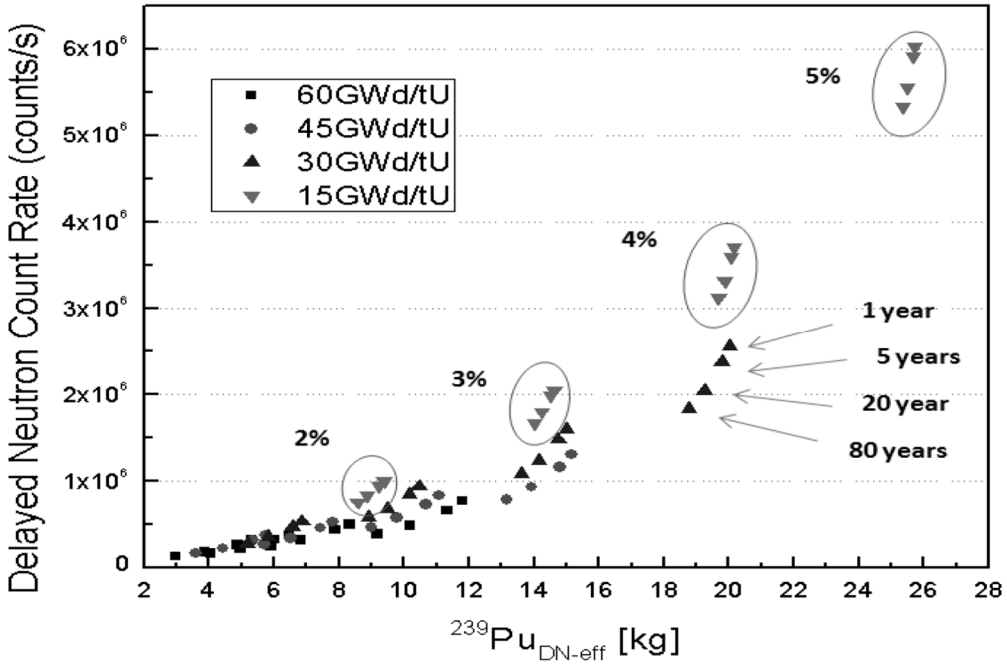

Figure 26: The delayed-neutron count rates from DN measurements of the 64 spent fuel assemblies from the first library (Section 2.3), as a function of their effective fissile content; reprinted from Blanc et al. [21] with permission from INMM.

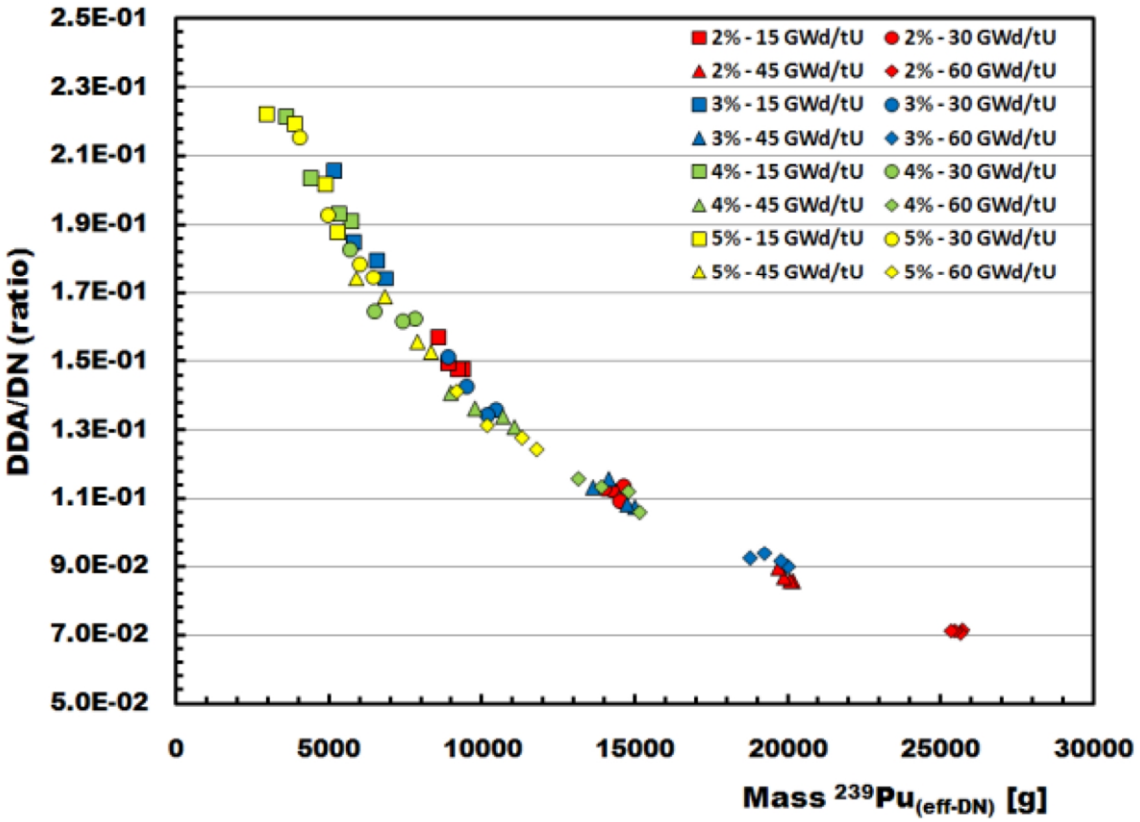

Figure 27: The ratio of the DDA signal to the DN signal for the 64 spent fuel assemblies in the first library (Section 2.3) as determined by the NGSI's integrated DDA and DN instrument; reprinted from Henzl et al. [172] with permission from INMM.

The combination of the DDA and DN signals leads to a better correlation, as shown in Figure 27. As explained earlier in Section 4.1.6.1, the two signals are independent because the DDA signal is sensitive to both fission and absorption whereas the DN signal is dominated by fission. Note that this explanation has nothing to do with the differences among the delayed-neutron production abilities of the three fissile isotopes, unlike the NGSI's explanation. In comparing a 4% enriched, 40 GWd/tU burned, 5 year cooled spent PWR assembly against a fresh PWR assembly, the changing fissile isotopics decreases the average number of delayed neutrons emitted per fission by roughly 20%, whereas the total fissile content decreases by more than 60%. Therefore, the error in assuming a constant value for the average number of delayed neutrons based on a middle value of burnup is only ±10%, roughly, whereas the fission term changes too much to be approximated as constant. Clearly then, the fission term of Equation 18 is the dominant variable, not the average number of delayed neutrons.

4.1.6.4 Limitations

The DN technique by itself suffers the same limitation as the CIPN, PNAR, and DDA techniques, in that it cannot distinguish between neutron absorption and production. Only in combination with one of these techniques can a significant separation between these two neutron processes be made. Also, the DN technique's results depend on the BIC set (Figure 26).

Furthermore, the DDA/DN instrument is heavy and can be expensive because of the cost of the ^{3}He detectors and the D-T neutron generator. In particular, the DN technique's need to produce enough delayed neutrons to overcome the passive neutron flux of the spent fuel assembly eliminates the use of a ^{252}Cf source and pushes the required D-T neutron generator (~10^{11} neutrons/s) to the upper ranges of that technology's generating capacity.

4.2 Distinguishing fissile material by neutron coincidence

Neutron-coincidence NDA techniques (abbreviated as NC techniques, below) can be more difficult to understand than the other kinds of neutron NDA techniques, so a longer introductory exposition is given here. The physics of the historical applications of NC techniques to samples other than spent fuel assemblies is discussed, because it is only by reference to these simpler historical cases that the much more difficult case of spent-fuel-assembly assay can be properly understood. Only passive NC techniques are considered here, however, so neither accelerator-driven systems [191, 192] nor Mihalczo's ^{252}Cf fission-chamber noise-analysis technique [193-196] is considered.

Passive NC techniques are similar to the TN technique insofar as they analyze the same passive neutron flux being emitted from the spent fuel assembly. Their superiority to the TN technique is just that they analyze the time sequence of the neutron detections. This analysis requires the use of neutron detectors with high detection efficiency, such as ^{3}He detectors, since the figure of merit for neutron-coincidence NDA techniques is the ratio of the square of the detection efficiency to the detector die-away time (ε^2/τ) (page 26 of Smith and Jaramillo [140], and Evans et al. [141]). Among the individual NC techniques, the distinctions are not so much distinctions of hardware as they are distinctions of ways to analyze the same coincidence data.

NC techniques attempt to determine the quantity of spontaneously fissioning isotopes in a sample (e.g., a can of MOX powder or a spent fuel assembly) by associating the coincident detection of neutrons with the coincident emission of multiple prompt neutrons from each spontaneous fission event. (See Table 6 and Figure 28.) Of course, even though multiple neutrons may be born simultaneously from a particular fission event, they likely will not be detected precisely simultaneously because they will take different, random paths to arrive at the detectors. This spatial transport of the neutrons thus smears the detection times of such simultaneously emitted neutrons. This dispersion in detection times caused by random variations in spatial transport will be referred to as "spatial die-away" in the following discussion. (The total die-away process is a combination of this spatial die-away and "material die-away," which is the dispersion caused by the creation or absorption of neutrons in material (isotopes) [130].) This spatial die-away dispersion thereby causes the detections of neutrons from many separate fission events to overlap in time. However, by detecting many neutrons over a long measurement time and then applying a probabilistic analysis, NC techniques are able to separate, on average, the accidental overlaps of neutrons born in separate, randomly occurring, spontaneous fission events, on the one hand, from the true coincidences of neutrons born in the same spontaneous fission event, on the other hand. To put it quickly: The accidental overlaps caused by spatial die-away tend to even out over many neutron detections since the spontaneous fission events occur randomly with respect to time and with respect to each other, whereas the coincident detections of neutrons born in the same fission event occur persistently and accumulate over many neutron detections because they are real coincidences and not random with respect to each other.

Figures 29 and 30 illustrate this coincidence between neutron detections and give an example of one kind of NC probabilistic analysis. Figure 29 is a classic representation of the coincidence between detected neutrons; it is known as the Rossi-alpha curve, named after

Bruno Rossi [197]. It plots the rate at which a second neutron is detected following the detection of a first neutron (called a "triggering" neutron), which occurs at time zero (the origin). It is thus similar to a plot of the conditional probability of detecting a second neutron given that a first neutron has been detected. The hump at the start of the curve represents the coincidence between neutrons, since neutrons that are emitted simultaneously are more likely to be detected close in time to each other. The hump dies away exponentially. Figure 30 illustrates one way to construct a Rossi-α curve from a time sequence of neutron detections.

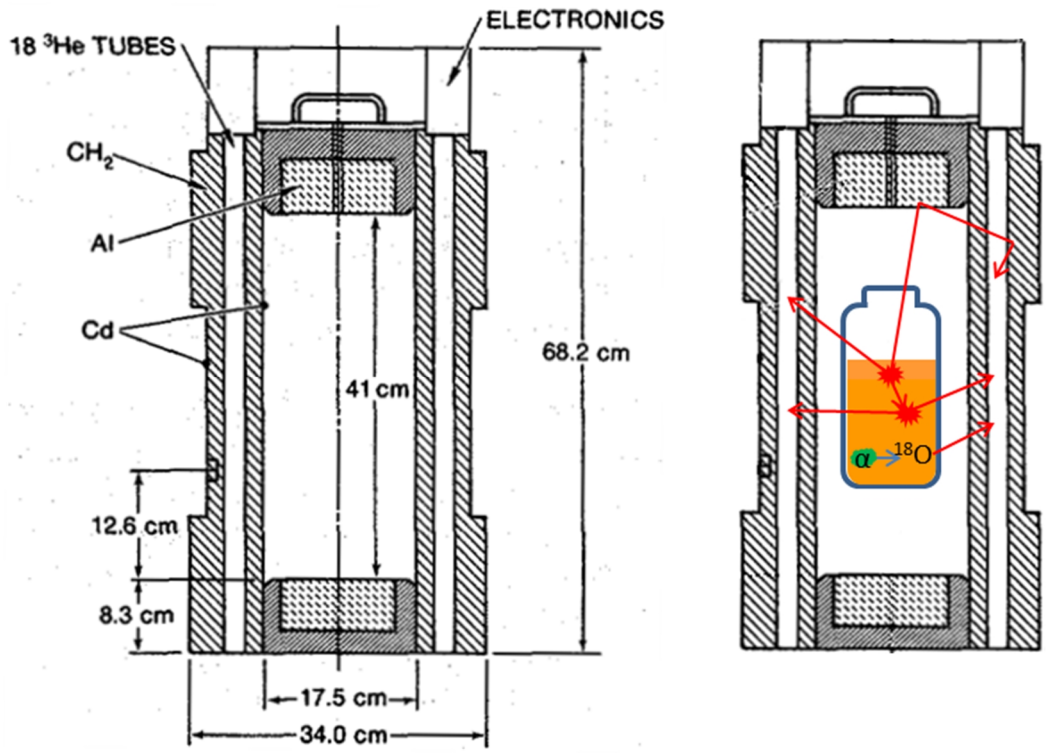

Figure 28: Left: A cross-sectional drawing of the upgraded High-Level Neutron Coincidence Counter (HLNCC-II) (; copied from Figure 17.5 in Reilly et al. [75]). Right: An illustration of spontaneous fission, induced fission, and (α,n) reactions producing neutrons from a sample.

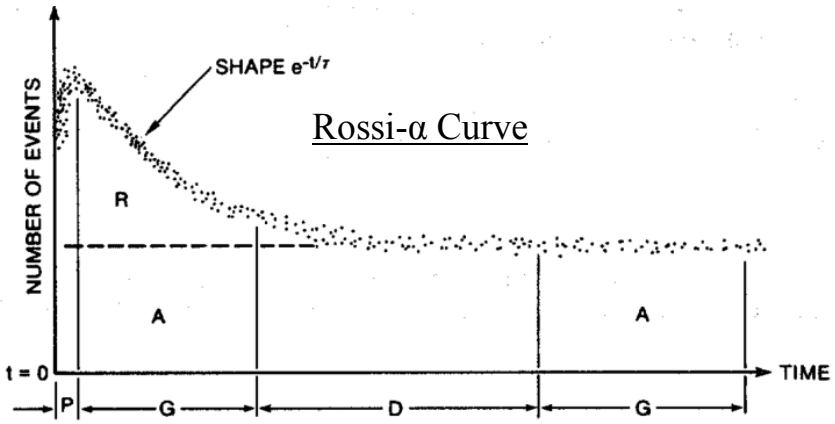

Figure 29: A sketch of a one-dimensional Rossi-α curve, which shows the rate at which second neutrons are detected as a function of the time after first neutrons are detected (which is the origin, $t = 0$). The dots in the curve have no real meaning, except insofar as they indicate that a true Rossi-α curve is a histogram; see Figure 30. Copied from Reilly et al. [75].

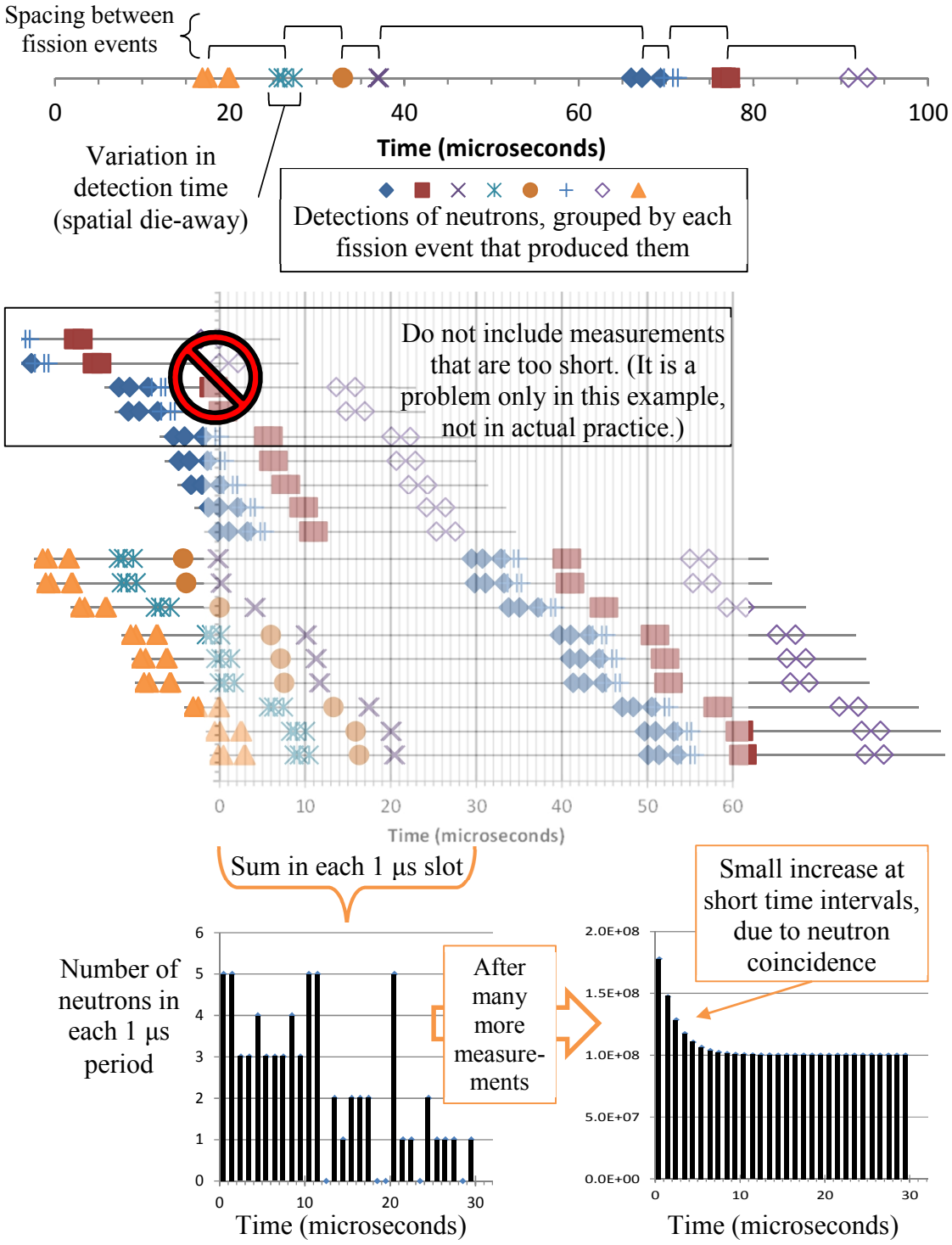

Figure 30: An example of creating a Rossi-α diagram from a time-sequence of neutron detections. Top: the time sequence. Middle: recording the data at each neutron detection, beginning with the first detection (bottom) and going to the last detection (top). Bottom Left: summing the number of neutrons that fall into each 1 μs slot, from 0 μs to 30 μs. Bottom Right: a speculation about the final Rossi-α curve after measuring many more time-sequences (note the change in the vertical scale). Reprinted from [206] with permission from ESARDA.

Of course, there are many other neutronic processes that can occur besides neutrons' birth in spontaneous fission, their transport, and their subsequent detection. Several such neutronic processes are included in the following list:

(1) Neutrons can be created spontaneously through processes other than spontaneous fission. In particular, (α,n) reactions are often a significant source of spontaneously generated neutrons. On their own, (α,n) neutrons simply increase the number of accidental coincidences, since they are effectively like spontaneous fissions that only emit one neutron each. When (α,n) neutrons induce fission, however, they create coincident neutrons from each induced fission event. Since the (α,n) neutron is absorbed in the induced fission event, the induced fission event appears to be a spontaneous fission event to the neutron detectors. However, the induced fission events are in isotopes other than the spontaneous-fission isotopes. Therefore, they cause NC techniques to overestimate the quantity of spontaneously fissioning isotopes. These effects of (α,n) neutrons are taken into account by using two parameters: (1) α, the ratio of (α,n) neutrons to spontaneous-fission neutrons; and (2) M_L, the neutron leakage multiplication of the sample (which is denoted just by M in Ensslin et al. [198]).

(2) Neutrons can leak out of both the sample and the neutron detectors, so that they are not detected at all. Neutron leakage reduces the expected number of neutron coincidences and causes NC techniques to underestimate the quantity of spontaneously fissioning isotopes. (It also reduces the expected number of induced fission events in each fission chain, but this point will be discussed in the context of induced fission, below.) Neutron leakage is part of the spatial die-away of the neutron population. The direct loss of neutron coincidences because of neutron leakage is taken into account by the use of a detection efficiency, ε.

(3) Neutrons can be captured by neutron absorbers, so that they are not detected at all. Neutron capture thus reduces the expected number of neutron coincidences and causes NC techniques to underestimate the quantity of spontaneously fissioning isotopes. (It also reduces the expected number of induced fission events in each fission chain, but this point will be discussed in the context of induced fission, below.) Neutron capture decreases the material die-away time of the neutron population, since it removes neutrons. The direct loss of neutron coincidences because of neutron capture is taken into account through the detection efficiency, ε, since its effect is indistinguishable from neutron leakage (unless the neutron detectors are moved around or enlarged).

(4) Neutrons can be created through induced fission in isotopes that are different from the spontaneous-fission isotopes (e.g., in fissile isotopes). Any neutron can induce fission: neutrons from spontaneous fissions, neutrons from (α,n) reactions, and neutrons from other induced fission events. Induced fission events from (α,n) reactions have been addressed in the previous point. Subsequent induced-fission events by neutrons from prior induced-fission events constitute *fission chains*. The important connection is therefore the one between spontaneous fission events and the fission chains that they initiate. The fission chains increase the material die-away time of the neutron

population because they create more neutrons. (See Figure 20, above, and page 5 of Pacilio [197], for example.)

Fission chains act as a second cause of real neutron coincidences besides the simultaneous emission of neutrons from the same fission event. Each fission event in a chain has a real correlation with every other fission event in the chain, including the initiating spontaneous-fission event. This correlation within a fission chain is in stark contrast to the utter lack of any correlation between spontaneous fission events. Whereas the accidental overlapping of neutrons from separate spontaneous fission events averages out over many neutron detections (as described above), the coincident detections of neutrons from separate induced-fission events in the same fission chain do not average out, because such neutrons do possess a real correlation to each other, albeit a weaker one than the correlation among neutrons from the same fission event. It is weaker because there is a finite and somewhat random time interval between fission events in a fission chain, whereas prompt neutrons from the same fission event are emitted simultaneously and instantaneously for all practical purposes.

The effect of fission chains on NC techniques depends on two main factors: the speed of the neutrons that induce the fission events (I = fast; II = slow) and the speed of the neutrons that are detected (a = fast; b = slow). Note that the meaning here of "the speed of the detected neutrons" refers to the speed with which they depart the sample chamber and enter a detector unit that includes not only the detector itself but also any moderator that surrounds the detector. The four possible pairs of these two main factors are discussed in turn:

(I-a) If the induced fission events are primarily fast fissions and if their neutrons are transported primarily as fast neutrons to the detector units, then the time intervals between the fission events in each fission chain usually are similar to or smaller than the time intervals between the detections of simultaneously emitted neutrons, which happen simply because the neutrons take different, random paths to the detectors (as discussed above). In other words, the increase in the material die-away time caused by fission chains is negligibly small in comparison to the spatial die-away time. In this case, all of the fission events in the fission chain appear to be one giant "superfission" to the neutron detectors, since all of their neutrons arrive at the detectors within the same general timespan as do the neutrons from a single spontaneous fission event. Böhnel was the first researcher to address this superfission approximation thoroughly [199-201], and the approximation is valid for many applications of NC techniques, such as the assaying of MOX powder. The size of the superfissions is an effect of the neutron multiplication (M_L) in the sample, so a knowledge of the multiplication enables the spontaneous fission to be separated from the induced fission. Lastly, neutron capture can be neglected in this case because the cross sections of neutron absorbers are small for fast neutrons.

(I-b) If the induced fission events are primarily fast fissions but their neutrons are transported primarily as slow neutrons to the detector units, then the sample

being assayed must have its nuclear material (both spontaneous and fissile isotopes) distributed in a heterogeneous and dilute fashion, and it must contain some moderating material. This situation describes the assay of drums of contaminated waste. Each small particle of nuclear material generates neutrons by spontaneous fission and then by induced fast fission within the same particle. The neutrons leave the particle and are moderated somewhat by the moderating material in the drum, but they do not then proceed to induce much thermal fission because of the dilute distribution of the particles of nuclear material. Instead, they leave the drum and are detected. This case is similar to the previous case in that the time between induced fissions is small in comparison with the spatial die-away time. The moderation in the drum actually increases the spatial die-away time. Therefore, the superfission approximation is valid here also. A difference in this case is that neutron capture cannot be neglected, since the slow neutrons may be captured within the drum while they are going to the detectors. This neutron capture can be taken into account by the detection efficiency, ε.

(II-a&b) When the induced fission events are primarily thermal fissions, it implies that there is significant moderating material in the sample, so most of the neutrons that reach the detectors will also be thermal neutrons, although a few fast neutrons will still survive the trip to the detectors. In this case of thermal fissions, the time intervals between the fissions in each fission chain are long, since each inducing neutron must undergo the thermalization process before it can induce the next fission. As discussed in Section 4.1.5.1 in the context of the DDA technique, the thermalization process is on the order of 2 μs in pure water, and this process must be repeated after each fission in the fission chain. By this fact, the material die-away time becomes significantly longer than the spatial die-away time, and the correlations among the detections of neutrons from different fission events in the same fission chain are stretched out over a significantly longer time period than are the correlations among neutrons from the same fission event. The superfission approximation is therefore inappropriate to make in this case. Instead, the simultaneously emitted neutrons from the fission events, both spontaneous and induced, produce coincident detections within a relatively short time period—that is, the spatial die-away time period caused by the random differences in the neutrons' transport paths to the detectors, as discussed above. These same neutrons also make additional coincident detections with the other neutrons from the other fission events of their fission chains, but these additional coincident detections occur over a much longer time period, namely, the material die-away time. (This slower, material die-away time is what is observed in reactor noise analysis [197].) A separation of the coincident detections into shorter coincidences (within the spatial die-away time) and longer coincidences (over the material die-away time) is thus a means of distinguishing between all fission events and

induced fission events only, respectively. (This separation is what the DDSI technique attempts to do; see Section 4.2.2.)

Neutron capture can be a severe problem in this case, because it intercepts not only those neutrons that are on their way to being detected but also those neutrons that are on their way to inducing the next fission events in the fission chains. Therefore, neutron capture in this case affects the multiplication (M_L) in addition to affecting the detection efficiency (ε).

The energy of the neutrons that are detected in this case is a secondary aspect, since as mentioned above, the same neutron moderation that causes most of the induced fission events to be thermal fissions also simultaneously causes most of the neutrons that may be detected to be thermal neutrons. Therefore, the much smaller flux of fast neutrons can be isolated only by discarding the much larger population of slow neutrons by means of a filtering material on the detectors, such as cadmium. The same information about the fission events is contained in both the fast flux and the slow flux, though, since the same fission events produce both the fast neutrons and the slow neutrons into which the fast neutrons eventually become through moderation. The difference between detecting fast neutrons and detecting slow neutrons is therefore just how the neutron interactions besides fission affect the NC instrument's ability to extract this information.

There are two main negative aspects to detecting the slow neutrons. The first is that the moderation process increases the overlapping of the detection of neutrons from different fission events (i.e., increases the spatial die-away time), causing the number of accidental coincidences to increase. The second is that neutron capture is more severe for the thermal-neutron population than for the fast-neutron population, since the cross sections for the neutron absorbers are greater for slow neutrons, in general. Therefore, if the count rate of fast neutrons is high enough to give sufficient statistics, it is better to count the fast neutrons than the slow neutrons because the coincidence information contained in the fast-neutron signal is cleaner.

In summary, the physical processes that must be considered when applying NC techniques to the most general samples include neutron production by spontaneous fission, neutron transport to the detectors (spatial die-away), neutron production by (α,n) reactions and other processes, neutron leakage, neutron absorption, and neutron production by induced fission. Neutron production by induced fission is subdivided into four cases: (I-a) fast-neutron fission and fast-neutron detection, (I-b) fast-neutron fission and thermal-neutron detection, (II-a) thermal-neutron fission and fast-neutron detection, and (II-b) thermal-neutron fission and thermal-neutron detection.

With this background of the physics, it is possible to understand the point-model assumption that is common to the historical applications of NC NDA techniques. The point model assumes that the sample being assayed produces the same neutron signal as if the sample would be compressed into a single point in space; that is, the sample can be modeled as an infinitesimally small point. Nevertheless, the spatial die-away time is still assumed to

have a finite length. Rather than being attributed to neutron scattering within the sample, the spatial die-away time is attributed to a very quick fast-neutron transport in the sample chamber followed by a longer neutron moderation and transport process in the polyethylene surrounding the ^{3}He neutron detectors. This attribution is why the literature often uses the term "detector die-away time" to refer to the spatial die-away time. It is clear, then, that the point model can be valid only for a fast-neutron flux within the sample, that is, for case (I-a) described above.

The point model can be divided into two constituent assumptions about two different spatial regions. The first assumption is the most basic one and is about the space within the sample itself. This part of the point model assumes that any effects of the sample's geometry on the interactions of the neutrons within the sample can be neglected. The second assumption adds to the first one and is about the space outside of the sample, between it and the neutron detectors. This part of the point model assumes that the positioning of the sample inside the NC instrument's assay chamber (or with respect to the neutron detectors) is irrelevant to the NC measurement. This second assumption usually cannot be assumed unless the NC instrument is intentionally designed to have the same probability to detect a given neutron regardless of where that neutron was born inside the assay chamber. Such an intentionally designed detection probability is known as "having a flat detection-efficiency profile within the instrument." It is seen, then, that the first part of the point model concerns the negligibility of the spatial distribution of the sample, whereas the second part concerns the negligibility of the spatial distribution of the NC instrument.

The assumption of the point model allows NC practitioners to define the detection efficiency, ε, in a unique way. Usually, the efficiency of a detector concerns the fraction of neutrons that it detects out of all the neutrons that pass through it; this definition makes no reference to the sample at all. One could broaden this definition slightly to be the fraction of neutrons that are detected out of all the neutrons that are emitted by the sample; this definition would consider that some neutrons leak out through the surfaces of the assay chamber that are not covered by detectors. The detection efficiency used for NC techniques, though, is even broader still: it concerns the fraction of neutrons that are detected out of all the neutrons that are created, regardless of whether or not they avoid being captured in the sample and escape successfully from the sample to be able to be detected. This definition excludes only neutrons that are absorbed in induced fission events, since those neutrons are multiplied (i.e., the net neutron profit of induced fission is greater than zero). Unlike the previous definitions, this definition thus includes neutrons that can never be detected (i.e., captured neutrons), not even by a repositioning of the neutron detectors. Such a broad definition makes sense only if neutron capture is relatively small and if the spatial aspects of neutron capture—namely, self-shielding—can be neglected. These conditions are satisfied only when the point model is valid, and the point model is valid only when the neutron flux within the sample stays fast, as discussed above.

Lastly, it can be recognized that NC techniques are similar to the differential die-away technique (DDA; Section 4.1.5). The DDA technique analyzes how a large pulse of neutrons dies away over time; the NC techniques analyze how many small pulses of neutrons—i.e.,

neutrons from spontaneous fission—die away over time. This comparison can be expressed symbolically as follows:

$$N(t) = N_{\text{DDA pulse}} e^{-t/\tau} = \sum_{i=1}^{\left(\frac{N_{\text{DDA pulse}}}{N_{\text{spont. fiss.}}}\right)} N_{\text{spont. fiss.}} e^{-t/\tau} \qquad \text{Equation 20}$$

There are two main differences between the dying away processes of the DDA and NC techniques. The first is that the DDA neutrons originate from outside the fuel assembly and go into the fuel assembly. They therefore have a different spatial distribution within the fuel assembly than the primary neutrons (from spontaneous fission) have, which may lead to different die-away times; i.e., the two τ variables on either side of Equation 20 may be slightly different. The second difference is that the starting time of the DDA pulse is controlled and well-known, whereas the starting time of each spontaneous fission event is random and unknown. Without the knowledge of the starting times of the spontaneous fission events, the summation of the die-away functions in Equation 20 cannot be performed directly, since it is impossible to "line up" the die-away curves. Therefore, NC techniques line up these die-away curves indirectly by using probability, as demonstrated in the Rossi-α example of Figure 30.

For this reason, the reader should be careful about interpreting NC results from Monte Carlo simulations (e.g., Figures 4 and 5 in Belian et al. [28] regarding DDSI). Whereas the starting times of the spontaneous fission events in a Monte Carlo simulation can be chosen and recorded, it is impossible to know them in real life unless some other, faster particles from the fission events, such as prompt gamma-rays or anti-neutrinos, are also measured. Therefore, die-away curves that come from Monte Carlo simulations are not exactly the same as die-away curves that come from NC measurements, such as Rossi-α curves (Figure 29). The Monte Carlo curves are plotting the dying away of the arrival times of neutrons at the detector, whereas the NC Rossi-α curves are plotting the dying away of the rate at which a second neutron is detected following the detection of a triggering neutron. In particular, the definitions of coincident detections is different. In a Rossi-α diagram, the detection of one neutron in a time gate following the detection of a triggering neutron constitutes a pair, whereas in a Monte Carlo arrival-time diagram, two neutrons must be inside the gate to constitute a pair. The Monte Carlo arrival-time diagram and the Rossi-α diagram are certainly related, but one should not apply the mathematics or analysis of one diagram to the other without first making the appropriate transformations.

4.2.1 Neutron Multiplicity counting (NM)

Name	Neutron Multiplicity counting (NM)
References	NGSI: [8, 25] Other: [198]
Measurement environment	In water (in air or other gas is also possible)
Passive vs. Active	Passive
Time dependency	Time-dependent
Particles detected	Neutrons
Type of detectors	^{3}He detectors
Particles' detected attribute	Coincidence of creation in fission events and fission chains
Governing physical properties of the fuel assembly	The number of primary neutrons (N_{PRI}) The leakage multiplication of primary neutrons (M_L) The absorption of neutrons, specifically The production of neutrons, specifically
Governing isotopes	Primary-neutron sources; fissile isotopes; neutron absorbers
Maturity	Has been used for many years to assay MOX powder, plutonium scrap, and drums of contaminated waste [198]; has not yet been tested on spent fuel assemblies
Limitations	Lack of an adequate theory to address the violation of the point model and the associated assumptions Cannot distinguish the reason for a loss of induced fission, whether it is because of a loss of fissile material or because of a loss of inducing neutrons because of neutron capture
Selected by the NGSI for prototype testing?	No

4.2.1.1 Principle of operation

Neutron Multiplicity counting (NM) is a passive technique and is an advanced form of neutron-coincidence counting. It analyzes not only the coincidence between pairs of detected neutrons but also the coincidence among triplets of detected neutrons. (NM could theoretically analyze higher-order multiplets, too, but this is not usually done.) Thus, whereas the one-dimensional Rossi-α curve shown in Figure 29 represents the coincidence between pairs of detections, a two-dimensional Rossi-α diagram represents the coincidences among triplets, respectively [202-205]. The time between the second and third detections is the second axis for plotting the two-dimensional Rossi-α surface [202].

In typical safeguards practice, Rossi-α diagrams are not used. Instead, a hybrid analysis known as shift-register analysis is employed [130, 206]. The details of how the neutrons are counted in shift-register analysis is described by Reilly, Ensslin, et al. [75, 198]. Here it is sufficient to say that shift-register analysis is practically an integration of the one-dimensional Rossi-α curve over two time periods: an early period that spans the coincidence hump and a late period that has no hump. (See Figure 31.) These time periods are called "gates." Neutron-coincidence counting (i.e., counting of pairs of detected neutrons) subtracts the (average) number of neutrons in the late gate (Region 2) from the (average) number of neutrons in the

early gate (Region 1), leaving only those neutrons that are truly coincident with the first neutron ($t = 0$). These real pairs are known as "doubles."

When taking data, the actual number of neutrons that are detected within a given gate varies, of course. By summing up the number of times each given number of neutrons is detected within the given gate, a histogram can be constructed of the numbers of neutrons in the gate. (See Figure 32 for an example.) The average number of neutrons in a gate is the same as the first moment (mean) of this histogram. The variance in the number of detected neutrons is related to the second moment (about the origin) of the histogram. (The variance is actually the second moment about the mean.) This variance is related to the number of triplets detected, given that a first neutron is detected (i.e., it is conditional). Neutron multiplicity counting uses a complicated algebraic counting theory to subtract the variance in the late gate from the variance in the early gate, roughly speaking, and it thereby isolates the real triplets from the accidental triplets [198, 207, 208]. These real triplets are known as "triples."

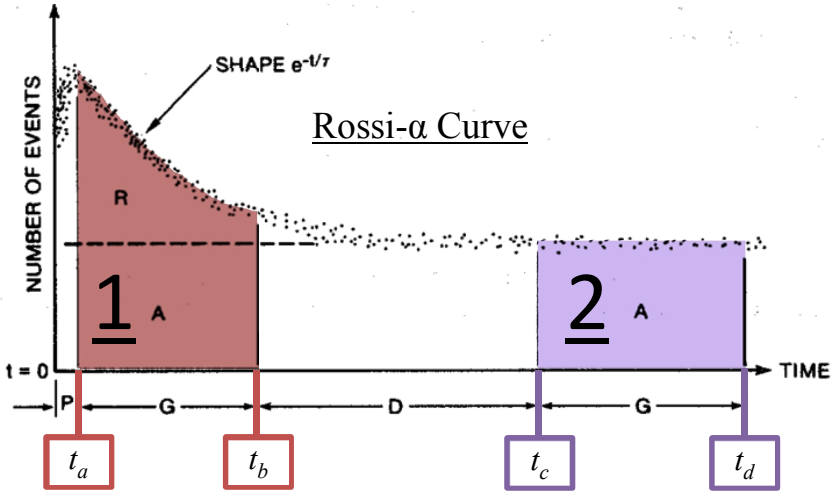

Figure 31: A modification of Figure 29, showing how the shift-register method is an integration of two regions of the one-dimensional Rossi-α curve. Reprinted from [206] with permission from ESARDA.

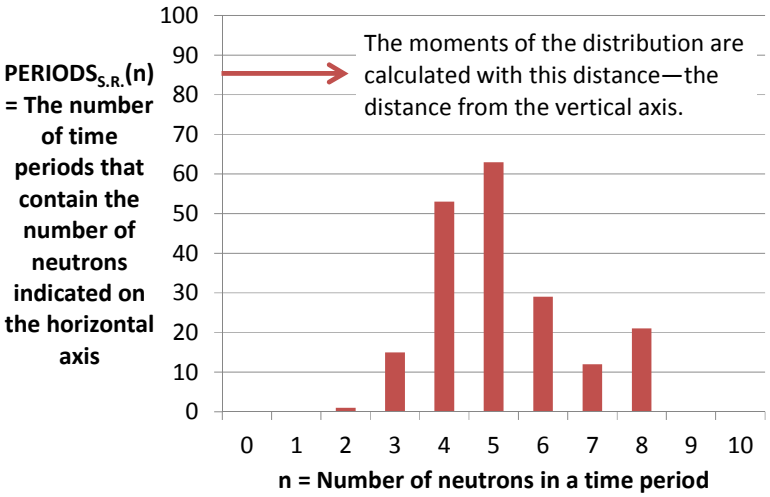

Figure 32: A histogram of the number of neutrons detected within a certain period of time following the detection of a first neutron (for a fictitious sequence of neutron detections). Reprinted from [206] with permission from ESARDA.

In the language of shift-register analysis, the average number of neutrons detected per unit time is the “singles” count rate; the average number of real pairs of neutrons detected per unit time is the “doubles” count rate; and the average number of real triplets of neutrons detected per unit time is the “triples” count rate. Note that the “per unit time” here represents a division of the number of counted items by the entire measurement time (e.g., hundreds to thousands of seconds), rather than the taking of the limit as time goes to zero. Also note that these “real” pairs and “real” triplets are not the same as the number of pairs or triplets detected within a randomly chosen time interval of the same length as the gate. Not only does such a randomly triggered gate contain accidental pairs in addition to the real pairs, but even more fundamentally, the neutrons in a gate that starts randomly must be treated with an independent probabilistic analysis, whereas the neutrons in gate that starts with the detection of a neutron must be treated with a conditional probabilistic analysis, i.e., conditional on the first detection.

Also note that the phrase *neutron multiplicity* in the name “Neutron Multiplicity counting” refers foremost to this detection of multiples of neutrons. It is true that the multiplicity of the neutrons emitted from each fission event does impact the multiplicity of the neutrons detected. In a sample with a fast neutron spectrum, no induced fission, and no (α,n) sources, these two multiplicities are closely connected. And in the applications of NM to samples with fast fission, the superfission approximation ties the multiplicity of neutrons from the entire fission chain to the multiplicity of the detected neutrons. In the application of NM to samples with thermal fission, though, the elongation of the correlations among the neutrons from the fission chains confuses the connection between the multiplicity of neutrons emitted from each fission event and the multiplicity of detected neutrons. Therefore, *neutron multiplicity* must refer primarily to the multiplicity of detected neutrons in the context of spent-fuel NDA.

4.2.1.2 The NGSI’s design

The NGSI did not design an instrument specifically for NM. Instead, NM was evaluated for an instrument designed to perform Differential Die-away Self Interrogation (DDSI) [25]. Therefore, see the DDSI design in Section 4.2.2.2. As discussed above, an NM measurement is like a TN measurement but with neutron detectors that have high efficiency.

4.2.1.3 Data analysis

The singles (S), doubles (D), and triples (T) (per unit time) of NM counting have traditionally been expressed as functions of the rate of spontaneous fission (F), the detector efficiency (ε), the ratio of (α,n) neutrons to spontaneous fission neutrons (α), and the leakage multiplication (M) (page 63 of Ensslin et al. [198]):

$$S = F\varepsilon M\nu_{s1}(1+\alpha) \qquad \text{Equation 21}$$

$$D = \frac{F\varepsilon^2 f_d M^2}{2}\left[\nu_{s2} + \left(\frac{M-1}{\nu_{i1}-1}\right)\nu_{s1}(1+\alpha)\nu_{i2}\right] \qquad \text{Equation 22}$$

$$T = \frac{F\varepsilon^3 f_t M^3}{6} \cdot \left\{ \nu_{s3} + \left(\frac{M-1}{\nu_{i1}-1}\right)[3\nu_{s2}\nu_{i2} + \nu_{s1}(1+\alpha)\nu_{i3}] + 3\left(\frac{M-1}{\nu_{i1}-1}\right)^2 \nu_{s1}(1+\alpha){\nu_{i2}}^2 \right\}$$

Equation 23

The other variables in these equations are assumed to be known. They are the doubles gate fraction (f_d); the triples gate fraction (f_t); the first, second, and third reduced moments of the spontaneous-fission neutron distribution (ν_{s1}, ν_{s2}, and ν_{s3}); and the first, second, and third reduced moments of the induced-fission neutron distribution (ν_{i1}, ν_{i2}, and ν_{i3}). These equations assume the point model and the superfission approximation (page 59 of Ensslin et al. [198]).

It may be helpful to consider the purpose of these three equations in the context of the traditional applications of NM (i.e., fast neutron spectrum in the sample). The singles count rate is nothing more than a TN measurement. The additional determination of the doubles count rate enables the spontaneous fission sources to be separated from the (α,n) sources, since (α,n) neutrons cannot create real pairs; that is, F and α are found. The additional determination of the triples count rate enables either the detector efficiency or the leakage multiplication to be determined, because the ratio of the triples to the doubles explores the difference between the observed fission multiplicity and the expected fission multiplicity based on the isotopes that are assumed to be fissioning. Neutron capture and leakage (smaller ε) will produce less multiplicity than expected, whereas leakage multiplication (M) will produce more multiplicity than expected.

Since there are four unknowns (F, ε, α, M) but only three measured quantities (S, D, T), the solution to this system of equations is indeterminate. The answer to this problem is to assume that one of the four unknowns actually is known, leaving only three unknowns. Then the system can be solved. Which of the four to assume depends on the particular sample being assayed. The point model for a homogeneous sample with significant multiplication (e.g., a can of MOX powder) allows ε to be assumed as constant in that case, whereas the small multiplication, heterogeneous distribution, and significant neutron capture in drums of contaminated waste suggest assuming M and finding ε in that case [198].

With regards to the application of NM to spent fuel assemblies, the NGSI chose to assume that ε is known and to examine F, α, and M. In this case, the spontaneous fission rate, F, is practically a function of the ^{244}Cm content only, for all but the least burned and least cooled spent fuel assemblies (Section 3.3.1). α and M are defined as before. In terms of the symbols used in the descriptions of the neutron-multiplication techniques (Section 4.1), F is practically $N_{PRI}/\bar{\nu}_{\text{Cm-244}}$ (where N_{PRI} is the number of primary neutrons per second); and M is M_L, the leakage multiplication of primary neutrons.

By Monte Carlo modeling of the 64 spent fuel assemblies from the first library (Section 2.3), the NGSI found the following results [25]: α is poorly determined by NM and is "small and rather uninteresting." F can be determined more accurately than α can, but the accuracy is still quite poor. M can be determined the most accurately and might be useful.

A problem in the NGSI's approach, though, is that, of the four unknown variables, α is actually the one that is best known *a priori*, not ε, since the spontaneous fission of ^{244}Cm

dominates the production of primary neutrons [75, 92]. Therefore, an approximation of α as being zero or some constant, small value would be reasonable. The NGSI's findings regarding α support this hypothesis.

In contrast, ε is expected to be quite variable due to the unknown and changing quantities of neutron absorbers in the fuel. Ordinarily, ε would depend also on neutron leakage as well as on neutron absorption. However, since the geometry of the spent fuel assembly does not change with the burning, enrichment, and cooling of the fuel (the BIC variables) and since the scattering of neutrons from water and from ^{238}U dominates the neutron diffusion, the neutron leakage probability likewise does not change with the BIC variables [209, 210]. (See also Section 6.2.3.) Therefore, changes in ε can be attributed primarily to changes in neutron absorption, which is an important variable not only for neutron detection directly but also as an influence on leakage multiplication via changes to the length of fission chains. Therefore, ε can be regarded as a measure of the extent to which the point model is violated.

Therefore, NM should probably be reevaluated based on an assumption of α and a solution for F, ε, and M. Not only would the substitution of ε for α provide more information on neutron absorption, but it should also improve the accuracies of F and M. Also, the utility of the triples rate (which is the key feature of NM) to the interpretation of DDSI (which is an advanced analysis of the doubles rate) should be evaluated.

4.2.1.4 Limitations

The NGSI found that the main problem with applying NM to spent fuel assemblies is that the uncertainty in the triples count rate is excessively large [8, 25]. This large uncertainty is caused by a very large accidental triples count rate. The NGSI attributed the large accidental triples count rate to the enormity of the passive neutron flux from a typical spent fuel assembly. However, the violation of the point model is also a major cause of the very large accidental triples count rate, particularly the increase in the spatial die-away times caused by neutron thermalization (e.g., see the characteristic die-away times on page 5 of Pacilio [197]).

Apart from the high accidental triples count rate, the biggest hurdle to applying NM to spent fuel assemblies is the development of a theory that applies when the point model is violated. As was said before, the NM equations (Equations 21 through 23) are predicated upon the validity of the point model. However, it seems that alternative NM equations for spent fuel assemblies might be able to be derived even though the point model is violated, since α is small and estimable and since neutron leakage can be taken as constant.

Lastly, as with most of the neutron-multiplication NDA techniques (Section 4.1), NM cannot distinguish well whether a reduction in the induced fission rate is caused by a reduction in fissile isotopes or by a reduction in neutron population because of neutron capture. If the triples rate could be good enough, NM might be able to use ε to sense the loss in count rate due to absorption of neutrons on their way to the detectors, because the triples-to-doubles ratio indicates the expected multiplicity of the fissions being detected. This ability would be an advantage over the neutron-multiplication techniques. Nevertheless, ε could not be used to distinguish between the aforementioned two causes of a reduction in the number of induced fissions, since there is no signal whatsoever from induced fissions that never occur.

4.2.2 Differential Die-away Self Interrogation (DDSI)

Name	Differential Die-away Self Interrogation (DDSI)
References	NGSI: [15, 26-28, 161, 211, 212] Other: [180, 213-215]
Measurement environment	In water (in air or other gas is also possible)
Passive vs. Active	Passive
Time dependency	Time-dependent
Particles detected	Neutrons
Type of detectors	^{3}He detectors
Particles' detected attribute	Coincidence of creation in fission events and fission chains
Governing physical properties of the fuel assembly	The number of primary neutrons (N_{PRI}) The leakage multiplication of primary neutrons (M_L) The production of neutrons, specifically
Governing isotopes	Primary-neutron sources; fissile isotopes; neutron absorbers
Maturity	Novel
Limitations	Large uncertainty or long measurement time, for low BU and small quantity of primary-neutron sources, because signal is weak Possibly poor statistics for absolute numbers of coincidence counts
Selected by the NGSI for prototype testing?	Yes, location uncertain [15]

4.2.2.1 Principle of operation

Differential Die-away Self Interrogation (DDSI) is a passive neutron-coincidence technique that is an advanced analysis of the doubles rate. (Please see the previous section on the NM technique for the definitions and explanations of neutron-coincidence terms such as "doubles rate.") DDSI's main feature is that it attempts to distinguish the two sources of neutron coincidence from each other: (1) coincidence from neutrons emitted in the same fission event and (2) coincidence from neutrons emitted in different fission events that are part of the same fission chain. These sources of coincidence were discussed previously in the prelude of this section on NC techniques (Section 4.2), specifically in item (4-II-a&b) of the list. The first kind of coincidence (from the same fission event) occurs on a shorter time scale than does the second kind of coincidence (from the same fission chain). Therefore, the two kinds of coincidence have two different die-away times. The measured Rossi-α curve is a sum of these two die-away curves, as illustrated in Figure 33. Therefore, DDSI is a hybrid between traditional NDA coincidence counting—which analyzes primarily the spatial die-away process—and traditional reactor noise analysis—which analyzes primarily the material die-away process. Such a hybrid technique is well suited to the NDA of spent fuel assemblies, which likewise fall between the extremes of small samples and large reactors.

The two die-away times are not really measured, *per se*, but instead the areas under the Rossi-α/die-away curve in the two relevant regions are integrated, as in a shift-register

analysis (Figure 31). These two counting intervals following each "first" (triggering) neutron are termed the "early gate" and the "late gate." Ordinarily there should also be a third, even later gate that measures the accidental coincidences, but this "accidentals" gate has not yet been included in the NGSI analyses of DDSI. It is expected to be considered in future NGSI work [212]. In the meanwhile, the counts in the early gates and late gates are being compared directly with each other, without a subtraction of accidental coincidences [212].

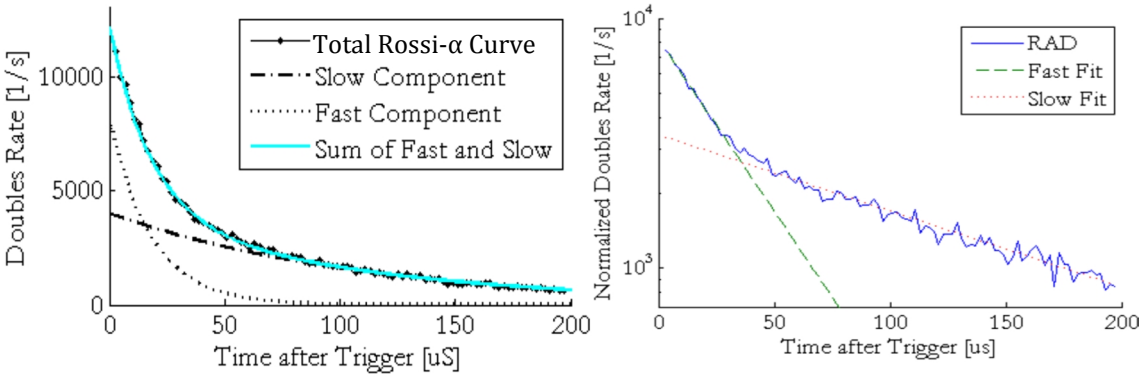

Figure 33: Left: a breakdown of the Rossi-α curve from a spent fuel assembly into its two die-away components (on a linear scale), as determined from Monte Carlo simulations of measurements with a DDSI instrument. Right: a semi-log plot illustrating the two components. Modified from Figures 7 and 10 in Kaplan et al. [212], with permission from INMM.

Note that the early NGSI publications described the two components of the Rossi-α/die-away curve differently [26-28, 161, 211]. They attributed the fast die-away time to neutrons from spontaneous fission and fast induced fission only; they called this die-away time as the "detector" die-away time (see Figure 34). They attributed the slow die-away time to neutrons from thermal induced fission and called it the "sample interrogation" die-away time.

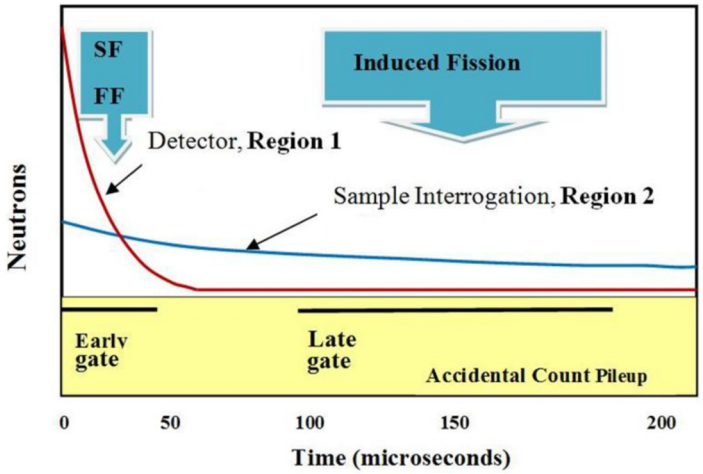

Figure 34: An early NGSI description of the physics of DDSI; copied from Schear et al. [27] with permission from INMM.

These early attributions and nomenclature were a consequence of a misunderstanding in this novel adaptation of neutron coincidence counting to spent fuel assemblies. In the traditional applications in which the point model is valid, the most influential cause of the spatial die-away time is the moderation of neutrons in the polyethylene surrounding the neutron detectors, which is why it is called the "detector" die-away time. Also, since the

neutron spectrum inside the assay chamber is fast in those applications, the most influential cause of thermal induced fission is the reflection of moderated neutrons from this polyethylene back into the assay chamber. This reflection is considered to be "interrogating" the sample, similar to the way reflected neutrons interrogate the spent fuel assembly in the PNAR technique. It seems likely, therefore, that this interrogation concept also was carried over from the idea of using neutron-coincidence counting in PNAR, as described in Section 4.1.2.2 and by Menlove et al. [153] and Evans et al. [154].

In truth, the point model is very much invalid for the case of spent fuel assemblies, mostly because of the presence of cooling water between the fuel pins. This water significantly moderates the neutrons *inside* the spent fuel assembly, in addition to the moderation in the detector's polyethylene. The first consequence of this neutron scattering inside the spent fuel assembly is that it lengthens the spatial die-away time of the thermal neutrons. As for fast neutrons, it merely attenuates them but does not greatly lengthen their spatial die-away time, so it is still valid to call the fast die-away time as the "detector" die-away time in DDSI. The second and more important consequence is that these neutrons that are moderated inside the spent fuel assembly can induce thermal fission immediately, without needing to travel to the detectors first. There is no two-step process of emission and then reflection. Thus, "sample interrogation" is a misnomer; the slow die-away time is actually caused by the correlations among the fissions of the fission chains, as in reactor noise analysis [197]. The third and most important consequence is that the thermal induced fission events contribute to the fast die-away time, along with the spontaneous and fast fissions. Since there is no two-step process for thermal induced fission, the thermal induced fission events do not occur only during a neatly separated time interval after all of the spontaneous and fast fission events. Moreover, the Rossi-α diagram is not even constructed in this way, since the "first" detected neutron (the triggering neutron) does not occur at the time of the fission event, nor does it have to be a neutron from a spontaneous fission; see Figure 30. Therefore, neutrons from thermal induced fission events do contribute to the early, "fast" coincidences that are measured by DDSI. This fact has recently been verified by the Monte Carlo simulations of Kaplan et al. of the NGSI [212]. Therefore, the interpretation of DDSI that has been presented above in this report is the correct one, and it has recently been adopted by the NGSI.

4.2.2.2 The NGSI's design

The NGSI's design of a DDSI instrument has gone through at least one iteration. Prior to 2012, the design was cylindrical and required the spent fuel assembly to be lowered into it from above (Figure 35). A lead (Pb) shield surrounded the fuel assembly to protect the ^{3}He neutron detectors from the assembly's intense gamma-ray emission. The outer circumference of the Pb shield was covered by a layer of Cd, to filter out the thermal neutron flux coming from the fuel assembly. The ^{3}He detectors were arranged in two rows around this circumference and outside the Cd layer. These detectors were embedded in polyethylene, and fins of Cd were also placed in the polyethylene, between the ^{3}He detectors. The purpose of these fins will be described later. The outer circumference of the polyethylene was covered by another layer of Cd to cut down the background thermal neutron flux. The instrument's steel housing was outside this outer Cd layer.

A new design was reported in 2012 [28]. This design has essentially the same components, but they are arranged in a rectangular U shape in cross section (Figure 36). This arrangement allows the DDSI instrument to be placed onto a spent fuel assembly from the side.

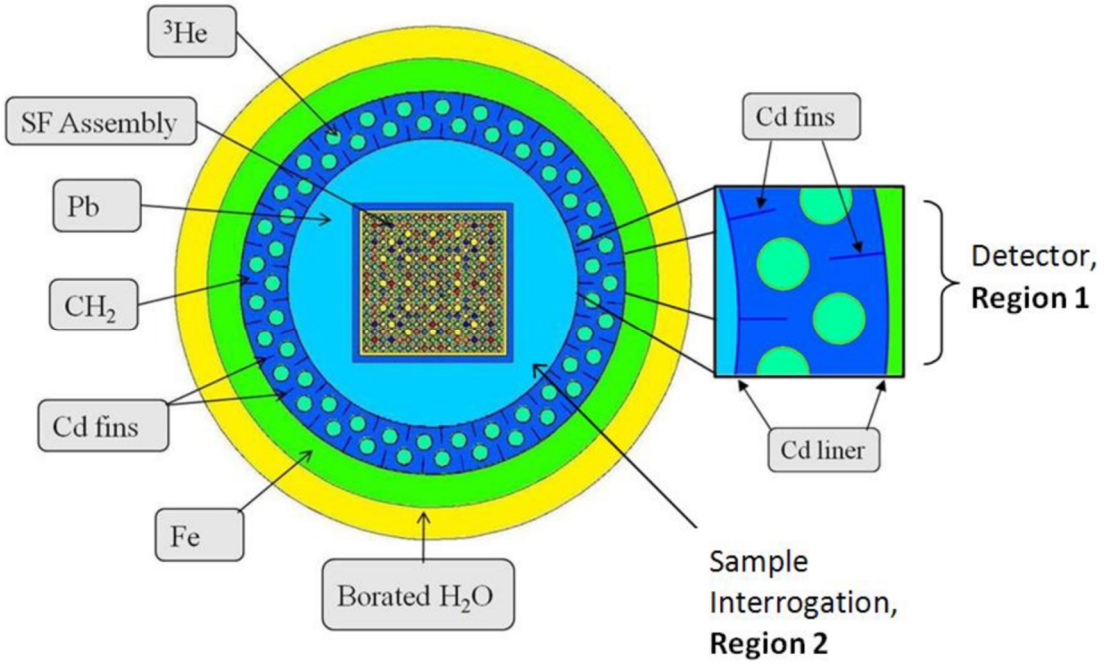

Figure 35: The pre-2012 version of the NGSI's design for a DDSI instrument, cross-sectional view; copied from Schear et al. [27] with permission from INMM.

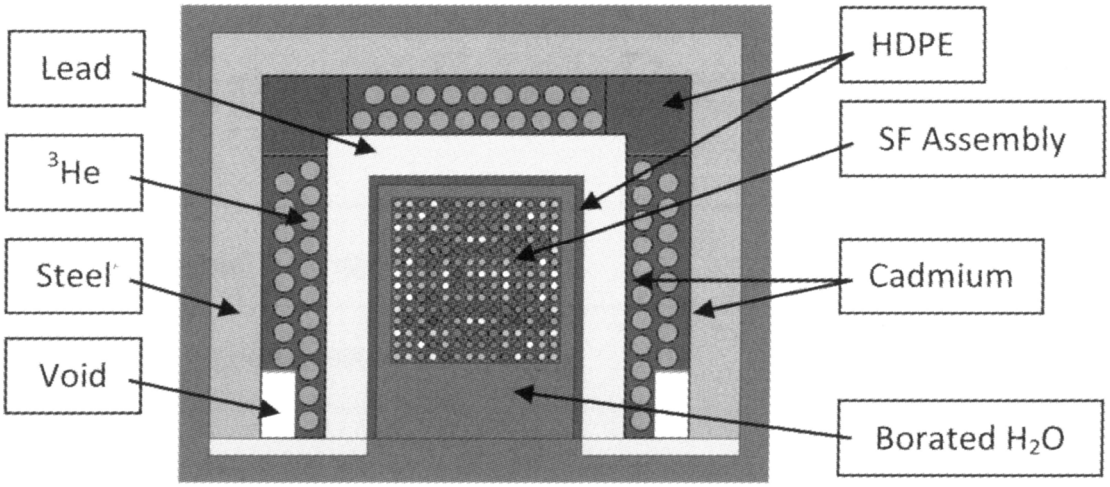

Figure 36: The 2012 version of the NGSI's design for a DDSI instrument, cross-sectional view; copied from Belian et al. [28] with permission from INMM.

The Cd fins in the DDSI instrument are a new feature among neutron-coincidence-counting instruments. Their purpose is to reduce the detector die-away time by capturing neutrons that stray too far away from a ^{3}He detector. Without the Cd fins, such neutrons would eventually arrive at the detector but at a time later than that of neutrons that scattered only in the polyethylene close to the detector. Their spatial or detector die-away time would thus be longer. In colloquial terms, the Cd fins force the neutrons to be detected either *immediately* upon reaching the detector region of the instrument or else not at all.

It may seem strange at first that the DDSI instrument should acquire a better signal by *not* detecting certain neutrons, i.e., those that run into the Cd fins. The advantage comes from having a cleaner signal with regard to the neutron coincidences, even though the overall magnitude of the signal decreases. The purpose of shortening the detector die-away time is to accentuate the distinction between it and the longer die-away time from fission-chain coincidences, since making this distinction is the chief goal of the DDSI analysis. In graphical terms, the kink in the elbow of the total Rossi-α/die-away curve shown in Figure 33 becomes more pronounced with the more distinction between the two constituent die-away curves.

4.2.2.3 Data analysis

Thus far, the NGSI's main metric for DDSI is the ratio of the count rate in the late gate to the count rate in the early gate [27]. This ratio will be called the "late-to-early" ratio hereafter, and it will be assumed that the gates will be chosen such that the early gate expresses primarily the fast die-away time and the late gate expresses primarily the slow die-away time. Since the count rate in the early gate is thus attributable to all kinds of fission (spontaneous, fast, and thermal) but the late gate is attributable only to induced, thermal fission chains, the late-to-early ratio is an indicator of the fraction of induced thermal fission relative to the total amount of fission. In other words, DDSI provides an indication of the strength of the second term of the neutron diffusion equation (Equation 3) relative to the sum of the strengths of the first and second terms, for the spent fuel assembly.

Importantly, neutron capture does not directly affect the early-gate's indication of total fission nor the late-gate's indication of induced fission, since neutron capture is a separate term (the third term) in the neutron diffusion equation. Neutron capture affects these indications only indirectly by reducing the numbers of neutrons detected and thus forcing the assay duration to be longer to accumulate sufficient statistics. (Note the important distinction that although neutron capture's shortening of the fission chains does affect the actual amount of induced fission, it does *not* affect DDSI's measurement of that actual amount of induced fission, which is the true issue of correlating between the NDA-measurements and physical-properties vector spaces; see Figure 82 and Section 6.2.1, below.) This fact means that these two DDSI measurements (actually taken simultaneously) are independent of the neutron leakage multiplication (M_L), which is a combination of both the second and third terms.

The DDSI also makes a third simultaneous measurement, namely, a TN measurement of all the neutrons emitted from the fuel assembly regardless of time coincidence. (In NC terminology, this measurement is the "accidental singles" rate.) As discussed in the TN and PNAR sections (4.1.1 and 4.1.2) and shown in Equation 7, a TN measurement *is* sensitive to neutron capture, since TN is sensitive to M_L and since capture is an integral part of M_L. Thus, when all three DDSI quantities—the early-gate measurement, the late-gate measurement, and the accidentals-gate (TN) measurement—are considered together, it is seen that all three of the variable terms of the neutron diffusion equation are represented in some fashion by one or more of these three quantities. The representation of all three terms is of the utmost importance to NDA logic, as will be explained in Section 6, and so DDSI's ability to provide such representation potentially makes it a very valuable NDA technique, as will be discussed in Section 7.

The NGSI also tried to make a direct correlation between the late-to-early ratio and the effective fissile content of the spent fuel assembly; the result is shown in Figure 37. (However, the late-to-early ratio in this figure is based on a Monte Carlo arrival-time analysis, which may have some problems, as discussed in the next paragraph.) The correlation exhibits the same kind of scatter in the data as the correlations for the neutron-multiplication NDA techniques (Figures 11, 14, 17, 25, and 26). Similar to the data analysis of the PNAR and CIPN techniques (Sections 4.1.2.3 and 4.1.3.3), a two-parameter correlation from both the late-to-early ratio and the singles count rate to the fissile content would reduce this scatter.

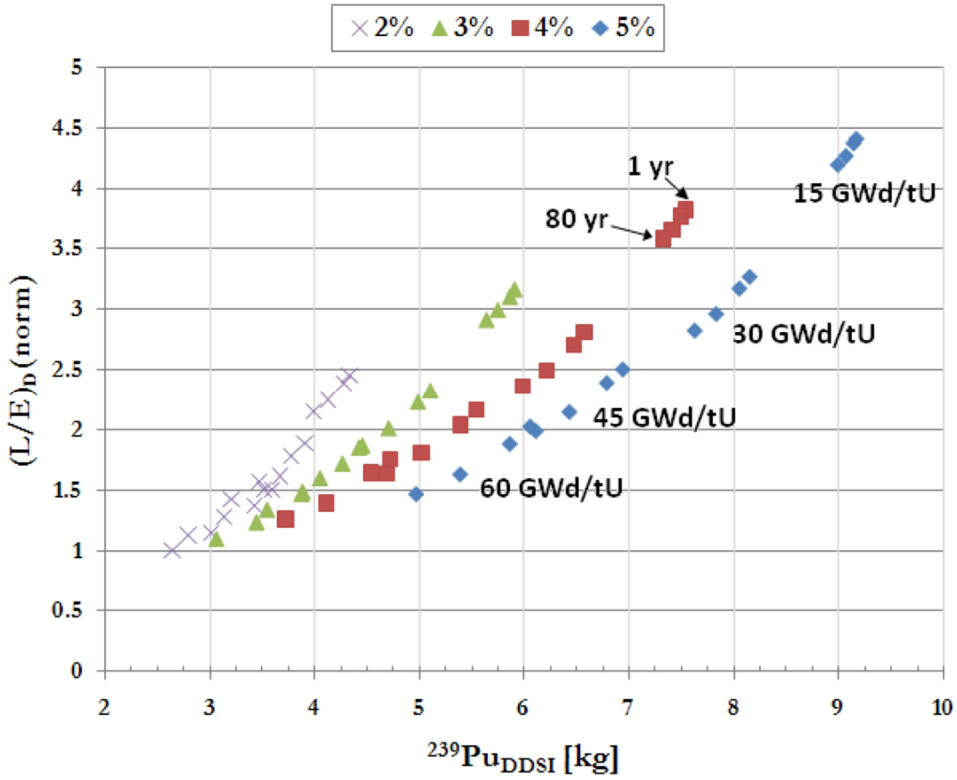

Figure 37: A correlation between the DDSI's late-to-early ratio and the effective fissile content of the 64 spent fuel assemblies from first library (Section 2.3); copied from Schear et al. [27] with permission from INMM.

The methodology for analyzing DDSI data is still in the early development stages, however. The NGSI's data analysis prior to the recent work by Kaplan et al. [212] was based only on Monte Carlo simulations of the distributions of arrival times of neutrons at the detectors. As mentioned previously at the end of the introduction to Section 4.2, the Monte Carlo arrival-time diagrams are not the same as Rossi-α diagrams. This fact led to some confusion and possibly to some mistakes in the earlier analyses. For instance, Schear et al. [27] applied the NM equations for Singles, Doubles, and Triples (Equations 21 through 23, above) to Monte Carlo arrival-time diagrams, but these equations require the subtraction of pairs and triplets from an "accidentals" gate, which was not included in the Monte Carlo analysis. Nevertheless, the Monte Carlo arrival-time diagrams have provided an initial understanding of the physics and characteristics of the DDSI technique, and the future work by the NGSI will make the connection to the experimentally measured data.

4.2.2.4 Limitations

The chief drawback of DDSI with regard to its equipment is its need for the thick and heavy Pb shield between the spent fuel assembly and the ^{3}He detectors. In addition to the bulkiness of the shield, the shield also adds to the distance separating the detectors from the fuel assembly. If it is considered that the Pb shield is part of the detector region, then this extra distance increases the detector die-away time. This effect needs to be investigated, in conjunction with a more general investigation of the violation of the point model (see below).

Another potential limitation that still needs to be investigated is how good the counting statistics will be for the three DDSI quantities: early-gate coincidences, late-gate coincidences, and accidental-gate total counts (TN). Certainly for fuel assemblies with low burnup, DDSI will face the same problem of poor statistics that the PNAR technique will (Section 4.1.2.4), since both techniques are passive techniques. Even for higher-burnup assemblies, though, the counting statistics of DDSI may not be very good, since like all NC techniques, DDSI's coincidence quantities depend upon the fraction of neutrons detected out of all the neutrons in the entire system, both fuel assembly and NDA instrument (i.e., the so-called "detection efficiency," ε; see the introduction to Section 4.2). The gross violation of the point-model assumption because of the presence of water in the fuel assembly and the massive Pb shielding around the assembly will probably make the detection efficiency to be poor, perhaps very poor, and this loss of efficiency will cause the accuracy of the early-gate and late-gate coincidence quantities to suffer. Additionally, the violation of the point model will probably skew the DDSI results significantly toward the outer rows of fuel pins, since the neutrons from those pins are more likely to survive the journey to the detectors.

At least two reference levels of accuracy can be identified: the accuracy of the late-to-early ratio and the accuracy of the absolute values of the coincidence counts in the early and late gates. The accuracy of the late-to-early ratio should always be superior (that is, easier to make good), because uncertainties that affect both gates should cancel out, somewhat or fully, in the ratio. The accuracy of the absolute counts in the gates should be more difficult to make good. In fact, the accuracies of the early and late gates should even be different from each other, with the accuracy of the early gate being better since it always gets more counts.

The varying levels of accuracy in the three DDSI measured quantities affect the utility of combining them to determine the three terms of the neutron diffusion equation, as discussed above and in Section 7. If only the TN and late-to-early-ratio quantities have decent accuracy, then DDSI can determine only these two independent quantities, not three, in actual practice. Another concern is that even though the three DDSI quantities are independent, they are only somewhat so; they are not at all close to being orthogonal. This description is evidenced by the fact that induced fission is part of all three quantities. In order to achieve an accurate three-dimensional correlation, then, it would be necessary to determine the three DDSI quantities to good levels of accuracy, which as has just been explained, may not be possible to do.

4.3 Distinguishing fissile material by neutron energy

Three of the NGSI's neutron-based NDA techniques (Table 10) determine the fissile content of a spent fuel assembly by the neutrons' interactions with the fissile isotopes' resonances at specific neutron energies. Since each isotope's resonances are unique to that isotope, these neutron-energy techniques make more or less direct measurements of the isotopes, rather than indirectly inferring the isotopes from their effects on the overall neutronic properties of the spent fuel assembly (Equation 3), which is what the other neutron-based NDA techniques do. In other words, the signals from the neutron-energy techniques are merely limited by the neutron-diffusion equation (Equation 3) rather than governed by it. By this fact, these neutron-energy techniques each have the potential for greater accuracy in the determination of the isotopic content than any single one of the other neutron-based NDA techniques. (See Section 6.)

There are three difficulties that these neutron-energy NDA techniques have in common and must overcome. The first difficulty is how to measure the neutrons' energies. Each of the three techniques measures the neutrons' energies in a different way. NRTA measures the energies in a neutron beam by the neutrons' times of travel down a flight tube of a specified length; this method is known as the time-of-flight method. LSDS measures the energies by the time that the neutrons take to slow down in a block of lead (Pb). SINRD measures the energies by whether or not the neutrons are absorbed in filter materials that allow only neutrons with sufficient energy to pass through. The second difficulty is that neutron energy is easily changed by neutron scattering, especially scattering from hydrogenous materials such as water. This fact is why the two active techniques, NRTA and LSDS, cannot operate if the spent fuel assembly is in water and why the passive technique, SINRD, is energy-sensitive only to the assembly's outer rows of fuel pins. The third difficulty is related to the second and is that neutron attenuation in general—whether scattering from the beam in NRTA or self-shielding absorption in LSDS and SINRD—tends to overwhelm these techniques' signals. The two active techniques—NRTA and LSDS—somewhat compensate for attenuation by demanding exceptionally strong neutron sources or long measurement times.

4.3.1 Neutron Resonance Transmission Analysis (NRTA)

Name	Neutron Resonance Transmission Analysis (NRTA)	
References	NGSI: [29-31, 216, 217] Other: [218-228]	
Measurement environment	In air or other gas	
Passive vs. Active	Active	
	One 8-pin measurement (PWR): [30]	$3 \cdot 10^{11}$ n/s ↔ 13 hour $1 \cdot 10^{13}$ n/s ↔ 20 min
	Thirty-six 8-pin measurements (≈ a full PWR assembly) at one axial position on the assembly:	$3 \cdot 10^{11}$ n/s ↔ 20 days $1 \cdot 10^{13}$ n/s ↔ 12 hour
Time dependency	Time-dependent (pulsed)	
Particles detected	Neutrons	
Type of detectors	^{3}He detectors or other kinds of detectors	
Particles' detected attribute	Energy	
Governing physical properties of the fuel assembly	Neutron energy resonances of specific isotopes (The resonances can be for scattering and capture as well as for fission.)	
Governing isotopes	All isotopes that have resonances for neutrons below about 50 eV, which includes all U and Pu isotopes, some Am isotopes, and some fission products [31]	
Maturity	Has been done for many years for cross-section measurements and on smaller samples of used nuclear fuel, but has not yet been done on entire fuel assemblies	
Limitations	Severe attenuation of the neutron beam through an entire fuel assembly, which forces the need either for extremely strong beams or for long measurement times Cannot be performed with the fuel assembly in cooling water, which attenuates the beam too much Beam must be aligned well with the fuel pins Cost of a strong pulsed neutron source Must be a dedicated facility because of the large size of the time-of-flight setup	
Selected by the NGSI for prototype testing?	No	

4.3.1.1 Principle of operation and the NGSI's design

Neutron Resonance Transmission Analysis (NRTA) is an active NDA technique that transmits a pulsed beam of neutrons through the fuel assembly. (See Figure 38.) The pulse contains neutrons over a span of energies. The resonances of the isotopes in the fuel preferentially remove neutrons with the resonant energies, thereby imparting a characteristic signature into the transmitted beam. (See Figure 39.) The transmitted beam is detected, and the resonance chasms in the detected spectrum are separated from each other by analysis. The

strength (depth) of a characteristic resonance chasm is related to that isotope's quantity in the sample. Conceptually, then, NRTA is somewhat like shining a flashlight beam through several sheets of translucent paper to see what is written on them.

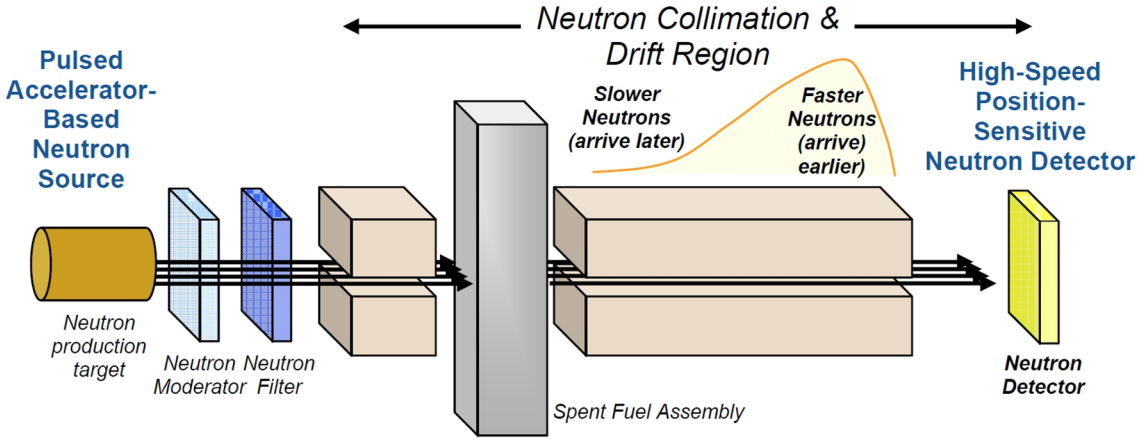

Figure 38: "Schematic representation of the NRTA measurement approach."
Copied from Chichester and Sterbentz [31] with permission from INMM.

This technique was originally used to measure the cross sections of pure-isotopic samples; the NDA application inverts this problem by using known cross sections to determine unknown composition. The equation is simply

$$I(E) = I_0(E)e^{-\Sigma\{Nx\sigma_t(E)\}}, \qquad \text{Equation 24}$$

where I is the transmitted intensity, E is the neutron energy, I_0 is the original intensity without the fuel assembly, x is the thickness through which the beam passes, N is the atomic volume density, and σ_t is the microscopic total cross section. The summation in the exponent covers the case when the sample consists of a mixture of isotopes; the quantities in the braces then change with each isotope. For a homogeneous mixture, the thickness x is the total thickness and can be brought outside the summation. (Schrack et al. [219] present this equation in a different form that also accounts for experimental uncertainty in the neutron energy.) The basic physics of NRTA are thus seen to be quite simple.

In NRTA, the energies of the neutrons are determined by the time-of-flight (TOF) method. In the TOF method, a pulse of neutrons of many energies is created at one end of a long "flight" tube, which is just a tube that either is evacuated or is filled with air or other gas. The neutrons travel down the flight tube, pass through the fuel assembly, and continue on to the neutron detector. (See Figure 38.) In order to protect the neutron detector from most of the background neutrons created by spontaneous fission in the fuel, a second flight tube (or collimator) is also used after the fuel assembly, between it and the neutron detector. The distance between the pulse source and the neutron detector is the flight length. Because the neutrons' energy is non-relativistic kinetic energy, the higher energy neutrons move faster and travel this flight length sooner than the lower energy ones do. By measuring the time between the start of the pulse and the detection of a neutron—that is, the time of flight—the energy of the detected neutron is determined (Table 12).

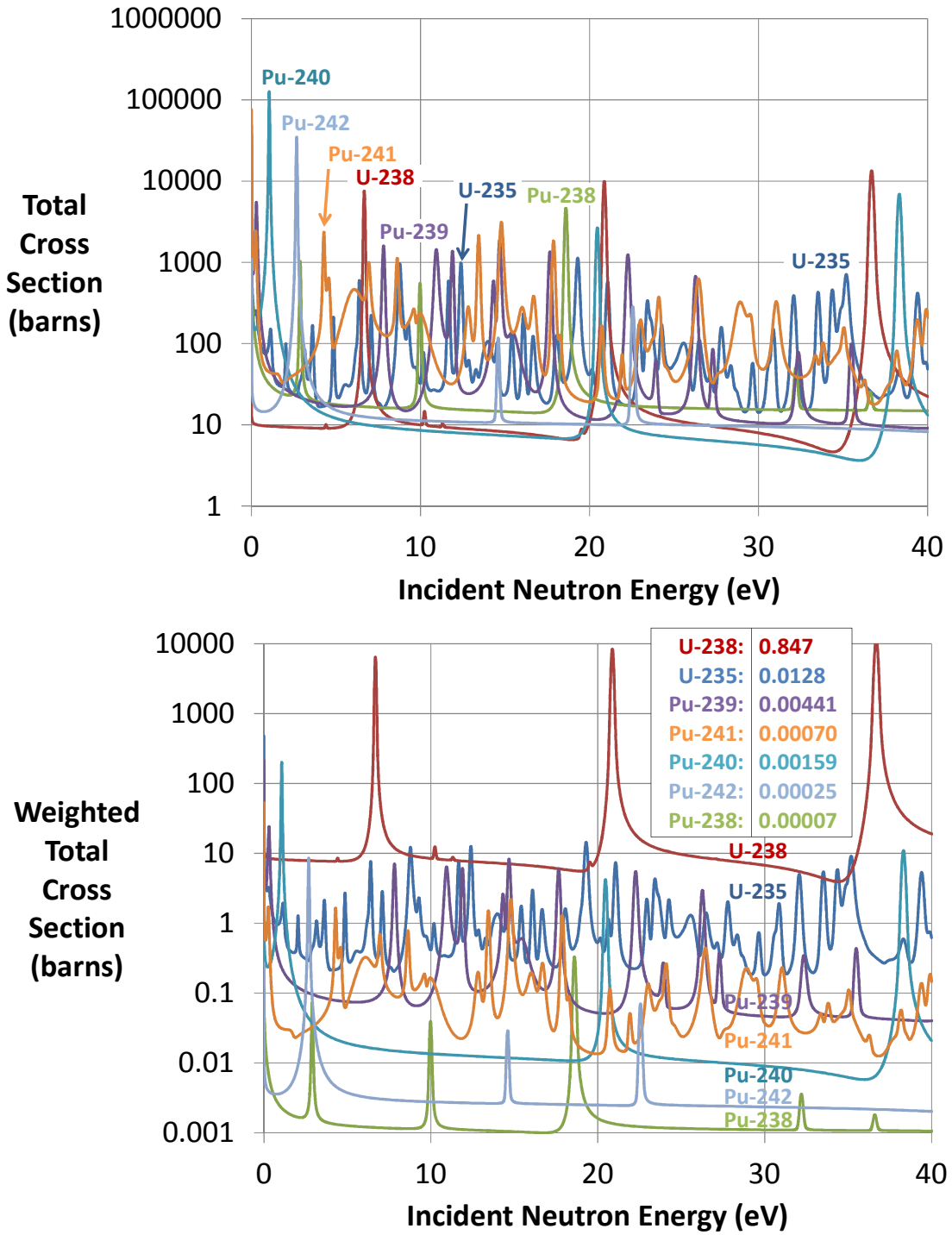

Figure 39: The total neutron cross sections of important U and Pu isotopes in used LEU and MOX fuel. Top: Cross section per nucleus. Bottom: Cross sections weighted by the average weight fractions of the isotopes in a PWR spent fuel assembly, 4% initial enrichment, 30 GWd/MT burnup, 5 years cooling time. The cross-section data are from ENDF [125] and were interpolated with the aid of Zerkin's plotting program [229]. The weight fractions are from LaFleur's Table E.1 [87] and are indicated in the table.

Table 12 also reveals that the detector must be able to count neutrons rapidly in order to distinguish among neutrons with high energies. For example, the difference between 19.9 eV and 20.0 eV is only 0.2 μs, so to distinguish between these energies, the detector must be able

to count at 500 kHz, at least (1 count/0.2 μs = 500 kHz). Between 39.9 eV and 40.0 eV, the time difference reduces to only about 70 ns, which corresponds to 1.4 MHz. Detectors that can count in the low megahertz range (1 MHz to 5 MHz) are available, so this level of energy resolution is achievable [31, 230]. Of course, these times of flight are specifically for a 5 m flight path; longer flight tubes increase the time differences between neutrons of different energies and thereby ease the count-rate requirements. Chichester and Sterbentz have determined that a 5 m flight path and an examination up to 40 eV should yield sufficiently good NRTA data while minimizing cost [30, 31].

Table 12: Time-of-Flight Calculations

Neutron Energy	Neutron Velocity	Time of Flight over a 5 m Distance
(eV)	(m/s)	(μs)
0.1	4374	1143.1
0.9	13122	381.0
1.0	13832	361.5
9.9	43520	114.9
10.0	43739	114.3
19.9	61702	81.0
20.0	61857	80.8
39.9	87369	57.23
40.0	87479	57.16
50.0	97804	51.12

Table 12 also indicates the maximum pulse rate of the NRTA system. If 0.1 eV is the lowest energy that will be investigated, then the pulses must be chronologically spaced at least by the flight time of the 0.1 eV neutrons—1143 μs. This time corresponds to 875 Hz. In actuality, the maximum pulse rate must be less than this value, because other processes besides the flight time, such as the moderation time, have not been included.

Much consideration has been paid to the availability of neutron sources for an NRTA system [30]. A neutron intensity of about 10^{13} neutrons per second, emitted isotropically in three dimensions, is required to achieve adequate statistics in a reasonably long measurement time of 12 hours per PWR fuel assembly [30]. This neutron source strength is beyond the capabilities of typical D-D neutron generators (10^5 to 10^8 neutrons/s) and D-T neutron generators (10^7 to 10^{10} neutrons/s) [182]. Therefore, a system based on an electron accelerator must be used instead. More specifically, a lower-neutron-energy, higher-neutron-flux system is desired, since only neutrons with 40 eV or less energy are useful. The NGSI's suggested configuration combines a linear electron accelerator, a high-Z target, and a photonuclear source, such as beryllium or heavy water [30]. The accelerator brings the electrons up to 10 MeV; they collide with the high-Z target to produce bremsstrahlung gamma-ray photons; and the gamma-ray photons induce photonuclear reactions in the beryllium or heavy water to produce high-energy neutrons. The neutrons then pass through a low-Z moderator to bring

their energies down to about 40 eV and less, at which point they enter the collimator/flight-tube to go to the fuel assembly and the detector. (See Figure 38.) Lastly, it would be most efficient to set up several flight tubes around the neutron source, because the source produces neutrons in all directions. Such a configuration, called "multiplexing," would conserve neutrons and would speed up the average measurement time per fuel assembly, since multiple fuel assemblies could be examined simultaneously from the same neutron source [30].

4.3.1.2 Data analysis

A simple example of how to analyze NRTA data is illustrated by Figure 40 and Equation 25. In this example, the 10.93 eV resonance of ^{239}Pu is analyzed. It is assumed that this resonance is sufficiently isolated from all other resonances and that the non-resonant attenuation of the beam has already been taken into account, perhaps through calibration. The transmitted strength of the beam at the resonance chasm, b, is measured as a proportion of the total transmitted beam outside the resonance chasm, $a+b$. Rearrangement of Equation 24 produces an equation for the transmission factor, T:

$$T(E_r) = \frac{I(E_r)}{I_0(E_r)} = \frac{b}{a+b} = e^{-Nx\sigma_t(E_r)} \qquad \text{Equation 25}$$

All these variables are known except for the ^{239}Pu density, N, so the equation can be solved for it. This example is simplified; in practice, computerized analyses are required to account for other variables, such as Doppler broadening and geometric effects [224, 225, 231].

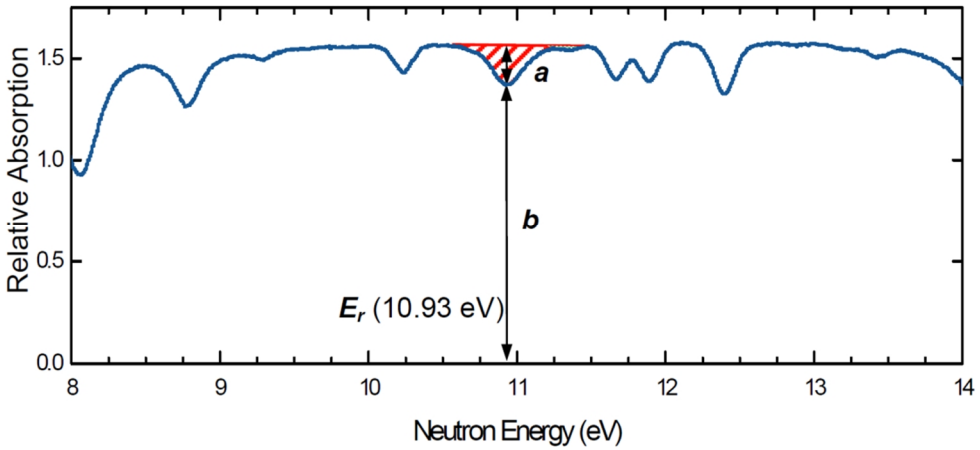

Figure 40: "Estimation of the transmission factor (T) using the 10.93 eV resonance depression from ^{239}Pu. The transmission factor T is simply given by $T = b/(a+b)$." Copied from Figure 10 in Sterbentz and Chichester [30].

A big advantage of NRTA is that any isotope with resonances can be examined, not just the fissile isotopes. Thus, the quantities of other minor actinides and certain fission products can also be measured; see Table 13. Chichester and Sterbentz at Idaho National Laboratory (INL) have demonstrated that the NRTA technique can detect all of the uranium and plutonium isotopes shown in Figure 39 except ^{238}Pu. They state that the NRTA technique can also detect ^{234}U, ^{241}Am, and ^{243}Am [31]. They have also identified six important fission products with resonances in the neutron-energy range from 0.1 eV to 40 eV: ^{99}Tc, ^{103}Rh, ^{131}Xe, ^{133}Cs, ^{145}Nd, and ^{152}Sm [29-31]. (In their first report, Chichester and Sterbentz also

discussed the measurement of the 18.3 eV resonance of ^{147}Sm as a possible way of determining the cooling time of a fuel assembly, since ^{147}Sm is a decay product of ^{147}Pm. It is not clear why this isotope was subsequently removed their list.) NRTA can therefore directly detect all these important isotopes, unlike most other NDA techniques.

Table 13: Isotopes that the NGSI claims can be measured in spent fuel by NRTA, along with the energies (in eV) of resonance chasms that were identified in the range of 0 eV to 40 eV in simulated NRTA transmission measurements [29].

^{99}Tc	5.9		
^{103}Rh	1.25		
^{131}Xe	14.4		
^{133}Cs	5.9		
^{145}Nd	4.35		
^{147}Sm	18.25		
^{152}Sm	8.1		
^{234}U			
^{235}U	3.6	4.8	8.8
	11.65	12.4	19.4
	32.0	33.5	34.4
	35.2		

^{236}U	5.45		
^{238}U	6.67	10.25	21.0
	36.8	66.3	81.1
	20.9	36.8	
^{239}Pu	0.3	10.9	11.9
	17.6		
^{240}Pu	1.05		
^{241}Pu	13.4		
^{242}Pu	2.65		
^{241}Am			
^{243}Am			

Conversely, NRTA is insensitive to most of the other isotopes that are present in spent fuel assemblies but are unimportant [31]. These isotopes include the oxygen of the UO_2 fuel pellets and the zirconium, tin, iron, chromium, niobium, nickel, carbon, and silicon of the Zircaloy-4 cladding. Hydrogen impurity in the cladding and the gaseous isotopes in air are also not able to be detected. The reason is that none of these isotopes have any resonance structure in the neutron-energy range from 0.1 eV to 40 eV. This insensitivity to these unimportant isotopes improves the signal-to-noise ratio.

4.3.1.3 Limitations

The first limitation of NRTA is the required strength of the neutron source versus the required measurement time. (See the discussion above in Section 4.3.1.1.) To assay a spent PWR fuel assembly within a day, the source must produce on the order of 10^{13} neutrons per second, which is beyond the capabilities of D-D and D-T neutron generators and is at the upper limits of systems based on electron linacs. Multiplexing, in which several spent fuel assemblies are assayed simultaneously from the same neutron source, seems to be the most promising way to bring the average measurement time per assembly down to a reasonable level. Of course, this solution means that NRTA would be applicable mostly to large measurement campaigns rather than to the ad hoc assaying of only one or two assemblies.

NRTA cannot measure a spent fuel assembly in water; the fuel assembly must be in gas or vacuum. The reason is that the water eliminates the signal because it scatters too many of the neutrons out of the neutron beam. This restriction may be the most severe limitation on the applicability of NRTA, since fuel assemblies must be cooled in water for at least the first five years after being discharged from the reactor [232]. Only well-cooled fuel assemblies can be analyzed by NRTA, and even then, forced air cooling may be necessary [30].

For similar reasons, the number of pins in a line that can be examined accurately by NRTA is restricted to about 8 pins; only limited information can be obtained from up to 12 pins. As the number of pins in a line increases, the NRTA signal becomes increasingly attenuated, primarily due to non-resonant scattering. This situation causes a problem for the examination of PWR fuel assemblies, which usually are in an array of 17 pins by 17 pins (Figure 41). By examining pins along the diagonals of the fuel assembly, though, the maximum number of pins through which the beam must pass is reduced to 12 pins, because several of the "pins" are not actually fuel pins but are empty guide tubes. The diagonals that contain more than 12 pins do not need to be measured, because the fuel assembly can be rotated so that those pins can be examined along other diagonals that contain 12 pins or fewer. Since only 8 pins can be examined thoroughly, though, the PWR geometry still prevents the accurate measurement of the innermost pins, which may be a problem in some cases.

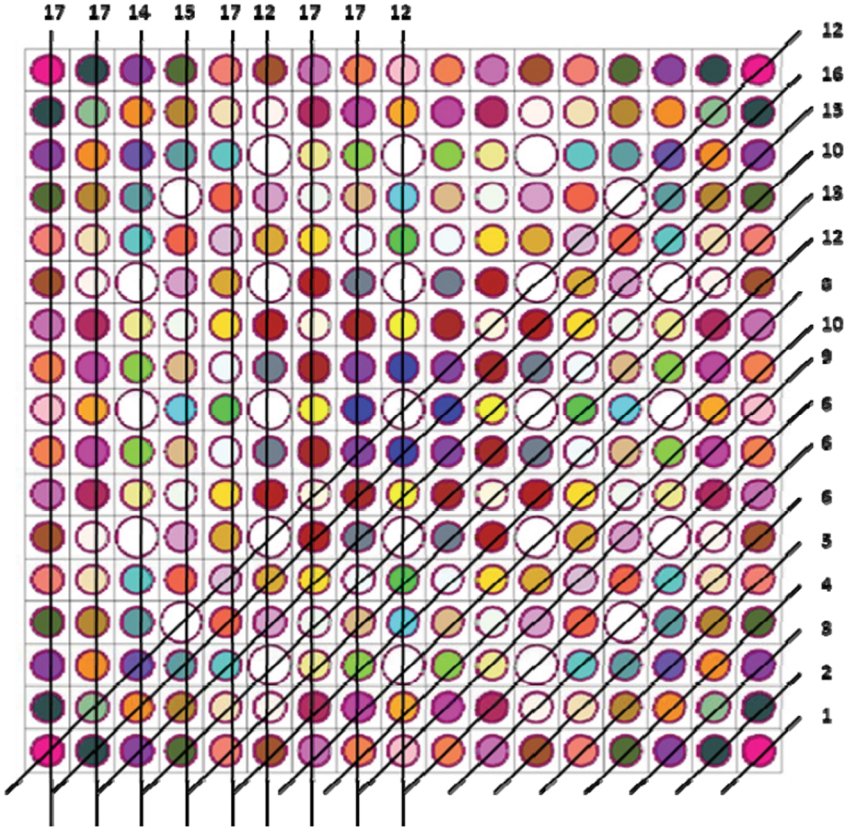

Figure 41: A "PWR 17 x 17 fuel assembly showing number of fuel pins in the vertical columns and [along the] diagonal lines." Copied from Sterbentz and Chichester [29].

The alignment of the fuel pins is a related issue. If the pins are not aligned precisely with the neutron beam, then many neutrons may miss one or more fuel pins. Although this situation would not change the relative proportions of the resonances, it would scale up the overall count rate of the entire spectrum. This increase would probably complicate the determination of the absolute quantities of the isotopes. The diameter of the neutron beam also plays a factor in this alignment problem. It appears that this alignment issue remains as an area for further research [29, 30].

4.3.2 Lead Slowing-Down Spectroscopy (LSDS)

Name	Lead Slowing-Down Spectroscopy (LSDS)
References	NGSI: [32, 33, 35, 36, 233-240] Other: [34, 181, 241-274]
Measurement environment	In air or other gas
Passive vs. Active	Active; neutron strength = 10^{13} n/s · 1 hour ≈ 10^{16} n [35, 240]
Time dependency	Time-dependent (pulsed)
Particles detected	Neutrons
Type of detectors	High-purity ^{238}U or ^{232}Th fission chambers, and perhaps ^{235}U, ^{239}Pu, and ^{241}Pu fission chambers
Particles' detected attribute	Energy
Governing physical properties of the fuel assembly	Neutron energy resonances for fission of fissile isotopes
Governing isotopes	Fissile isotopes; neutron-capturing isotopes, especially those with capture resonances between 0.1 eV and 10 keV
Maturity	Has been done for many years for cross-section measurements and on smaller samples of used nuclear fuel, but has not yet been done on entire fuel assemblies
Limitations	Cannot be performed with the fuel assembly in cooling water Cannot be performed if there is a significant amount of moderating material in the fuel assembly or assay chamber. This includes hydrogen absorption into the zircaloy cladding. Self-shielding of the fuel assembly Cost of the lead and of the strong neutron source Probably must be a dedicated facility because of the large size and weight Difficulty of obtaining, transporting, and using fission chambers made from ^{239}Pu and ^{241}Pu (if used)
Selected by the NGSI for prototype testing?	No

4.3.2.1 Principle of operation and the NGSI's design

Lead slowing-down spectroscopy (LSDS) is an active NDA technique in which the nuclear fuel assembly is placed into the middle of a large block of lead (Pb). (See Figure 42.) A neutron generator creates a pulse of neutrons in the middle of this block of Pb, near to the fuel assembly. The neutrons in the pulse scatter throughout the block of Pb, and some leak out. Many stay inside the block, though, and pass back and forth through the fuel assembly as they scatter off the Pb nuclei. As the neutrons scatter, they slow down, first by inelastic collisions and then, below about 100 keV, by elastic collisions (Figure 43). LSDS works during the lower energy part when only elastic collisions occur; usually the energy range below 10 keV is considered [32, 262]. As the neutrons slow down and lose energy, their energies pass through the energy resonances for fission of the fissile isotopes inside the fuel assembly. So at

the times when the energy of the neutrons matches the energy of an isotope's fission resonance, the atoms of that particular isotope have a much higher probability of fissioning.

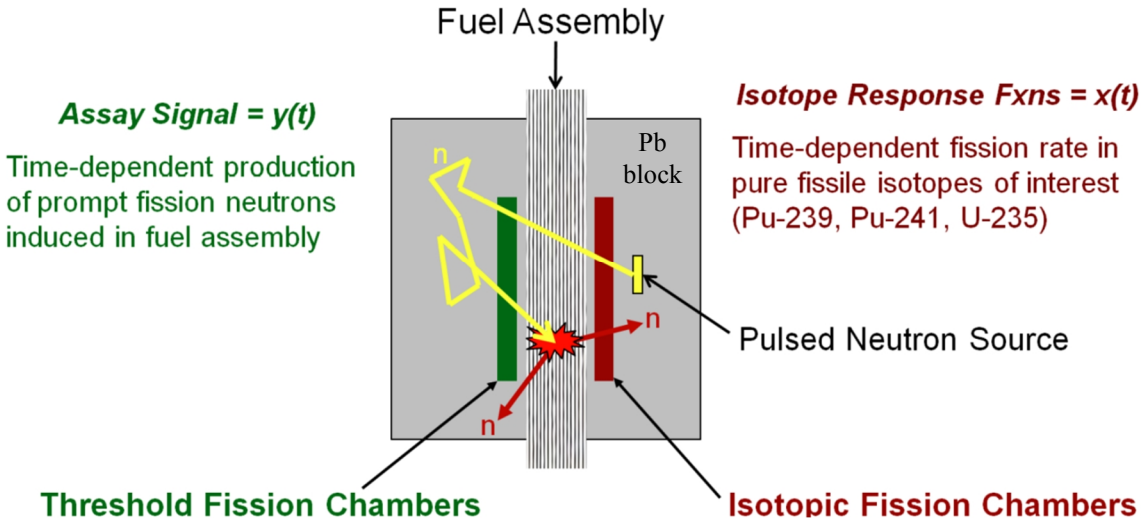

Figure 42: Schematic of a lead-slowing-down spectrometer; modified from Kulisek et al. [33].

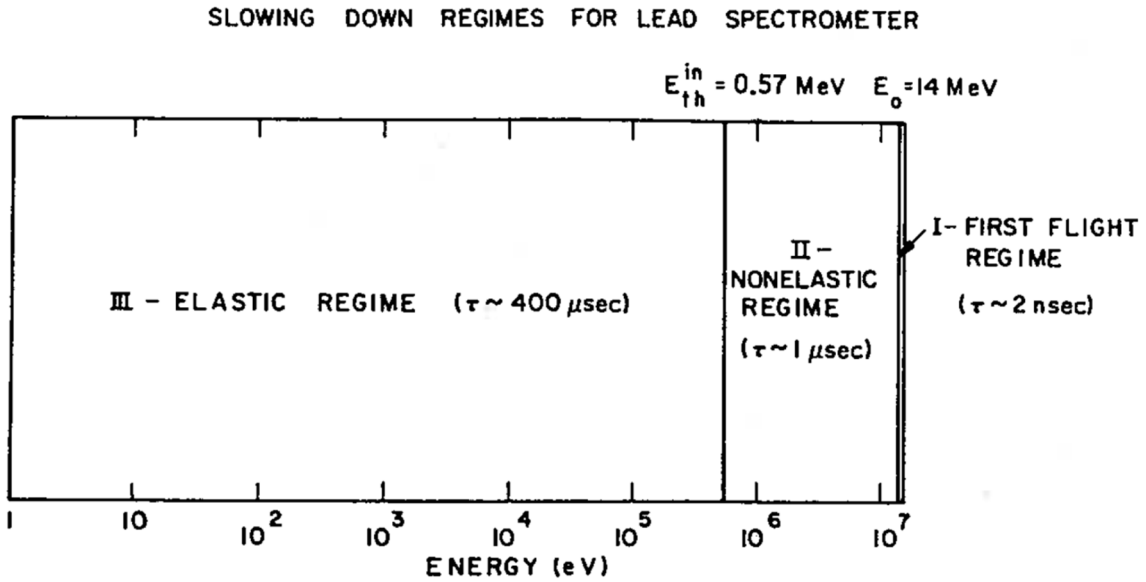

Figure 43: "The different energy regimes and corresponding characteristic times for lead," from Sawan and Conn [248].

As those atoms fission, they release several neutrons. These fission neutrons can be distinguished from the pulse's neutrons by the fact that the fission neutrons have high energy (greater than 1 MeV, on average), whereas the pulse's neutrons have low energy (below 10 keV). Indeed, these fission neutrons are so fast that they are above the fission threshold energies of ^{238}U and ^{232}Th, which are about 1 MeV. For this reason, special fission chambers, called threshold fission chambers, are placed next to the fuel assembly in the Pb block. These fission chambers do not contain any fissile material but contain only ^{238}U or ^{232}Th. Therefore, they do not react with the pulse's neutrons except at the very start, when the neutrons are still above 1 MeV. Later, during the interrogation phase (below 10 keV), these threshold fission chambers react only when fissile isotopes in the fuel assembly fission and release fast

neutrons. The threshold fission chambers' signals therefore correspond to the fission events in the fuel assembly. The time at which a fission event occurs corresponds to the energy of the neutrons that induce the fission, as will be explained next.

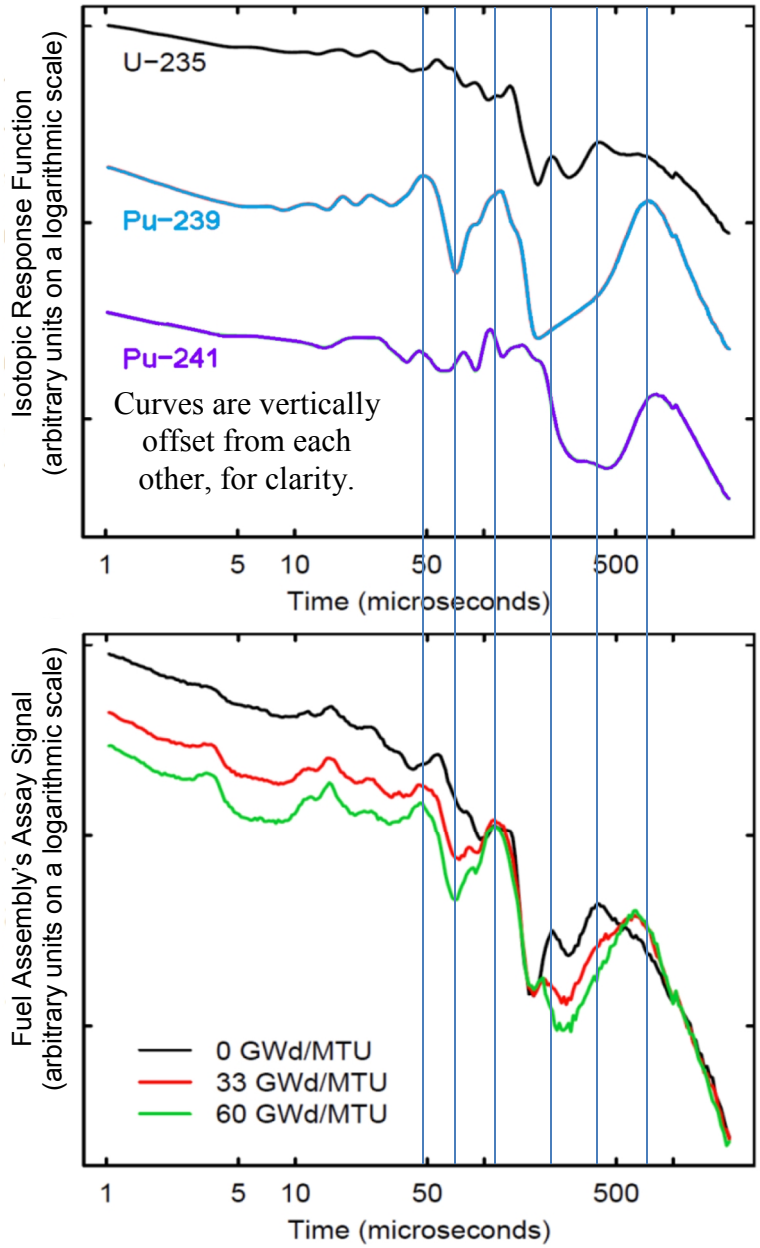

Figure 44: Top: the LSDS response of the three main fissile isotopes (as measured by the isotopic assay fission chambers). Bottom: the LSDS response of an entire fuel assembly (as measured by the threshold fission chambers), with burnup as a parameter. Modified from Smith et al. and Kulisek et al. [33, 233].

LSDS is similar to NRTA in that the time-dependent response of the nuclear fuel to a pulse of neutrons from an external source is measured, with the energy of the neutrons being directly correlated to the time dependence. In both techniques, the energy of the neutrons is a precise function of the time after the beginning of the pulse, so by measuring the *time* at which a neutron is detected, we can know the *energy* of that neutron. The unique energy-

dependent resonance signatures of the various isotopes, particularly the fissile isotopes, appear in this time-dependent response. (See Figure 44 for an example.) Thus, the isotopic composition of the fuel can be found by analyzing the time-dependent and energy-dependent response of the fuel to the neutron pulse.

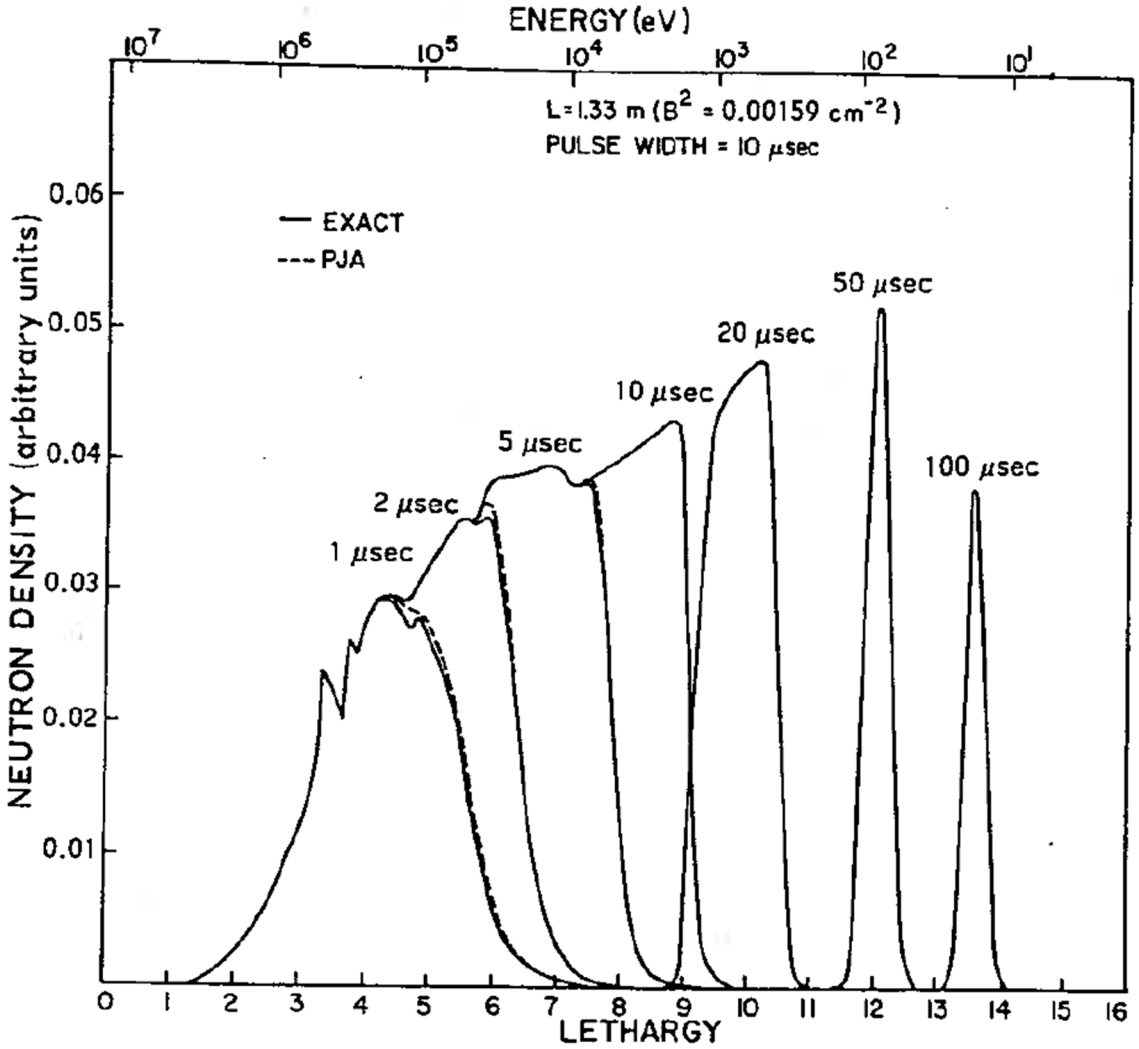

Figure 45: "The neutron density as a function of energy and time for a pulse width of 10 μs in the University of Wisconsin [lead slowing-down spectrometer]" Copied from Figure 3 in Sawan and Conn [248]. Copyright 1974 by the American Nuclear Society, La Grange Park, Illinois

The initial and major difference between NRTA and LSDS is that, while NRTA determines the energies of the neutrons in the pulse by their times of flight, LSDS determines their energies by the time that it takes for them to slow down in a large Pb block. In NRTA, the pulse is first moderated to have a broad energy spectrum, so that it contains neutrons of various energies; and the flight tube then merely sorts them in order of decreasing energy. In LSDS, the entire pulse slows down together via scattering collisions with the Pb nuclei (Figure 45). Therefore, in NRTA, the flight tube serves only to *indicate*, to the detector, the energy of each neutron; the energy of the neutron as it interacts with the sample has no connection at all with the flight tube. In contrast, the moderation in Pb in LSDS serves the dual purposes of *changing* the neutrons' energy to cause them to interact with the sample and

of *indicating* this energy to the detectors. It simultaneously achieves both purposes by changing the energy in a precise and consistent way after the beginning of the pulse.

Previously, NRTA was compared to shining a flashlight beam through sheets of paper, but this metaphor does not suitably describe LSDS. Instead, LSDS is more like heating up an unknown object with a pulse of heat and then letting it cool down. As the object cools down over time, it emits a certain signal whenever the temperature equals some "resonant" temperature. Although we cannot directly measure the temperature with a thermometer, we do know how fast it cools down, so by measuring the time after the heating pulse, we know its temperature. The temperatures at which the object emits signals are characteristic of its composition.

Of course, only fission produces a signal. Isotopes that capture neutrons reduce this signal. Geometric effects, especially the effect known as "self-shielding," also complicate the total signal. These aspects will be discussed in Section 4.3.2.4.

The NGSI did not select a specific kind of neutron generator for the LSDS; they simply stated that they expect to need a total of about 10^{16} neutrons to achieve a reasonably accurate assay [33]. For an assay time of one hour, this strength implies a generation rate of 10^{12} to 10^{13} neutrons per second. This rate is above that of typical D-D and D-T neutron generators (10^{8} n/s and 10^{10} n/s, respectively [182]), so it requires making photoneutrons by creating an electron beam with an electron accelerator and striking it against a heavy-metal target, as is done for the NRTA technique; see Section 4.3.1.1. For example, the lead slowing-down spectrometer at Rensselaer Polytechnic Institute (RPI) uses an air-cooled, tantalum target that is placed in the middle of the spectrometer [274].

4.3.2.2 Derivation of the time-energy relationship

Much of the recent literature about LSDS has quoted Lee et al. [259] for the equation that relates the slowing-down time to the energy of the neutrons:

$$E = \frac{k}{(t + t_0)^2} \qquad \text{Equation 26}$$

Unfortunately, this reference gives no indication of the source of this equation and therefore leaves the impression that it is purely empirically derived. This is not the case, however. Actually, this relationship was published in a different form in the first international paper on LSDS, by Bergman et al. in 1956 [241]. This paper does not give a derivation, however. Williams [275] comes close to deriving it from the general theory but stops short of presenting it in a simple form. (The argument of the delta function in Equation 9.220 on page 424 in his book must be set equal to zero and solved.) Conn and Sawan [246] finish this connection mathematically in Equation 7 of their paper, yet the context is complicated and prevents a ready grasp of the result. The mathematics in Pál and Pázsit's paper is also complicated [267]. Chabod [181] lists a couple of references for derivations, but neither of them is conveniently available in English. Cramer et al. [249] give a simple derivation, but it is in an obscure internal report from Knolls Atomic Power Laboratory that is difficult to obtain. In 2002, the American Nuclear Society republished Lamarsh's 1966 book on nuclear reactor theory—*not* on LSDS—which contains a simple derivation (Section 6-17) of the form

of the equation reported by Bergman et al [276]. In short, a clear and simple derivation of Equation 26 as applied to LSDS is difficult to find in the literature.

For this reason and because the purpose of this report is to give an intuitive understanding of the theory, a simple and heuristic derivation that is similar to Cramer's and Lamarsh's derivations will be given here. This seemingly enigmatic relationship (Equation 26) can surprisingly be derived by considering the simple formula, "Distance = Speed * Time," for the neutrons. The "distance" here is the mean free path between collisions, λ, which is the reciprocal of the transport macroscopic cross section, Σ_{tr}; and of course, the neutron speed is related to the neutron energy ($E=mv^2/2$). In Pb, Σ_{tr} is basically constant with energy over the range from 10 keV down to thermal energies (0.01 eV) [125]. Therefore, λ is also constant over this energy range.

The time, t_i, between the i^{th} pair of collisions is therefore given by the simple formula:

$$t_i = \frac{\lambda}{v_i} \qquad \text{Equation 27}$$

Here, v_i is the neutron's velocity after the first collision of the pair. If we consider a succession of n collisions, then the total time for these n collisions to occur is given by summing up these times:

$$t = \sum_{i=0}^{n} t_i = \sum_{i=0}^{n} \frac{\lambda}{v_i} = \lambda \sum_{i=0}^{n} \frac{1}{v_i} \qquad \text{Equation 28}$$

During these n collisions, the neutron velocity declines from an initial velocity v_0 to a velocity v.

We now make the transition from a discrete summation to a continuous integration, under the assumption that each collision produces an infinitesimal loss of velocity. This approximation is not too bad for a heavy moderator like Pb, as will be shown below. Equation 28 then becomes as follows:

$$t = \lambda \int_{\tilde{n}=0}^{\tilde{n}=n} \frac{1}{\tilde{v}} d\tilde{n} \qquad \text{Equation 29}$$

Here, tildes are used to indicate the dummy variables of integration.

The next step is to convert the variable of integration from being the number of collisions to being the velocity:

$$t = \lambda \int_{\tilde{v}=v(\tilde{n}=0)}^{\tilde{v}=v(\tilde{n}=n)} \frac{1}{\tilde{v}} \left(\frac{d\tilde{n}}{d\tilde{v}}\right) d\tilde{v} = \lambda \int_{\tilde{v}=v_0}^{\tilde{v}=v} \frac{1}{\tilde{v}} \left(\frac{d\tilde{v}}{d\tilde{n}}\right)^{-1} d\tilde{v} \qquad \text{Equation 30}$$

The change in velocity per collision is the derivative, $d\tilde{v}/d\tilde{n}$.

The following step uses equations in terms of neutron lethargy, u, instead of neutron velocity. Lethargy is defined with reference to a maximum neutron energy, E_0, which in this case, is the initial energy of the pulse:

$$\tilde{u} = \ln\frac{E_0}{E}$$ Equation 31

Therefore, we apply the chain rule:

$$\frac{d\tilde{v}}{d\tilde{n}}\cdot\frac{d\tilde{E}}{d\tilde{v}}\cdot\frac{d\tilde{u}}{d\tilde{E}} = \frac{d\tilde{u}}{d\tilde{n}} = \xi, \text{the average change in lethargy per collision}$$ Equation 32

This quantity, ξ, is a constant for elastic scattering and is simply a function of the atomic mass of the nuclei, A (e.g., A = 204, 206, 207, or 208 for the natural Pb isotopes):

$$\xi = 1 - \frac{(A-1)^2}{2A}\ln\left(\frac{A+1}{A-1}\right)$$ Equation 33

So for ^{208}Pb, ξ equals 0.009585, a small number that justifies our earlier approximation of infinitesimal loss of velocity per collision. The change in energy with velocity and the change in lethargy with energy are given as follows:

$$\tilde{E} = \tfrac{1}{2}m\tilde{v}^2 \text{ therefore } \frac{d\tilde{E}}{d\tilde{v}} = m\tilde{v}$$ Equation 34

$$\tilde{u} = \ln\frac{E_0}{E} \text{ therefore } \frac{d\tilde{u}}{d\tilde{E}} = -\frac{1}{\tilde{E}}$$ Equation 35

(m is the mass of the neutron.) Plugging these quantities into Equation 32 produces an expression for $d\tilde{v}/d\tilde{n}$:

$$\frac{d\tilde{v}}{d\tilde{n}} = \frac{\xi}{\frac{d\tilde{E}}{d\tilde{v}}\cdot\frac{d\tilde{u}}{d\tilde{E}}} = \frac{\xi}{(m\tilde{v})\left(-\frac{1}{\tilde{E}}\right)} = -\left(\frac{\xi\tilde{E}}{m\tilde{v}}\right)\left(\frac{\frac{1}{2}m\tilde{v}^2}{\tilde{E}}\right) = -\frac{\xi\tilde{v}}{2}$$ Equation 36

Thus, $d\tilde{n}/d\tilde{v} = -2/\xi\tilde{v}$, and Equation 30 can be evaluated:

$$t = \lambda\int_{\tilde{v}=v_0}^{\tilde{v}=v}\frac{1}{\tilde{v}}\left(-\frac{2}{\xi\tilde{v}}\right)d\tilde{v} = \frac{2\lambda}{\xi}\int_{\tilde{v}=v}^{\tilde{v}=v_0}\frac{1}{\tilde{v}^2}d\tilde{v} = \frac{2\lambda}{\xi}\left(\frac{1}{v}-\frac{1}{v_0}\right)$$ Equation 37

Equation 37 is basically the form given by Bergman et al [241]. Substituting the energy for the velocity (Equation 34) and rearranging produces the form derived by Conn and Sawan [246] and used by Lee et al. [259]:

$$E = \frac{k}{(t+t_0)^2}$$
$$\text{where } k = 2m\left(\frac{\lambda}{\xi}\right)^2 \text{ and } t_0 = \frac{2\lambda}{\xi v_0}$$ Equation 38

Thus, it has been shown that the heart of LSDS is actually not very complicated; it is "Distance = Speed * Time" for the neutron pulse, as the neutrons bounce around off the Pb atoms inside the Pb cube of the spectrometer.

Other values for k and t_0 in Equation 38 can be derived theoretically [181] or experimentally [241, 248, 272]. Indeed, Pál and Pázsit say that the values in Equation 38 are not just inaccurate but wrong, having been derived from a bad assumption [267]. Nevertheless, this derivation is easy to understand and illustrates the basic physical concepts.

The width of the pulse in the time-energy spectrum is also critically important in LSDS. If the pulse width is narrow, then the energy resolution is correspondingly good, so that the resonances of the isotopes can be resolved. Otherwise, the signal is blurry and worthless. As Figure 45 illustrates, the pulse width in pure lead is narrow. In fact, even if the pulse is wide initially (as in Figure 45), it will become narrower as it scatters in the lead, through a process called "energy focusing." Williams explains energy focusing in this way: "[I]n a given time interval, neutrons with a larger velocity undergo more collisions and thus lose more energy than neutrons of lower velocity," (pages 421 and 422 of Williams [275]). So for a wide initial pulse, the neutrons that arrive later in the lead block "catch up" to the earlier ones. This energy focusing seems contradictory to the steady-state development of the 1/E energy spectrum, in which neutrons spread out over an energy range as they scatter. The resolution of this paradox probably lies in the fact that energy focusing occurs for a time-dependent neutron population, whereas the 1/E spectrum describes a steady-state neutron flux.

The ideal pulse width, for a Gaussian energy distribution for the pulse, is given as follows:

$$\text{Full Width at Half Maximum} = \frac{\Delta E}{E} = \sigma \cong \sqrt{\frac{8}{3A}} \cong 11.4\% \text{ for Pb} \qquad \text{Equation 39}$$

The recent papers by the research team being led by the Pacific Northwest National Laboratory (PNNL) [33, 36, 234, 236] erroneously quote the paper by Lee et al. [259] as a source for this expression; it is actually not in this paper anywhere. According to Sawan and Conn, this expression comes from a Grueling-Goertzel model of the asymptotic dispersion in energy (Equations 9-11 in Sawan and Conn [248]), though they do not actually derive it there or in their earlier paper [246]. The expressions by Bergman et al. (Equations 8 and 9 and Equation 10 in their appendix [241]), by Williams (page 422 [275]), and by Chernikova et al. (their Equation 3 [272]) seem to be slightly different. (See also Sawan and Conn's discussion of this point [248].) The group at Los Alamos National Laboratory uses similar equations that may have been partially empirically derived [32, 261, 263].

One immediate and important consequence of Equation 39 is that neutron scattering off light elements, especially hydrogen for which $A = 1$, causes the pulse to broaden. Thus, it is absolutely imperative to remove as many light elements as possible from the spectrometer and from the fuel assembly. Keeping the fuel assembly immersed in water during the measurement is thus impossible; the fuel assembly must be cool enough that it can be air cooled. (The U.S. Nuclear Regulatory Commission says that fuel assemblies must be cooled in water for at least the first 5 years after being discharged from the reactor [232].) Even in dry fuel assemblies, some hydrogen exists in the zirconium alloy of the fuel-pin cladding; the alloy absorbs the hydrogen from the cooling water during the burning of the fuel in the reactor [32]. Gavron et al. [32] reported that this hydrogen in the cladding did not affect their ability to detect fissile isotopes with LSDS, but Smith et al. [236] reported that when hydrogen was

included in their simulations, the error in the plutonium content increased to 7%, from a no-hydrogen value of 2%. Becker et al. [274] show some simulation results of the effects of hydrogen in the lead of the spectrometer. Furthermore, instruments that contain light elements, such as some scintillator detectors, either must not be used or must be specially treated. (For example, Chernikova et al. [272] recommend covering a scintillator detector with ^{6}Li.)

4.3.2.3 Data analysis

Various ways to analyze the LSDS data, such as those presented in Figure 44, have been suggested. They can be classified into two main groups: (1) those that examine only selected portions of the time/energy spectrum at which the fissile isotopes produce dominating, resonant signals, and (2) those that try to fit the entire spectrum by a superposition of ideal signals from pure isotopes. Note that the original usages of LSDS, as proposed by Bergman et al. [241], were the studying of the physics of the slowing down of neutrons and the measuring of the energy dependencies of the absorption cross sections of various isotopes. Since those purposes were different from the current purpose of examining the isotopic content of spent fuel assemblies, those approaches to collecting and analyzing data are not applicable in the current case and will not be discussed here.

Krinninger, Wiesner, and Faber's 1969 paper [244] was one of the first to discuss the use of LSDS for assaying the isotopic content of used nuclear fuel. They used the first type of data analysis—that of examining only selected parts of the energy spectrum—and compared the signal in the 0.3 eV region, where ^{239}Pu has an exceptionally strong fission resonance, against the general signal in the thermal region (0.025 eV). Cramer et al. [249] in 1976 also took a similar approach to determining the axial variability of the ^{233}U enrichment in special fuel pins. The 1974 paper by Sawan and Conn [248] was similar to these but examined higher-energy resonance regions because of the self-shielding of ^{239}Pu at this strong resonance (explained below in the next subsection) and because of the long die-away time of thermal neutrons. In recent years, Chernikova, Romodanov, and other researchers in Sweden and Russia have also adopted this approach and have called it "time intervals matrix analysis" [269, 270, 272].

Figures 46 and 47 show Sawan & Conn's and Romodanov's group's choices for appropriate time intervals. Both have chosen the two ranges from 60 μs to 80 μs and from 100 μs to 130 μs, roughly defined; and Romodanov et al. have included other intervals as well. Sawan & Conn performed a direct solution of their 2 x 2 matrix to calculate the masses of ^{235}U and ^{239}Pu, whereas Romodanov et al. find these masses by minimizing a function (Equation 40) that describes their higher dimensional matrix. The basic idea in both cases is to adjust the estimates of the masses ^{235}U and ^{239}Pu to produce the same count rates as the measured count rates in these intervals.

The minimization equation for time-intervals matrix analysis is as follows [269, 272]:

$$J = \sum_{j=1}^{n} \left\{ \left(\sum_{i=1}^{k} f_{i,j} \right) - F_j \right\} \qquad \text{Equation 40}$$

Here, J is the function to be minimized; F_j is the measured count rate in the j^{th} time interval; n is the number of time intervals to be analyzed; $f_{i,j}$ is the contribution of the i^{th} isotope to the

fission rate in the j^{th} time interval; and k is the number of fissile isotopes being considered. (Note that the meanings of the i and j indices have been swapped here, relative to their original meanings by Chernikova et al. [272], in order to match the meanings in the reports by PNNL. Thus, "i" can now be interpreted as standing for "*isotope*.") Romodanov, Chernikova, et al. considered each isotopic contribution function, $f_{i,j}$, to be a function of the concentrations of ^{235}U and ^{239}Pu in the fuel [272], which may have been an attempt to account for the impact of the neutron absorption in one isotope on the fission rate of another. Unfortunately, this way of dealing with neutron absorption is not only incomplete but also obscures, rather than reveals, its effects. It is incomplete because it considers only absorption in ^{235}U and ^{239}Pu, and it obscures the effects by including them in the inner summation in Equation 40. Therefore, it seems better to leave these $f_{i,j}$ functions as only functions of one isotope (the i^{th} isotope) and to deal with absorption in a different way, as in the second data analysis method, which will be described next.

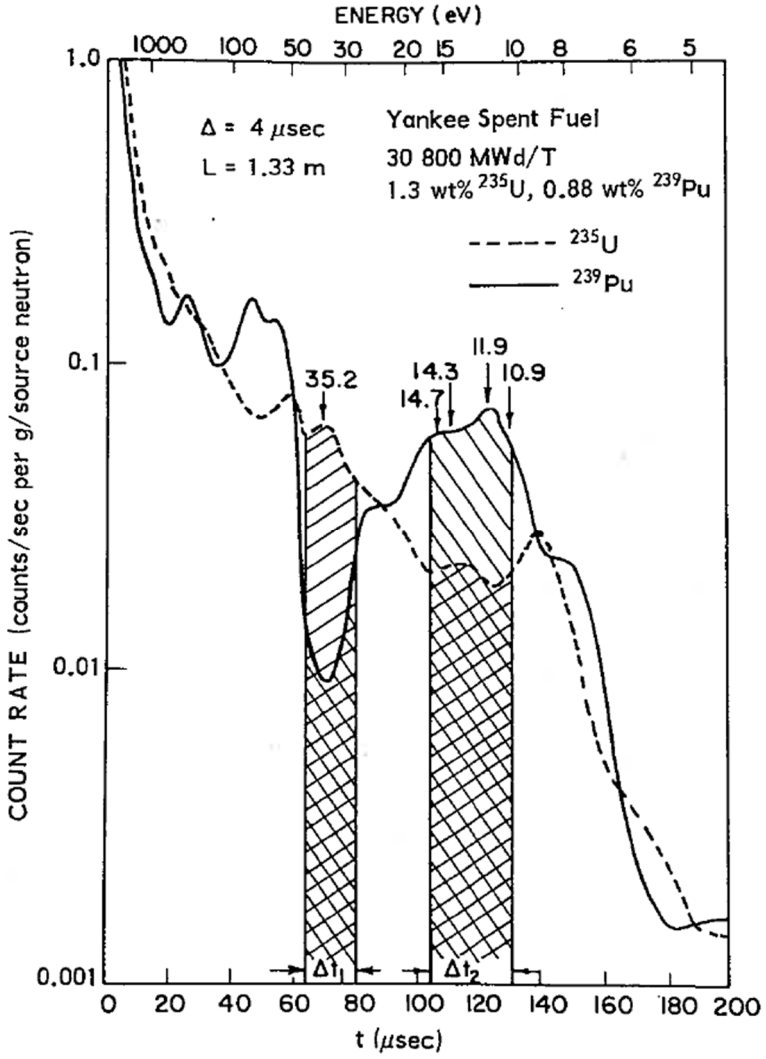

Figure 46: "Uranium-235 and ^{239}Pu count rates for spent-fuel pin ST2 (30 800 MWd/T)." This figure illustrates Sawan & Conn's choice of two time intervals in which ^{235}U and ^{239}Pu have strong resonant signals.Copied from Figure 15 in Sawan and Conn [248].

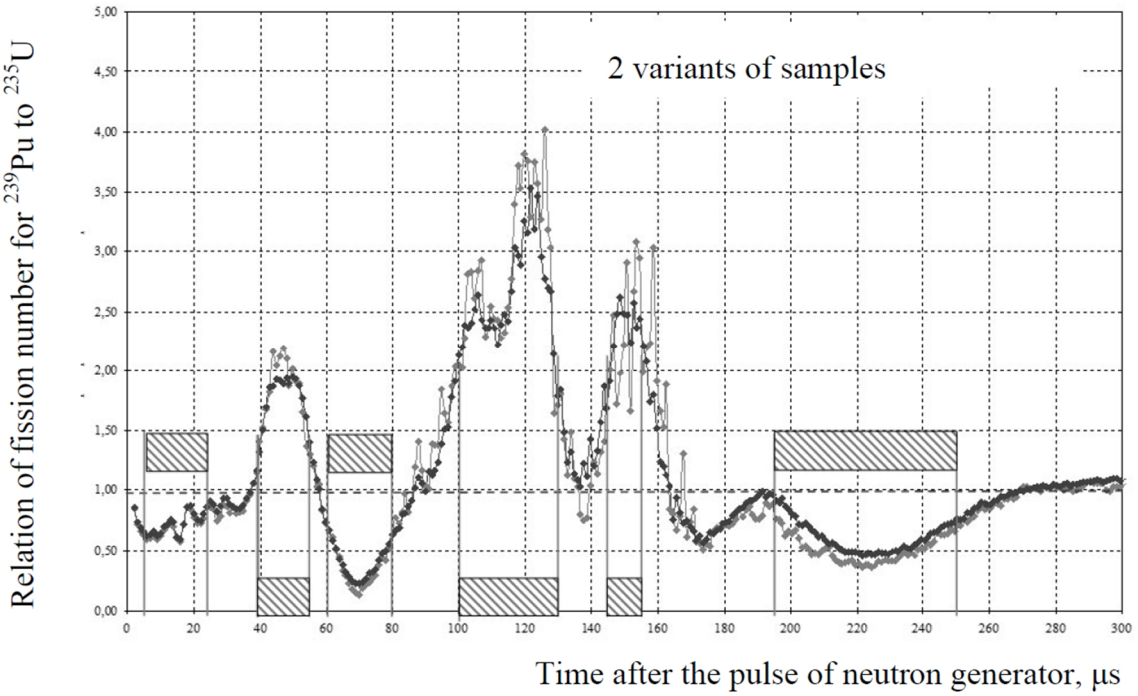

Figure 47: The ratio of the number of fissions of ^{239}Pu to the number of fissions of ^{235}U, as a function of the time after the initial neutron pulse in LSDS. The shaded areas indicate the ranges that are used in the time-intervals matrix technique, which is being used in Russia and Sweden. Copied from Romodanov et al. [269] with permission from the authors.

The second type of data analysis—that of analyzing the entire energy spectrum—has been championed by the RPI/PNNL team in the United States since as early as 1990 [252]. The basic idea is that the total response of the fuel assembly to the interrogating neutrons, which is measured by the threshold fission chambers, must be the superposition of the individual responses of all the isotopes in the fuel assembly. (This total response of the threshold fission chambers is also called the "threshold assay" signal.) In its most conceptually simple incarnation, this method calculates the ideal response of each isotope according to its published fission cross-section data. The strength of each isotope's signal in the superposition ideally corresponds to the amount of that isotope in the fuel assembly. Thus, the total, threshold assay signal is "de-convoluted" by adjusting the weighting of each isotope's signal until the superposition matches the measured signal, and the resulting values of the weighting coefficients represent the quantities of the isotopes.

If the individual isotopic signals would be represented by analytical functions or by a high-resolution discrete distribution, then this process would be similar to Fourier analysis, in which an arbitrary function (like the threshold assay signal) is fitted by a superposition of weighted sinusoidal basis functions (like the ideal signals from the individual isotopes). In practice, though, a rough, discrete distribution is used; the 2011 PNNL variation uses only 162 time bins to cover the interval from 20 μs to 2000 μs [33]. This rough approximation then actually becomes like the time-intervals matrix-analysis method, with the only difference being that all of the time intervals over the entire interrogation period are now included in the analysis instead of only a few. Indeed, the maximum-likelihood-estimation process used in PNNL's method is very similar to the minimization used in the time-intervals matrix-analysis

method; the equations look alike (Equations 40 and 41), except that PNNL's equation uses logarithms [33, 269]:

$$R = \sum_{j=1}^{n} \{ y(t_j) - Y(t_j) \ln[y(t_j)] \} \qquad \text{Equation 41}$$

Here, R is the function to be minimized, in the maximum-likelihood estimation; t_j is the j^{th} time interval; $Y(t_j)$ is the measured count rate in this interval; and $y(t_j)$ is the calculated count rate as given by Equation 42.

$$y(t_j) = C \cdot f(t_j) \sum_i \left(\frac{m_i}{A_i} \right) \bar{\nu}_i \, X_i(t_j) \qquad \text{Equation 42}$$

Here, C is a proportionality constant; $f(t_j)$ is the self-shielding function for time interval j; m_i and A_i are the mass and atomic number of isotope i, so that m_i/A_i is the number of nuclei of isotope i in the fuel assembly; $\bar{\nu}_i$ is the average number of neutrons emitted per fission of isotope i; and X_i is the number of fissions of isotope i in the j^{th} time interval, per nucleus and assuming no self-shielding. The self-shielding function, $f(t)$, is defined as the ratio of the average neutron flux in the fuel assembly to the neutron flux at the threshold fission chambers:

$$f(t) = \frac{\bar{\phi}_{fuel}(t)}{\phi_{detectors}(t)} \qquad \text{Equation 43}$$

Thus, $f(t)$ incorporates neutron absorption in all isotopes and is a single factor that affects all isotopes equally, which is why $f(t)$ is a prefactor in Equation 42 and is not dependent on the isotopes in the summation, in contrast with the approach of Romodanov et al.

It appears that the genesis of this second type of data analysis (PNNL's method) may have been the adoption of the use of isotopic fission chambers in the RPI lead slowing-down spectrometer, since it seems that both concepts appeared at the same time [252]. Unlike the threshold chambers that use purified fissionable material—^{232}Th or ^{238}U—the isotopic fission chambers use pure fissile material—^{235}U or ^{239}Pu. The fissile isotopes have much larger fission cross sections at the lower energies of the interrogating neutrons than at the higher energies of the fast neutrons produced by fission in the fuel assembly. For this reason, the isotopic fission chambers basically measure the interrogating neutron pulse rather than the fission events in the fuel assembly, which are measured separately by the threshold fission chambers.

RPI used the isotopic fission chambers to measure experimentally the responses of the pure fissile isotopes to the interrogating neutron pulse, rather than calculating these responses from the published fission cross-section data. (See Figure 44, for example.) Mathematically, the function X_i in Equation 42 became a measured function instead of a calculated one. With such experimental data available, the logical next step for RPI was to try to use the isotopic-fission-chamber spectra as basis functions to "de-convolute" the threshold assay signal. Indeed, in the first application of isotopic fission chambers, they were put down into the middle of the fuel assembly, so that they would then "see" the same neutron flux as the fissile material in the fuel pins, and thus their signals would be very representative of the signals from this material.

Of course, putting these fission chambers into the middle of the fuel assembly was relatively to do easy when only mock-up fuel assemblies made from fresh fuel were being measured [252]. For highly radioactive, spent fuel assemblies, this task would be much more daunting. Therefore, in later designs, the isotopic fission chambers have been relocated to just outside the fuel assembly, in the Pb block, similar to where the threshold fission chambers are. A correction factor is applied to compensate for this change in location [265]. This latter setup is much more reasonable for measurements on actual spent fuel assemblies.

One difficulty with the use of isotopic fission chambers that seems not to have been addressed yet is the difficulty of obtaining and using fission chambers made with ^{239}Pu or ^{241}Pu. Such fission chambers are more rarely produced commercially than are those that use ^{235}U, and they may be subject to more stringent safeguards and transportation requirements [38].

4.3.2.4 Limitations

LSDS as applied to spent fuel assemblies requires a strong pulsed neutron source (10^{16} total neutrons) [35, 240]. According to PNNL, the primary reason is the low efficiency with which the threshold fission chambers (^{238}U or ^{232}Th) can detect the fast neutrons from the induced fission events in the fissile material [240]. For this reason, LANL is developing a ^{4}He-recoil fast-neutron detector that would have much greater detection efficiency that the threshold fission chambers [240]. Ideally, greater detection efficiency could reduce the neutron-source requirements by a factor of one thousand [240]. As for the passive neutron flux generated by the spent fuel assembly itself, a study by LANL showed that it would not impact the LSDS analysis [32], and an LSDS measurement by RPI of a 96 g PuBe neutron source was able to overcome its passive neutron flux [35, 237, 274], which was probably on the order of 10^{6} or 10^{7} neutrons/s [277].

LSDS's requirement for a complete absence of water or other moderating materials in the assay chamber and in the spent fuel assembly has been discussed at the end of Section 4.3.2.2.

Self-shielding may be the biggest obstacle to using LSDS to assay spent fuel assemblies. Self-shielding occurs when the material in the outer portion of the fuel assembly (and in the outer region of each fuel pin) absorb so many of the neutrons that significantly fewer of these neutrons are able to reach (spatially) the inner fissile atoms and induce a signal from them. Self-shielding thus causes the amount of induced fission to be much less than it otherwise should be for the actual amount of fissile material in the fuel assembly. From another perspective, the amount of fission in the fuel assembly depends upon (1) the amount and spatial distribution of the fissile material and (2) the spatial distribution of the neutron flux throughout the fuel assembly (Equation 3). Self-shielding refers to a reduction in the amount of fission due to changes in this second quantity, the spatial distribution of the neutron flux.

The meaning of *self* in *self-shielding* needs clarification. A strictly limited meaning is that *self* refers only to each isotope individually, so that only the neutron absorption in the same isotope can contribute to the self-shielding of that isotope. In general and in the safeguards NDA literature specifically, *self* refers to the entire object or sample—in this case, a fuel assembly [274, 278]. In this meaning, any neutron absorption in the fuel assembly—in any isotope and regardless of whether the absorption produces fission—contributes to self-

shielding. This broader meaning encompasses a physical phenomenon that is important to LSDS, namely, the reduction in the fission signal from the fissile isotopes caused by non-fission-inducing capture in other isotopes. (See Figure 7 in Becker et al. [274] for an example of self-shielding of ^{235}U by resonance capture in ^{238}U, in a fuel pin.) For all these reasons, this report uses the broader definition, too.

In a basic sense, self-shielding causes LSDS to underestimate the fissile content of a fuel assembly. Self-shielding also complicates the fitting of the threshold assay signal, though, because self-shielding is energy dependent. It follows the energy dependencies of the absorption cross sections, with the strength of the self-shielding increasing directly with the strength of the cross sections. This fact is why the self-shielding coefficient, f, in Equation 42 is a function of time (energy).

The various proponents of the time-intervals matrix-analysis method (e.g., Krinninger et al., Sawan and Conn, and Romodanov et al.) have pointed out that the method—as they have developed it thus far—works only as long as self-shielding is ignored [244, 248, 269, 272]. The time-intervals matrix-analysis method partially avoids this problem by choosing time intervals in which the resonances of the fissile isotopes are isolated, but self-shielding still affects these time intervals and the overall results. The work by PNNL's team is more advanced, therefore, because they have already begun to address this problem. At first, it may seem that, by including in the analysis many portions of the time-energy spectrum that contain little information about the fissile isotopes, the PNNL method is making the problem more difficult than it needs to be. The benefit, though, is that these other intervals contain information about the neutron absorption in the other isotopes and can therefore help to determine the extent of the self-shielding.

There are a few different ways to determine the self-shielding function, $f(t)$. One way is to try to derive $f(t)$ analytically, using the published absorption cross section data of various isotopes. The recent PNNL effort in this regard has been to treat the fuel assembly as a parallelepiped that is homogeneous—specifically ignoring the space between fuel pins [33, 237]. The PNNL report states that this assumption is probably the reason that the analytical $f(t)$ does not match the simulation results very well. Another way to derive $f(t)$ is to reconstruct it from simulations of a suite of similar fuel assemblies, such as are in the NGSI's Spent Fuel Library (Section 2.3). The way that $f(t)$ varies over the fuel assemblies in the library is broken down into a matrix of basis vectors [33, 237]. The function $f(t)$ is then treated as a function of the masses and of the coefficients of these basis vectors, so that the minimization done in Equation 41 now must include these coefficients as variables, in addition to the isotopic masses. This empirical approach seems to yield better results than the analytical approach [33, 237]. A third way is to use neural networks to describe $f(t)$, but this way requires extensive calibrations [262]. In summary, the problem of determining the self-shielding function is a complicated and on-going area of LSDS research; therefore, further details of these approaches will not be given here.

4.3.3 Self-Interrogation Neutron Resonance Densitometry (SINRD)

Name	Self-Interrogation Neutron Resonance Densitometry (SINRD)
References	NGSI: [15, 37-287] Other: [288]
Measurement environment	In water (in air or other gas is also possible)
Passive vs. Active	Passive
Time dependency	Time-independent (continuous)
Particles detected	Neutrons
Type of detectors	Fission chambers: ^{235}U only (practically) or ^{235}U, ^{239}Pu, and ^{241}Pu (ideally)
Particles' detected attribute	Energy
Governing physical properties of the fuel assembly	For absolute measurements The number of primary neutrons (N_{PRI}) The leakage multiplication of primary neutrons with reflection (ARR·M_L; Section 4.1.2.3) For relative measurements The proportion of fission in ^{239}Pu to fission in ^{235}U
Governing isotopes	Primary-neutron sources; fissile isotopes; neutron absorbers
Maturity	Novel; early prototype tests in air only
Limitations	Limited sensitivity to inner fuel pins because of neutron scattering; only the three outer rows of pins can be measured fully. Large uncertainty or long measurement time, for low BU and small quantity of primary-neutron sources, because signal is weak Difficulty of obtaining, transporting, and using fission chambers made from ^{239}Pu and ^{241}Pu (if used)
Selected by the NGSI for prototype testing?	Yes, primarily at the Post Irradiation Examination Facility (PIEF), Daejeon, Republic of Korea [15]

4.3.3.1 Principle of operation

Self-Interrogation Neutron Resonance Densitometry (SINRD) is a passive technique that measures several portions of the energy spectrum of the neutrons being emitted from a sample. In a SINRD instrument, multiple fission chambers (FCs) are used as the neutron detectors. Several of them are covered with various kinds of neutron absorbing materials, which act like filters that are sensitive to neutron energy. They effectively limit the ability of the fission chambers that they cover to detecting only neutrons that have energies greater than the cutoff energies of these materials. With these multiple fission chambers and filters, the SINRD instrument can measure three distinct regions of the neutron energy spectrum: fast neutrons, epithermal neutrons around the 0.3 eV resonance of the fissile isotopes, and thermal neutrons. These regions are illustrated in Figure 48.

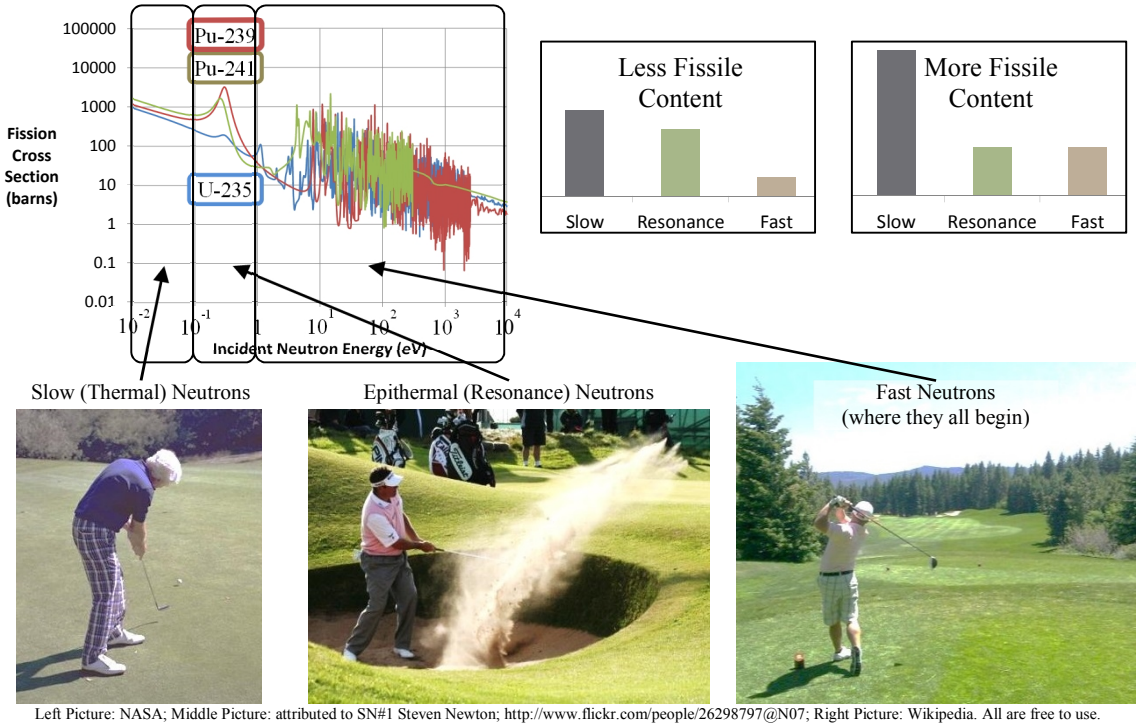

Left Picture: NASA; Middle Picture: attributed to SN#1 Steven Newton; http://www.flickr.com/people/26298797@N07; Right Picture: Wikipedia. All are free to use.

Figure 48: An illustration of how the resonance fission of fissile material can alter the neutron energy spectrum. SINRD relies on the comparisons among these three energy categories of neutrons to detect fissile material.

SINRD operates by comparing the magnitudes of the neutron fluxes in these three energy regions. If the count rate within the resonance region is substantially reduced in comparison to what would be expected from the count rates of the fast and thermal neutrons, then this decrease can be attributed to the absorption of neutrons in the 0.3 eV resonances of the fissile isotopes (i.e., to a resonance chasm at this energy). Of course, such resonance absorption in fissile isotopes leads to fission and the production of more neutrons. These fission neutrons begin as fast neutrons, though, and not as 0.3 eV neutrons, so the resonance chasm is undisturbed by such fission. However, the chasm is disturbed by neutron scattering and slowing down, which will be discussed below.

4.3.3.2 The NGSI's design

The NGSI's configuration of the SINRD instrument that was evaluated in Phase I contained four kinds of fission chambers (FCs): one bare FC without any filter and three other FCs, each with a different filter [37]. (Figure 49 is a schematic of this Phase I design; Figure 50 is a photograph of the prototype to be tested on PWR fuel at the Post Irradiation Examination Facility in the Republic of Korea [15].) The filters were boron (in the form of boron carbide, B_4C), gadolinium metal (Gd) with hafnium metal (Hf), and cadmium metal (Cd). The absorption cross sections of these elements and the fractions of the neutrons that they allow to pass (as functions of neutron energy) are shown in Figure 51.

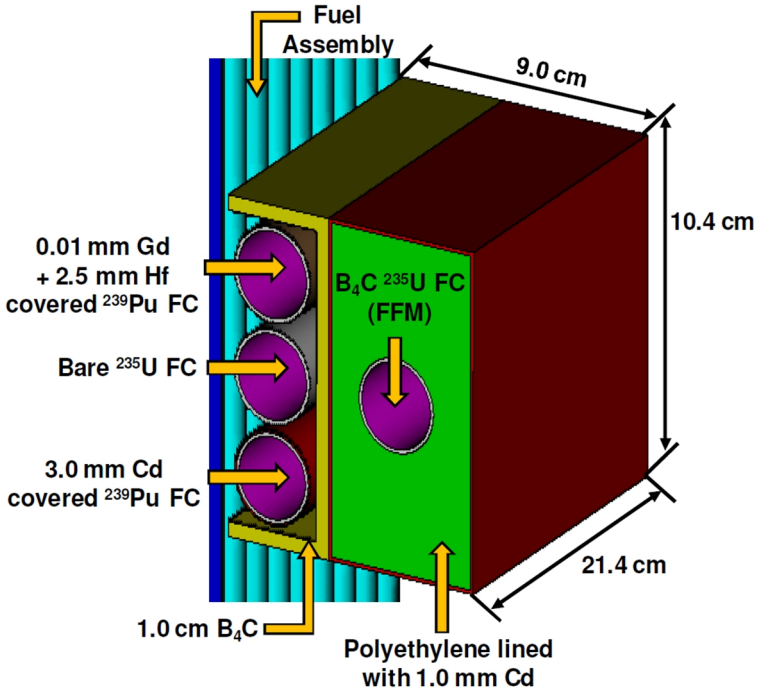

Figure 49: Configuration of the SINRD instrument that was evaluated in Phase I of the NGSI Spent Fuel NDA Project copied from Hu et al. [284].

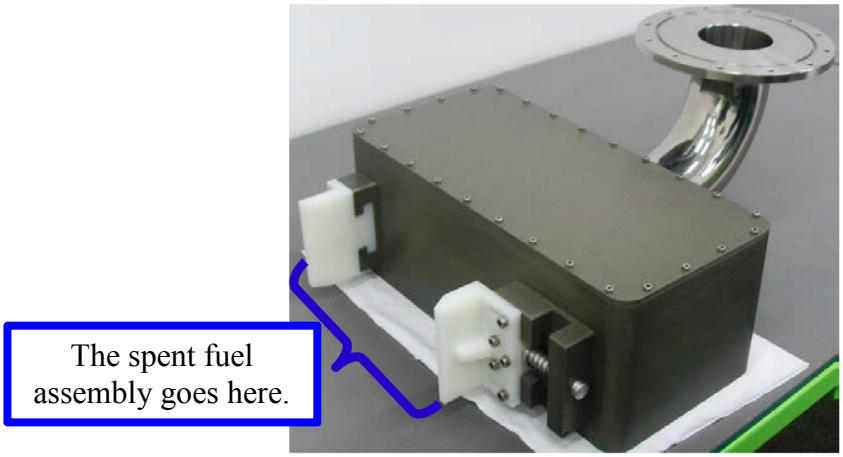

Figure 50: Photograph of the NGSI's SINRD instrument to be tested on PWR fuel at the Post Irradiation Examination Facility in the Republic of Korea; modified from Tobin et al. [15].

In this design, the bare FC detects mostly thermal neutrons, because of the exponentially increasing cross section of ^{235}U with decreasing neutron energy. The FC that is covered with 0.01 mm of Gd and 2.5 mm of Hf detects neutrons either with energy between 0.13 eV and 0.6 eV or with energy greater than 3 eV. (The Gd removes neutrons with energy below 0.13 eV, and the Hf absorbs additional neutrons between 0.6 eV and 3 eV.) The FC that is covered with 3.0 mm of Cd detects primarily neutrons with energy above 1.3 eV. The difference between the count rates of the (Gd+Hf)-covered FC and the Cd-covered FC represent the neutrons in the energy window that spans the 0.3 eV resonances of the fissile isotopes (Figure 48). Lastly, the FC that is behind the 1.0 cm shield of B_4C detects primarily fast neutrons, with energy above 3.8 keV. Therefore, this last FC is called the *fast fission*

monitor (FFM). The polyethylene behind the B_4C takes these fast neutrons and slows them down to thermal energy to increase the efficiency with which the FC detects them. Nevertheless, they are still considered to have been the fast neutrons in the energy spectrum coming from the fuel assembly. In summary, the three sets of FCs—(1) the bare FC, (2) the (Gd+Hf)−Cd window FCs, and (3) the FFM—together detect the distortion of the energy spectrum caused by 0.3 eV resonance absorption (and corresponding fission) in the fissile isotopes. (See Figure 48.)

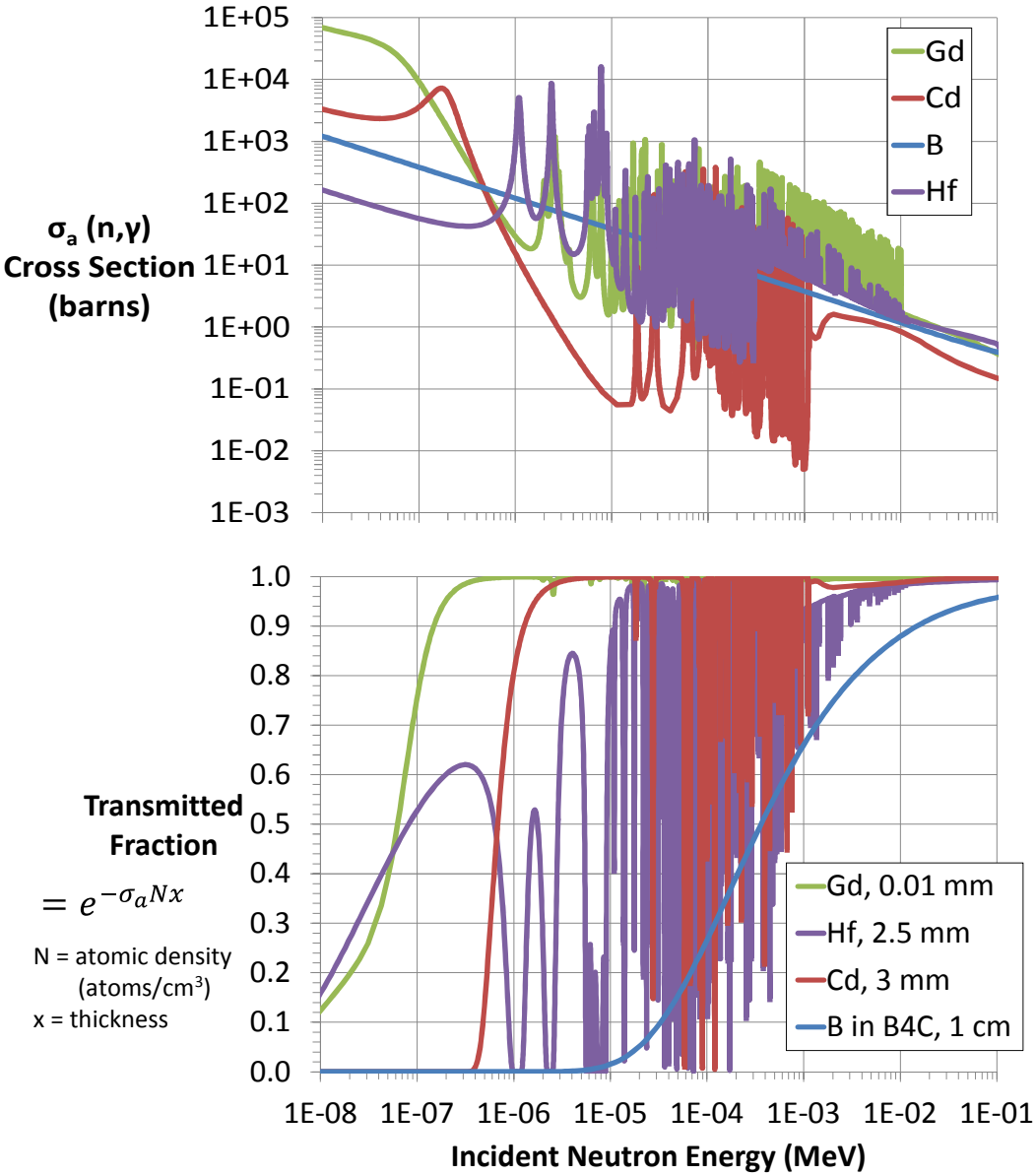

Figure 51: Top: the microscopic cross section of several elements (with natural isotopic abundance) that are used as filters in the NGSI's SINRD instruments. Bottom: the fractions of neutrons, as functions of energy, that are transmitted through the indicated thicknesses of these elements.

The use of the Gd−Cd window is what makes SINRD superior to total neutron counting (TN). The window helps the SINRD instrument to distinguish between the fissile isotopes, on

the one hand, and the primary-neutron-generating isotopes, on the other. (Recall that primary neutrons are generated by (α,n) reactions and spontaneous fission, whereas secondary neutrons are generated by induced fission.) A TN (total neutron) measurement—whether of the fast flux only, the thermal flux only, or the entire flux—can yield the same count rate from a fuel assembly with no fissile material but much primary-neutron-emitting material (i.e., ^{244}Cm) as from a fuel assembly with a small amount of primary-neutron-emitting material but much neutron multiplication in fissile material. (See Equation 3 and Section 4.1.1.) In contrast, a SINRD measurement that shows large thermal and fast fluxes but a *relatively* small 0.3 eV resonance flux is clearly indicative of the multiplication caused only by fissile material.

The use of Hf in conjunction with the Gd-covered FC is intended to mitigate the effect of the radiative capture of neutrons in the 1.06 eV resonance of ^{240}Pu. Without the Hf, the Gd−Cd window spans this ^{240}Pu resonance and cannot distinguish its resonance chasm from the 0.3 eV resonance chasm caused by the fissile isotopes. Of course, the fission of the fissile isotopes produces more neutrons, whereas the radiative capture by the ^{240}Pu does not. (It produces γ rays.) In the context of spent fuel measurements, though, this combination of a strong resonance chasm (caused by the absorption in ^{240}Pu) with a small total neutron flux (because ^{240}Pu does not multiply neutrons) will be interpreted as being due to less primary-neutron-emitting material (i.e., less ^{244}Cm and less burnup) and more fissile material in the fuel than is actually the case. In order to avoid this false interpretation, it is necessary to make the Gd−Cd window to be insensitive to resonance absorption in ^{240}Pu. This goal is achieved by adding the Hf to absorb all (or almost all) of the neutrons within the ^{240}Pu resonance energy range (0.6 eV to 3 eV). Of course, this Hf reduces the total number of neutrons that are counted within the (Gd+Hf)−Cd window, but at least the neutrons that are counted—or rather, are not counted but are absent—can then be confidently attributed only to fissile resonance absorption and not to ^{240}Pu resonance absorption.

As has just been described, the main way in which SINRD distinguishes fissile material is by comparing the three energy ranges of neutrons. Since all three fissile isotopes have resonances near 0.3 eV within the (Gd+Hf)−Cd window, SINRD primarily analyzes the fissile isotopes together as one group. SINRD can be improved, though, by using three sets of FCs, with each set using a different fissile isotope—one with ^{235}U, one with ^{239}Pu, and one with ^{241}Pu. Because these isotopes have different fission resonance peaks outside the (Gd+Hf)−Cd energy window, these sets of FCs are not equally sensitive to the same neutron flux. For instance, ^{235}U has eight clear resonance peaks (plus several other shoulders on these peaks) in the span between the 0.3 eV resonance and the next highest resonance of ^{239}Pu, at 7.81 eV; and ^{241}Pu has five resonance peaks in this same span. Each isotope's set of FCs is particularly sensitive to that isotope's resonance chasms outside the (Gd+Hf)−Cd energy window, even without any human attempt to bracket those resonance chasms with filters, as is done with the 0.3 eV resonance chasm. (This principle that "like fissile isotopes detect like fissile isotopes" is actually the origin of the word *self* in the name *Self-Interrogation Neutron Resonance Densitometry* and was the operating principle in the early experiments from which the SINRD NDA concept grew [288].) Thus, comparing the signals of the sets of FCs with one another can lead to a determination of the isotopic content of the fissile material—especially if calibrations with different isotopic mixtures are performed beforehand. Such calibrations

could be made with fuel assemblies of various burnups, initial enrichments, and cooling times, such as has been simulated by Hu, LeFleur, and colleagues, for example [37, 38].

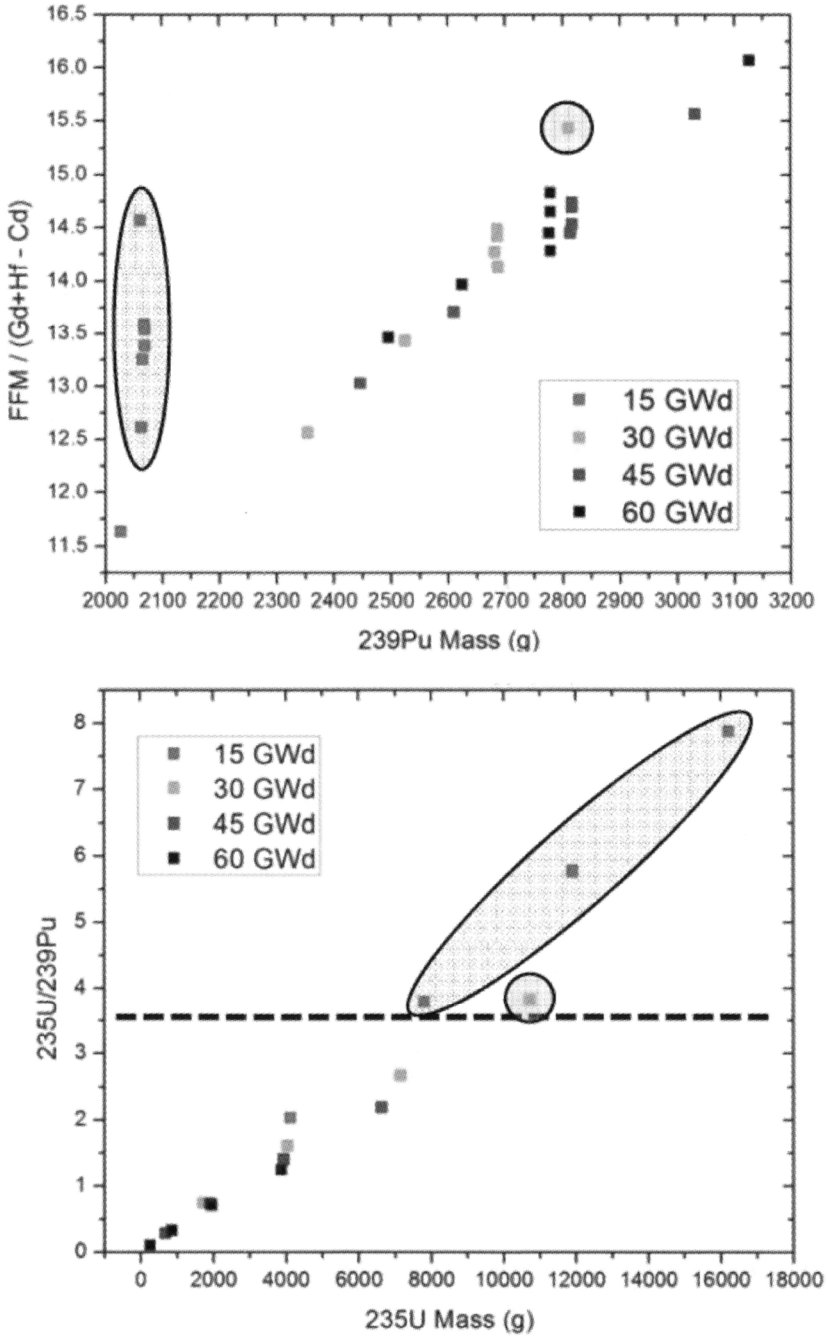

Figure 52: The correlation between one of the SINRD ratios and the ^{239}Pu mass in the fuel assembly (top figure), showing that the residual ^{235}U content at low burnups (bottom figure) ruins the correlation with the ^{239}Pu. Low burnup is less than 30 GWd/tU; such data are circled in the figure. Copied from Hu et al. [37] with permission from INMM.

FCs with ^{239}Pu or ^{241}Pu are much more rarely produced commercially than are ^{235}U FCs, and they may be subject to more stringent safeguards and transportation requirements [38]. For these reasons, the NGSI design of the SINRD instrument uses only ^{235}U FCs [37]. Therefore, to determine the plutonium content of a fuel assembly without any other information, the NGSI SINRD instrument must rely on good calibration data and on limiting

measurements only to those fuel assemblies that have burned for at least 30 GW-days/metric-ton-U [37]. (See Figure 52.) Such fuel assemblies have burned enough of the ^{235}U so that what remains has a negligible influence on the (Gd+Hf)−Cd window's count rate in comparison to the influences of the ^{239}Pu and ^{241}Pu, which increase in the fuel as it burns. This criterion is reached more quickly (i.e., at lower burnup) than just a mere comparison of the ^{235}U mass with the ^{239}Pu and ^{241}Pu masses would indicate, since the 0.3 eV resonance peak of ^{235}U is much smaller than those of the Pu isotopes (Figure 48). The summary point here is that a SINRD instrument that uses all ^{235}U FCs can distinguish among the fissile isotopes only with the help of the fact that the burning of the fuel changes their relative proportions in a unique way.

4.3.3.3 Data analysis

The SINRD data for an LEU fuel assembly can be analyzed by referring to the figures in LaFleur et al. [38]. In the following instructions, "*Bare*" refers to the count rate in the bare FC, "*Window*" refers to that in the Gd−Cd window or the (Gd+Hf)−Cd window, and "*FFM*" refers to that in the fast-flux monitor. The first analysis is to use *Bare* as a total neutron (TN) measurement. Since the TN count rate depends largely upon the amount of ^{244}Cm in the fuel, it serves as a way to estimate the burnup of the fuel.

Next, the SINRD data can be analyzed for ^{235}U and ^{239}Pu, specifically. The sequence for determining the mass of ^{235}U in the fuel assembly is as follows:

- Measure, by chemistry, the boron content of the cooling water.
- Measure *Window* and *Bare* for the unknown fuel assembly; and take the ratio, denoting it by "*raw*" to indicate that that it has not yet been normalized: $\left(\frac{Window}{Bare}\right)_{raw}$
- Normalize this ratio by the same ratio as was previously determined by measurements on a fresh fuel assembly; denote this normalized result with the subscript, "*measured*":

$$\frac{\left(\frac{Window}{Bare}\right)_{raw}}{\left(\frac{Window}{Bare}\right)_{fresh\ fuel}} = \left(\frac{Window}{Bare}\right)_{measured}$$

- Use this ratio with Figure 53 (which is a copy of Figure 10(a) in LaFleur et al. [38]) to determine the fraction of ^{235}U in the fuel. Note that this figure depends significantly on the amount of boron in the cooling water, but it does not depend significantly on the initial enrichment. Also note that this curve is approximately linear.

The sequence for determining the mass of ^{239}Pu in the fuel assembly is similar and is as follows:

- Measure, by chemistry, the boron content of the cooling water.
- Measure *FFM* and *Window* for the unknown fuel assembly; and take the ratio, denoting it by "*raw*" to indicate that that it has not yet been normalized: $\left(\frac{FFM}{Window}\right)_{raw}$

- Normalize this ratio by the same ratio as was previously determined by measurements on a fresh fuel assembly; denote this normalized result with the subscript, "*measured*":

$$\frac{\left(\frac{FFM}{Window}\right)_{raw}}{\left(\frac{FFM}{Window}\right)_{fresh\ fuel}} = \left(\frac{FFM}{Window}\right)_{measured}$$

- Use this ratio with Figure 54 (which is a modified version of Figure 7 in LaFleur et al. [38]) to determine the fraction of ^{239}Pu in the fuel. (This figure is similar to Figure 52, but the abscissa is the ^{239}Pu fraction of the heavy metal, not the ^{239}Pu absolute mass, and the ordinate has been normalized, as in the previous step.) Since the result depends on the boron content of the water, choose either the left or right figure according to the measured boron content. If the initial enrichment is otherwise known, then choose the appropriate curve within that figure to determine the ^{239}Pu content; otherwise, an unknown initial enrichment can be interpreted as an error in the value of the ^{239}Pu content. Note that these curves are approximately linear.

There are several assumptions in these sequences for determining the masses of ^{235}U and ^{239}Pu in the fuel assembly. Note that it is initially assumed that the fuel assembly is indeed LEU and not MOX. Different curves would be used if the fuel would be MOX. (See LaFleur et al. [38] for these curves.) Also, ^{241}Pu has been ignored in these analysis sequences, although not in the MCNPX simulations on which the figures have been based. Further calibration, simulation, and analysis work would be necessary for determining the ^{241}Pu. Lastly, it is important to recognize that, although Figures 52 through 54 show relations with ^{235}U and ^{239}Pu fractions, these fractions were determined by burning the fuel, not by artificially adding these isotopes to otherwise fresh, depleted-uranium fuel. The abscissas of these figures are thus actually the fractions of these isotopes in the presence of all the other isotopes that come with burning the fuel, such as neutron absorbers.

The determination of ^{235}U and ^{239}Pu by these analyses could be improved in a couple of ways. First, the calculation could be iterated, by using the determination of the residual ^{235}U and the burnup to estimate the initial enrichment more accurately. Figures 53 and 54 can be used more precisely if the initial enrichment is known. Secondly, other FC ratios could be used in addition to those in Figures 53 and 54. These ratios in these figures were chosen because they are roughly linear, whereas the curves for other ratios are not linear. Nevertheless, if graphical analysis is performed or if these non-linear curves are approximated with polynomials or other functions, then the curves of the other ratios could be used. By using several FC ratios to calculate several values for the fissile masses and then comparing these values, the accuracy of the results may be improved, and so would be the confidence that the results were not spoofed.

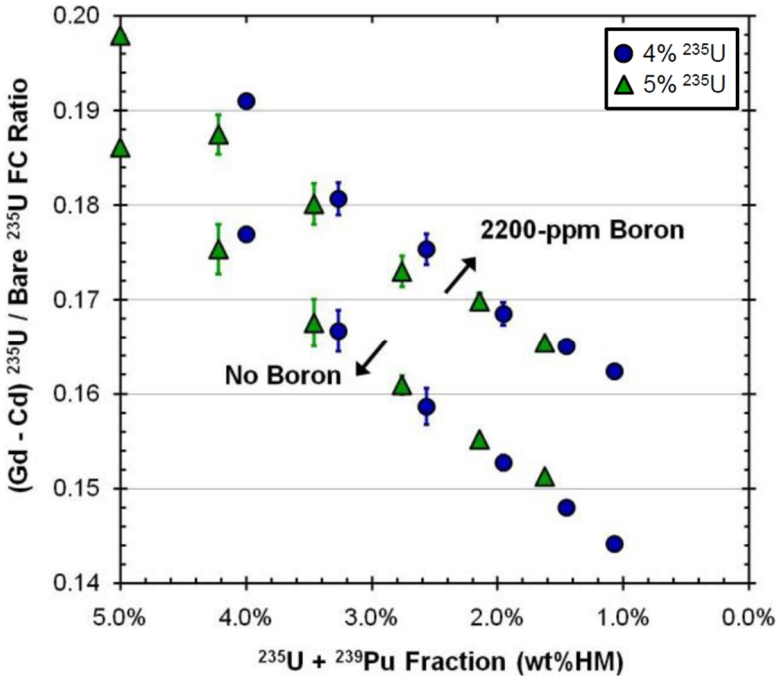

Figure 53: The relationship between the *Window*-to-*Bare* SINRD ratio and the fraction of ^{235}U in the fuel. Copied from Figure 8.10 in LaFleur [87] with permission from the author.

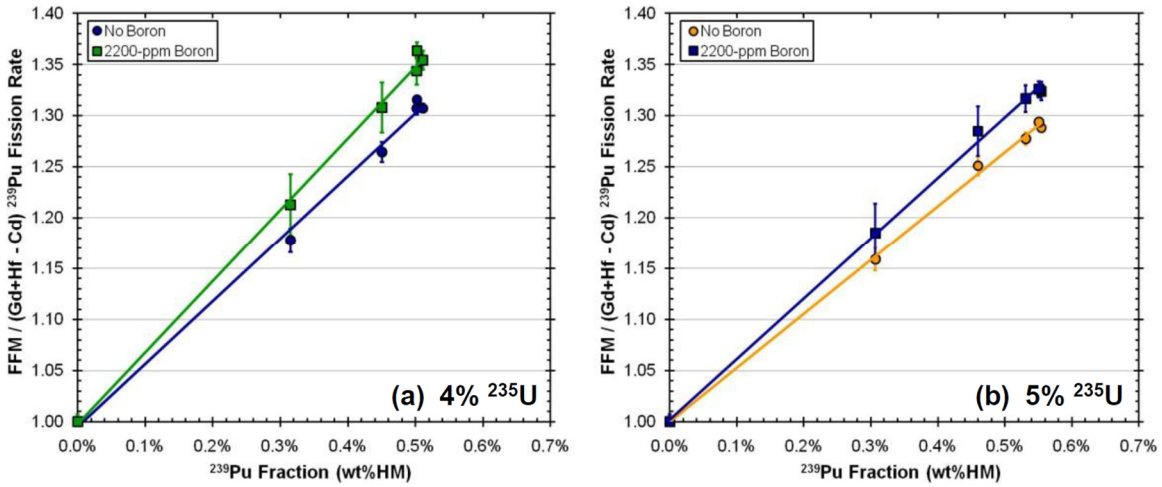

Figure 54: The relationship between the *FFM*-to-*Window* SINRD ratio and the fraction of ^{239}Pu in the fuel. Copied from Figure 8.5 in LaFleur [87] with permission from the author. Note that the lines pass through the origin (0.0%, 1.00) because the *FFM*-to-*Window* SINRD ratio has been normalized by the ratio's value for a fresh LEU fuel assembly.

4.3.3.4 Limitations

An important limitation of the SINRD technique is the loss of the resonance-chasm signal because of the slowing down of neutrons through scattering in water. The basic physics of neutron scattering says that the final energy of a neutron, after it has elastically scattered off a nucleus, is equally likely to be any energy within a certain range that is determined by the mass of the nucleus (Equation 2-73 in Duderstadt and Hamilton [289]). This fact necessarily implies that a peak in the neutron density (or flux) at a certain energy cannot migrate down to lower energies as those neutrons scatter. Instead, the peak diminishes, as those neutrons end

up with a variety of lesser energies. (In considering such a peak, it is obviously necessary to exclude the peak of the Maxwellian distribution of the thermal neutrons. The discussion here is speaking only of a peak in the epithermal or fast regions.) Likewise, if a resonance chasm in the neutron density (or flux) is considered instead of a peak, then the chasm also must diminish rather than migrate, since the neutrons that surround and define the chasm undergo the same scattering process. Although this phenomenon occurs with scattering off nuclei of any mass, it is most pronounced with scattering off hydrogen, in which it is possible that the neutron can end up with zero energy by a full transfer of its momentum to the nearly equally sized proton. Since hydrogen is plentiful as a constituent of the cooling water and has a significant neutron-scattering cross section, resonance chasms cannot survive if the neutrons travel more than about 1 cm through the water [130].

This fact is of critical importance for SINRD measurements on spent fuel assemblies in cooling water. It means, first of all, that the SINRD instrument must be placed as close as possible to the fuel assembly—even touching it, if possible—because the resonance-chasm signal is lost if there is a water gap of even 1 cm between the instrument and the fuel assembly. Secondly, it means that the resonance chasms from the fuel pins in the interior region of the assembly cannot be detected by a SINRD instrument on the outside of the assembly. Such fuel pins do contribute to the total neutron flux emitted by the assembly—especially to the thermal flux—by increasing the total reactivity of the assembly, and this increase can be seen by the SINRD instrument. But without the resonance chasms from the interior pins, the SINRD instrument cannot distinguish whether those pins consist of primary-neutron-generating material (e.g., curium) or of secondary-neutron-generating material (i.e., fissile isotopes), as discussed earlier.

This consequence—that the SINRD signal consists primarily of the fuel pins closest to the SINRD instrument—has been verified by a series of MCNPX simulations, based on the case of a 17 x 17 PWR assembly of unburned, 0% enriched uranium fuel (i.e., perfectly depleted, fresh fuel) [37]. In each simulation of the series (except the base case), one (and only one) row of fuel pins was replaced with pins of burned, typical LEU fuel; and the signal, in a SINRD instrument outside the assembly and on a side that was parallel to the row, was simulated. By normalizing each simulation to the base case, it was determined that only the three rows of pins that are closest to the SINRD instrument have a significant effect on the count rate in the (Gd+Hf)−Cd window. Moreover, the SINRD instrument in these simulations was touching the assembly; so that if the SINRD instrument would be offset from the assembly by 0.5 cm, for instance, then perhaps only the first row or only the first and second rows would contribute to the signal in the (Gd+Hf)−Cd window. There is a slight uncertainty in the results because of the fact that certain rows have more guide tubes and fewer fuel pins than other rows do. Nevertheless, this series of simulations has provided an important rule of thumb for the application of the SINRD technique to spent fuel assemblies in water—namely, that SINRD measures mostly the outer three rows of pins. With regard to the data analysis sequences mentioned earlier, this fact implies that the outer three rows largely govern where the "*measured*" ratio data points fall on the plots in Figures 53 and 54; and the effects of the inner pins may move the data points so slightly as to be negligible in comparison to the inherent uncertainty of the curves in these figures.

Thus, even if SINRD instruments are located on all four sides of the fuel assembly, the inner 11 x 11 pins may not be able to be clearly evaluated. This corollary was partially supported by other simulations of SINRD measurements in various pin-diversion scenarios, in which spent fuel pins were replaced by depleted uranium dioxide pins [87]. Diversions of large numbers of pins (e.g., 56 pins) in the central region were able to be detected, but smaller numbers (e.g., 16 pins) were difficult to detect. Moreover, it was not clear if the cause of the ability to detect the inner pins was primarily the absence of fissile isotopes in the DU pins or rather the absence of ^{244}Cm isotopes in those pins, instead. This distinction is important because it indicates the quality of the SINRD instrument, specifically its superiority over total neutron counting because of its ability to detect fissile material and not just ^{244}Cm (burnup). If there would be no such distinction between the absence of fissile isotopes and the absence of Cm in this diversion scenario, then the advantage of the SINRD instrument would be more or less limited to the outer three rows of pins. A caveat to this conclusion is that perhaps the additional SINRD information about the fissile content of the outer three rows does somehow reduce the uncertainty in the total neutron count rate coming from the inner pins.

Lastly, since SINRD is a passive technique like PNAR and DDSI, it has the same difficulty of having large uncertainties in the measured count rates or needing long measurement times when the neutron flux that is emitted from the fuel assembly is weak. Thus, SINRD may be impractical for measuring fresh or slightly burned fuel assemblies. For example, when the NGSI made a SINRD measurement on a fresh fuel assembly in air, they put a ^{252}Cf source either next to it or inside of it to provide a sufficient neutron flux [39].

5. The photon-based NDA techniques

In this section, the five photon-based NDA techniques of the NGSI (Table 1) are described and discussed. At the beginning of the subsection of each NDA technique, a short summary table is given that lists the prominent characteristics of that technique. Afterward, the principle of operation, the design of the NGSI's version of the NDA instrument, the method by which the data are analyzed, and the limitations of the technique are described.

The five techniques are categorized in Table 14 according to the genesis, or origin, of the photons that are measured, and the rest of this section will follow this categorization. In three of the techniques, the photons are created from fission events, whether the fission events that occurred previously while the fuel assembly was in the nuclear reactor, or the fission events that are actively induced in the fuel assembly during the NDA measurement. In two of the techniques, the photons come from fluorescence of the atoms of interest, whether from their electrons or their nuclei. This categorization highlights a fundamental physical principle of these photon NDA techniques, namely, that the ones that measure photons from fission are necessarily governed by the neutronic physics of the fuel assembly as well as by the photonic physics, whereas the ones that measure photons from fluorescence can be substantially independent of the neutronic physics. This concept is discussed in Sections 6.2.2 and 6.2.3.

Table 14: The five photon-based NDA techniques, categorized according to the genesis of the photons

The Genesis of the Photons	The Photon-Based NDA Techniques
Fission	DG: Delayed Gamma spectroscopy (DG)
	TG: Total Gamma-ray counting (TG)
	PG: Passive Gamma spectroscopy (PG)
Fluorescence	NRF: Nuclear Resonance Fluorescence
	XRF: X-Ray Fluorescence

In contrast to the neutron measurements in most of the neutron NDA techniques (except those in Section 4.3), the measurement of the radiation's energy is an essential aspect of the all of the photon NDA techniques except the total gamma-ray counting (TG) technique. The reason is that the energy of a gamma-ray is much easier to measure than the energy of a neutron, and furthermore, it is highly desirable to measure the energy of the radiation emitted by an atom, whenever possible, because it is usually the only aspect of the radiation that is characteristic of the atom. This is to say that in most cases, only the energy of the radiation provides conclusive information about what kind of atom emitted it. The reason why gamma-ray energy is easier to measure than neutron energy will be discussed below.

The details of how photons are detected and their energies are measured will not be given in this report. The reader is referred instead to a textbook on radiation detection, such as the classic book *Radiation Detection and Measurement* by Knoll [290]. A brief description of the types of detectors to be used in these NDA techniques will suffice here. The main type of detector for most gamma-ray and X-ray spectroscopic NDA techniques is the high-purity-germanium (HPGe) detector (and its antecedent, the lithium-drifted-germanium detector,

Ge(Li)). The reason is that this type of detector has the best energy resolution of any commonly available type. The superior energy resolution not only speeds the assay time by providing a better signal-to-noise ratio; it also enables certain methods of data analysis that cannot be performed with lower-quality data. On the other hand, the HPGe detector also has one of the smallest maximum count rates among commonly available detectors. The maximum is 100 kHz (i.e., 10^5 detections per second) at most [46, 291], and 20 kHz is a more realistic, conservative value for a typical maximum count rate [56]. Other types of gamma-ray detectors have worse energy resolution but may have higher maximum count rates. For example, cerium-doped lanthanum bromide ($LaBr_3$(Ce)) scintillator detectors have about 18 times worse energy resolution than HPGe detectors have [56, 292], but they can count at least 15 times as fast as HPGe detectors [56], i.e., up to 1 MHz and beyond [291, 293]. Other types of scintillator detectors that have been used in NDA work include NaI(Tl) scintillators and CdZnTe (also known as CZT) scintillators. For certain NDA techniques and methods of data analysis, the higher maximum count rates of these scintillator detectors as compared to that of HPGe detectors outweigh their worse energy resolution. An additional advantage of these scintillator types is that they are often cheaper than HPGe detectors.

As said above, the energy of gamma-rays is easier to measure than the energy of neutrons that are about 1 MeV or less (i.e., fission-spectrum and slower neutrons). The reason is that the energy of gamma-rays is not separable into kinetic energy and rest-mass energy, as is the energy of neutrons. The goal in the measurement of gamma-ray energy is to absorb the gamma photon completely, whereas the goal in the measurement of neutron energy is to measure only the kinetic energy. The range of gamma-ray energies of interest to spent-fuel NDA is from tens of kiloelectron-volts to several megaelectron-volts, and in a gamma-ray detector, all of this photon energy goes toward making electric charge that can be detected and analyzed. The ionization energies of most of the gases used in ionization chambers and proportional detectors is between 10 eV and 25 eV (Table 5.1 in Knoll [290]); and the energy to create an electron-hole pair in a chilled germanium detector is about 3 eV (Table 11.1 in Knoll), in a NaI(Tl) scintillator is about 20 eV (page 237 in Knoll), and in a CZT scintillator is about 4.5 eV (Table 13.5 in Knoll); so each gamma photon can be expected to create thousands of fundamental units of charge (e) or more in any gamma-ray detector. In contrast, while the kinetic energy of fast neutrons can be measured directly by ionization in recoil detectors, the kinetic energy of thermal and epithermal neutrons cannot, since it is well below these minimum ionization energies of detectors. Even if charge is created by releasing some of the rest-mass energy of a thermal or epithermal neutron (939.6 eV) through a neutron reaction, the neutron's kinetic energy is so minor in comparison to the released energy (i.e., to the Q value of the reaction) that it is effectively overwhelmed and lost to the detector. Thus, the direct measurement of a thermal or epithermal neutron's kinetic energy in a detector is practically impossible. Nevertheless, thermal and epithermal neutrons have essential importance to the neutronic physics of spent fuel assemblies; the 0.3 eV neutron resonance of ^{239}Pu is just one example. Therefore, neutron energy must be measured in an indirect way, such as the three ways described in Section 4.3: by the neutron's time of flight (NRTA), by its slowing-down time (LSDS), or by its absorption in filters (SINRD). Such indirect ways of

measuring neutron energy are much more cumbersome than the direct way of measuring gamma-ray energy in a detector.

5.1 Distinguishing fissile material by the gamma-rays it emits from fission

Three kinds of gamma-rays that are emitted by fission can be recognized, according to their time of emission. Prompt gamma-rays are created at the instant of the fission event itself; delayed gamma-rays are created somewhat later from the decay of short-lived fission products; and even-more-delayed gamma-rays are created hours to years after the fission event has occurred. Such “more-delayed” gamma-rays are often called passive gamma-rays in the context of spent-fuel NDA, since they are continuously emitted from the fuel without the need for any additional excitation from the outside. Generally, prompt gamma-rays are not used for spent-fuel NDA, since an external neutron source would be required to create them; and in that case, the neutron signal is more informative than the prompt-gamma-ray signal, since the gamma-ray energy is not informative and since the neutron signal is less attenuated. Therefore, only delayed gamma-rays and passive gamma-rays are used as NDA signals. The NDA techniques that exploit these gamma-ray signals are discussed in this section.

5.1.1 Delayed Gamma spectroscopy (DG)

Name	Delayed Gamma spectroscopy (DG)
References	NGSI: [40-49] Other: [294-301]
Measurement environment	In water, primarily; but in air has also been considered [47]
Passive vs. Active	Active neutron source; minimum source = $1 \cdot 10^{11}$ neutrons/s [48]
Time dependency	Time-dependent (long-pulsed "one pass" or short-pulsed)
Particles detected	Gamma-rays
Type of detectors	High-purity germanium (HPGe) detectors for detailed spectroscopy [48]; lanthanum bromide ($LaBr_3$) for rough spectroscopy [48] and for totals counting of high-energy gamma-rays only [300]
Particles' detected attribute	Energy
Governing physical properties of the fuel assembly	For absolute measurements The leakage multiplication of external-source neutrons with reflection (ARR·$M_{L,ext}$; Section 4.1.3.3), but specifically isolating the amount of induced fission from the amount of neutron absorption For relative measurements The proportion of fission in ^{239}Pu to fission in ^{235}U
Governing isotopes	Fissile isotopes; neutron absorbers
Maturity	Has been tested on small samples of fissile materials in various forms of packaging Has been used to measure the fission rates in single fuel pins that have been slightly irradiated in a zero-power research reactor [299]
Limitations	Requires a strong neutron source to overcome the passive gamma-ray flux from the spent fuel assembly Attenuation of the gamma-rays from the inner pins makes it difficult to determine the absolute amount of fission
Selected by the NGSI for prototype testing?	Yes, at the Central Storage of Spent Nuclear Fuel (CLAB), Sweden [15]

5.1.1.1 Principle of operation

Delayed Gamma spectroscopy (DG) is an active technique in which neutrons are injected into the spent fuel assembly, induce fission, and produce gamma-rays that are emitted from the fuel assembly and detected. Thus, the interrogating radiation is neutron radiation, but the detected radiation is gamma radiation. The gamma radiation that is measured by the DG technique is not the prompt gamma radiation from the fission events themselves but rather is the delayed gamma radiation that comes from the radioactive decay of the fission products.

Thus, the gamma-ray detection is performed not simultaneously with the neutron irradiation and but rather during a separate measurement time period after the irradiation.

As with delayed neutrons (Section 4.1.6.1), the total amount delayed gamma radiation is emitted over an extended period of time after the fission event [298]. Therefore, the DG technique can be performed either with many repetitions of a short cycle of irradiation and detection or with only a few repetitions of a long cycle of irradiation and detection. The shorter cycle produces a stronger signal from the fission products with shorter half-lives, while the longer cycle may be easier to implement in some situations. The NGSI has examined both kinds of cycles [48].

Because the interrogating radiation (neutrons) is different from the detected radiation (gamma-rays), the DG technique exhibits aspects of the physics of both kinds of radiation. The effects of the neutron irradiation will be discussed first, followed by the aspects of the gamma-ray detection.

The neutron irradiation of the spent fuel assembly can be described by the neutron diffusion equation (Equation 3) or a similar neutron-transport equation. Therefore, the number of fission events that are induced, the absolute amounts of the fission products that are produced, and the absolute gamma-ray activities that are emitted are all dependent on the same neutronic physical properties of the spent fuel assembly on which the neutron-based NDA techniques are dependent (Section 4). In this sense, the DG technique is very similar to the DN technique (Section 4.1.6) and has the same problem, namely, that the absolute DG signals are likewise dependent upon the burnup, initial enrichment, and cooling time of the spent fuel assembly (i.e., the BIC set of variables; see Section 6.2). On the other hand, a beneficial similarity is that the DG technique is likewise able to isolate the induced-fission term of Equation 3, as illustrated by equations corresponding to the DN equations (Equations 18 and 19):

$$S_{PRI} + (\bar{\nu} - 1)\Sigma_{\mathrm{f}}\phi_{irr} - \Sigma_{\mathrm{a,capture}}\phi_{irr} - D\nabla^2\phi_{irr} = \frac{1}{v}\frac{\partial\phi_{irr}}{\partial t} \qquad \text{Equation 18}$$

$$Gamma\ Activity \propto \int_{\mathrm{Irradiation}} \Sigma_f \phi_{irr} dt' \qquad \text{Equation 44}$$

Therefore, as with the DN technique, an integration of the DG technique with any of the neutron NDA techniques that can observe only neutron multiplication (i.e., PNAR, CIPN, and DDA) should be particularly useful.

The detection of gamma-rays permits the use of gamma-ray energy spectroscopy to determine relative information about specific fissile isotopes. The energies of the gamma-rays that are emitted from fission products during their radioactive decay are usually characteristic to the emitting isotopes. (See Figure 55, for example.) Therefore, the activity of each set of characteristic-energy gamma-rays corresponds to the quantity of the emitting fission product. Next, the isotopic distribution of the fission products depends both on the fissioning isotope and on the energy of the incident neutron that induces the fission. (See Figure 56, and note that independent, not cumulative, fission yields are important for DG since its objective is to observe their gamma-emitting radioactive decay within short timeframes following fission.)

For the fissile isotopes, an approximation can be made that only thermal-neutron-induced fission is important since their thermal-fission cross sections are very much larger than their fast-fission cross sections. Therefore, the differences in the quantities of the emitting fission products can be related to differences in the amounts of fissile and fissionable that have fissioned. Thus, by measuring the activities of gamma-rays with specific energies, the quantities of the emitting fission products can be determined, from which the quantities of the fissioning isotopes can be determined. In practice, various factors, such as gamma-ray attenuation, typically cause the uncertainties in the absolute quantities to be unacceptably large and thus restrict the determined quantities to being relative to each other rather than absolute. (See the bottom of Figure 57, for example.)

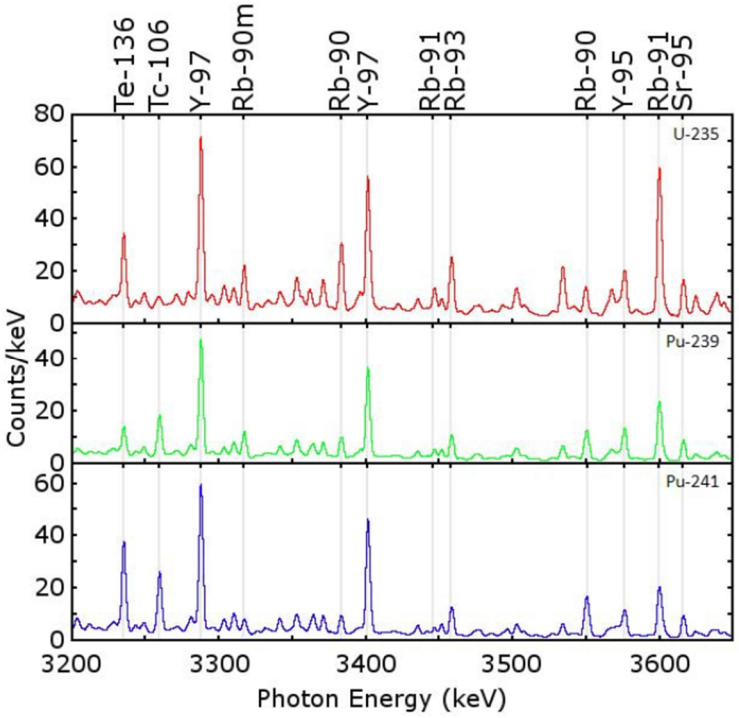

Figure 55: "Example pulse-height spectra of active-interrogation signal for pure U-235, Pu-239, and Pu-241 for a HEDGS measurement protocol of 10-seconds on, 10-seconds off and 10 minutes of total interrogation time." Copied from Campbell and Smith [41] with permission from INMM.

It is important to recognize that the fast fission of ^{238}U can contribute a significant DG signal (Figures 56 and 57) that can cause errors in the interpretation of the overall DG signal. The fast fission of ^{238}U produces a distribution of fission products that is fairly similar to that of the thermal fission of ^{239}Pu [298]. Therefore, the signal from the fast fission of ^{238}U can be misinterpreted as being from the presence of more ^{239}Pu than actually exists in the fuel. In fresh fuel, the gamma-rays emitted from the β-decay of the ^{239}Np that is created by neutron capture in ^{238}U can provide information on the quantity of ^{238}U in the fuel, which might help to resolve this problem, but in spent fuel, these ^{239}Np gamma-rays are overwhelmed because they are all at relatively low energy [294]. Marrs et al. have noted that although the cumulative fission-product yields for the mass-132 chain are similar for both 14 MeV neutron fission of ^{238}U and thermal fission of ^{239}Pu, the independent yields are different [298]. Therefore, they suggested examining the time dependence of the gamma-ray activity from ^{132}I

as a means of distinguishing between ^{238}U and ^{239}Pu. They had some difficulty with this approach, however, and furthermore it is unclear whether the same approach can be used if the fast fission of ^{238}U is by Watt-fission-spectrum neutrons [303] rather than by 14 MeV neutrons. The conclusion is that, with the current state of the art, the fast-fission of ^{238}U must be minimized in the DG technique as it must be in the DN technique also (Section 4.1.6.1). Such minimization consists only of minimizing the fast fission by the irradiating neutrons, by moderating them to below 1 MeV before introducing them to the spent fuel assembly. Nothing can be done to minimize the fast fission of ^{238}U by the fast neutrons that are born from induced fission in the fissile isotopes.

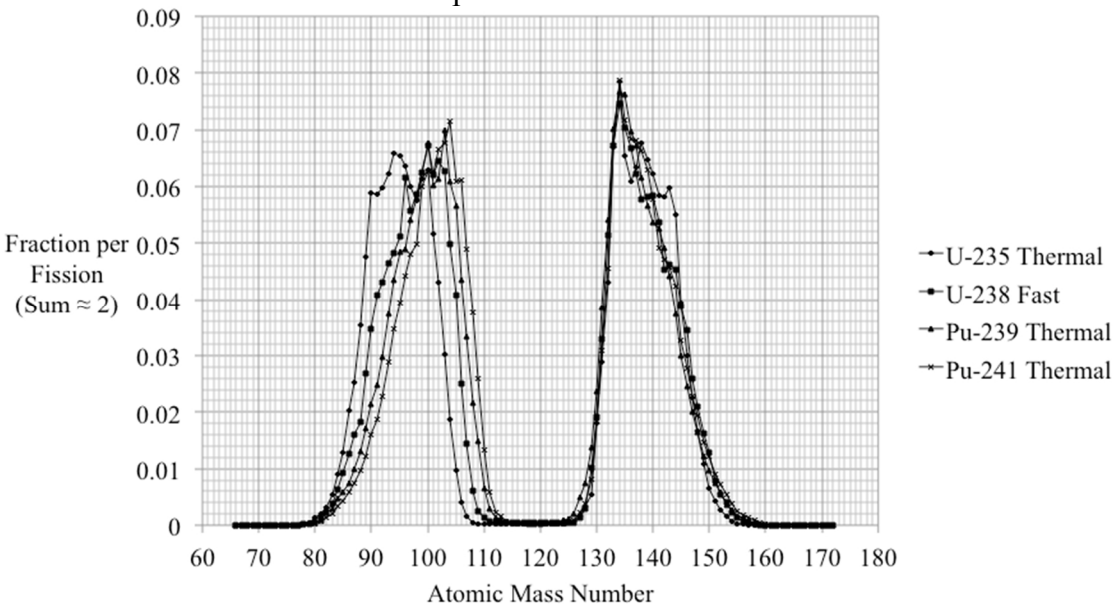

Figure 56: Independent fission yields from neutron-induced fission (thermal = 0.0235 eV; fast = 500 keV). Data are from ENDF/B-VII.1 [125] in the Flexible Database Explorer [302].

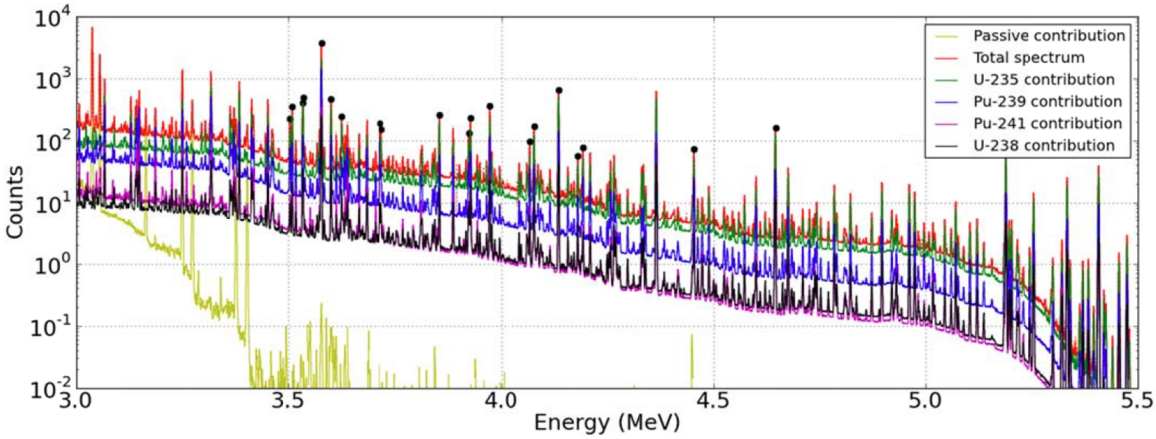

	Atom Fraction		
	U-235	Pu-239	Pu-241
Normalized to fissile content	0.350 ± 0.020	0.424 ± 0.026	0.226 ± 0.056
Normalized to U-235 content	1.000 ± 0.020	1.213 ± 0.037	0.646 ± 0.156

Figure 57: Top: "Calculated HPGe delayed gamma-ray spectra for [BU = 60 GWd/tU, IE = 5%, CT = 5 years] (from NGSI spent fuel library). Black markers indicate peaks used for demonstration of the response de-convolution algorithm that determines relative fissile isotopic content." Bottom: Corresponding results. Copied from Mozin et al. [49] with permission from INMM.

Mozin et al. [48] point out that the signal from ^{241}Pu is also very similar to that from ^{239}Pu, so a separation between these two isotopes may be difficult to achieve in practice.

5.1.1.2 The NGSI's designs

The NGSI's investigation into the DG technique was split between two parallel teams, one at Pacific Northwest National Laboratory (PNNL) and the other from the University of California (Berkeley) (UCB), Lawrence Berkeley National Laboratory (LBL), and Idaho State University (ISU). The results of both teams were roughly similar, and they made a joint publication near the end of Phase I of the NGSI's project [48].

Both NGSI teams have emphasized examining the gamma-rays that have energies above 3.0 MeV. The primary reason is that the passive gamma-ray background from the long-term cooling of the spent fuel drops off to very low activities above this energy [48]. (See Figure 57.) The PNNL DG team has focused specifically on the energy range between 3.2 MeV and 3.65 MeV (Figure 55) for the additional reasons that the attenuation coefficient of lead (Pb) is both at its minimum and fairly constant within this range [41, 44]. (See Figure 65 in Section 5.1.3.4, below.) The gamma-rays in this range are therefore preferentially less attenuated by lead shielding and are also all attenuated by the same amount such that the sizes of their peaks are not distorted relative to each other. Because of this focus on the high-energy portion of the spectrum, the PNNL team named their technique, "High Energy Delayed Gamma Spectroscopy," with the acronym "HEDGS" [41].

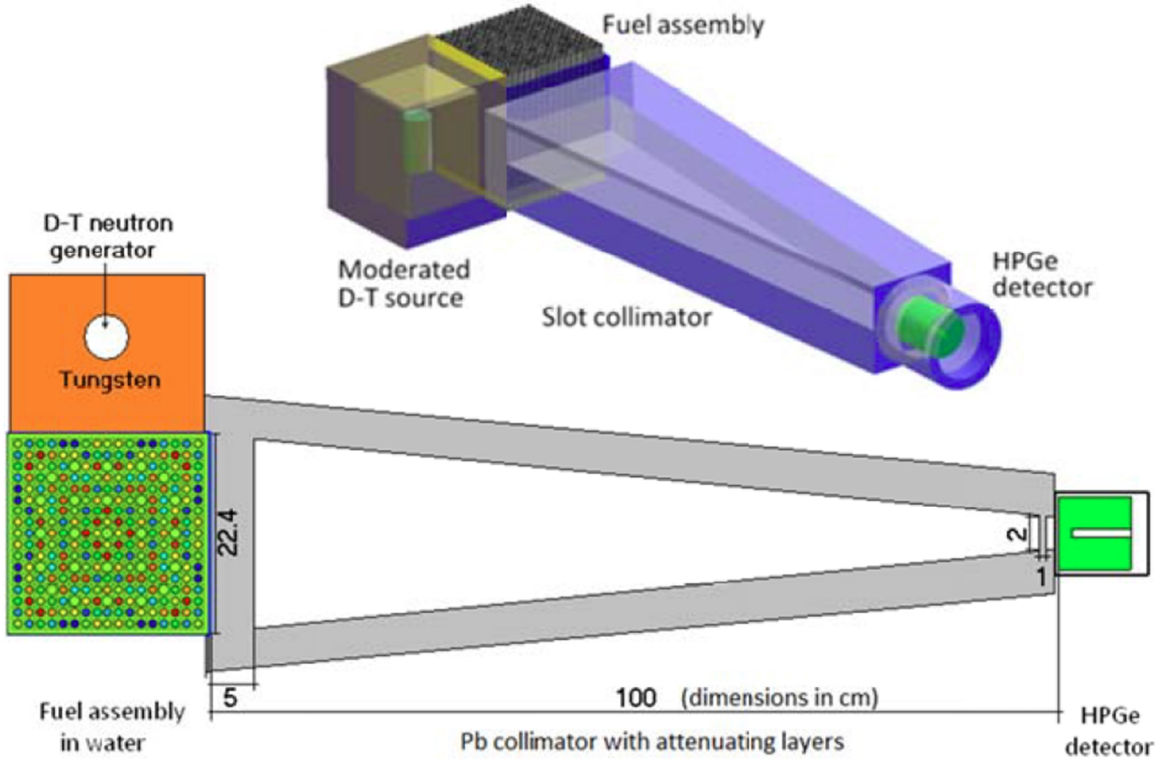

Figure 58: DG instrument designs proposed by the UCB/LBL/ISU team.
Copied from Mozin et al. [49] with permission from INMM.

Each team has proposed different DG equipment (Figures 58 and 59). Although both teams have proposed using a D-T neutron generator and an HPGe detector, the other aspects of the

designs are different. The UCB/LBL/ISU team has nominally proposed using tungsten as the neutron-moderating, spectrum-tailoring material around the neutron generator [49], whereas the PNNL first proposed using iron and then changed to Pb after making a comparative analysis [47]. As said in the previous subsection, the neutrons from the D-T generator must be moderated in order to minimize the fast fission of ^{238}U. The D-T generator produces neutrons with 14 MeV energy [182]. Other differences are discussed in the following paragraphs.

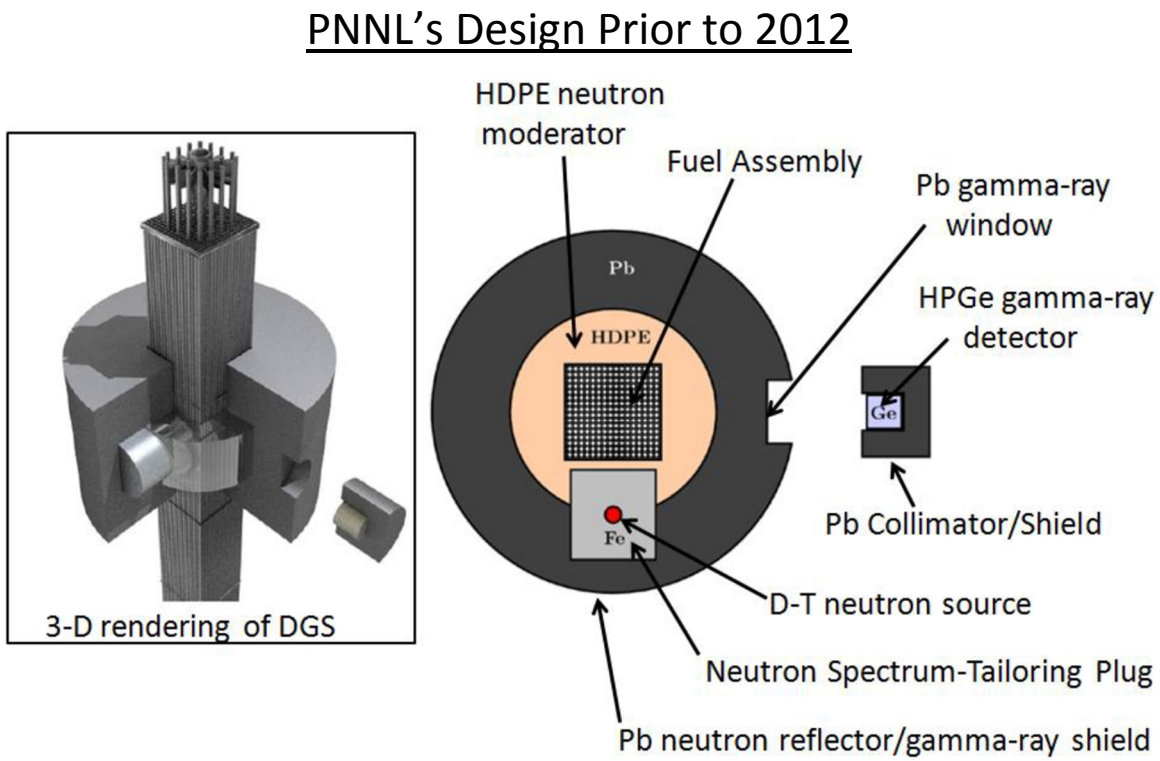

Figure 59: DG instrument designs proposed by the PNNL team.
Copied from Kulisek et al. [47] with permission from INMM.

The PNNL team initially assumed that the spent fuel assembly would be in air during the DG measurement [41, 47]. Based on this assumption, they surrounded the fuel assembly first with high-density polyethylene (HDPE) and then with a Pb shield, in order to moderate the interrogating neutrons, reflect them back into the assembly, and provide some radiation protection for the environment surrounding the DG instrument. They cut a cylindrical notch in this Pb shield to serve as a window for observation by the HPGe detector, but they left a portion of the thickness of Pb in the window to attenuate the passive gamma-ray background being emitted by the spent fuel assembly. The HPGe detector was offset from the window by a distance that was left undetermined but was to be based on a compromise between the increased gamma-ray flux from being closer and the decreased neutron-radiation damage to the detector from being farther [47]. No significantly additional collimation between the window and the HPGe detector was necessary because the Pb shield itself provided sufficient shielding.

In the 2012 design, the PNNL team changed the assumption to assuming that the spent fuel assembly (and the DG instrument) is in water. The water provides sufficient neutron moderation so that the HDPE around the fuel assembly can be removed from the design. The Pb shield and window have been retained, though.

In contrast, the UCB/LBL/ISU team has always assumed the fuel assembly would be in water. (See Figure 3 of Mozin et al. [42].) Therefore, although they initially included Pb shielding in their design [42], they eventually removed it and instead have chosen to use a slot collimator between the fuel assembly and the HPGe detector to manage the gamma-ray flux (i.e., count rate) and to protect the detector. The slot collimator is made from Pb and has a field of vision that spans the width of the fuel assembly [49].

Another difference between the designs of the two NGSI teams is the duty cycle of the measurement. The UCB/LBL/ISU team has chosen to focus on what they have called a “one-pass” approach, which consists of only one, long period of irradiation (30 minutes or more) that is followed by one, long period of counting the delayed gamma-rays (also 30 minutes or more) [49]. The PNNL team has chosen the opposite, “pulsed” option, consisting of many repetitions of a short irradiation period (10 seconds) and a short counting period (also 10 seconds). The total measurement time of PNNL’s design can last from tens of minutes to an hour or more [48]. This 20 second duty cycle is still much longer than the 2 second duty cycle of the NGSI’s DN instrument design (Section 4.1.6.2), presumably because the gamma-rays are emitted over a much longer time period (tens of minutes to hours) than are the delayed neutrons (the longest half-lives in Table 11 in Section 4.1.6.1, above, are slightly less than one minute). As was said in the previous subsection (5.1.1.1), the advantage of the “pulsed” duty cycle is the increase in the average gamma-ray activity of the isotopes with shorter half-lives, whereas the advantage of the “one-pass” duty cycle is simplicity.

5.1.1.3 Data analysis

The NGSI and most of the other literature have emphasized using the DG signal to determine the relative proportions of fission in the fissile isotopes rather than the absolute, total amount of fission. Therefore, this kind of relative analysis will be discussed first, and absolute analysis will be discussed afterward.

5.1.1.3.1 Relative data analysis

The determination of the relative proportions of fission in the fissile isotopes is based upon separating the measured DG spectrum into its component contributions from the pure fissile isotopes, including a correction for the contribution from ^{238}U. This partitioning is possible because of the differing energies of the gamma-rays emitted from the differing amounts of different fission products created from the various fissile isotopes, as explained above. The analysis thus consists of scaling the spectral contributions of the pure fissile isotopes (and of ^{238}U) in such a way that the measured spectrum is reproduced. This scaling or fitting is typically done by a least-squares regression algorithm. The resulting scaling factors indicate the relative proportions of fission in the fissile isotopes.

This spectral separation (or de-convolution) can be performed with regard to the entire spectrum, a limited range of the spectrum, or specific gamma-ray peaks within the spectrum. As mentioned in the previous subsection (5.1.1.2), both NGSI teams focused on the high-energy portion of the spectrum. Using simulated DG results, the UCB/LBL/ISU team performed fitting of the range from 3.5 MeV to 5.0 MeV, while the PNNL team performed fitting of the range from 2.5 MeV to 4.8 MeV [48]. (This fitting range by PNNL was larger than their targeted range of 3.2 MeV to 3.65 MeV because they used the extra portions of the spectrum to account for the gamma-ray background; see page 7 of Campbell et al. [44].) In addition to these fittings of relatively broad spectral portions, the UCB/LBL/ISU team also tried fittings based on more limited data portions. They performed two kinds of fittings based only on the set of the ten most intense gamma-ray peaks in the high-energy region [48]. In one kind of fitting, they took a 25 keV wide slice of the spectrum surrounding each peak and performed the fitting on this set of spectral slices. In the other kind of fitting, they determined the area under each peak (i.e., the total number of counts comprising each peak) and performed the fitting on the set of peak areas. They found that the fitting over the broad spectral region provided the best, most accurate results [48].

The NGSI teams primarily analyzed simulated spectra that had excellent energy resolution corresponding to the expected resolution from HPGe detectors. In addition, the UCB/LBL/ISU team also analyzed simulated spectra corresponding to a $LaBr_3(Ce)$ detector, which has worse energy resolution. Not surprisingly, they found that the fits to the HPGe spectra were more accurate than the fits to the $LaBr_3(Ce)$ spectra [48].

Some of the previous, non-NGSI work also focused on relative data analysis, such as the works by Beddingfield and Cecil [295], Firestone et al. [297], and Marrs et al. [298]. Such work was also based on peak areas or intensities, like the UCB/LBL/ISU team's analysis of the relative peak areas of the ten most intense high-energy peaks. The foremost difference between this previous work and the NGSI work is that the previous work merely identified gamma-ray peaks that are particularly indicative of the fission of specific isotopes (e.g., ^{235}U vs. ^{239}Pu) and formed ratios of such peaks to identify and distinguish between pure materials. Unlike the NGSI's work, this previous work did not extend the analysis to determining the proportions of fission in mixtures of fissionable isotopes, which is the condition of spent fuel assemblies.

For this reason, the least-squares fitting that was done by Marrs et al. (Section 3.1 of their paper [298]) is not the same as the least-squares fitting that the NGSI teams did. The fitting by

Marrs et al. was used only to determine accurately the intensity of a peak for which the source isotope was already known. In this fitting, the measured peak was compared to the expected peak position and shape corresponding to the known isotope. In contrast, the NGSI teams used least-squares fitting to reconstruct the measured spectral portions or peaks as a superposition of unknown constituent contributions from multiple fissionable isotopes. Thus, the fitting by Marrs et al. was a preliminary step of preparing the data to be analyzed subsequently in the form of a ratio, whereas the fitting by the NGSI teams was the main data analysis itself. From a mathematical perspective, Marrs' use of a single ratio to apportion the induced fission between two possible isotopes (e.g., ^{235}U and ^{239}Pu) is an exactly constrained system of equations, whereas the NGSI's use of multiple peaks and/or swaths of the spectrum for such apportioning leads to an over-constrained system of equations that requires least-squares fitting to obtain the best fit. Performing the apportioning based on *multiple* ratios, on the other hand, would likewise require a similar least-squares fitting.

It appears that the NGSI has not yet considered in detail such an analysis based on multiple ratios [48]. As mentioned before, the UCB/LBL/ISU team did perform an analysis based on multiple peaks, but the peaks were chosen according to their strength rather than their parent fission isotopes (e.g., ^{235}U or ^{239}Pu) [48, 49]. If the peaks would instead be chosen selectively according to the information that they provide about the parent fission isotopes, then the least-squares fitting of these multiple peaks might be more efficient than the fitting of the entire high-energy portion of the spectrum yet suffer little loss of accuracy.[2]

Marrs et al. [298] gave five criteria for selecting the most informative gamma-ray peaks: (1) The peaks should either be unique to the parent fission isotope or be produced roughly equally by all the fissile isotopes (i.e., insensitive to the fission isotope). Ratios of the former kind to the latter kind (e.g., corresponding to ^{235}U/(^{235}U + ^{239}Pu)) are useful for subsequent analysis because they are easier to calculate and tend to have less temporal volatility than ratios of unique-isotope peaks (e.g., ^{235}U/^{239}Pu) [295]. (2) The peaks should not be affected by the energy of the incident neutrons that induce the fissions, unless an analysis of the energy spectrum of the incident neutron flux is specifically desired. (3) The peaks should not overlap other gamma-ray peaks from the gamma-ray background, such as from neutron-activated structural materials in the surrounding environment. Presumably, this background would also include the passive, self-generated gamma-ray flux in the case of a spent fuel assembly. (4) The peaks should not overlap other delayed-gamma-ray peaks from other isotopes to the extent that the peaks cannot be resolved from each other. Alternatively, if there are contributions from other, unresolved peaks, the contributions should be small and easily corrected for. (5) Lastly, the pairs of peaks used in ratios should be close in energy to each other "in order to minimize the energy-dependent corrections for absorption and detector efficiency in an actual diagnostic measurement" [298].

The peaks selected by Marrs et al. [298] probably would not be useful for spent-fuel NDA because they are too low in energy (between 500 keV and 2560 keV). Marrs et al. were concerned with using the DG NDA technique for forensic analysis following a nuclear

[2] This choice between fitting peaks and fitting an entire spectrum is similar to the choice of analysis of LSDS data, between time intervals matrix analysis and spectral de-convolution (Section 4.3.2.3). The difference with DG is that self-shielding is not as much of an issue in the relative analysis of DG data as it is in LSDS analysis.

explosion, and presumably the gamma-ray background in this energy range in such a measurement would be less than that in a spent-fuel measurement. Nevertheless, their five criteria might be useful for selecting similarly informative gamma-ray peaks in the higher energy region. In that case, the development of a DG analysis based on least-squares fitting of multiple informative ratios for the application to spent-fuel NDA might be a fruitful area for future work.

5.1.1.3.2 Absolute data analysis

The NGSI teams mentioned the possibility of using the DG signal to determine the amount of induced fission (or the fission rate) in the spent fuel assembly, but they did not investigate it [48]. They mentioned that factors such as neutron absorption would have to be taken into account; these factors are those expressed in Equations 18 and 44 on page 123 (Section 5.1.1.1). Thus it is seen that the absolute measurements depend on the BIC variables (see Section 6, below), just as most of the neutron-based NDA techniques do. On the other hand, the DG technique's ability to perform energy spectroscopy does confer one advantage to it, namely, the ability to separate directly the actively generated, delayed gamma-rays from the self-generated, passive gamma-rays. In comparison, the actively generated, delayed neutrons in the DN technique are indistinguishable from the self-generated, passive neutrons and the secondary neutrons. Since all neutrons appear to be the same to the detectors in the DN technique, it is only by solving Equations 18 and 19 simultaneously (along with some other information) that the total delayed-neutron flux can be identified.

The separation between the active and passive gamma-ray fluxes in the DG techniques can be made in two ways. One way is to identify specific gamma-ray peaks that can come either only from the short-lived, actively generated fission products or only from the long-lived, burnup-generated fission products. This way is basically what Kröhnert et al. [299, 301] did in their work. They chose the ^{142}La (2542 keV), ^{89}Rb (2570 keV), ^{138}Cs (2640 keV), and ^{95}Y (3576 keV) gamma-ray lines as representative delayed-gamma-ray lines, and they identified the ^{137}Cs (662 keV) and ^{154}Eu (1276 keV & 1596 keV) gamma-ray lines as representative passive gamma-ray lines. The other, more simple way is to divide the entire energy spectrum into a low region (less than 3 MeV) and a high region (greater than 3 MeV) and to recognize that the gamma-rays in the high region come almost totally from the short-lived, actively generated fission products. In this second, simple way, the energy resolution of the energy spectrum is largely unimportant, since only the total counts in each region are important. Thus, a more robust yet lower resolution gamma-ray detector, such as a $LaBr_3$(Ce) detector, can be used for making measurements in this second way. The reason that Kröhnert et al. [299, 301] did not use this second way for their experiments is probably because the delayed gamma-rays in the high-energy region were too weak, on account of the irradiation intensity being limited by the maximum power of the zero-power PROTEUS research reactor. In contrast, the strength of the NGSI's proposed D-T generator should be sufficient to produce a good high-energy signal.

The basic parts of an absolute analysis can be seen in the equations that Kröhnert et al. [299, 301] used to calculate the absolute fission rate, F, in a fuel pin based on the measurement of a gamma-ray peak at energy E_γ. (See also the similar equations in Phillips et

al. [127] (Equation 1) and in Chapter 8 of Reilly et al. [75] (Equations 8-1 and 8-10).) This fission rate corresponds to the spatial integration of the fission term in Equation 18 and is expressed as follows:

$$F = \frac{N_{net}(E_\gamma)}{\varepsilon(E_\gamma) att(E_\gamma) b(E_\gamma) C} \qquad \text{Equation 45}$$

Here, N_{net} is the net count area of the peak; ε is the detector's efficiency for detecting gamma-rays at that energy; *att* is an attenuation factor that accounts for the solid angle covered by the detector and also their attenuation from their point of generation to the detector; b is the branching intensity of the gamma-ray peak; and C is the correction factor for the buildup of the fission products during irradiation and also their decay during and after irradiation. This last correction factor, C, incorporates the time integration in Equation 44 and is expressed by the following form in the case that isomers of the fission products are neglected:

$$C = \left(\frac{Y_{ind,2}}{\lambda_2} + \frac{i_{12}\lambda_1 Y_{cum,1}}{\lambda_2(\lambda_1 - \lambda_2)}\right)(1 - \exp(-\lambda_2 t_i))\exp(-\lambda_2 t_c)(1 - \exp(-\lambda_2 t_a)) + \left(\frac{i_{12}\lambda_2 Y_{cum,1}}{\lambda_1(\lambda_2 - \lambda_1)}\right)(1 - \exp(-\lambda_1 t_i))\exp(-\lambda_1 t_c)(1 - \exp(-\lambda_1 t_a)) \qquad \text{Equation 46}$$

Index 1 refers to the direct parent of the detected fission products, and index 2 refers to the fission product itself. Y_{ind} is the effective independent fission yield; Y_{cum} is the effective cumulative fission yield; λ is the decay constant; t_i is the irradiation time; t_c is the cooling time; and t_a is the measurement time. The fission-product yields, Y, are weighted composites of the corresponding yields from the individual fissionable isotopes, as follows:

$$Y = a_{U\text{-}235}Y_{th,\,U\text{-}235} + a_{U\text{-}238}Y_{f,\,U\text{-}238} + a_{Pu\text{-}239}Y_{th,\,Pu\text{-}239} + a_{Pu\text{-}241}Y_{th,\,Pu\text{-}241} \qquad \text{Equation 47}$$

Here, the a variables are weighting coefficients; the subscript *th* refers to thermal-neutron-induced fission; and the subscript *f* refers to fast-neutron-induced fission. Note that the thermal fission of ^{238}U and the fast fission of the fissile isotopes are all negligible in comparison with the given fission terms. Lastly, these equations thus far refer to the calculation of the fission rate from only one gamma-ray peak. If multiple peaks are used, then a least-squares fitting of the fission rates determined from the various peaks is necessary to find the most accurate value. If a range of the energy spectrum is used to calculate the fission rate, then the right-hand-side of Equation 45 must be integrated over that range, with C being redefined to accommodate the fact that various fission products contribute at various energies. Thus, C would probably have to be defined empirically in this latter case.

Equations 45 through 47 reveal the basic parts of an absolute analysis. The neutron-induced fission during irradiation produces a certain amount of fission products, Y, per fission (Equation 47). These fission products both build up and decay, so the per-fission quantities Y must be adjusted to reflect these changes, producing C (Equation 46). The possibility that the fission products may decay in ways other than those that produce the expected gamma-ray of the desired energy must be taken into account through b; the fact that some gamma-rays that are produced will not arrive at the detector is taken into account through *att*; and the ability of the detector to properly detect the gamma-rays of the given energy is expressed through ε

(Equation 45). The net count area, N_{net}, is experimentally measured and produces the fission rate when divided by the expected number of gamma-ray counts per fission (i.e., the denominator of Equation 45).

The chief difficulty with absolute analysis is the complications of determining the attenuation factor, *att*. This attenuation factor is based on the geometrical arrangement of the radiation source (e.g., the fuel pin or assembly) and the detector. The determination of the transport and attenuation of the gamma-rays from their points of origin to the detector is difficult enough once their points of origin are known, but these points of origin—that is, the spatial distributions of the fission products—are also variable and depend on the spatial distributions of both the fissionable isotopes and the interrogating neutron flux. Thus for the case of a spent fuel assembly, the attenuation factor, not just the quantities of the fission products, also changes with the BIC set, especially with the axial burnup profile. These geometric considerations as expressed through the attenuation factor can be quite difficult to handle accurately, as Kröhnert et al. discovered when they tried to compare measurements of fresh fuel in one position with measurements of burnt fuel in another position, relative to the detector [301]. It is for this reason that most researchers, including Kröhnert et al., endeavor to express even absolute fission rates as relative ratios of fission rates from two samples that have been measured in the same geometrical configuration, since many geometric influences cancel in such ratios. Likewise, the nondestructive assay of spent fuel assemblies by the DG technique will almost certainly need to use calibration to take care of such geometric influences empirically.

5.1.1.4 Limitations

The DG NDA technique has a few limitations. Firstly, it requires a strong neutron source to produce enough low-energy, delayed-gamma-ray activity that can overcome the self-generated, passive gamma-ray activity from the spent fuel assembly and/or to produce enough high-energy, delayed-gamma-ray activity to obtain sufficient counting statistics in a reasonable period of time. As said before, the NGSI has focused on the high-energy region. Secondly, the DG technique has difficulty to determine the absolute amount of fission because of the attenuation of the gamma-rays from the inner pins. This attenuation is the most severe limitation. Thirdly, the gamma-ray detector of choice, namely, a high-purity germanium detector, is limited both by its inability to process count rates greater than about 100 kHz and by its relatively short lifetime caused by sensitivity to damage by fast neutrons (see Kulisek et al. [47]). The fact that the neutrons that the D-T generator produces start out at 14 MeV instead of with a lower-energy, Watt fission spectrum [303] exacerbates the fast-neutron damage to the detector.

On the other hand, it is notable that DG does not suffer the same limitation as the DN technique regarding the separation among the two source terms and the induced-fission term of Equation 19. The energy spectroscopy of the DG technique allows it to directly determine the fission rate by distinguishing the actively induced, delayed gamma-rays from the self-generated, passive gamma-rays and from the prompt gamma-rays from spontaneous and induced fission, according to their different energies.

5.1.2 Total Gamma-ray counting (TG)

Name	Total Gamma-ray counting (TG) (also known as gross gamma-ray counting)
References	NGSI: [15] Other: [9, 75, 142, 145, 304, 305]
Measurement environment	In water (in air or other gas is also possible)
Passive vs. Active	Passive
Time dependency	Time-independent (continuous)
Particles detected	Gamma-rays
Type of detectors	Ion chambers, if energy spectroscopy is not also being performed PG detectors, if energy spectroscopy is being performed; the TG signal is a by-product in this case
Particles' detected attribute	Existence (quantity)
Governing physical properties of the fuel assembly	The total gamma-ray activity of the long-lived fission products (i.e., those with half-lives greater than a few days)
Governing isotopes	Main: ^{137}Cs, ^{134}Cs, ^{154}Eu Lesser: ^{95}Zr, ^{95}Nb, ^{144}Ce+^{144}Pr
Maturity	Currently in use
Limitations	Attenuation of the gamma-rays from the inner pins makes it difficult to detect partial defects and to determine the actual total gamma-ray activity of the assembly
Selected by the NGSI for prototype testing?	Yes, in every proposed combination; see Table 2

5.1.2.1 Principle of operation

Total gamma-ray counting (also known as gross gamma-ray counting) is the most basic gamma-ray NDA technique. It is merely the measurement of the self-generated gamma-ray flux that is emitted from the fuel assembly. Therefore, it is a passive and time-independent technique. The self-generated gamma-ray flux originates from the radioactive decay of fission products that were created by the fission of atoms during the burning of the fuel assembly in the nuclear reactor. As described in Section 3.3.4, the total rate of passive gamma radiation can be on the order of 10^{15} photons/s for a spent fuel assembly (30 GWd/tU, 5 years cooled, both PWR and BWR) [87]. After a cooling time of one month approximately, the total gamma-ray flux is dominated by the six isotopes shown in Figure 60, namely, ^{95}Nb (half-life = 35 days), ^{95}Zr (half-life = 64 days), ^{144}Pr (half-life = 17 minutes, in secular equilibrium with parent ^{144}Ce with half-life = 285 days), ^{134}Cs (half-life = 2.1 years), ^{154}Eu (half-life = 8.6 years), and ^{137}Cs (half-life = 30.1 years). (See also Fig. 14 in Cobb et al. [306].) Although other fission products besides the six listed ones do produce measurable fluxes of gamma-rays that can be distinguished with energy-sensitive gamma-ray detectors (see the PG technique), they do not contribute substantially to the total gamma-ray flux. Of course, there is a small

contribution of gamma-rays associated with the self-generated neutron reactions initiated by primary neutrons (e.g., from spontaneous fission), but this contribution is negligible. The total gamma-ray flux is thus considered to be produced directly by burnup and to be modified by the cooling time since the discharge of the spent fuel assembly from the reactor (Figure 61).

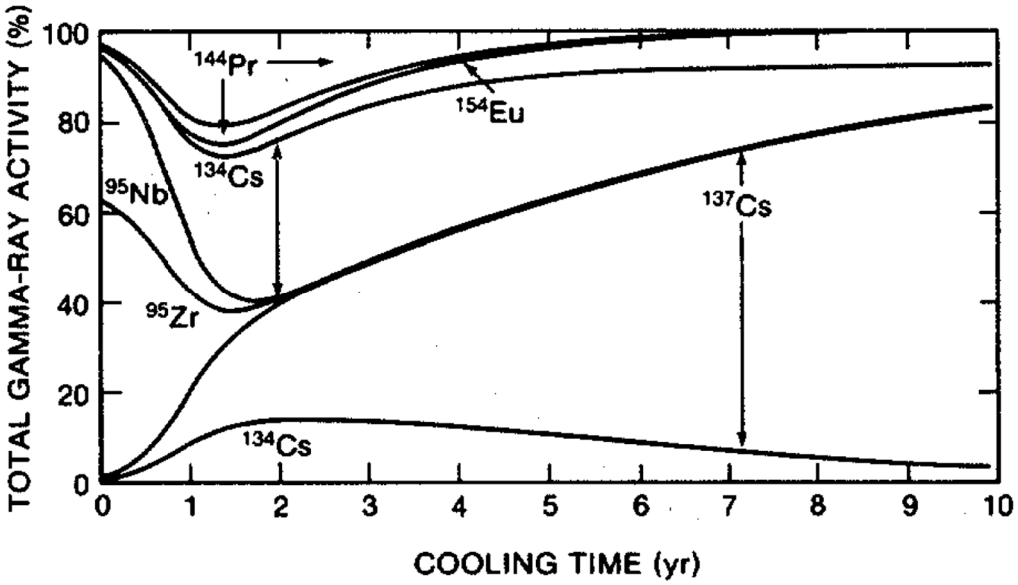

Figure 60: "An example of the variation in fission product gamma-ray activity as a function of cooling time, with each major gamma ray given as a percentage of the total activity. Note that ^{144}Pr and ^{134}Cs each have two major gamma rays shown. The curves are based on measurements of a PWR fuel assembly with an exposure of 12.18 GWd/tU and a cooling time of 2 yr. The extrapolation to longer and shorter cooling times was done by calculation."
Copied from Fig. 18.6 in Reilly et al. [75].

After the two shortest-lived fission products in the list—that is, ^{95}Nb and ^{95}Zr—have decayed away, the total gamma-ray activity (count rate) can be represented by a power law:

$$C_\gamma = a(\mathrm{BU})(\mathrm{CT})^{-b} \text{ for CT} > 12 \text{ months} \qquad \text{Equation 48}$$

The reason that these two isotopes cannot be included in this equation is that their concentrations in the spent fuel assembly at the time of discharge from the reactor depends on the reactor's recent operating history and the proximity of reactor control materials to the assembly in the reactor (Section 18.3.4 of Reilly et al. [75]). After the remaining isotopes besides ^{137}Cs have substantially decayed away relative to the activity of ^{137}Cs, the total gamma-ray activity is then represented by the exponential decay of ^{137}Cs:

$$C_\gamma = a(\mathrm{BU})e^{-\lambda(\mathrm{CT})} \qquad \text{Equation 49}$$

Historically, these equations have been used in conjunction with an *a priori* knowledge of the cooling time of the spent fuel assembly. Thus, a TG measurement combined with CT gives the BU of the assembly. The constants *a* and *b* are usually determined empirically by plotting and fitting the results from measurements of a range of spent fuel assemblies from the same spent fuel pool. Outlying fuel assemblies show up clearly on such a plot [145, 148]. Thus, the TG technique is used primarily for comparative measurements against a relative calibration curve rather than to assay a single spent fuel assembly against an absolute standard.

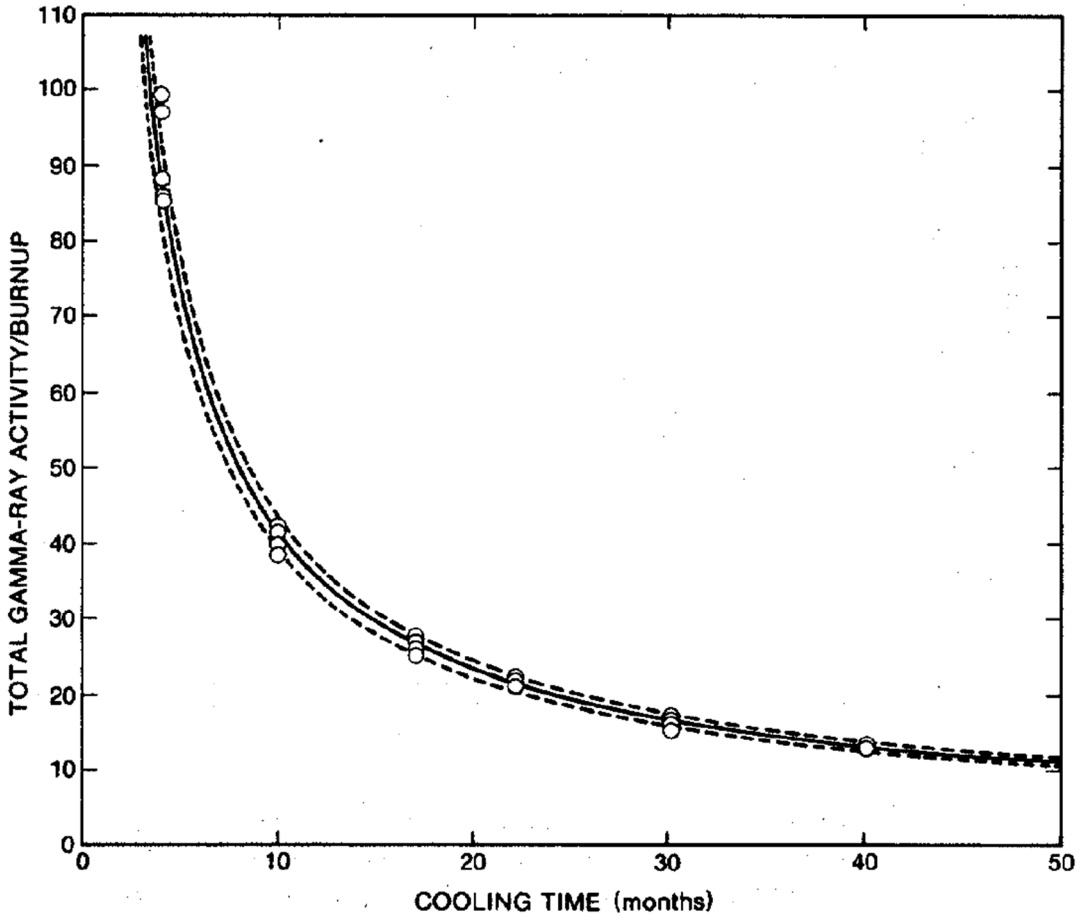

Figure 61: "Measured total gamma-ray activity divided by burnup as a function of cooling time for PWR fuel assemblies. The fitted curve illustrates how the total gamma-ray activity can be used to verify the consistency of operator-declared values for burnup and cooling time." Copied from Fig. 18.7 in Reilly et al. [75].

Total gamma-ray counting is currently used in IAEA safeguards, such as in the Fork detector (FDET) and the Safeguards MOX Python (SMOPY) detector [7, 9, 75, 143, 146]. The FDET uses an ion chamber to measure the total gamma-ray flux; the SMOPY detector uses a CdZnTe detector to perform passive gamma-ray spectroscopy (PG). The fuel assembly is raised out of its rack in the spent fuel pool, the detector is placed next to the assembly (usually near the midplane), and the measurement is made. (See Figure 10.) The Fork and SMOPY detectors also include neutron detectors besides the gamma-ray detectors.

5.1.2.2 The NGSI's design

The NGSI plans to include ion chambers in all of its prototype NDA instruments, to make TG measurements. For example, ion chambers were included in the PNAR instrument that was used to measure spent fuel assemblies at the Fugen Advanced Thermal Reactor (Figure 13). A main benefit of including such a TG-measurement capability in all the instruments is that the high TG count rate allows the NDA personnel to measure the axial burnup profile of a fuel assembly very quickly. This high detected count rate is made possible not only by the intense, passive gamma-ray flux but also by the ion chamber's ability to detect this flux without becoming overwhelmed by dead time, i.e., by its high maximum count rate.

5.1.2.3 Data analysis

The data analysis consists of employing Equation 49 or Equation 57, along with *a priori* knowledge of the cooling time, to determine the burnup of the fuel assembly. The fitting constants in these equations must come from measurements on a full cohort of similar spent fuel assemblies.

5.1.2.4 Limitations

The TG signal from the inner pins of the fuel assembly is attenuated by the outer pins. Therefore, TG is not sensitive to partial defects, in general. Furthermore, the existing method for analyzing TG data requires information from the reactor operator, either the burnup or the cooling time. Also, the TG method is largely insensitive to the initial enrichment of the fuel assembly, because the main gamma-ray emitter, ^{137}Cs, is produced in practically equal amounts by the fission of ^{235}U and the fission of ^{239}Pu. This attribute of the TG method is a benefit, rather than a limitation, in many cases.

5.1.3 Passive Gamma spectroscopy (PG)

Name	Passive Gamma spectroscopy (PG)
References	NGSI: [50-53] Other: [75, 78, 79, 102, 127, 142, 146, 306-324] Other (tomography):[325-332]
Measurement environment	In water (in air or other gas is also possible)
Passive vs. Active	Passive
Time dependency	Time-independent (continuous)
Particles detected	Gamma-rays
Type of detectors	High-purity Germanium (HPGe) detectors for detailed spectroscopy; other types of energy-sensitive gamma-ray detectors for lower-quality results
Particles' detected attribute	Energy
Governing physical properties of the fuel assembly	The gamma-ray activities of the governing isotopes listed below
Governing isotopes	Main: ^{137}Cs, ^{134}Cs, ^{154}Eu Lesser: ^{95}Zr, ^{95}Nb, ^{144}Ce+^{144}Pr, ^{106}Ru+^{106}Rh
Maturity	In use in the SMOPY detector [146] and in the enhanced Fork detector [314]; also tested extensively on spent fuel assemblies around the world for many years [307]
Limitations	Attenuation of the gamma-rays from the inner pins makes it difficult to detect partial defects Different attenuation of gamma-rays of different energy makes it difficult to form accurate ratios
Selected by the NGSI for prototype testing?	Yes, at the Central Storage of Spent Nuclear Fuel (CLAB), Sweden [15]

5.1.3.1 Principle of operation

Passive Gamma spectroscopy (PG) is a passive NDA technique that consists of measuring the energy spectrum of the gamma-ray flux being emitted from the spent fuel assembly. (See Figure 62 for an example.) This passively emitted gamma-ray flux is generated by the radioactive decay of the fission products that were created by the burning of the fuel assembly in the nuclear reactor. This gamma-ray flux is therefore directly proportional to the number of fission events that occurred in the fuel assembly while it was being burned in the reactor, which is to say that the PG signal is proportional to burnup, in general. (See also Equations 48 and 49 for TG counting, above.)

PG spectroscopy is the same as TG counting except that PG spectroscopy identifies the gamma-rays from particular fission products by measuring their characteristic energies. This ability allows the practitioners of PG spectroscopy to form ratios of the intensities of gamma-rays from two different isotopes. The goal is to infer BU by accounting for CT. A solution for

both BU and CT is possible if the two isotopes in the ratio have either different production rates from BU (i.e., different polynomial dependencies on BU) or different half-lives or if they have both differences. Then the two equations for the two isotopes are independent and can be solved simultaneously.

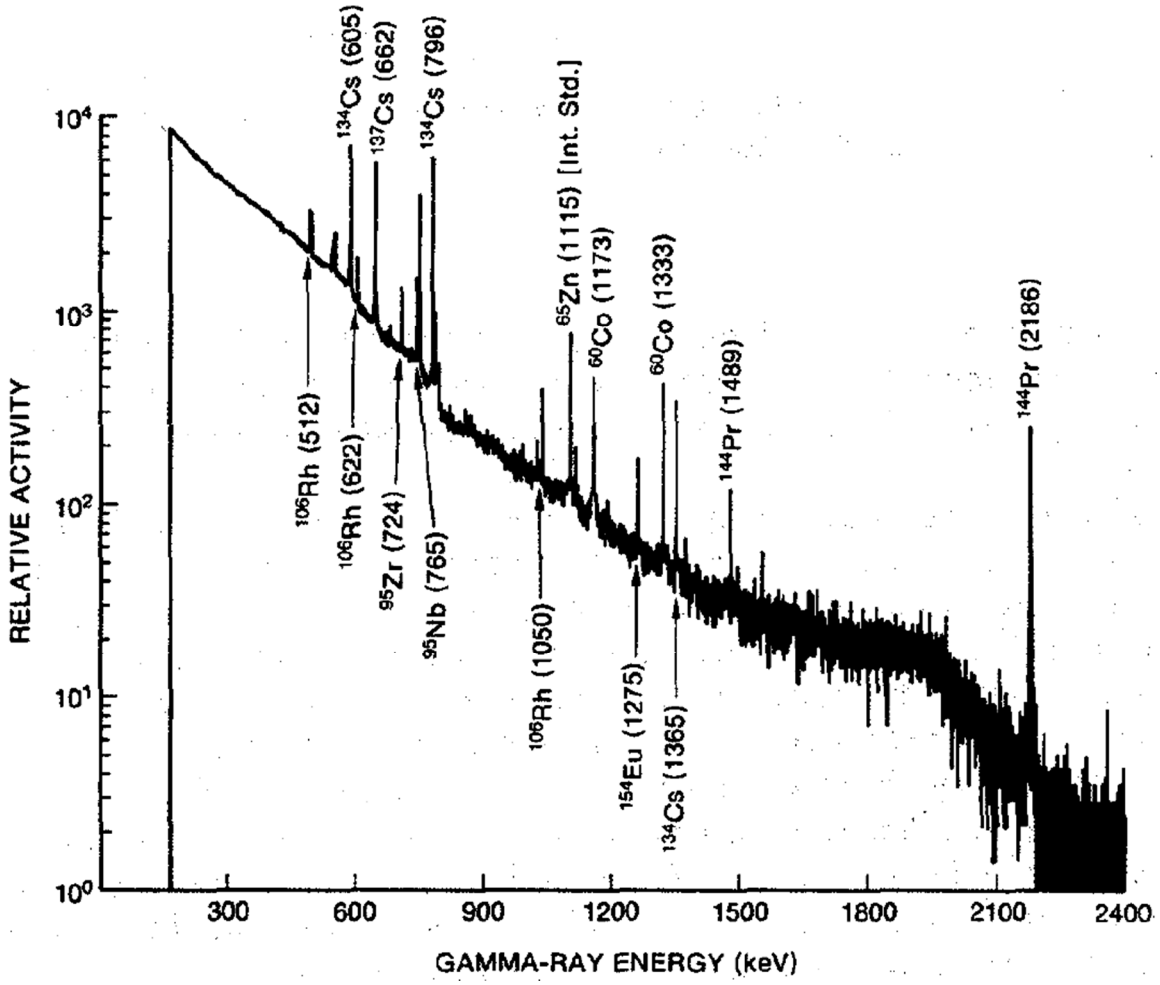

Figure 62: "Gamma-ray spectrum of a PWR fuel assembly with an exposure [burnup] of 32 GWd/tU and a cooling time of 9 months." Copied from Figures 1.14 and 18.3 of Reilly et al. [75].

The pair of ^{134}Cs and ^{137}Cs is an example that exhibits both of these differences. Their half-lives are different (2.1 years for ^{134}Cs vs. 30.1 years for ^{137}Cs) , and their production from BU is different. The production of ^{137}Cs is proportional to BU to the first power, because the fact that it is a direct fission product means that only one neutron—the neutron that induces the fission—is necessary to create it. In contrast, the production of ^{134}Cs is proportional to BU to the second power, because ^{134}Cs is produced by neutron capture in ^{133}Cs, which comes primarily from the beta-decay of ^{133}I, which is a direct fission product. (See page 62 and Figure A-4 in Phillips et al. [127].) Thus, the production of a ^{134}Cs atom requires two neutrons: one to induce the fission to make the ^{133}I and another to transmute the ^{133}Cs to ^{134}Cs. Because of both of these differences, the pair of equations that express the gamma-ray peaks of these isotopes as functions of BU and CT can be solved simultaneously for these variables, as follows [317]:

$$a_{137}i_{137} = \mathrm{BU} \cdot e^{-\lambda_{137}\cdot \mathrm{CT}} \quad \text{Equation 50}$$

$$a_{134}i_{134} = \mathrm{BU}^2 \cdot e^{-\lambda_{134}\cdot \mathrm{CT}} \quad \text{Equation 51}$$

$$\mathrm{BU} = \left[\frac{a_{134}i_{134}}{(a_{137}i_{137})^{\left(\frac{\lambda_{134}}{\lambda_{137}}\right)}}\right]^{\left(\frac{\lambda_{137}}{2\lambda_{137}-\lambda_{134}}\right)} \quad \text{Equation 52}$$

$$\mathrm{CT} = \left(\frac{1}{\lambda_{134}-2\lambda_{137}}\right)\ln\left[\frac{(a_{137}i_{137})^2}{a_{134}i_{134}}\right] \quad \text{Equation 53}$$

Here, i is a gamma-ray-peak intensity; a is a calibration or fitting constant; λ is a decay constant; and the subscripts "134" and "137" correspond to the two isotopes, respectively.

Only a few fission products have been identified as having sufficient intensity and other essential qualities to serve as indicators of burnup, and these are listed in Table 15. Note that this table does not include the gamma-rays that are emitted by the radioactive decay of the uranium and plutonium isotopes themselves, because as Cobb et al. [306] pointed out, "…their gamma rays (< 450 keV) are obscured by the Compton scattering of the higher energy gamma rays from the fission products." Of the fission products listed in Table 15, only three isotopes—^{137}Cs, ^{134}Cs, and ^{154}Eu—have half-lives that are long enough to be used after the spent fuel assembly has cooled more than about ten years (see Figure 60). Each of these isotopes emits gamma-rays of more than one energy; Willman et al. [317] focused on using the 662 keV peak from ^{137}Cs, the 795 keV peak from ^{134}Cs, and the 1275 keV peak from ^{154}Eu. The ^{154}Eu isotope deserves special mention: Even though it has a large neutron-capture cross section and should therefore asymptotically approach a saturation level in the reactor, it actually does not saturate and instead reflects well the total irradiation history of typical LWR fuel assembly (see page 70 of Phillips et al. [127]). This ability may be related to the fact that it is produced by multiple pathways. Lastly, it can be noted that none of these isotopes nor any other passive gamma-ray-emitting isotope produces a significant amount of gamma-rays with energies above about 3.5 MeV (Figure 57); the High-Energy Delayed Gamma Spectroscopy (HEDGS) technique (Section 5.1.1) exploits this fact.

5.1.3.2 The NGSI's design

For Phase I of the Spent Fuel Nondestructive Assay Project, the NGSI evaluated a PG spectroscopy system that uses a collimated, high-purity-germanium (HPGe) detector, as illustrated in Figure 63. In this configuration, the HPGe detector is located above the spent-fuel pool and over to one side, presumably where personnel can access it. The detector communicates with the spent fuel assembly via a long collimation tube. The water in the spent fuel pool thus serves not only to shield personnel from radiation but also to collimate the gamma-ray flux for the HPGe detector. This configuration has been used before in previous PG spectroscopy measurements of spent fuel assemblies [97, 127, 307].

Table 15: "Isotopes measurable by gamma rays in a typical irradiated fuel assembly." Copied from Table 18-3 in Reilly et al. [75], which was derived from Table V in Cobb et al. [306].

Fission Product Isotopes	Half-Life	Fission Yield in ^{235}U (%)	Fission Yield in ^{239}Pu (%)	Gamma-Ray Energy (keV)	Branching Ratio (%)
^{95}Zr	64.0 days	6.50	4.89	724.2	43.1
				756.7	54.6
^{95}Nb	35.0 days	6.50	4.89	765.8	99.8
^{103}Ru	39.4 days	3.04	6.95	497.1	86.4
				610.3	5.4
^{106}Ru-Rh	366.4 days	0.40	4.28	622.2	9.8
				1050.5	1.6
^{134}Cs	2.06 yr	1.27×10^{-5} [a]	9.89×10^{-4} [a]	604.7	97.6
				795.8	85.4
				801.8	8.7
				1167.9	1.8
				1365.1	3.0
^{137}Cs	30.17 yr	6.22	6.69	661.6	85.1
^{144}Ce-Pr	284.5 days	5.48	3.74	696.5	1.3
				1489.2	0.3
				2185.6	0.7
^{154}Eu	8.5 yr	2.69×10^{-6} [a]	9.22×10^{-5} [a]	996.3	10.3
				1004.8	17.4
				1274.4	35.5
Activation Products					
^{54}Mn	312.2 days			834.8	100.0
^{58}Co	70.3 days			811.1	99.0
^{60}Co	5.27 yr			1173.2	100.0
				1332.5	100.0

[a] Europium-154 and ^{134}Cs values are given only for direct production of the isotope from fission. Actually, each of these isotopes is produced primarily through neutron absorption. For PWR fuel material irradiated to 25 GWd/tU, the "accumulated fission yields" of ^{154}Eu and ^{134}Cs were calculated as 0.15% and 0.46%, respectively.

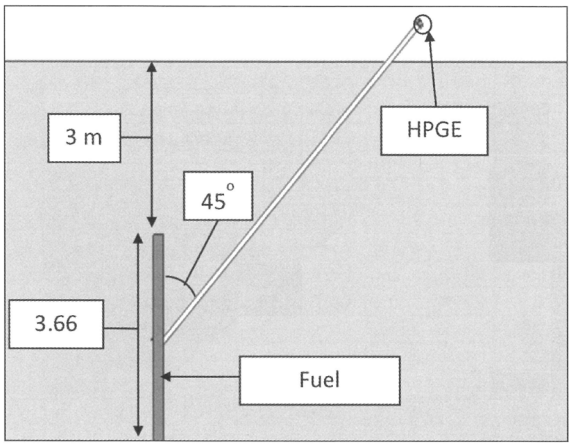

Figure 63: Setup for making PG spectroscopy measurements.
Reprinted from Galloway et al. [53] with permission from INMM.

Although this configuration was the one examined in Phase I, it may not be the configuration that is actually deployed during prototype testing in Sweden [15]. One problem with it is that the long collimation tube prevents it from being structurally integrated with other NDA techniques into a single instrument. Furthermore, all Swedish BWR nuclear power plants and the interim spent-fuel storage facility at CLAB already possess a collimator that is built into a wall of the spent-fuel pool [317, 329]. The collimator is like a horizontal, sealed hole through the side wall of the pool. By putting a spent fuel assembly in front of the collimator on the pool side, a PG measurement can be made with a HPGe detector at the other end of the collimator on the outside of the pool, at the same height. In this case, the pool's wall serves as radiation shielding for the equipment and personnel making the PG measurement. Since such setups are already available in Sweden, a separate PG spectroscopy setup for the NGSI-related testing may not be necessary.

It should be noted that the main reason that the long collimator is necessary is because the HPGe detector cannot handle a high count rate, i.e., more than a few hundreds of kilohertz [46]. Other types of gamma-ray detectors that can handle higher count rates can be placed closer to the spent fuel assembly. For example, the SMOPY detector [146] and the enhanced Fork detector [78, 79, 314] are positioned next to the spent fuel assembly and use CdZnTe (CZT) detectors with only short collimators. Similarly, the gamma-ray tomography instrument that has been tested in Finland and Sweden used Si(Li) and CZT detectors in relatively close proximity to the spent fuel assembly [330]; see Section 5.1.3.4.

5.1.3.3 Data analysis

The basic equations for calculating BU and CT from PG data are Equations 50 through 53, though modified for whichever two isotopes are being used, of course. Corrections for attenuation are discussed qualitatively in the next subsection (*Limitations*); quantitative details are presented in Chapters 8 and 18 of Reilly et al. [75].

5.1.3.4 Limitations

The most difficult problem of PG spectroscopy is the attenuation of the gamma-rays. Attenuation affects the assay in three main ways: (1) by limiting the ability to detect partial defects, (2) by introducing uncertainty regarding the representativeness of the measured signal to the characteristics of the entire fuel assembly, and (3) by introducing errors into ratios of two gamma-ray peaks by altering (3-a) their sampled volumes and (3-b) their detection efficiencies. These ways will be discussed in turn.

As with TG counting, it is difficult, if not impossible, to detect partial defects by conventional PG spectroscopy, because the gamma-rays from the inner pins cannot be detected well because they are too attenuated by the outer pins. A Monte Carlo simulation study in 1983 by Phillips and Bosler [333] found that 92% of the ^{137}Cs signal (661.6 keV) and 73% of the ^{154}Eu signal (1275 keV) come from the outer three rows of fuel pins in a spent PWR fuel assembly. (This study is also referenced on page 548 of Reilly et al. [75].)

A modification to PG spectroscopy that has potential to detect partial defects is gamma-ray tomography [330]. (See the list of references in the introductory table, above.) Several measurements are made as the fuel assembly and the gamma-ray detectors are rotated relative

to each other, and the various views are combined synthetically to create a two-dimensional, cross-sectional image of the gamma-ray activities of the assembly's fuel pins. The tomography is enhanced by measuring only high-energy gamma-rays, which necessarily must have experienced fewer scattering collisions on their way to the detector, since scattering reduces the gamma-ray energy. For example, Jansson et al. [331] performed tomography of a recently discharged, spent fuel assembly by measuring the 1596 keV gamma-ray peak from the decay of ^{140}La to ^{140}Ce, the ^{140}La itself (half-life = 1.68 days) being in secular equilibrium with the fission product ^{140}Ba (half-life = 12.75 days). This particular kind of measurement is feasible only at very short cooling times, obviously. Also, tomography's ability to detect fuel-pin diversions is limited [330]. Furthermore, nuclear-material assay cannot be done with gamma-ray tomography (as yet).

Because attenuation causes a conventional, non-tomographic PG system to detect gamma-rays from only the outer three or four rows of fuel pins of the assembly, a question arises about the extent to which that gamma-ray signal is representative of the entire spent fuel assembly. The NGSI spent significant effort on answering this question [51, 53]. The answer is connected with how the burnup is distributed transversely across the spent fuel assembly. For example, if the edge pins of the fuel assembly have burned more than the center pins, a PG measurement will overestimate the burnup of the entire assembly.

"Fortunately, there are a few factors that act to minimize the variance in the transverse burnup profile. First of all, the IE [initial enrichment] profile of a given model of fuel assembly from a given manufacturer should be consistent from fuel assembly to fuel assembly for commercial reasons. This consistency in the IE profile will carry over into more consistency in the BU profile and will thus minimize the uncertainty in the NDA correlations. Secondly, reactor operators generally strive to flatten the neutron flux transversely across the reactor core as much as possible, because doing so increases the total power that can be generated without reaching a maximum allowed temperature or heat flux at any particular point in the reactor. Thirdly, edge assemblies in the first power cycle are typically moved to another location in the reactor core for the second and subsequent power cycles, to produce a more even burning of the fuel. Therefore, the variance over the transverse profile caused by BU is often not very great, as Ezure [91] has observed for BWR fuel assemblies and as Galloway et al. [53] have indicated for PWR fuel assemblies." (Reprinted from [210] with permission from Elsevier.)

Attenuation introduces error directly into the determination of ratios of gamma-ray-peak intensities, in two ways, at least. Firstly, attenuation within the fuel assembly causes the sampled volumes of gamma-rays with different energies to be different. The attenuation coefficient of a given material is a function of the gamma-ray's energy. (See Figures 64 and 65 for example; see also Figure 3.21 in Lamarsh and Baratta [74].) Therefore, the same fuel-assembly material will attenuate different-energy gamma-rays differently, so that the less attenuated gamma-rays can originate from deeper within the fuel assembly yet still be detected than can the more attenuated gamma-rays. The sampled volume of the less attenuated gamma-rays is thus greater than the sampled volume of the more attenuated gamma-rays. For example, as mentioned above, Phillips and Bosler [333] calculated that 92% of the detected 661.6 keV gamma-rays from ^{137}Cs come from the outer three rows of fuel pins

in a PWR assembly, whereas only 78% of the 1275 keV gamma-rays from ^{154}Eu do, since they are less attenuated. This effect skews the ratio of the two gamma-rays from what would be expected from the quantities of the two isotopes in the fuel. Such differences in the sampled volumes can be calibrated away [75], but the effect does cause the result to be more sensitive to the consistency of the geometry of the measurement.

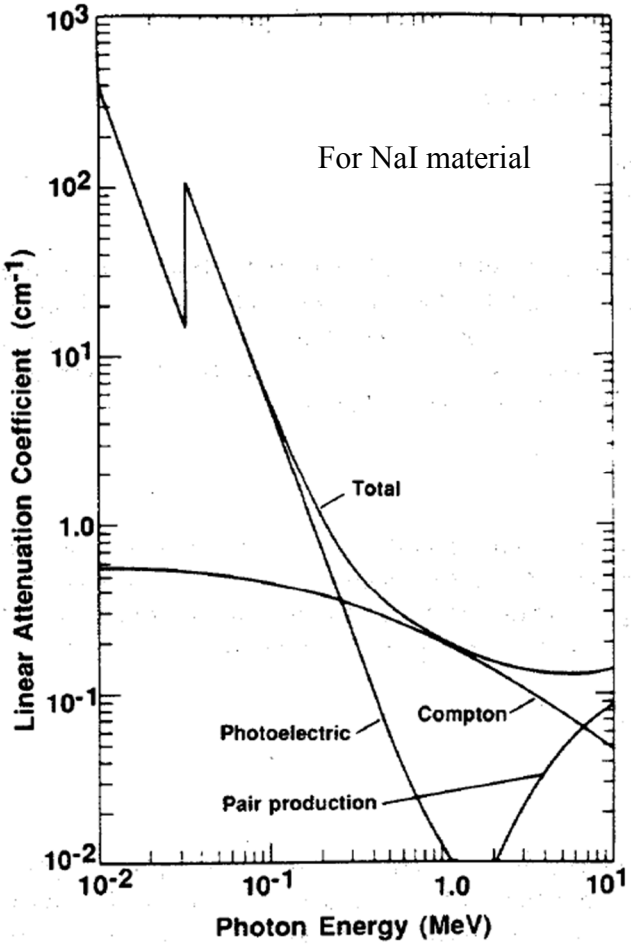

Figure 64: "Linear attenuation coefficient of NaI showing contributions from photoelectric absorption, Common scattering, and pair production." Modified from Figure 2.3 in Reilly et al. [75].

The second way that attenuation introduces error into the ratios of gamma-rays is by the "attenuation" within the detector itself—that is, by the percentage of the gamma-ray's energy that is deposited in the detector and thus detected. This detection efficiency depends on the gamma-ray's energy, again because the attenuation coefficient of the detector's material is a function of the gamma-ray's energy. As with the first effect of attenuation, this second effect can be calibrated away for a given detector, and since it is inherent to the detector, it is less sensitive to the geometry of the measurement.

Another limitation, discussed already (Section 5.1.3.2), is that HPGe detectors cannot handle count rates greater than about hundreds of kilohertz; their dead time becomes too great. Even though the high-energy gamma-ray count rates are well below this limit, the low-energy gamma-ray count rates are well above it. This limitation forces practitioners of PG spectroscopy to use long collimators or thick shielding or different, lower-resolution detectors.

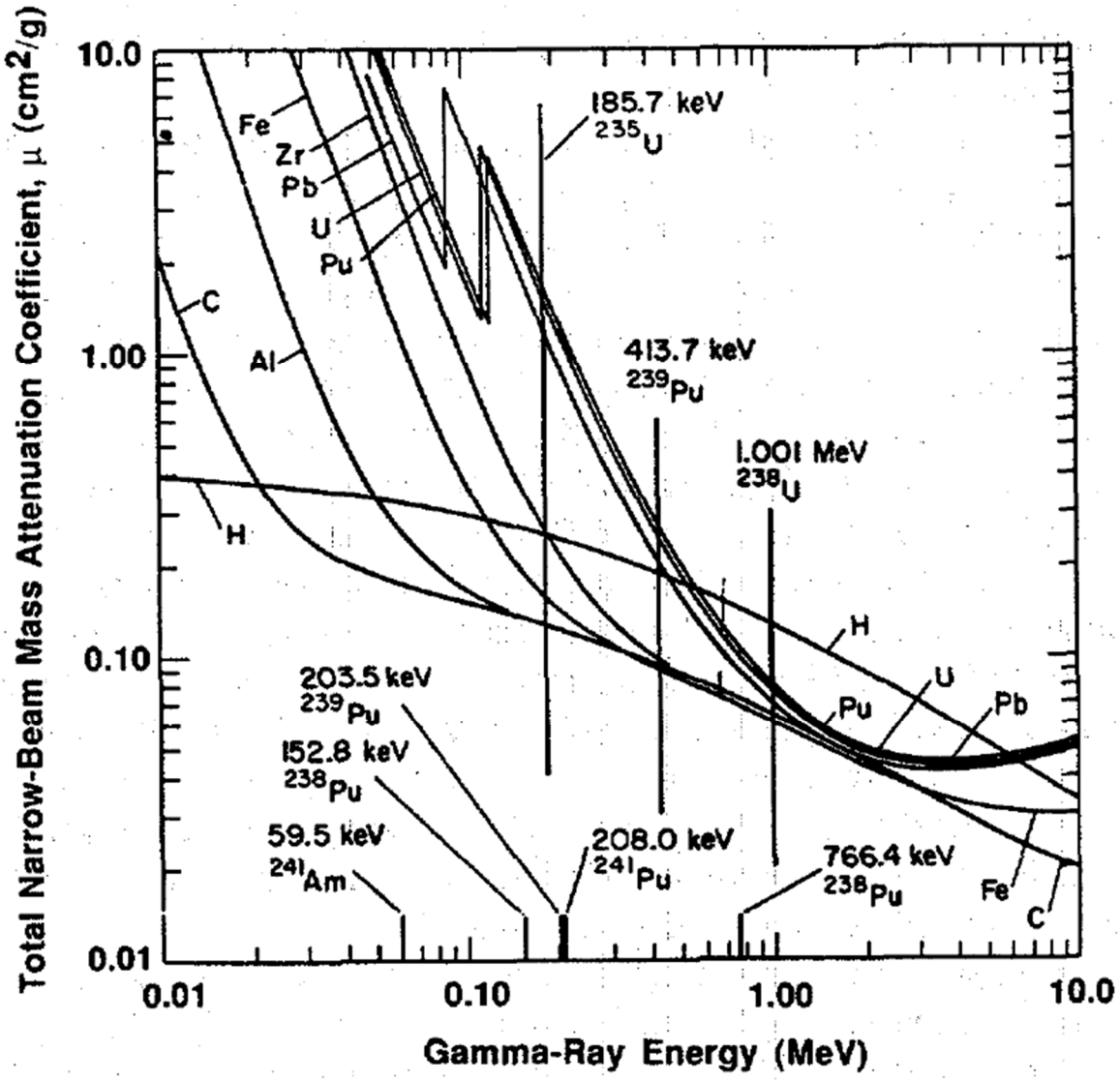

Figure 65: "Mass attenuation coefficients of selected elements. Also indicated are gamma-ray energies commonly encountered in NDA of uranium and plutonium" Copied from (Figure 2.12 in Reilly et al. [75].

5.2 Distinguishing fissile and other isotopes by their fluorescence of gamma-rays and X-rays

Fluorescence is the almost instantaneous emission of light radiation (i.e., photons) by an atom or nucleus after it has been excited by radiation. (Phosphorescence is similar, but the light is emitted over a longer period of time.) The key attribute of fluorescence that makes it valuable for NDA is that the emitted photons are at energies (wavelengths) that are characteristic of the emitting nucleus or atom. Thus, the unique energies of fluorescence photons both imbue them with information about the quantities of the fluorescing isotopes in the spent fuel assembly and allow them to be distinguished from other photons.

In the fluorescence NDA techniques, the exciting radiation comes from outside the atom or nucleus. In the broadest sense, the gamma-rays that come from fission could be considered as similar to fluorescence or phosphorescence photons, since at some point in the past, neutron radiation excited nuclei to unstable states, causing them to emit characteristic photons eventually. This association is typically not made, however. Only excitation by alpha, beta, or gamma radiation (or X-radiation) that does not lead to a nuclear reaction is considered as producing fluorescence.

Two types of fluorescence are considered in this section: fluorescence of gamma-rays by the nuclei of atoms, and fluorescence of X-rays by the electron clouds of atoms. In addition to this distinction of the origin of the photons, the gamma-rays generally have much higher energy than the X-rays.

5.2.1 Nuclear Resonance Fluorescence (NRF)

Name	Nuclear Resonance Fluorescence (NRF)
References	NGSI: [54-57] Other: [323, 334-396]
Measurement environment	In water (in air or other gas is also possible)
Passive vs. Active	Active
Time dependency	Time-independent (source is pulsed, but physics and data collection are instantaneous)
Particles detected	Gamma-rays (or neutrons for the photofission variation)
Type of detectors	High-purity germanium (HPGe) detectors for the best energy resolution; other types of energy-sensitive gamma-ray detectors for lower resolution; neutron detectors for the photofission variation
Particles' detected attribute	Energy (or quantity, for the IRT method)
Governing physical properties of the fuel assembly	The quantities of the fluorescing isotopes in the fuel assembly
Governing isotopes	Any heavy isotope of interest, including ^{235}U, ^{238}U, ^{239}Pu, ^{240}Pu, ^{241}Pu, and ^{242}Pu
Maturity	Has been performed for scientific measurements with pure and mixed targets; is being developed for cargo inspection [371]; has not yet been tested on spent fuel
Limitations	Needs a very strong gamma-ray source with the gamma-rays being at the correct, resonance energy Must be a dedicated facility because of the large size of the electron accelerator, the shielding around the gamma-ray detectors, and the need for a separate measurement station in the transmission configuration
Selected by the NGSI for prototype testing?	No

5.2.1.1 Principle of operation

Nuclear resonance fluorescence (NRF) is an active gamma-ray technique. Unlike in the technique of delayed-gamma spectroscopy (Section 5.1.1), both the interrogating radiation and the detected radiation in the NRF technique are gamma radiation (except in the photofission variant, which detects neutrons, as will be discussed below). In NRF, a gamma-ray beam that spans a range of energy is passed through the spent fuel assembly. The gamma photons that have energies that match the resonance energies of a specific isotope induce fluorescence in the nuclei of that isotope. In fluorescence, a nucleus absorbs a photon and goes to an excited energy state, and then it immediately de-excites (relaxes) and re-emits the photon, usually in a direction that is different from the incident direction. These re-emitted, fluorescence gamma-rays radiate in all directions (though not isotropically), so they are distinguishable from the gamma-ray beam. Furthermore, their preferred directions of

scattering both are different from the preferred directions from other types of photon scattering and are indicative of the polarization of the gamma-ray beam and the spin of the fluorescing nuclei [341]. Also, the re-emitted, fluorescence photons maintain energies that are characteristic of the isotope (Figure 66), in contrast with other scattering processes (particularly Compton scattering) that decrease the energy of the scattered gamma photon in non-characteristic ways. Thus, the fluorescence gamma-rays carry information about the quantity of the fluorescing isotope in the spent fuel assembly, and they can be distinguished from other gamma-rays by their energy. In summary, NRF gamma-rays represent the quantity of the fluorescing isotope in the spent fuel assembly, and they can be distinguished (and therefore measured) primarily by their energy but also by their direction, to a lesser extent.

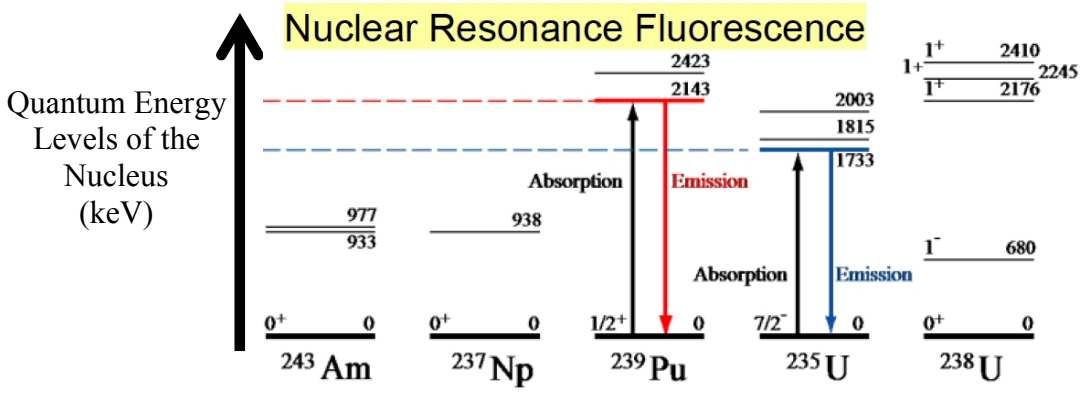

Figure 66: Quantum energy levels of several isotopes, to illustrate NRF. A 2143 keV gamma-ray beam will induce fluorescence only in ^{239}Pu nuclei (red), whereas a 1733 keV gamma-ray beam will induce fluorescence only in ^{235}U nuclei (blue). Modified from Figure 1 in Seya et al. [397] with permission from INMM.

Though the concept of NRF is as simple as equating the number of fluorescence gamma-rays proportionately with the number of fluorescing nuclei, the implementation of NRF as an NDA technique requires overcoming significant scientific and engineering challenges. These challenges are included in the following list:

- Creating the gamma-ray beam in an economic way yet with enough gamma-ray intensity
- Distinguishing the fluorescence gamma-rays from the gamma-rays that are scattered out of the beam by other means
- Distinguishing the fluorescence gamma-rays from the gamma-rays that are self-generated in the spent fuel assembly by radioactive decay processes
- Detecting and counting the gamma-ray photons fast enough so that these two kinds of distinguishing can be completed in a reasonably short amount of time

Other challenges exist, but these are the main ones, which if solved, would enable NRF to be a viable NDA technique.

Notably, the attenuation of the gamma-rays by the spent fuel assembly is not included in this list of challenges for NRF, which is unlike the cases of the other photon-based NDA techniques. The two reasons are (1) that NRF uses high-energy gamma-rays that are not attenuated as much as are the lower-energy photons in the other NDA techniques and (2) that the one-dimensional geometry of the NRF gamma-ray beam allows transmission

measurements to be insensitive to the three-dimensional geometry of the spent fuel assembly. (Such transmission measurements will be described and discussed in the next subsection.) This insensitivity to attenuation makes NRF unique among the 14 NGSI NDA techniques.

The next subsection (Section 5.2.1.2) will describe the equipment and configuration of an NRF NDA system and will simultaneously discuss the various ways to address the main challenges listed above. The remainder of this subsection (Section 5.2.1.1, *Principle of operation*) will be devoted to describing the main aspects of the physics of nuclear resonance fluorescence itself. The four aspects that will be discussed are (a) the angular dependence of the scattered (fluorescence) gamma-ray photons, (b) the energy of the gamma-ray beam that is used to induce NRF, (c) the energy of the fluorescence photons, and (d) the comparison of the energies of photons scattered by NRF versus the energies of photons scattered by other photon-scattering mechanisms.

(a) Gamma-ray photons that are scattered by the process of nuclear resonance fluorescence are not scattered isotopically, in general. Instead, they are scattered preferentially into certain angles, because of the requirements of the physics of spin [56, 334, 340, 341]. Figure 67 shows the preferred angles for the cases of spin 1/2 nuclei, such as ^{239}Pu. (The angles are referenced from the direction of the incident gamma-ray beam.) Isotopes with even mass numbers (e.g., ^{240}Pu) have different preferred angles than these. Because of all these angular preferences, the relative angle between a gamma-ray detector and the spent fuel assembly must be taken into account when directly measuring NRF-scattered photons, to achieve the best accuracy. According to Figure 67 and Section 3.1 of Shizuma et al. [396], the error from assuming isotropic scattering is about 10%.

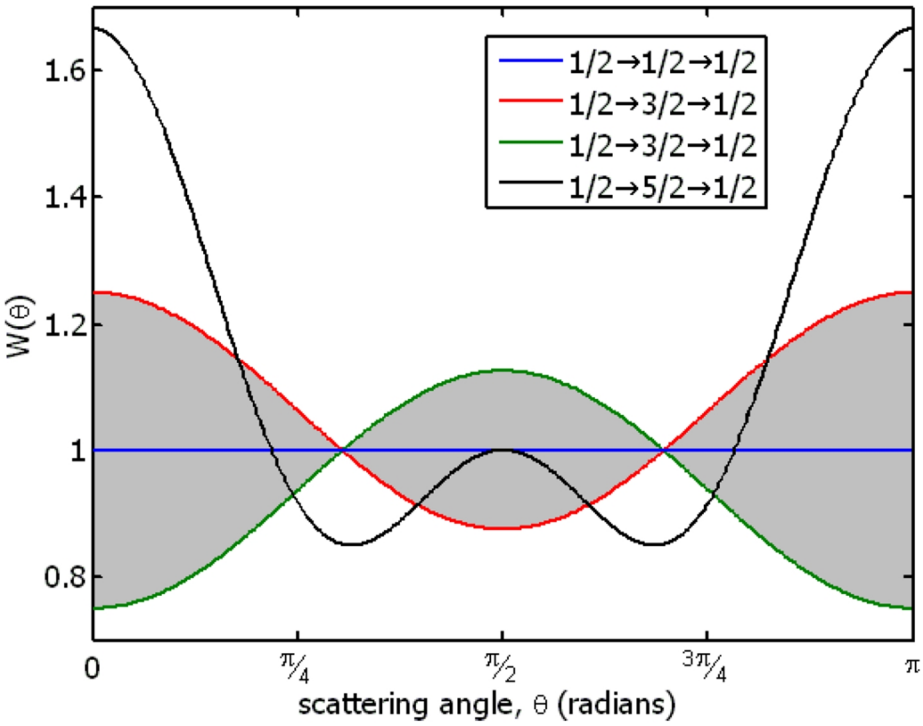

Figure 67: The angles into which NRF photons are preferentially scattered (corresponding to the shaded regions), for the case of spin 1/2 nuclei, such as ^{239}Pu. The overall transitions are from the ground state and back to the ground state. The transition to the spin 5/2 level (black line) rarely occurs. Copied from Figure 2.1 in Ludewigt et al. [56].

As Figure 67 and this estimate of error by Shizuma et al. indicate, though, NRF scattering is symmetric about the nucleus, even though not isotropic. This feature of NRF is in contrast to the angular dependencies of other scattering processes, both elastic and inelastic, most of which preferentially scatter gamma-rays into the forward angles. (Nuclear Thomson scattering is an exception [398].) Therefore, the NRF signal in the backward angles is greater on a relative basis than in the forward angles; that is, the signal-to-noise ratio is better for the backscattered photons.

Nevertheless, it should be kept in mind that the background noise from these other processes can still be stronger than the NRF signal even at the backward angles. This situation occurs when the amount of the fluorescing isotope—which contributes the NRF scattering and some non-resonant scattering—is much less than the amounts of the other isotopes—which contribute only non-resonant scattering. An example of this situation is backscattered-configuration measurements of the small concentrations of plutonium isotopes in a spent-fuel assembly. See Table 4.1 in Ludewigt et al. [56] regarding this background from bremsstrahlung sources and Section 3.3 in Shizuma et al. [396] regarding this background from quasi-mono-energetic sources.

(b) Nuclear resonance fluorescence can be induced by gamma-ray beams of many different energies. “Because NRF states are simply excited nuclear states, possible NRF gamma-ray energies range from tens of keV up to many MeV. However, for the purpose of using NRF to assay materials, photons of energy between 1.5 and 4 MeV are most useful.” [56] Two reasons why energies lower than 1.5 MeV are not useful are (1) that the passively generated gamma-ray background from the spent fuel assembly is large in this region (see Figures 57 and 62, for example) and (2) that these lower energy photons are much more attenuated during their transport in and through the spent fuel assembly (see Figure 65, for example). The two drawbacks of higher-energy gamma-rays are (1) they are more expensive to produce and (2) the higher-energy resonance states of many isotopes are not yet known as well as their lower-energy states are known. The efficient production of higher energy gamma-rays will be discussed in the next subsection, and further NRF experiments on pure isotopes will extend the knowledge of resonance states to higher energies (see References [342, 350, 356, 364, 384], for example).

(c) Nuclear resonance fluorescence is an elastic and coherent scattering process. It is elastic because after the scattering event, no additional particles exist besides the photon and the atom, and neither the photon nor the atom is left in an excited state. That is, the kinetic energy of the system is conserved, and no potential energy is created. The scattering is also coherent in the sense that the photon scatters off the entire nucleus simultaneously, such that the momentum of the photon is transferred to the entire nucleus rather than to one individual nucleon [399]. Since the mass of the entire nucleus is much greater than the mass of an individual nucleon, the photon effectively ricochets off the nucleus without transferring much of its energy to it, so that the energy of the scattered photon is almost the same as the energy of the incident photon.

The energy transferred from the photon to the nucleus is the nucleus’ recoil energy and is on the order of tens of electron-volts for collisions with high-energy gamma-rays. For example, it is 13.4 eV for the scattering of 2431 keV photons off ^{239}Pu (page 7 of Ludewigt et

al. [56]). The energy that the photon loses in the scattering event would thus be negligible except for the fact that it is just sufficient to shift the scattered photon off the resonance energy of the fluorescing isotope. Even after taking Doppler broadening into account, the energy width of a nuclear resonance is not as large as tens of electron-volts. Therefore, the scattered photon *cannot induce fluorescence a second time*. The scattering cross section for the once-scattered photon is thus non-resonant and much smaller. This fact is essentially beneficial for the application of NRF as an NDA technique because it drastically reduces the self-shielding of the fluorescing isotope and of the spent fuel assembly as a whole. The fluorescence photons are thus more able to escape the fuel assembly and be detected.

The above description of NRF as an elastic and coherent scattering process assumes that the nucleus is left in its ground energy state after the scattering event. (Figure 66 illustrates only such relaxations to the ground state.) It is also possible, though, for the nucleus to de-excite (relax) from the initial, high-energy excited state to another, less excited state. In this case, the NRF scattering event is inelastic because the nucleus is left in an excited state, and the scattered photon has less energy than the incident photon by an amount equal to this energy of the nucleus's excited state (plus the recoil energy). Often the excited state is the first excited state [396], but sometimes another excited state is the dominant one, such as the third excited state (46 keV) in the case of de-excitation from the 1815.2 keV state in ^{235}U [400]. Thus, there are two possible outcomes of an NRF scattering event: (1) elastic scattering that leaves the nucleus in the ground state and preserves the photon's energy and (2) inelastic scattering that leaves the nucleus in an excited state and subtracts this energy from the photon's final energy. Importantly, the energies of both kinds of fluorescence photons are characteristic of the fluorescing isotope, since both the ground and excited states are characteristic. In the following discussion, these two kinds of NRF photons will be referenced as *ground-state photons* and *excited-state photons*, respectively.

(d) Other elastic scattering processes besides nuclear resonance fluorescence exist, namely, Rayleigh scattering, nuclear Thomson scattering, and Delbrück scattering. (These three scattering processes will be collectively abbreviated as *RTD scattering*.) In Rayleigh scattering, the photon scatters coherently off the entire electron cloud of the atom [399]. In nuclear Thomson scattering, the electromagnetic field of the photon induces oscillatory motion of the positively charged nucleus, which in turn, re-emits the photon in a different direction [398]. In Delbrück scattering, the photon scatters off a dipole consisting of a positron-electron pair that exists in the strong Coulombic field in the vicinity of a nucleus [401]. These three scattering mechanisms are all considered to be coherent and to sum coherently. Since they all leave the atom in an unexcited state, they are all elastic scattering mechanisms. Finally, by virtue of the fact that they are all coherent scattering mechanisms, they transfer momentum from the photon to the entire atom and thus preserve the energy of the photon (less the minor amount of recoil energy).

For the sake of explanatory contrast and because it is a very prevalent scattering mechanism in NRF NDA, Compton scattering will also be quickly described now. Compton scattering is the inelastic and incoherent scattering of a photon from only one electron in the atom. Since only one electron is involved, Compton scattering is incoherent. Because of the lesser mass of the electron as compared with the mass of the entire atom, the transfer of

momentum from the gamma-ray photon to the electron is accompanied by a transfer of energy that is sufficient to eject the electron from its bound orbit. The sum of the final energies of the electron and the photon do not equal the incident photon energy because some potential energy remains in the atom since it is now ionized. Thus, Compton scattering is also inelastic. (A distinction should be noted between Compton scattering off a bound electron in an atom and Compton scattering off a free electron in an electron beam; the latter must be elastic since there is no ionization involved.)

The fact that RTD scattering is elastic causes some difficulty for NRF as an NDA technique. Since the energy of ground-state NRF photons is the same as the energy of photons scattered by RTD scattering, they cannot be distinguished easily by their energy. In a measurement of the energy spectrum of backscattered photons, such NRF-scattered gamma-rays appear only as a small resonance peak that is superimposed on a large background of these RTD-scattered gamma-rays [396].

The measurement of the excited-state NRF-scattered photons may be particularly useful in this case. In contrast with the energy of ground-state photons, the energy of excited-state photons is distinctly different from the energy of scattered photons from the elastic RTD scattering of incident photons *at the fluorescence energy*. As long as the incident beam *contains no photons at the same energy as the excited-state NRF scattered photons*, there can be no RTD scattered photons at that energy, so that the excited-state gamma-rays stand out well in the measured energy spectrum against the relatively much smaller gamma-ray background in that energy region. Of course, if the energy width of the incident gamma-ray beam is so large that it also contains such lower-energy incident photons, then those photons will undergo elastic RTD-scattering and will overlap with the excited-state photons. Such a situation is no better than the overlapping of RTD-scattered photons and ground-state NRF-scattered photons at the fluorescence energy. Thus, the utility of the excited-state photons depends on the energy width of the incident gamma-ray beam. In summary, for the specific NDA configuration of a narrow-energy incident beam and a measurement of backscattered photons, the signal-to-noise ratio for a measurement of excited-state photons should be better than for the measurement of ground-state photons [396].[3]

5.2.1.2 The NGSI's design and other designs, and data analysis

The use of NRF as an NDA technique is relatively new. For this reason, the NGSI examined several different methods of inducing, detecting, and analyzing the NRF signal. Rather than discussing each of these configurations as a separate whole, this report will proceed step by step through the NRF NDA technique and discuss the possible variants of each step, beginning with the generation of the gamma-ray beam, following it as it interacts with the spent fuel assembly, and ending with the detection of the characteristic NRF signal. The following discussion will also include some newer aspects that were not examined in the NGSI's Phase I report [56].

[3] It should be noted that for the heavy actinides of interest, the energy of the excited-state photons from inelastic NRF scattering is still greater than the Compton edge that is produced in the gamma-ray detector by the higher-energy photons from elastic NRF and RTD scattering (i.e., incident-energy, resonant-energy, ground-state energy photons). That Compton edge is approximately 256 keV less than the ground-state energy [290]; the difference between the excited state and the ground state is less than this amount.

The characteristic signal that is produced by the NRF process is revealed both by the photons that NRF scatters and by the photons that it does not scatter. In the first case, the NRF-scattered photons are detected directly, such as with gamma-ray detectors that are located behind the spent fuel assembly at the backscattered angles. This first case is called a "backscattered" measurement. (See Figure 68.) In the second case, it is the *absence* of the NRF-scattered photons, in the gamma-ray beam after it has passed through the fuel assembly, that is detected. This second case is called a "transmission" measurement. The benefits and difficulties of each type of measurement will be discussed below.

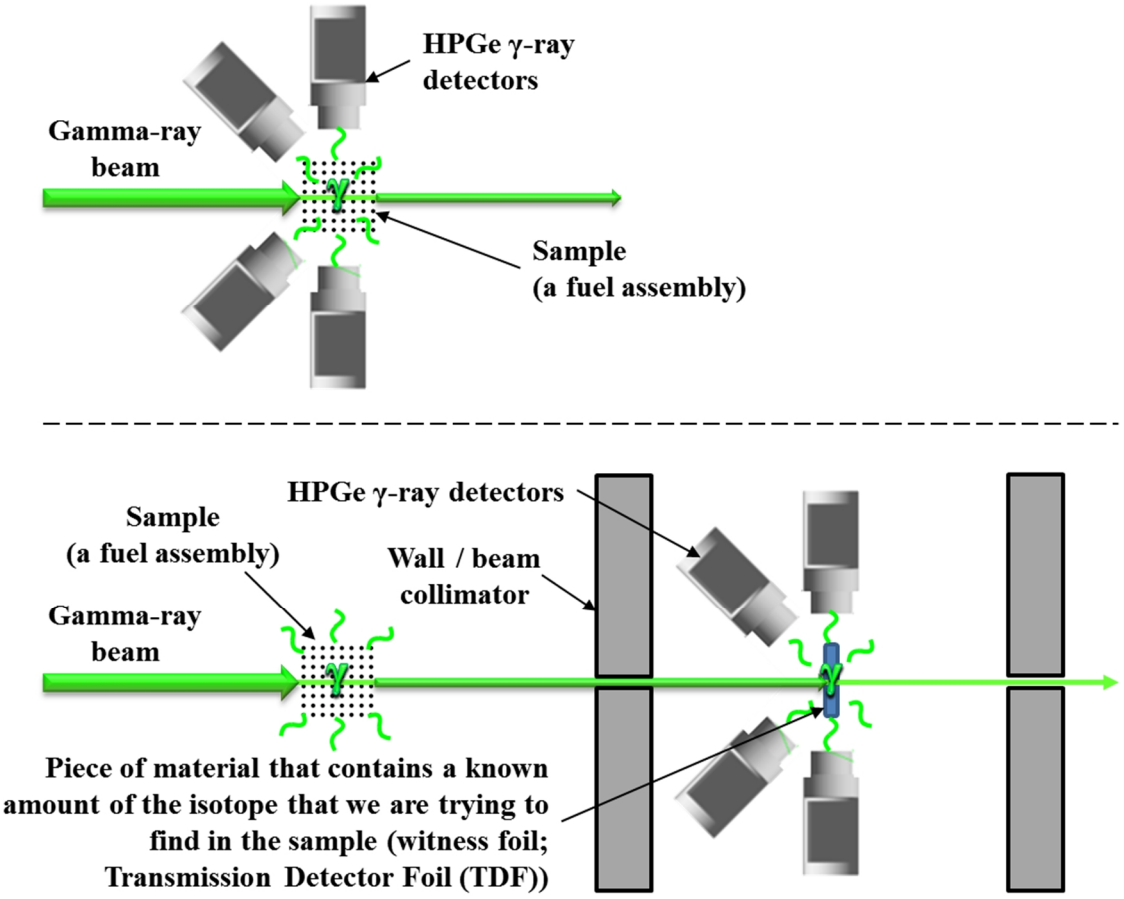

Figure 68: Top: NRF backscattered-measurement configuration. Bottom: NRF transmission-measurement configuration

5.2.1.2.1 Production of the gamma-ray beam

To date, there are two main ways to produce a high-energy gamma-ray beam, and the NGSI explored them both: (1) by bremsstrahlung and (2) by inverse Compton scattering [56, 340]. Bremsstrahlung (braking radiation) is created when a charged particle is negatively accelerated (i.e., decelerates), such as when a high-energy electron is slowed down and eventually stopped in a material. Bremsstrahlung gamma-ray sources for the NRF technique operate by accelerating electrons to high energy and then ramming them into a high-Z (heavy) target, such as tungsten; photons of all energies up to the incident electron energy are created as the electrons come to a stop (Figure 69). Inverse Compton scattering occurs when a low-energy photon collides with a higher-energy electron, and the electron gives up some of its

energy to the photon (Figure 70). Inverse-Compton-scattering sources for NRF operate by accelerating an electron beam to high energies and then crossing the electron beam with a beam of light; inverse Compton scattering occurs at the point where the beams collide and converts the low-energy photons into high-energy gamma-ray photons. When a laser is used as the beam of light, such gamma-ray sources are called laser-Compton-scattering sources, abbreviated as LCS sources. LCS sources are the only inverse-Compton-scattering sources that will be discussed in this report. Each of these two kinds of gamma-ray sources, bremsstrahlung and LCS, will be discussed next in more detail.

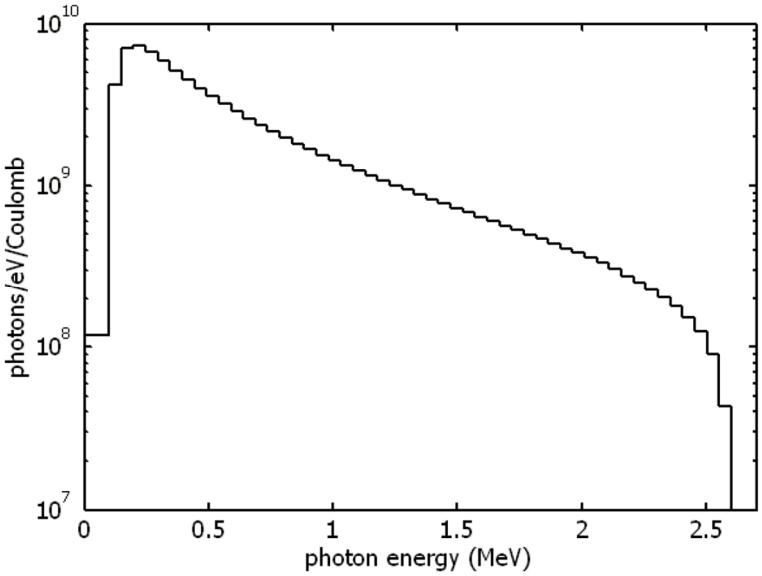

Figure 69: An example of an energy spectrum of photons created by a bremsstrahlung source. The spectrum was computed by Monte Carlo (MCNPX) for photons created by 2.6 MeV electrons normally incident upon 102 μm thick Au foil backed by 1 cm thick Cu, and leaving within 3.57° of the initial electron trajectory. Copied from Figure 2.6 in Ludewigt et al. [56].

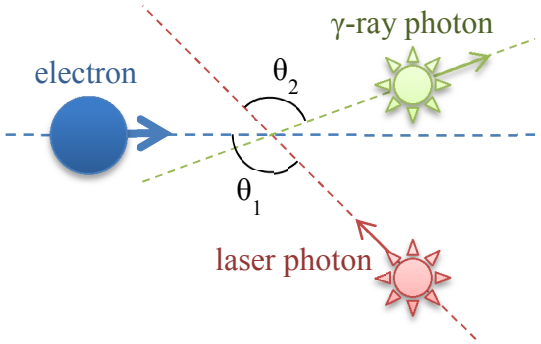

Figure 70: Schematic of inverse Compton scattering

As Figure 69 illustrates, bremsstrahlung has a continuous energy spectrum. The analytical formula that describes the energy spectrum of bremsstrahlung that is created from relativistic electrons is complicated and so will not be presented here; Figure 69 will serve as a representative description, instead. The two important yet conflicting characteristics of bremsstrahlung are (1) that it is easy to produce, since electrons are relatively easy to accelerate to high energies and shoot at a high-Z target, yet (2) that the vast majority of the bremsstrahlung photons are at energies other than the energy of the nuclear resonance that the

gamma-ray beam is supposed to excite in the fuel assembly. Tersely, it can be said that a bremsstrahlung gamma-ray source makes many useless photons cheaply. Increasing the highest ("endpoint") bremsstrahlung energy by increasing the electron-beam energy does not help, because even though doing so does make more photons at the NRF energy, it also simultaneously increases the background in the gamma-ray detector. (For example, changing the endpoint energy in Figure 69 from 2.6 MeV to something higher would not help.) The background increases because some of the higher-energy photons (i.e., photons with energy higher than the NRF energy) are also scattered (by various processes) into the detector, where they create a Compton continuum that overlaps with the NRF signal at the lower, NRF energy. Thus, the signal-to-noise ratio does not improve or even becomes worse.

An even more important problem that is caused by this excess of useless photons from a bremsstrahlung source is that the detector is forced to count all of the photons that reach it even though most of them are useless. That is, the detector does not know *a priori* that a given photon is at a meaningless energy; it must count it first before it can realize that fact. However, gamma-ray detectors are limited in the number of photons that they can count per second, that is, in their counting rates. This limitation is especially severe for HPGe detectors, which have the best energy resolution; their limit is a few hundred kilohertz [46]. By making many useless photons, a bremsstrahlung source overloads the gamma-ray detectors, causing them to reach their rate limits more quickly (i.e., at a lower flux of useful, NRF-energy photons in the beam) than does a source that produces only useful photons at the proper, NRF energy. This rate-limit problem will be discussed more in later paragraphs.

In contrast with a bremsstrahlung source, an LCS source makes photons only within a narrow energy band, which can be tuned to be centered at the desired NRF energy. For this reason, LCS sources are also called quasi-mono-energetic sources. (Other kinds of quasi-mono-energetic sources exist but will not be discussed here.) The energy of the LCS gamma-ray beam depends on the electron beam's energy and on the relative angles among the electron beam, the laser beam, and the collimator through which the gamma-ray beam passes to go to the fuel assembly. The relationship among the gamma-ray energy (E_γ), the laser-photon energy (E_L), the electron kinetic energy (E_e), the collision angle (θ_1), and the scattering angle (θ_2) (see Figure 70) is as follows [351, 357]:

$$E_\gamma = \frac{E_L(1-\beta\cos(\theta_1))}{1-\beta\cos(\theta_1-\theta_2)+\frac{E_L}{E_e}(1-\cos(\theta_2))} \qquad \text{Equation 54}$$

where $\beta = \sqrt{1-\gamma^{-2}}$ and $\gamma = \left(\frac{E_e}{0.511\ \text{MeV}}\right) + 1$ = the Lorentz factor

A collimator can be used to isolate the gamma-rays being scattered at the certain angle that corresponds to the desired gamma-ray energy. Small uncertainties in the angles, in the width of the collimator, and particularly in the electron beam's energy cause the gamma-ray beam not to have precisely one energy but to have a narrow energy distribution. This fact is why LCS sources are called not "mono-energetic" but rather "quasi-mono-energetic." Figure 71 shows an example of the energy distribution of an LCS beam at the HIγS facility at Triangle Universities Nuclear Laboratory in Durham, North Carolina [385]. The full widths at half

maximum (FWHMs) of the LCS gamma-ray beams in that work were about 4% to 5% for beam energies from about 3 MeV to 6 MeV, according to Hammond's Table 5.1 [385]. (See also Figure 1 in Tonchev et al. [344].) Another example of an LCS beam energy distribution is Figure 3 in Kikuzawa et al. [355]. According to Kikuzawa et al. [355], a typical LCS gamma-ray beam exhibits "a gradual increase in the γ-ray intensity at low energies and a sharp decrease at high energies," so the distribution is not quite Gaussian. The energy spread of the 5.7 MeV gamma-ray beam in Kikuzawa's experiment was 7% full width at half maximum (FWHM) [355].

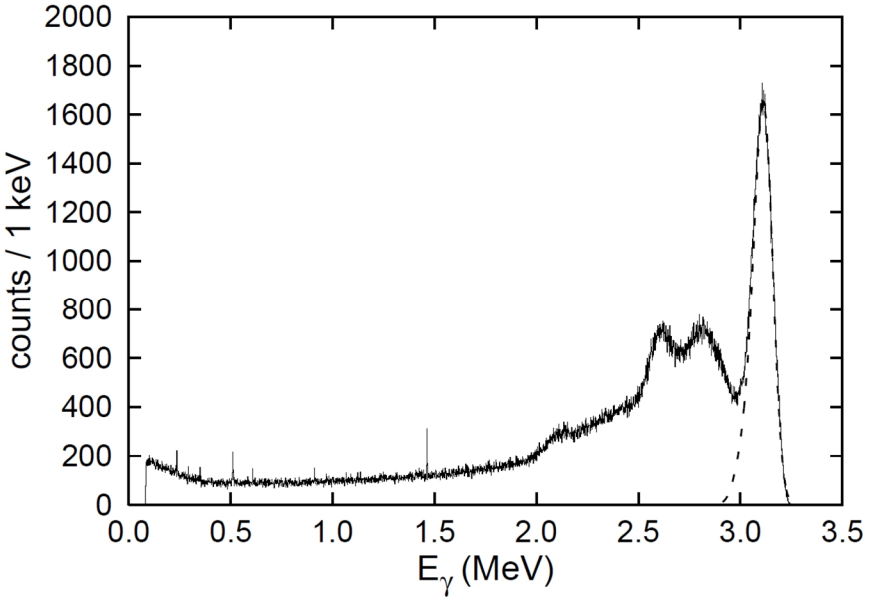

Figure 71: The measured (solid line) and actual (dashed line) energy distribution of a typical quasi-mono-energetic LCS gamma-ray source (E_γ = 3.1 MeV). The measured curve is different because it exhibits the characteristics of the detector itself (i.e., the detector response). Copied from Figure 5.8 in Hammond [385] with permission from the author.

Though the much narrower energy distribution of LCS gamma-ray beams is much more conducive to NRF measurements than that of bremsstrahlung sources, the main operational problem with LCS gamma-ray beams is that they have historically been weaker than bremsstrahlung beams. (LCS sources can also be larger and more expensive to build.) Table 2 in Kneissl et al. [340] compared LCS and bremsstrahlung beams at the state of the art in 1996; the LCS source produced 0.15 photons/(s·eV), whereas the bremsstrahlung source produced 1000 photons/(s·eV). Since this comparison is per unit of energy, it is a fair comparison for the NRF application, which uses only photons in a certain energy range. If it is assumed that bremsstrahlung sources have not changed much since 1996 because such technology was already mature by that time, an updated comparison can be made according to the characteristics of recent LCS sources. The LCS source used by Kikuzawa et al. [355] produced about $1 \cdot 10^5$ photons/s, corresponding to about 0.3 photons/(s·eV), and the LCS source used by Hammond produced about $1 \cdot 10^6$ photons/s to $1 \cdot 10^7$ photons/s, corresponding to about 10 to 200 photons/(s·eV). Thus, it can be said roughly that current LCS technology produces beams that are weaker than bremsstrahlung beams by one to three orders of magnitude.

It should be noted that the proper measure of a gamma-ray source is the spectral brightness[4], which is defined as follows:

$$\text{Spectral Brightness} = \frac{(\text{Number of photons})}{(\text{Time})\cdot\left(\begin{matrix}\text{Angular}\\ \text{Divergence}\end{matrix}\right)\cdot\left(\begin{matrix}\text{Beam}\\ \text{Cross-sectional}\\ \text{Area}\end{matrix}\right)\cdot\left(\begin{matrix}\text{Energy}\\ \text{Bandwidth}\end{matrix}\right)} \qquad \text{Equation 55}$$

$$\text{Units of Spectral Brightness} = \frac{\text{photons}}{\text{s}\cdot\text{mrad}^2\cdot\text{mm}^2\cdot(0.1\%\ \text{Bandwidth})} \qquad \text{Equation 56}$$

For an LCS source, the angular divergence, beam cross-sectional area, and energy bandwidth are all connected, so the previous, rough comparison on the basis of energy (eV) is not invalid.

A new generation of LCS sources is now being constructed with more advanced laser and accelerator technology. These LCS sources hope to achieve gamma-ray beams with greater spectral brightness, primarily by decreasing the emittance of the electron beam but also by increasing the fluxes of photons and electrons so as to increase the scattering collision rate. Emittance describes the "tightness" of each electron bunch in the electron beam; a smaller emittance means a "tighter" beam. An electron beam with a smaller emittance not only has a narrower energy distribution but also is more likely to interact with the photon beam. The new LCS sources reduce the emittance by using each electron bunch in the beam only one time, after which the bunch is discarded. (By "one time," it is meant that each electron bunch passes through the laser beam only one time, regardless of how many of its electrons actually undergo Compton scattering.) In this way, the various processes that tend to increase the emittance in a synchrotron or storage ring are not given an opportunity to affect the beam [351].

The laser part of the new LCS sources is also being improved. New super-cavities are being designed that collect the laser light between mirrors (e.g., see Hajima et al. [351]). The laser photon flux is thereby increased, so that the rate of scattering interactions is also increased.

Two main varieties of these new LCS sources will be described here. The first kind is a linear accelerator (linac) that runs on X-band radiofrequency (RF) power (11.424 GHz, for example), which is a higher frequency than conventional S-band RF power (3 GHz, for example) [362, 368, 370, 403]. By using the higher X-band frequency, the linac can be made to be shorter, thus saving space; the ultimate goal is to make the LCS source semi-portable by truck [370]. The electron bunches are sent to a beam dump after the LCS interaction position. An early, initial goal for spectral brightness of this kind of source has been 400 photons/(s·eV) [368], though it is desired to go up to 10^6 photons/(s·eV) [370]. Another advantage of this X-band LCS source is that X-band linacs have been built before, so the technology is not untried [370]; only the application to an LCS gamma-ray source is new.

The second kind of LCS source is a superconducting, energy recovery linac (ERL). The "energy recovery" feature is that after the LCS interaction position, the beam is not sent straightaway to a dump but rather is wrapped around again to the start of the linac [351].

[4] See Mills et al. [402] for the standardization of this terminology.

Instead of being accelerated in the linac, though, the used electron bunches are introduced in such a way that they are decelerated by the RF waves. The energy of the bunches is thus transferred to the RF waves, which are simultaneously accelerating new electron bunches. In this way, the energy of the used electron beam is largely recovered by being used to accelerate the new electron beam. The used electron beam is then dumped after this deceleration process. The anticipated spectral brightness is about $7 \cdot 10^6$ photons//(s·eV) [357]. In summary, one kind of new LCS source emphasizes reduced size and more proven linac technology, whereas the other kind emphasizes energy efficiency; but both kinds are expected to produce gamma-ray beams that are brighter than existing LCS sources.

5.2.1.2.2 Measurement of the backscattered photons

As the gamma-ray beam passes through the spent fuel assembly, some of the photons are scattered by NRF into the backward angles, and these photons are the ones that are detected in the "backscattered measurement" configuration of the NRF NDA technique. The configuration is illustrated in the top of Figure 68. Figure 72 is an example NRF backscattered measurement, taken on pure ^{240}Pu (in an aluminum container) with a bremsstrahlung beam. (Note that a spectrum from a spent fuel assembly would have a much greater background than the background in this figure.) The NRF peaks are denoted with arrows. For assay, the heights of the NRF peaks would be determined with curve-fitting routines, and then the amount of the isotope of interest in the sample would be determined from these heights according to a predetermined calibration.

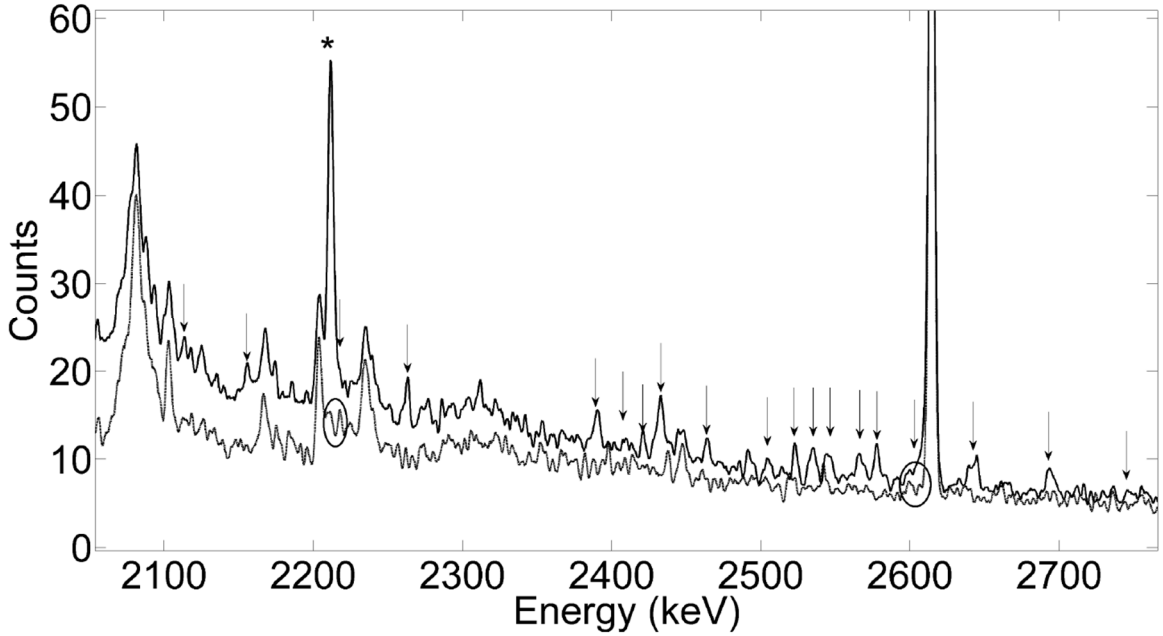

Figure 72: "NRF spectrum of the ^{240}Pu target (solid line) and radioactive target background (dashed line) in the γ-ray energy range from 2 to 2.8 MeV. The arrows indicate the 18 γ-rays corresponding to the nine populated NRF states. The asterisk denotes the ^{27}Al resonance at 2212.0 keV and the circles indicate relatively low-intensity regions in the background spectrum upon which ^{240}Pu γ-rays are expected." [384] Reprinted Fig. 3 with permission from B. J. Quiter, T. Laplace, B. A. Ludewigt, S. D. Ambers, B. L. Goldblum, S. Korbly, C. Hicks, C. Wilson, Physical Review C, 86, 034307, 2012. Copyright 2012 by the American Physical Society.

The benefit of this configuration is that the NRF-scattered photons themselves are detected directly, with their energy being the means by which they are distinguished from photons that are scattered by other processes. Thus there can be little confusion about the interpretation of the signal, except for the issue of self-shielding attenuation of the signal by the spent fuel assembly, which will be discussed below. This idealized clarity of interpretation of the NRF signal is the main advantage of the backscattered-measurement configuration.

There are three main disadvantages to the backscattered-measurement configuration: (1) the self-shielding attenuation by the spent fuel assembly that was just mentioned, (2) the enormous gamma radiation background that the spent fuel assembly itself produces, and (3) the relatively small concentration of the isotope of interest in the assembly. These will now be discussed in turn.

As explained in Section 5.2.1.1, *Principle of operation*, the subtraction of the recoil energy of the nucleus from the energy of the scattered photon is just enough to move the scattered photon's energy off the resonance so that the photon does not experience resonant scattering again on its way out of the spent fuel assembly. This fact does not mean, though, that the scattered photon cannot experience *nonresonant* scattering on its way out of the spent fuel assembly. Indeed, many NRF-scattered photons do experience such subsequent nonresonant scattering by all manner of scattering processes, whether coherent or incoherent, or elastic or inelastic. They also can be absorbed, such as in photofission if the photon energy is high enough. The extent of this attenuation by nonresonant scattering and absorption depends on the type and amount of the spent-fuel-assembly's material through which the NRF-scattered photon must pass on its straight-line path to the detector, and this path depends, of course, on the position in the fuel assembly at which the NRF scattering event took place. The attenuation is thus a geometric problem, in that it depends on the geometric (spatial) configuration of the material of the spent fuel assembly.

The geometric arrangement of a spent fuel assembly is fixed and well-known prior to the NDA measurement; and though its composition changes somewhat because of burnup, its ability to attenuate gamma-rays does not change significantly, since the total amount of heavy metal (the electrons of which dominate the gamma-ray attenuation) does not change significantly. Therefore, the self-shielding attenuation of the NRF-scattered gamma-rays can be predicted for the NRF NDA of spent fuel assemblies, either by calculations or Monte Carlo simulations or by calibrations with known, standard fuel assemblies. (The adjective *self-shielding* comes from the fact that the spent fuel assembly itself is shielding the detectors from being able to observe the NRF-scattered gamma-rays.) A correction factor can then be applied to the measured NRF signal to account for the fraction of it that was lost to the self-shielding. The self-shielding attenuation becomes a serious problem only when the geometry and composition of the sample being assayed are *not* known beforehand, such as when assaying blobs of formerly molten fuel after a reactor meltdown. In this case, there is no accurate correction factor for the unknown spatial configuration, so the assay accuracy suffers considerably.

The second main drawback to the backscattered-measurement configuration is the enormous gamma radiation background that the spent fuel assembly itself produces. This background is on the order of 10^{15} photons/s for a spent PWR fuel assembly [87]. The

background does not contribute many gamma-rays at the same energies as the resonance energies of the NRF signal, as long as those resonance energies are high enough (refer to Figures 57 and 62). Thus, the background does not directly reduce the signal-to-noise ratio. Instead, the background easily overwhelms the gamma-ray detectors' maximum count rate, which was discussed in the previous subsection. To bring the count rates down below the detectors' maximum limit, narrow collimators and/or thick filters of heavy metal must be put in front of the detectors. These collimators and filters do not reduce the signal-to-noise ratio (in fact, they often improve it), but they do reduce the absolute magnitude of the signal. More precisely, the wasting of the detectors' limited counting ability on the counting of many useless, low-energy photons is what reduces the absolute magnitude of the NRF signal that can be counted in a given amount of time.

The third main drawback is that scattering processes other than NRF also create a significant background in backscattered measurements, as explained in Section 5.2.1.1, *Principle of operation*. Since this non-resonantly scattered background consists of photons that originally came from the gamma-ray beam, it is distinct from the background generated by the spent fuel assembly itself, and it cannot be avoided. In the backscattered-measurement configuration, the much greater amount of non-resonant-scattering material than fluorescing material in the spent fuel assembly produces a background that is correspondingly much greater. Again, Table 4.1 in Ludewigt et al. [56] and Section 3.3 in Shizuma et al. [396] present data for this case. In contrast, the isotopic purity of the transmission detector foil (TDF) in a transmission-measurement configuration (see the next section) increases the strength of the NRF signal relative to the non-resonant background.

Note that the neutron radiation background of the spent fuel assembly is probably not a problem for the backscattered-measurement configuration. Unlike the neutron radiation in the case of delayed-gamma (DG) measurements (Section 5.1.1), which includes the 14 MeV neutrons from the D-T neutron generator, the neutron radiation in the NRF case is only the passive flux from the spent fuel assembly, most of which originates from fission and with a Watt energy distribution [303]. The fission Watt distribution is at less energy than 14 MeV. Therefore, the fast-neutron damage to the gamma-ray detectors in an NRF backscattered-measurement configuration should be much less than the damage in a DG instrument [47], perhaps to the point of being negligible.

5.2.1.2.3 Measurement of the transmitted photons

As the gamma-ray beam passes through the spent fuel assembly, many photons are absorbed or scattered out of the beam by various processes. Additional photons are removed from the beam at the resonance energies, because the NRF cross-section is cumulative with the cross-sections of the other scattering and absorption processes. Thus, the characteristic NRF signal from the isotope of interest is imparted to the gamma-ray beam in the form of chasms at the resonance energies, i.e., extra depletions of photons at those energies relative to the overall depletion at all energies. "This is like analyzing the light from the sun for elemental absorption lines to determine which elements are in the sun's atmosphere." [391] Thus, the amount of the isotope in the spent fuel assembly can be determined if the resonance chasms and the overall attenuation can both be measured. This concept is the basis of the

transmission-measurement configuration. It is basically the gamma-ray analogue of the NRTA NDA technique (Section 4.3.1). The bottom of Figure 68 illustrates the configuration, and Figure 73 is an example of some transmission-measurement data, taken on ^{239}Pu with an LCS beam.

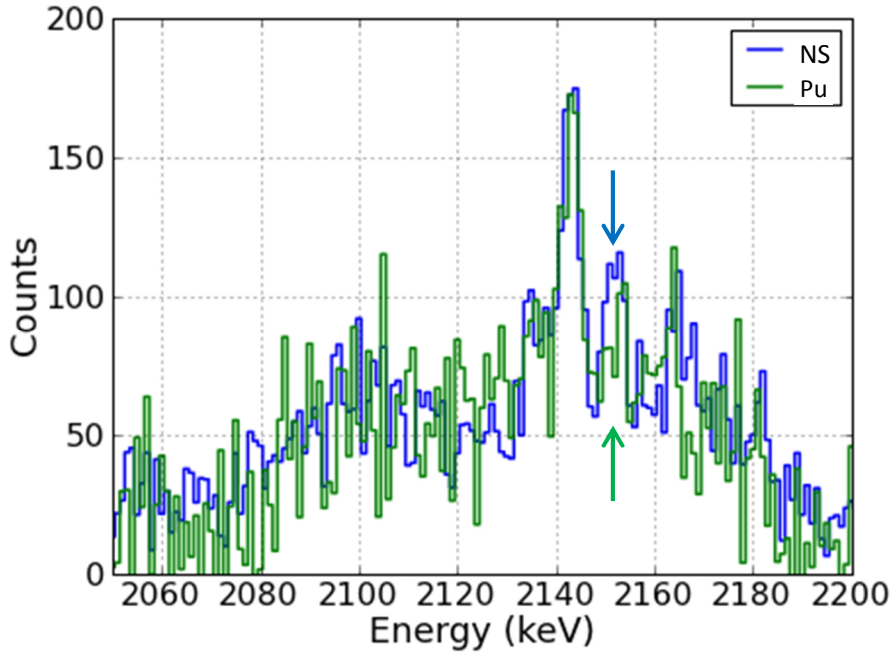

Figure 73: Transmission NRF measurement of ^{239}Pu, using an LCS gamma-ray beam with a nominal energy of 2140 keV. "NS" means a measurement with no sample, just the Pu witness foil; "Pu" means a measurement with both the ^{239}Pu sample and the Pu witness foil. In general, the NS line is higher than the Pu line because of resonance absorption in the ^{239}Pu target in the latter case. The energy state at 2150 keV (arrows) seems to be the strongest resonance state in this energy region. Received from Christopher Angell; see the similar figure (Fig. 4) in Angell et al. [391].

The advantages of a transmission measurement are the inverse of the disadvantages of a backscattered measurement, namely, (1) that the measurement is unaffected by the geometry of the sample being measured, whether spent fuel assembly or melted debris, (2) that it can be made separately from the presence of the self-generated gamma-ray background of the spent fuel assembly, and (3) that the isotopic purity of the TDF (discussed below) increases the strength of the resonant, NRF signal relative to the background that is produced by non-resonant scattering processes. An additional advantage is that the non-resonant, elastic, coherent scattering (i.e., RTD scattering, Section 5.2.1.1) that occurs in the spent fuel assembly does not interfere with the transmission measurement as it does with the backscattered measurement; it merely contributes to the overall attenuation of the beam.

The geometry of the sample (e.g., spent fuel assembly or melted fuel debris) is largely irrelevant because the gamma-ray beam is almost purely one-dimensional. The order in which the beam passes through two different materials, for example, does not affect their attenuation of the beam, as Figure 74 shows. To find the spatial distribution of the isotopes of interest in the sample, the beam can be rastered across the sample, or the sample can be rastered through the beam and/or rotated.

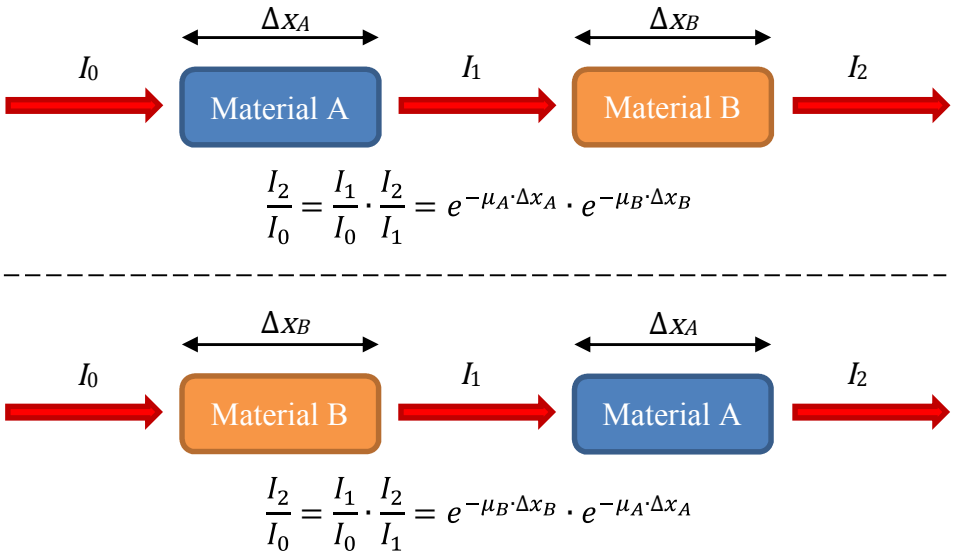

Figure 74: The order in which a one-dimensional beam passes through two different materials does not affect the total attenuation of the beam.

Therefore, the only effect of the geometry is what is called “notch refill,” which is when higher energy photons undergo one or more incoherent, inelastic scattering event (e.g., Compton scattering) that puts them exactly at the resonance energy yet still keeps them traveling in roughly the same direction as the rest of the photons in the beam so that they can also pass through any collimators that are placed downstream of the sample. (Another mechanism of notch refill could be that the higher energy photons produce photoelectrons that then produce new photons at the lower energy.) Thus, notch refill is the filling-in of the resonance chasms (i.e., the “notch”) in the transmitted beam, which makes it seem that less of the isotope of interest is in the sample than is actually there. Essentially, notch refill is a consequence of the beam not having precisely one dimension but rather having some finite cross-sectional area and angular dispersion. It also is exacerbated by increasing the thickness of the sample, so that a spent fuel assembly would produce more notch refill than a thin foil would. The NGSI examined the effects of notch refill and found them to be negligible in comparison with other, larger sources of uncertainty in the measurement [56]. Pruet et al. [346] also investigated notch refill and found that it should not be an issue with LCS gamma-ray beams; it needs only to be considered for bremsstrahlung beams.

As Figure 68 indicates, the transmission measurement can be made in a room that is separate from the location of the sample. The wall between the sample and the transmission-measurement setup contains a hole through which the beam can pass, so that the wall acts as a collimator for the beam and as a shield against all the scattered and self-generated radiation from the sample. In this way, the self-generated radiation from the sample has no impact on the transmission measurement. (The fraction of the self-generated radiation that just happens to line up with the collimator must be very small.) The gamma-ray detectors do not have to waste precious counting time on those useless photons.

One potential disadvantage of the transmission-measurement configuration is the inverse of the advantage of the backscattered-measurement configuration, namely, that the NRF-

scattered photons from the sample are not detected directly. Only their absence from the beam is detected. This fact can be a problem if the amount of the isotope of interest in the sample is too great, such as might be the case when using NRF to assay plutonium pits from nuclear weapons. In this case, the NRF scattering in the sample removes practically all of the resonance-energy photons from the transmitted beam, such that there is no longer any sensitivity to small changes in the amount of isotope; that is, the resonance chasms "hit the bottom." In typical samples such as spent fuel assemblies, the quantities of the isotopes of interest (e.g., ^{239}Pu) are so small that this case does not even come close to occurring; gross attenuation by non-resonant processes is reached well beforehand.

A much more practical hindrance for spent fuel assemblies is that the transmitted beam also cannot be analyzed directly, in general. (It might be possible do to with photofission, which is discussed below.) The gamma-ray beam is far too intense for a gamma-ray detector to resolve its energy spectrum adequately; that is, the count rate is far too high. It would be like trying to stare at a laser beam or at the sun. Furthermore, even if a detector could handle the count rate, the energy resolution of the detector would be much too coarse to see the resonance chasms in the spectrum, which are very narrow in energy. Narrow resonance peaks still give some signal in a coarse-resolution detector, but narrow resonance chasms are lost.

Instead, the beam must be analyzed indirectly, by the additional signal that it creates in another, well-known sample. This indirect analysis is like looking at the partial reflection that a laser beam or sunbeam makes on a sheet of paper that is placed in the beam. Such a signal or "reflection" is less intense than the beam yet still conveys its essential characteristics. The "sheet of paper" in the NRF transmission measurement is a well-characterized sample that contains a precisely known amount of the isotope of interest. This well-known sample is called a transmission detector foil (TDF) by the NGSI [56, 393]; it is also known as a witness foil [352, 383]. With a TDF, the transmitted beam can be analyzed indirectly.

The fundamental premise of using a TDF is that the TDF scatters photons in the beam in characteristic ways so as to preserve the information that is possessed by the resonance chasms in the beam. The most obvious method to ensure this correlation is to measure the NRF-scattered photons from the TDF; this method is why the TDF contains a known amount of the isotope of interest. The logic of the transmission measurement is then as follows: If there is less NRF scattering in the sample (fuel assembly), then there will be more NRF scattering in the TDF because more resonance-energy photons will have been preserved in the beam. Conversely, if there is more NRF scattering in the sample (due to more of the isotope of interest being present), then there will be less NRF scattering in the TDF, because the resonance chasms in the transmitted beam will be deeper. Thus, the magnitude of the NRF signal from the TDF is inversely proportional to the magnitude of the NRF scattering in the sample.

The original concept for measuring the NRF signal from a TDF has been essentially to make a backscattered NRF measurement of the TDF, as Figure 68 shows. The heights of the NRF peaks are analyzed as in a backscattered measurement, but in this case, they are related *inversely* to the amount of the isotope of interest in the sample, according to a predetermined calibration. Some aspects that make this measurement more simple and accurate than a backscattered measurement of a sample (fuel assembly) are (1) the geometry of the TDF is

well-known and optimized, (2) the TDF lacks a significant amount of self-generated radiation, and (3) the quantity of the isotope of interest in the TDF is large and optimized to yield a large NRF signal, particularly as relative to the background produced by non-resonant scattering processes. Nevertheless, such non-resonant scattering processes do still occur in the TDF and still produce a background, and the larger that is the energy width of the gamma-ray beam is the larger that this background will be. This principle is yet another drawback of bremsstrahlung beams, and it can even lead to overloading the count rates of the detectors if the combination of intensity and energy-width is sufficiently severe.

A late development in the use of NRF as an NDA technique has been the recognition that the NRF signal from the TDF may not need to be distinguished from the background of the other kinds of scattering coming from the TDF in order to obtain meaningful and accurate information about the NRF scattering in the sample (e.g., fuel assembly) [56, 373, 386, 391, 393]. In other words, the heights of peaks may not need to be determined with curve-fitting. As long as the NRF scattering is a significant fraction of the total scattering from the TDF, the total scattering—i.e., without energy resolution—can be measured instead and then compared against a reference signal without any NRF scattering. This simplification can be made because a reduction in the NRF signal from the TDF (namely, that caused by NRF scattering in the sample) is likewise a reduction in the total signal from the TDF, albeit a proportionally smaller one. The lack of a significant amount of self-generated radiation from the TDF ensures that any such changes in the total signal are attributable only to changes in the transmitted gamma-ray beam caused by attenuation in the sample. The need for the NRF signal from the TDF to be a significant fraction of the total signal means that this method cannot be used profitably with bremsstrahlung gamma-ray beams; narrow-energy-width LCS beams are required. Also, the Compton continuum and 511 keV positron-annihilation photons that are created by Compton scattering and pair production within the TDF itself can similarly preclude this approach unless they are either filtered out (see Section 5.2.1.2.4) or are rejected by some minimal degree of energy resolution in the detector (about 10%). Since the combined magnitude of the Compton continuum and annihilation peak increases at least as fast as with the square of the atomic number ($> Z^2$) [74], only light elements such as lithium do not produce a substantially interfering background; heavy actinides certainly do.

This method has been called variously as the “calorimetric” method [56], the “Dual Isotope Notch Observer (DINO)” method [373], the “average nuclear resonance absorption (NRA)” method [386], and the “Integral Resonance Transmission (IRT)” method [391]. (Technically, the DINO method also incorporates a second TDF as a constituent part of the method, as will be discussed below.) To avoid confusion with other averages and with the totally separate NDA technique of calorimetry, this report will henceforth refer to this method as the IRT method unless specifically referring to the unique, two-TDF configuration that is the DINO method.

The IRT method is particularly well-suited to take advantage of weak NRF resonances that HPGe detectors have difficulty to resolve above the RTD-scattering background. From a consideration of the nuclear physics that underlies the NRF process, it is expected that heavy isotopes with odd mass number (such as ^{239}Pu) should have many weak resonances that heretofore have not been able to be observed above background noise [391, 393]. Since such

weak resonances cannot be observed, they cannot contribute to a traditional analysis based on NRF peaks. On the other hand, when taken together, they do contribute significantly to the magnitude of the total NRF, resonant-scattered signal, which is exactly what the IRT method analyzes. Therefore, in the case that the energy width of the gamma-ray beam is fixed and given, the NRF scattering from the unresolved resonances adds more strength to the total NRF signal, which is measured by the IRT method. Alternatively, when considering a variable energy width, it is profitable to increase the energy width to pick up additional signal from unresolved resonance states only as long as the additional NRF signal from those states increases the overall proportion of the NRF signal to the total signal.

Figure 75 illustrates the way that the IRT method uses the TDF, namely, by the principle of self-interrogation. The inherent energy resolution with which a TDF can analyze the beam is the energy widths of the resonances themselves, which is on the order of one electron-volt. This energy resolution is much better than the energy resolution of even the best HPGe detectors. Resonance states from two different isotopes might appear to overlap when measured with a HPGe detector, yet a TDF will be able to determine if they actually overlap. Furthermore, the resonance states of the TDF always interact with the corresponding resonance chasms in the gamma-ray beam even if those resonance chasms are too shallow (i.e., weak) for an HPGe detector to detect them because of background noise. This fact is what the IRT method exploits.

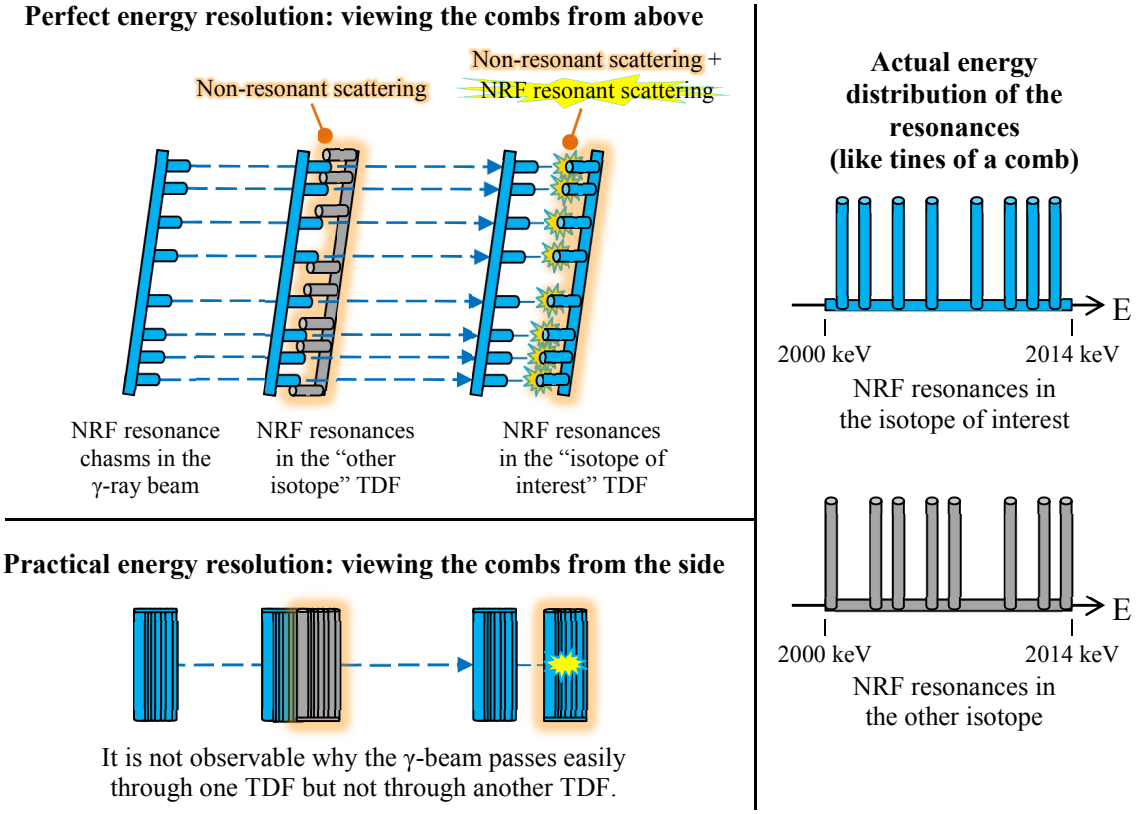

Figure 75: Schematic showing how a TDF can give an accurate, high-resolution, total signal from resonance chasms even if the individual chasms cannot be resolved with a detector because they are either too close together (in energy) or too shallow (weak).

The DINO method puts a second TDF, made of depleted uranium, into the transmitted gamma-ray beam and makes a separate backscattered measurement of it [373]. The purpose of this second TDF is to produce a purely non-resonant (non-NRF) scattered signal from the transmitted gamma-ray beam. This purely non-resonant signal can then be used to normalize the signal from the first TDF, which does include significant resonant scattering from the isotope of interest. The non-resonant signal from the second TDF also acts as a measurement of the total attenuation of the gamma-ray beam by the sample (fuel assembly). A beam flux monitor that is located after both TDFs also helps to account for the total attenuation by the sample. The DINO method also uses a Ta filter (see the next section) in front of the detector for the first TDF to cut down on the Compton continuum and annihilation peak that it produces and thereby to increase the signal-to-noise ratio [373].

Lastly, a variant of the transmission-measurement configuration that uses photofission has also been proposed [386]. It relies on the fact that the resonance states that produce NRF are the same ones that produce exceptionally large amounts of photofission (i.e., large, resonant, photofission cross-sections). Therefore, if the energy of the gamma-ray beam is above the threshold for inducing photofission (approximately 5 MeV), then the TDF will produce resonant photofission neutrons in addition to producing NRF scattered gamma-rays. By measuring these neutrons, one can determine the magnitudes of the resonance chasms in the transmitted gamma-ray beam. Alternatively, one could use specialty fission chambers made from the isotopes of interest as the TDFs, in which case the photofission events themselves would be directly detected. Either way, this photofission method is essentially the same as the IRT method but with the signal being a neutron or fission signal instead of a gamma-ray signal.

5.2.1.2.4 Detectors and filters

It has been mentioned several times that gamma-ray detectors are limited to maximum count rates. These count rates depend on several factors, so only rough magnitudes are discussed here. Present high-purity germanium (HPGe) detectors are limited to 100 kHz (i.e., 10^5 detections per second) at the very most [46, 291]; the NGSI used a more realistic, conservative maximum of 20 kHz in their study [56]. Cerium-doped lanthanum bromide ($LaBr_3$(Ce)) detectors have about 18 times worse energy resolution than HPGe detectors have [56, 292], but they can count at least 15 times as fast as HPGe detectors [56], i.e., up to 1 MHz and beyond [291, 293]. $LaBr_3$(Ce) have better energy resolution and faster decay times than NaI(Tl) detectors [292], so only $LaBr_3$(Ce) are considered here as the representative of scintillator detectors. In summary, HPGe detectors have the best energy resolution but a slower count rate, whereas other detectors, such as $LaBr_3$(Ce), have faster count rates but at worse energy resolution. The NGSI examined various aspects of this trade-off and the impact on the final assay time and accuracy [56]. For the IRT method in particular, the use of fast, low-resolution detectors is purely advantageous, since the method largely disregards the energy spectrum anyway.

High-*Z* materials—that is, materials made from heavy elements, where *Z* equals the number of protons—can be placed in front of gamma-ray detectors in order to filter out preferentially the low-energy photons from the gamma-ray flux that reaches the detectors. As

Figures 64 and 65 have illustrated (Section 5.1.3.4), material attenuates lower-energy photons more readily than higher-energy photons, and higher-Z material like lead (Pb) is more effective at such attenuation than is lower-Z material. Since the NRF signal, whether in a backscattered configuration or in a transmission configuration, is at high energy, a high-Z filter can be used to accentuate it relative to the lower-energy background. Of course, such filters do still somewhat attenuate the higher-energy, NRF signal, which then necessitates an increase in the gamma-ray beam strength or in the assay duration to compensate for the lost NRF signal strength. In practice, high-Z filters are used primarily when the gamma-ray beam strength is already excessively strong such that it overwhelms the maximum count-rate limit of the detectors. In this case, the high-Z filters bring the count rate back down under the limit while minimizing the loss of the NRF signal. The thickness of the filter is selected to achieve the optimum count rate for the detectors.

5.2.1.3 Limitations

The current foremost limitation on the use of NRF as an NDA technique is its lack of development. Although experiments on samples of pure isotopes have produced promising results, NRF has not yet been used to assay nuclear fuel. The higher-intensity LCS gamma-ray beams that are predicted to be necessary for such assaying are currently under construction. On the assumption that such gamma-ray sources will be completed on-schedule and will subsequently be used to carry out the essential proof-of-concept experiments, the state of the art of NRF as an NDA technique should look very different in three to five years from now.

Another limitation is the size and cost of the equipment that is used to produce the gamma-ray beams. Electron accelerators, even off-the-shelf, X-band electron accelerators, are relatively large and expensive in their capital costs as compared with the equipment of other NDA techniques; electricity and other operating costs can also be significant. Lasers and laser cavities can also be expensive. For these reasons, it seems likely that the first NRF NDA facilities will be large, permanent installations in locations close to the nuclear material to be assayed; the nuclear material (e.g., spent fuel assemblies or melted debris) will need to be transported to and from the NRF NDA facility.

Another limitation that has not yet been thoroughly considered is the availability of the TDFs for the transmission-measurement configuration. Ideally, the TDFs would be purely one isotope; practically, a combination of TDFs of well-known isotopic mixtures might also be feasible. In either case, certain isotopes may be difficult or prohibitively expensive to obtain and to transport. For example, pure ^{235}U, ^{239}Pu, and ^{241}Pu are special nuclear materials; furthermore, ^{241}Pu decays with a half-life of only 14.35 years to ^{241}Am, which thus contaminates any TDF containing ^{241}Pu. Such considerations are another reason why the first NRF NDA systems are likely to be stationary installations that have their own TDFs.

Apart from the foregoing pragmatic limitations, there is an important inherent limitation to NRF that involves a trade-off among the strength of the gamma-ray beam, the energy width of the beam, the energy resolution of the gamma-ray detectors, the count rate of the detectors, and the thickness of any high-Z filtering material that may be placed in front of the detectors to reduce the gamma-ray flux that impinges upon them. The “weakest link in the chain” of the

NRF NDA technique is the maximum count rate of the gamma-ray detectors. The second weakest link is the spectral brightness of the gamma-ray beam, since it is directly governed by the cost and size of the equipment used to produce it. The challenge is to optimize the above factors to obtain the fastest and most accurate assay while satisfying these two constraints.

Ideally, the gamma-ray source should be as strong as possible in order to produce a strong NRF signal and thereby to reduce the assay time that is required to achieve a given level of statistical precision. On the other hand, the gamma-ray detectors are limited to a maximum count rate. Increasing the gamma-ray strength beyond the point at which the detectors reach their maximum count rate is futile, since more NRF signal is worthless if the detectors cannot detect it. Two ways exist to improve this aspect of system performance: (1) reduce the number of non-NRF, useless photons that the detectors must count and (2) increase the maximum count rate of the detectors.

The useless photons can be reduced (1a) by reducing the energy width of the beam, since only photons at the resonance energy levels are meaningful, and (1b) by filtering out some of the low-energy, useless photons from the gamma-ray flux that reaches the detectors. Reducing the energy width of the beam (1a) implies increasing its spectral brightness, which requires the use of advanced technologies like those described above for LCS beams. High-Z filters (1b) simultaneously reduce some of the high-energy NRF signal as they filter out the low-energy photons, which then implies that the gamma-ray beam strength must be increased to compensate for the lost NRF signal.

The maximum count rate of the detectors (2) can be increased but only at the expense of their energy resolution (apart from a major, transformative breakthrough in detector technology). The loss of energy resolution makes the determination of NRF-peak heights much more difficult and inaccurate, and such determination is the basis of the backscattered-measurement configuration and the original version of the transmission-measurement configuration. The IRT version of the transmission measurement—because it does not need to analyze peak heights—avoids this difficulty and can therefore make profitable use of the lower resolution but higher count-rate detectors.

In summary, the NRF NDA technique will be limited by the size and cost of the equipment used to produce the gamma-ray beam, the cost and availability of TDFs, and the maximum count rates of the gamma-ray detectors.

5.2.2 X-Ray Fluorescence (XRF)

Name	X-Ray Fluorescence (XRF)
References	NGSI: [58-68] Other: [404-408] Active XRF for fuel pins: [14, 409]
Measurement environment	In water (in air or other gas is also possible)
Passive vs. Active	Passive (The active kind of XRF is not considered here.)
Time dependency	Time-independent (continuous)
Particles detected	X-rays
Type of detectors	High-purity-germanium (HPGe) gamma-ray detectors
Particles' detected attribute	Energy
Governing physical properties of the fuel assembly	Gamma and beta radioactivity (determines the absolute magnitudes of the X-ray count rates) Radial distribution of the Pu within each outer pin
Governing isotopes	Elemental U and Pu (individual isotopes are irrelevant)
Maturity	Is used in other nuclear applications (mostly active XRF) and has been tested on spent fuel pellets but has not yet been used with spent fuel assemblies
Limitations	Cannot analyze isotopic vectors, only elements Can analyze only the outer fuel pins, so it is useless for detecting partial defects Depends on the radial profile of Pu within the fuel pellets May need different collimators for fuel assemblies with different levels of radioactivity
Selected by the NGSI for prototype testing?	No

5.2.2.1 Principle of operation

X-ray fluorescence (XRF) can be either a passive technique or an active technique, but in the NGSI Spent Fuel NDA Project, only the passive XRF technique was considered. Therefore, only the passive XRF technique will be considered in detail in this report.

X-rays are photons with less energy than gamma-rays, and whereas gamma-rays originate from the nuclei of atoms, X-rays originate from the electron clouds of atoms. Since all the isotopes of a given element have the same electron cloud, X-rays do not carry any information about the isotope of the nucleus; they carry information only about the element. Nevertheless, each element produces X-rays with its own characteristic energies. An X-ray photon is produced when an electron transitions down to a lower energy level in the electron cloud (Figure 76); the energy of the X-ray is the energy difference between the initial and final electron energy levels. This production of an X-ray is called X-ray fluorescence. Since each element has characteristic electron energy levels, the X-rays that it produces are also characteristic of that element. In this way, XRF can be used to distinguish among two or more elements—such as uranium and plutonium—in a sample, such as a spent fuel assembly. Table 16 lists the major X-rays from uranium and plutonium, and some examples of the X-ray fluorescence peaks from lead, uranium, and plutonium are presented in Figures 77 and 78.

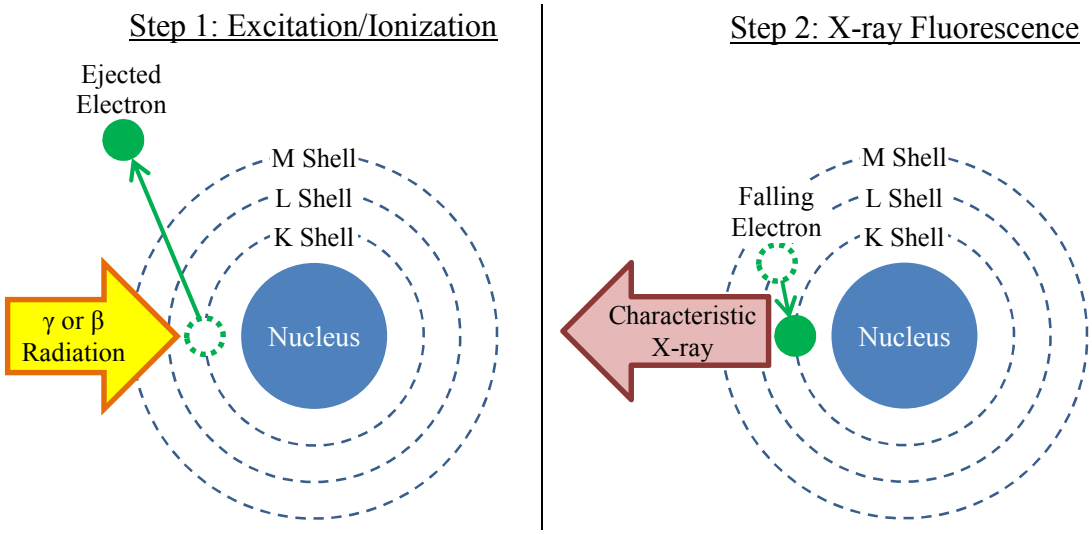

Figure 76: Schematic of how X-ray fluorescence occurs, as a high-energy electron moves to a lower-energy shell to fill a vacancy

Table 16: Energies and relative intensities of the major X-rays from uranium and plutonium. Modified from Table 1-1 in Reilly et al. [75].

	Levels	Energy (keV)		Relative Intensity (100 is maximum)	
X-ray	(Final − Initial)	Uranium	Plutonium	Uranium	Plutonium
$K_{\alpha 2}$	$K - L_2$	94.67	99.55	61.9	62.5
$K_{\alpha 1}$	$K - L_3$	98.44	103.76	100.0	100.0
$K_{\beta 1}$	$K - M_3$	111.30	117.26	22.0	22.2
$K_{\beta 2}$	$K - N_{2\text{-}5}$	114.5	120.6	12.3	12.5
$K_{\beta 3}$	$K - M_2$	110.41	116.27	11.6	11.7

Data are from C. M. Lederer and V. S. Shirley, editors, *Table of Isotopes* , 7th edition, John Wiley & Sons, Inc., New York, 1978.

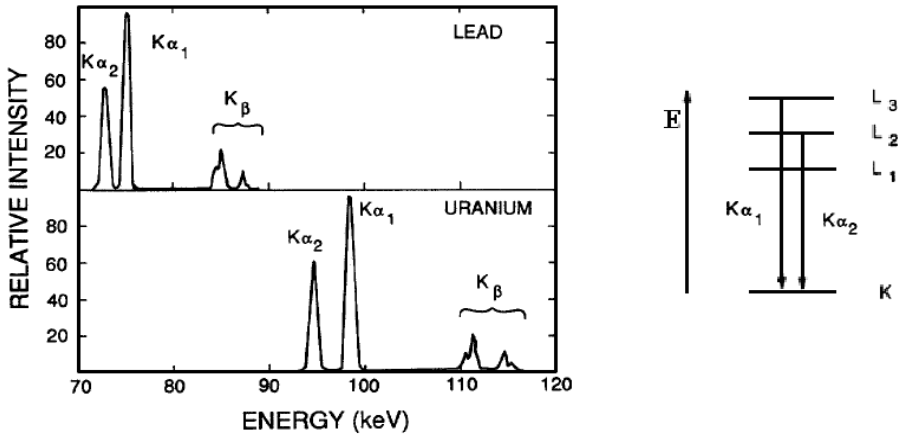

Figure 77: "Characteristic x-ray spectra from lead and uranium. Note that the pattern is the same but shifted in energy." Copied from Figure 1.6 in Reilly et al. [75].

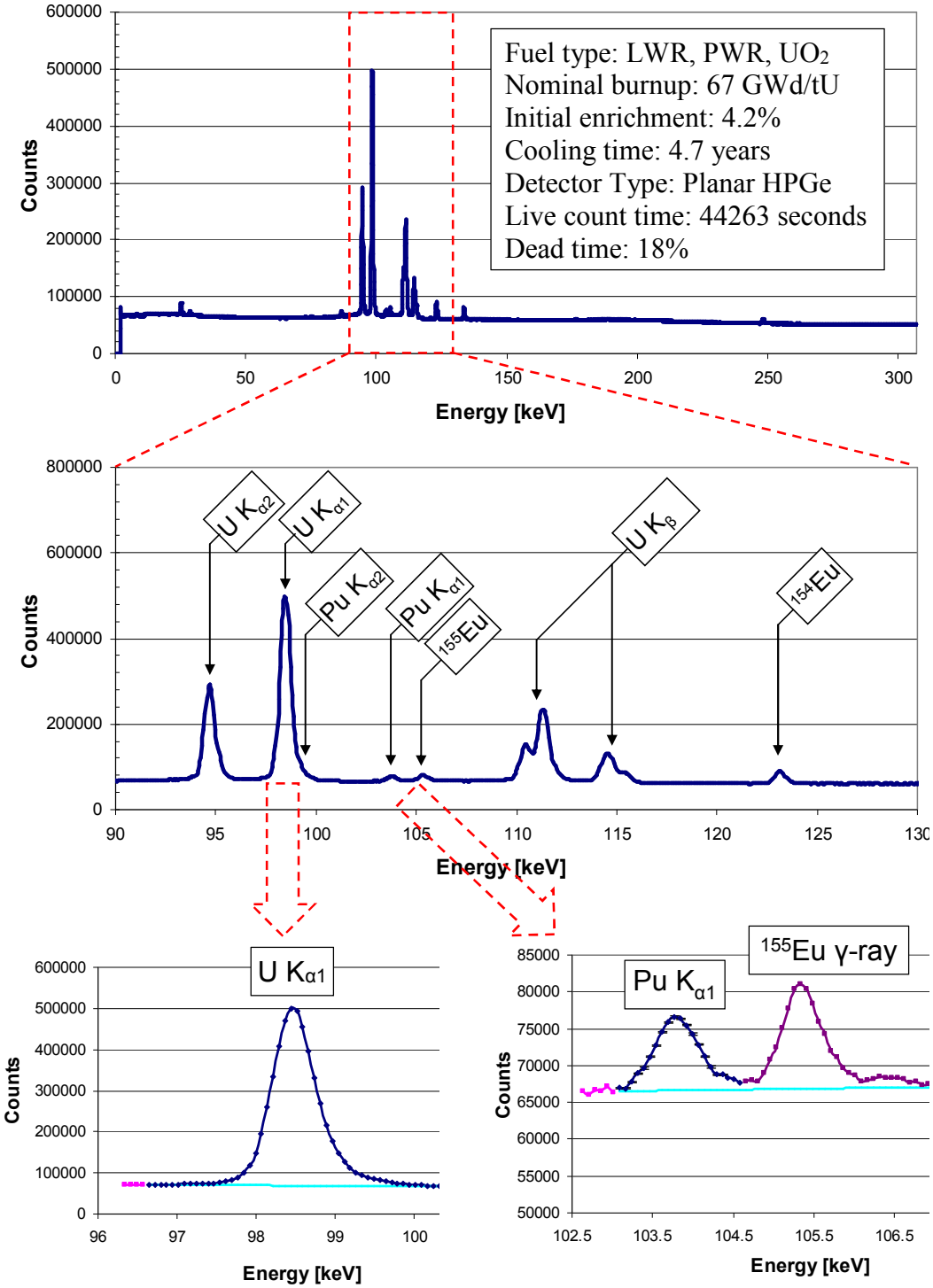

Figure 78: XRF measurement, with a planar HPGe detector, of part of a spent fuel pin (Label 649C) from the North Anna nuclear reactor in Virginia. Modified from Figures 2 and 14 in Freeman et al. [67]; see also the NGSI Phase 1 report [68].

As said above, an X-ray photon is produced when an electron moves to a lower energy shell around the nucleus. For this transition to take place, a vacancy in the lower energy shell must first be created. Such a vacancy can be created when radiation from an external source strikes the atom. The radiation types that are of most interest in spent-fuel NDA are gamma

radiation (photons) and beta radiation (electrons and also positrons, to a lesser extent). When an energetic photon or electron strikes one of the inner electrons around the nucleus (e.g., a K-shell electron), it can transfer enough energy and momentum to that inner electron to excite it to a higher level or to eject it from the atom, thus creating the vacancy. If the electron is ejected, the atom has then been ionized, at least temporarily.

Both types of ionizing radiation, gamma and beta, are present in large amounts in spent fuel assemblies, since they are produced from the radioactive decay of the fission products. Prior to the NGSI study of XRF, it was not known how much of the excitation of the atoms in the fuel pellets is caused by the gamma radiation and how much is caused by the beta radiation. In their study of single spent-fuel pins (not assemblies), the NGSI found that the gamma-rays were responsible for about 90% of the production of the XRF signal while the beta-rays were responsible for only about 10% [62, 64, 65, 67, 68]. The fraction that is attributable to the gamma-rays is expected to be greater for spent fuel assemblies, because the gamma-rays coming from the inner fuel pins are able to reach the outer fuel pins to excite their atoms, whereas the beta-rays (electrons) coming from the inner fuel pins are attenuated and stopped before they reach the outer pins. This fact is important for simulating XRF measurements, because the transport of gamma-rays is much easier to simulate in Monte Carlo programs than the transport of beta-rays is. Therefore, the NGSI was able to neglect safely the contribution from the excitation by beta-rays, in most cases.

Though this report deals only with passive XRF, it is appropriate to note here the main difference of passive XRF from active XRF. The hybrid K-edge densitometry (HKED) technique will be used as the representative active X-ray NDA technique. In HKED, the radiation that excites the atoms in the sample is a beam of X-radiation from an external source, typically an X-ray tube but sometimes a synchrotron [14]. The beam that comes out of the X-ray tube contains X-rays with a range of different energies. A monochromating crystal is placed in the beam to diffract only X-rays with a certain energy (wavelength) into a certain angle, thereby creating a separate beam only of X-rays with that particular energy. The energy of this monochromatic beam is chosen to be either just below or just above the K edge of the element that is being investigated in the sample. After making two separate measurements at these two energies, the amount of the element in the sample can be determined by comparing the difference in the attenuation of the beams through the sample. Simultaneously to these K-edge measurements, an X-ray fluorescence measurement can also be made. (This duality of measurement type is why the HKED technique is called “hybrid.”) As the X-ray beam is being attenuated by the sample, it is simultaneously exciting the electrons of the atoms in the sample and causing the atoms to fluoresce at their characteristic energies. These fluorescence X-rays are detected and analyzed in the XRF measurement. This XRF measurement is fundamentally the same as a backscattered NRF measurement (Section 5.2.1.2.2), just at lower photon energies.

In contrast with these active X-ray measurements, passive XRF uses the spent fuel’s own gamma and beta radioactivity to excite the atoms and induce fluorescence; no external source of radiation is required. Also, this passive gamma and beta radioactivity is not monochromatic but rather has a very wide range of energy. Therefore, there can be no K-edge densitometry associated with the passive XRF technique. It can be noted that in the HKED technique, the

XRF measurement does not actually require that the X-ray beam be monochromatic; the K-edge measurement is the one that requires the monochromaticity. In fact, the active XRF measurement does not even require that the external radiation beam must be X-rays; one could use an electron beam, as is done in energy-dispersive and wavelength-dispersive X-ray spectroscopic measurements with electron microscopes. Thus, the only fundamental difference between the passive and active XRF techniques is the origin of the exciting radiation, whether it is internal or external to the sample, even though the practices of the two types of techniques can be very different.

The attenuation of X-rays is an important feature and limitation of XRF. Estimations of the attenuation in the fuel and in the cooling water can be made as follows. From Table 16, it is seen that the X-ray energies of interest are around 100 keV. If it is assumed that most of the attenuation in the fuel is caused by the uranium, that the mass attenuation coefficient of uranium for 100 keV X-rays is 2.5 cm^2/g, that the density of the fuel is 10.4 g/cm^3, and that the density of the uranium in the fuel is 9.2 g/cm^3, then the calculation of the attenuation shows that about 70% of the X-rays are attenuated within half a millimeter of travel through the fuel. (See the equation in Figure 74.) As for the attenuation in the cooling water, the mass attenuation coefficient of water for 100 keV X-rays is about 0.16 cm^2/g, so that about 70% of the X-rays are attenuated within 8 cm of travel through the water. These estimations show that very few of the X-rays that originate in the inner pins will survive to be detected by the detectors. XRF essentially measures only the outer row of fuel pins in a spent fuel assembly and is therefore unable to detect partial defects.

Another conclusion from the consideration of X-ray attenuation is that unlike in the gamma-ray NDA techniques, heavy-metal filters, such as lead (Pb), cannot be used in front of the X-ray detectors to reduce the count rate. In the gamma-ray techniques, the relatively lower energy X-rays are background noise that the filters preferentially remove. In XRF, these same lower-energy X-rays are the signal itself, which should not be removed. Instead of using filters to remove unwanted higher-energy photons, the X-ray detectors can be made thin, so that the higher-energy photons preferentially pass through the detectors without depositing much of their energy in them. For this reason, the NGSI has recommended the use of thin, planar HPGe detectors [65, 67, 68]; see the next subsection (5.2.2.2).

A further comparison with the passive gamma spectroscopic technique (PG, Section 5.1.3) reveals the nature of the photon radiation flux coming from the spent fuel assembly and thereby further explains the principles of the XRF technique. The PG technique endeavors to detect and measure the characteristic gamma-rays being emitted from important isotopes in the spent fuel, such as ^{134}Cs, ^{137}Cs, and ^{154}Eu. These gamma-rays are characteristic and meaningful because they are at discrete energies. Essentially then, these gamma-ray signals must be comprised of *unscattered* photons, because of the fact that since inelastic, incoherent scattering dominates the total scattering, the photons lose energy almost every time that they scatter and then become no longer characteristic of the originating isotope. Such inelastically, incoherently scattered photons constitute the Compton continuum in the photon flux that is emitted from the fuel assembly (which is distinct from a Compton continuum created in the detector itself). Again, this Compton continuum is merely background noise for the PG technique. Some of the photons in this continuum *pick up meaning again*, though, as they

interact with the fuel pellets in the outer fuel pins via X-ray fluorescence. The X-ray fluorescence process essentially discretizes (or quantizes) again a portion of the photon continuum, thereby imparting information about the fluorescing elements to those photons. It is largely these “recycled” photons that the XRF technique measures and exploits.

An important question that arises from this vantage point is whether the additional rows of pins behind the outermost row contribute more to the Compton continuum—that is, to the noise—or more to the X-ray fluorescence of the outer pins—that is, to the signal. The NGSI investigated this question with Monte Carlo simulations and found that the background and the signal both increase by almost equal proportions with each row that is added behind the outer row [67, 68]. Therefore, the number of rows of fuel pins in a spent fuel assembly does not substantially affect XRF measurement results.

5.2.2.2 The NGSI’s design

The NGSI focused on understanding the XRF signal rather than on designing an optimal XRF instrument. Designing an instrument would have been the next step if the XRF instrument had been selected for prototype testing in Phase II of the Spent Fuel NDA Project. Nonetheless, the Phase I study did reveal some principles to guide the design of an XRF instrument, particularly since the study involved actual measurements of spent fuel pins from the North Anna nuclear reactor (see Figure 78 and References [62, 67, 68]) and from the Three Mile Island Unit 1 nuclear reactor [58, 59, 64, 65].

All of the XRF instrument designs presume the use of a collimator, to reduce the photon flux that the detector receives and thereby bring the count rate below the detector’s maximum limit. Some important aspects of the orientation of the collimator with the spent fuel assembly are the length of fuel pin that influences the measurement, the presence of obstructing objects, and the distance between the assembly and the collimator. Although the collimator gives only a very limited areal view of a fuel pin and removes the X-rays from outside this viewed portion, this portion of the fuel pin that is in line with the collimator is not the only portion that is important. The portions above and below this point are also important, because the gamma-rays from these neighboring portions can induce XRF in the viewable portion. Nevertheless, the length of these important neighboring portions is short. The NGSI calculated that only 2 cm of fuel pin length either above or below the centerline of a 0.1 cm radius, 5 cm long collimator make a significant contribution to the detected XRF signal [67, 68]. Of course, the presence of any structural material on the assembly, such as a band or spacer, will block much of the signal, so the XRF measurement must be made with a clear line of sight to the fuel pins. Similarly, the distance between the fuel assembly and the collimator will attenuate the XRF signal, not only because of the well-known inverse-square law but also because of attenuation by the water that fills this distance. The NGSI’s Monte Carlo simulations indicated that 2 cm of water would reduce the signal-to-background ratio of the Pu $K_{\alpha 1}$ peak roughly by 30% [67, 68], and this number agrees with an analytical calculation of attenuation that is based on the numbers given in the previous subsection (5.2.2.1). Note that the attenuation by water necessitates that the collimator be sealed to keep water out of it.

The NGSI study of an XRF measurement of a spent fuel assembly assumed that the collimator would be a pin-hole collimator that would be 80 cm long and have a diameter that could be varied from 0.1 cm to 0.3 cm. The larger-diameter collimators would be used for measurements of the less-burned, more-cooled fuel, since such fuel would produce smaller photon fluxes; the flux after 80 years of cooling is typically about 20 times less than the flux after only 1 year [67, 68]. In this case, a larger-diameter collimator would reduce the assay time by keeping the detector's count rate near its maximum limit. How the collimator diameter would be changed in the field was not addressed in the study.

A pin-hole collimator was chosen rather than a slot collimator because it was expected that the count rate with a slot collimator would be too high for the detector. This choice is unlike some past choices for collimators for passive gamma spectroscopy (PG); a slot collimator was used for the PG measurements of MTR fuel assemblies by Phillips et al. [127], for example. A slot collimator has the advantage that the entire width of a fuel assembly can be measured at once, thus automatically providing an average value over the width without the need to scan it with the instrument. Unlike an XRF instrument, though, a PG instrument can also make use of a high-Z filter in front of the detector to reduce the count rate within acceptable limits. An XRF instrument must rely solely on the collimator to reduce the count rate, thus necessitating the use of a pin-hole collimator.

As mentioned in the previous subsection (5.2.2.1), a thinner detector is better for X-ray measurements than a thicker detector because it records a cleaner signal and slightly reduces the count rate by not detecting some of the higher-energy gamma-rays. The higher-energy gamma-rays, which are not of interest for XRF, tend to pass right through thinner detectors because of the energy dependence of attenuation, as illustrated in Figure 64. Not only does this avoidance of high-energy gamma-rays reduce the total count rate of the detectors (albeit negligibly so, perhaps), but more importantly, it also reduces the Compton continuum that such gamma-rays create inside the detector. This Compton continuum overlaps the lower-energy X-ray signals, so reducing it is good. For this reason, a planar detector geometry is better than a coaxial geometry. The NGSI used Monte Carlo simulations to examine the effect of different thicknesses of the HPGe crystal in a planar detector on the signal-to-noise ratio, and they found that the optimal thickness is approximately 0.5 cm.

The NGSI examined only HPGe detectors in their XRF study, but this type is not the only type that has been used in XRF studies in the past. For example, Ahmed et al. [405] used CdZnTe (CZT) detectors to make XRF measurements of irradiated CANDU fuel bundles. That study was interested primarily in verifying that the fuel bundles were irradiated, rather than in assaying the bundles' plutonium content, however; so the authors examined only the uranium XRF peaks, not the much weaker Pu peaks. For Pu assay, the energy resolution of a CZT detector may not be sufficient to separate the Pu peaks from the uranium and ^{155}Eu peaks (Figure 78).

Separately from the NGSI study, researchers at Texas A&M University have examined the use of a diffraction crystal in an XRF measurement, to remove unwanted low-energy and high-energy photons from the detected photon flux and thereby to improve both the signal-to-noise ratio and the detector's counting performance [407, 408]. A diffraction crystal is a single crystal and takes advantage of the fact that although the X-rays from U and Pu XRF are

hard (high-energy), their wavelengths (0.124 Å, or 12.4 picometers, for 100 keV X-rays) are still long enough to be on the order of the spacing between the closest planes of atoms in the crystal lattice. These close planes are not defined by the spacings between the atoms in a single unit cell of the crystal, which are much longer than such wavelengths, but are rather defined by the spacing between atoms from multiple unit cells, such that the plane cuts through a single unit cell at a strange angle. The Texas A&M researchers used the (404) plane of a quartz crystal for their simulation work; that is, they oriented the quartz crystal relative to the collimated beam of photons coming from the spent fuel assembly so as to use this plane for diffraction.

As the photons pass through the diffraction crystal, the crystal diffracts them and bends their direction of travel into specific angles according to their energies (wavelengths). Thus, the X-rays of different wavelengths travel outward in different angles from the crystal. This result is somewhat like the separation of white light into constituent colors by a prism, although the physical mechanism is different (diffraction vs. refraction). For photons with such short wavelengths, the angles of diffraction are small: 8.447° for the 103.7 keV Pu $K_{\alpha 1}$ X-ray and 9.225° for the 95 keV U $K_{\alpha 2}$ X-ray. (See Table 2 in the 2011 paper [407].)

The differences among the diffraction angles of the various X-rays are too small to use as a basis for separating the X-rays from each other with collimators of reasonably short length. Nevertheless, the diffraction is sufficient to separate the important X-rays *as a group* from all of the irrelevant lower-energy and higher-energy photons. A secondary collimator can be placed behind the diffraction crystal. The collimator has a conical annular slot at the proper range of angles. The important X-rays are diffracted just enough to pass through the slot. Higher-energy photons are not diffracted enough and hit the central cone of the collimator, while lower-energy photons are diffracted too much and hit the outer ring of the collimator. The detector is placed behind the secondary collimator and is therefore exposed only to the flux of X-rays within the important range. In this way, the signal-to-noise ratio is improved while the total count rate is simultaneously reduced.

Note that a diffraction crystal is difficult to use in this way for the higher-energy, gamma-ray NDA techniques. This use is feasible with the XRF technique because the X-ray photons have sufficiently long wavelengths to diffract significantly, but the wavelengths of the higher-energy gamma-rays are much shorter. Gamma-rays are able to reflect off multi-layer mirrors at grazing-incidence angles, though, so a similar separation of desired gamma-rays from background may be possible to achieve with such mirror optics [323].

5.2.2.3 Data analysis

The NGSI's method of analysis of XRF data is straightforward. The areas under the U Kα1 peak (at 98.4 keV) and the Pu Kα1 peak (at 103.7 keV) are measured after subtracting the background. A correction is made for the overlap of the Pu Kα2 peak (at 99.6 keV) with the U Kα1 peak, by estimating the area of the Pu Kα2 peak from the area of the Pu Kα1 peak (62.5% of it; see Table 16) and then subtracting it from the measured area of the U Kα1 peak [67, 68]. The ratio of the area of the Pu Kα1 peak to the corrected area of the U Kα1 peak is then a measure of the ratio of the mass of Pu to the mass of U in the fuel pin. The correlation between these two ratios is linear and is determined from simulations of measurements or

from experimental measurements and careful destructive analysis; see Figure 79. (Destructive analysis must take into account the radial distribution of Pu in the fuel pin, as discussed in the next subsection, 5.2.2.4, *Limitations*.)

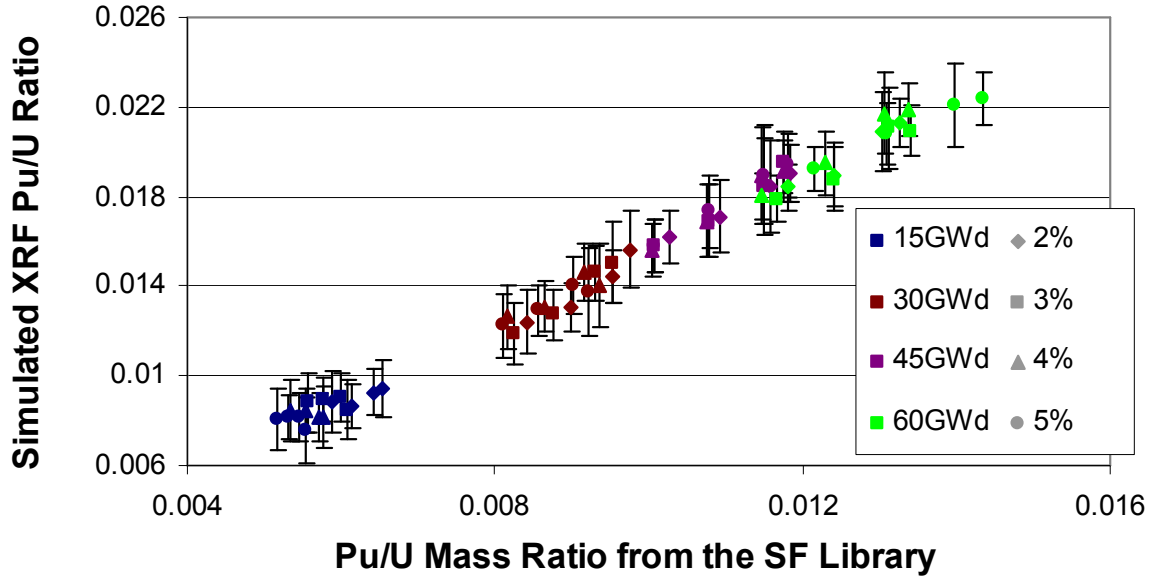

Figure 79: The correlation between the Pu/U XRF ratio and the Pu/U mass ratio, as determined by the NGSI's simulation studies. Burnup is indicted by color, and initial enrichment is indicated by symbol shape. Copied from the NGSI Phase 1 report [68].

It should be noted that Stafford made the correlation to the Pu/U mass ratio via a secondary correlation to burnup as determined by a PG spectroscopic measurement of the $^{134}Cs/^{137}Cs$ ratio [65]. Such a correlation to burnup is not an inherent part of the XRF technique, but it allows one to create the correlation to Pu/U mass ratio without performing destructive analysis, by taking advantage of existing correlations among the $^{134}Cs/^{137}Cs$ ratio, the burnup, and the Pu/U mass ratio.

The NGSI's Monte Carlo simulations of the experimental XRF measurements of spent fuel pins produced count rates that were four times smaller than the experimentally measured count rates [68]. (The earlier publication [67] reported an even larger discrepancy.) The reason for the discrepancy was unclear. Nonetheless, the Pu/U peak ratio and the relative magnitude of the nearby ^{155}Eu gamma-ray peak were consistently the same between the simulations and the experimental measurements. Since these peaks represent the important physics and results of an XRF measurement, the discrepancy in the absolute magnitude of the simulated signal has been considered to be nonessential.

5.2.2.4 Limitations

The XRF technique has several limitations, some of which have already been mentioned. As said above, XRF can analyze only elements, not isotopes. Also, it can analyze only the outer fuel pins of a spent fuel assembly, so it is unable to detect partial defects. Furthermore, the magnitude of the photon flux decreases significantly with increasing cooling time, which might necessitate using larger-diameter collimators with longer-cooled fuel to keep the assay time reasonably short.

One potentially important limitation that has not yet been discussed is the effect of the radial distribution of the Pu in the spent fuel pellets. The NGSI accounted for this radial distribution in their burnup and XRF measurement simulations by dividing up the fuel pellets into several radial regions [67, 68]; see Figure 80, for example. The radial distribution is important because the self-shielding of the X-rays by the fuel pellet is great. As said above (Section 5.2.2.1), approximately 70% of 100 keV X-rays are attenuated by travel through only 0.5 mm of fuel pellet, so X-rays that originate from Pu in the center of the fuel pellet are unlikely to survive the transit to the edge of the pellet to escape and be detected. Fortunately, as Figure 80 exemplifies, Pu is preferentially created on the exterior of a UO_2 fuel pellet during the burning of the fuel in the nuclear reactor, because the fuel pellet's self-shielding of the resonance-energy neutrons that produce Pu by capture in ^{238}U is also great. Therefore, most of the Pu X-rays are not attenuated. Furthermore, the NGSI examined the variation of the radial profile of Pu among all 64 spent fuel assemblies in the first spent fuel library (Section 2.3) and found that although the profile did vary among the assemblies, it varied only slightly and in a predictable way with burnup, initial enrichment, and cooling time. They recommended, though, that this variation should be investigated further since the first spent fuel library was created from idealized, not realistic, burnup simulations [68]. Any uncertainty in the Pu radial profile would translate directly into uncertainty in the XRF measurement results, since XRF cannot account for the radial profile. Lastly, this limitation also implies that XRF is probably unsuitable for assaying MOX fuel, since the radial distribution of the Pu in MOX fuel pellets is not just a function of burnup but is sometimes intentionally varied in the creation of the fuel pellets to improve the fuel's performance in the reactor [410].

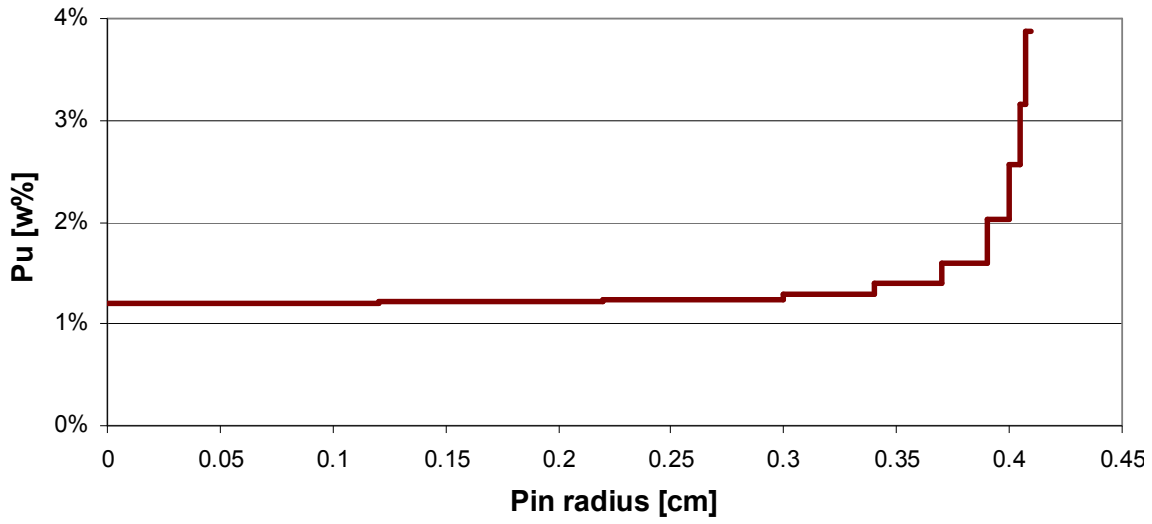

Figure 80: Radial distribution of the Pu in the spent fuel pellet from which the data in Figure 78 were measured. The distribution contains ten regions and is the result of a burnup simulation. Copied from Freeman et al. [67, 68].

Another limitation of XRF is the inherently long assay time when only a single pair of pin-hole collimator and detector is used for the measurement. The NGSI found that 10 hours would be needed for a reasonably accurate assay (approximately 4% uncertainty) [67, 68]. The reason is that, unlike with NRF in which the strength of the fluorescence-inducing

radiation source can be controlled and optimized, the radiation source of passive XRF is inherent to the spent fuel assembly and cannot be changed. This fact means that the XRF signal-to-noise ratio of a given, collimated beam is practically fixed. Since the diameter of the collimator is likewise fixed for a given photon flux from the fuel assembly and the maximum count rate of the given type of detector, the only way to speed up the assay, without employing some trick like using a diffraction crystal, is to use more collimators and detectors. Such a solution is certainly possible, but it obviously increases the size, weight, and cost of the XRF instrument.

6. A critique of the current practice of NDA of spent fuel assemblies

In a recent publication, one of the authors critiqued the current practice of NDA of spent fuel assemblies, both the practice of the NGSI and that of the rest of the safeguards community [210]. This section summarizes that publication by repeating selected portions of it, with permission from Elsevier. In so doing, this section provides a paradigm by which to understand how the NGSI's fourteen advanced NDA techniques can be applied in the most effective way. The focus of this summary is on the NDA of enriched-uranium assemblies; for the NDA of mixed-oxide (MOX) assemblies, the reader is referred to the original publication.

6.1 Introduction: An overview of NDA practice and the statement of the problem

The safeguards community uses NDA to characterize spent fuel assemblies for materials-accountancy purposes, specifically for the determination of their fissile and plutonium content. This current practice of NDA on spent fuel assemblies is illustrated in Figure 81. First, experiments (or simulations) are conducted to measure many fuel assemblies from a pertinent range of values of burnup (BU), initial enrichment (IE), and cooling time (CT).[5] (These three variables will be called collectively as the "BIC set" of variables in the following discussion; see also Section 3.2.) Historically, these BIC variables have been chosen because their values for a given fuel assembly are usually easy to determine from its records and because they seem to characterize spent fuel assemblies to a large extent. The measured quantity and the BIC variables are averages over the transverse cross-section of the fuel assembly and may also be averages over the axial length. By these experiments or simulations, the measured quantity is correlated to the BIC set, so that any future measurement on an unknown fuel assembly can be interpreted.

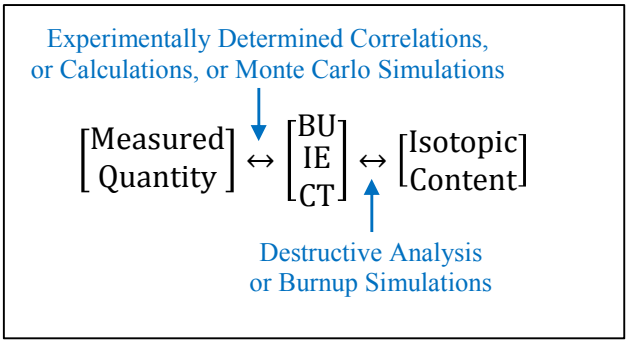

Figure 81: The current logic of NDA practice for safeguards. Reprinted from [210] with permission from Elsevier.

Second, the values of the BIC set are correlated with the characteristic of interest, i.e., the fissile or plutonium content. In the past, destructive assays were performed on the range of fuel assemblies to determine their isotopic content and establish the correlation. The current practice is to conduct burnup simulations to create the correlation.

In summary, the current NDA practice is to make two correlations to logically connect the measurement of a fuel assembly to its characteristics of interest via its BIC-set value. One

[5] The cooling time is assumed to be within a practical range: greater than a few days so that all of the very-short-lived neutron poisons (like ^{135}Xe) have decayed away, but less than about one century.

correlation is between the measured quantity and the BIC set. The other correlation is between the BIC set and the isotopic content.

The problem with these measurements is illustrated in Figures 11 (TN), 14 (PNAR), 17 (CIPN), 25 (DDA), 26 (DN), 37 (DDSI), and 52 (SINRD). The problem is that one measured value (on the vertical axis of each figure) corresponds to a range of possible values of the fissile content (on the horizontal axis). It is therefore impossible to obtain an accurate determination of the fissile content by using only one measured quantity in the absence of other information.

Burr et al. [135] have quantified this type of uncertainty that is exhibited in all these NDA techniques. They chose to analyze the PNAR technique as a representative example. Through Monte Carlo simulations, they showed that the fissile content of a spent fuel assembly can be predicted to a high degree of accuracy (accounting for 99.7% of the variance) by a parametric equation that uses only the three BIC variables as the parameters (Equation 1 in their paper). This equation was derived from a wide subset of the BIC domain and is therefore valid over that wide subset (though with the caveat that the fuel assemblies being examined were themselves merely the product of burnup simulations). They furthermore made the contrasting observation that if only the PNAR signal is used to determine the fissile content, then the relative error standard deviation (RESD) in the fissile content varies from 15% to 69% (as a function of the variation of the measurement RESDs from 1% to 20%, that is, as a function of the errors in the count rates themselves). These numbers confirm the argument made above, that the one measured quantity—the PNAR signal in this example—cannot determine the fissile content accurately.

The obvious solution to this problem is to use additional information to obtain an accurate determination. Such information can be added implicitly or explicitly. It can be added implicitly by applying the NDA only to a limited set of fuel assemblies, such as fuel assemblies from the same spent-fuel pool. In this way, most of the variables are implicitly kept fixed or within a tight dynamic range [127], and so the relationship collapses more or less to a one-to-one relationship (bijection). Such NDA results are inherently relative, applying only to fuel assemblies within the limited set, and so they are most useful just for checking for outlying fuel assemblies (Bevard et al. [2], Sections 3.4 and 7.1). Explicitly adding more information to the NDA measurement enables more general correlations to be made. If the BU, IE, or CT of the fuel assemblies is known *a priori* from their records or burnup simulations, then this information can be used to select a more accurate correlation between the measured NDA quantity and the fissile content. For example, Burr et al. [135] have shown that including accurate values of BU and CT (or of IE and BU) along with the NDA signal when calculating the fissile content produces a more accurate result than using just the NDA signal alone.

Burr's results also reveal that this kind of uncertainty in all these NDA techniques can be classified neither as random error (since knowledge of one or more BIC variables improves the result) nor as short-term systematic error (since the discrepancies are not all in one general direction), according to the commonly used definitions in the book of International Target Values [411]. Instead, the uncertainty is not inherent to each fuel assembly itself but is rather the uncertainty of choosing the fuel assembly to be measured—i.e., where its unknown BIC-

set value happens to be in relation to the calibration curve through the BIC-set domain. It is this choosing that is random. The explicit addition of information about the values of one or more BIC variables for a given fuel assembly therefore reduces the uncertainty by assisting the NDA practitioner to adjust the calibration curve to be more appropriate for interpreting the NDA measurement result for that given fuel assembly.

The following sections explain the physical reasons behind this phenomenon that has been merely observed by Burr et al.: why this uncertainty exists and why the knowledge of the BIC set, in particular, reduces this uncertainty. Various parts of these explanations are well-known in the literature; the originality of this work is the collection of these parts into a cohesive whole—a paradigm—that provides both a clearer interpretation of past results and the ability to predict ways to improve NDA practice. The priority is thus to derive an understanding from physical principles rather than to address specific pragmatic concerns. Such an understanding will nonetheless be useful for directing other research to address such concerns.

6.2 Theory: The nature of the vector spaces in NDA practice

6.2.1 The existence of the vector space of physical properties

The first step to constructing a better paradigm for NDA practice is to recognize explicitly that a vector space of the physical properties of the spent fuel assembly at the time of the NDA measurements should be included in the overall logic of Figure 81. The result is shown in Figure 82. The physical properties are physical in the sense of being related to the *physics* of the generation and transport of neutrons, photons, heat, or other particles or energy throughout the fuel assembly. The physical properties may be able to be detected directly (e.g., the gamma-ray activity), or they may need to be deduced (e.g., the multiplication of neutrons).

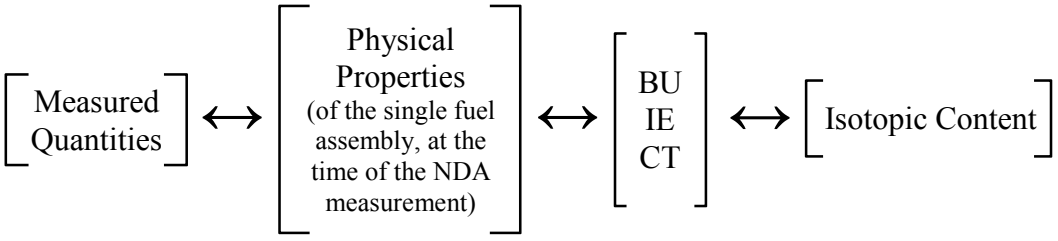

Figure 82: The corrected logic for proper NDA practice on spent fuel assemblies. Reprinted from [210] with permission from Elsevier.

The reason that the physical-properties vector space must be recognized and included is that the physical properties are the current characteristics of a fuel assembly and can be repeatedly determined or verified, whereas the BIC set describes only the past history of the assembly and therefore cannot be repeated for that particular assembly. This is to say that the NDA measurements are actually measuring the physical properties, *not* the BIC variables, in contradiction to the common parlance in both the safeguards and burnup-credit communities. For example, the only way to actually measure BU is to measure it *while* the fuel assembly is being burned in the reactor, such as by putting a neutron-flux monitor next to the fuel assembly or by detecting the antineutrinos associated with fission events [412]. This contradiction may have originated with total (energy-independent) gamma-ray measurements, since the gamma-ray activity of a spent fuel assembly is almost completely comprised of

gamma-rays emitted from the radioactive decay of fission products. The gamma-ray activity is thus an indication of the number of fissions that have taken place—that is, an indication of the burnup. Most physical properties, especially the neutronic properties, cannot be so closely identified with a particular BIC variable, though; and even the gamma-ray activity depends on CT as well as on BU. It is therefore more correct to recognize and include explicitly the physical-properties vector space in the logic of NDA practice, and this addition is an essential part of the following arguments.

6.2.2 The dominance of the neutronic physics

The next step is to recognize that the neutronic physics is the most important physics of a spent fuel assembly and actually governs all the other relevant physics. This conclusion is supported by three obvious facts. First, the burning of nuclear fuel in a nuclear reactor is a neutronic process: neutron-induced fission. Second, uranium and plutonium are required to be determined and safeguarded precisely because of their fissile isotopes. Third, the residual reactivity of a spent fuel assembly—which is important for ensuring criticality safety—is also a neutronic property. Therefore, the processes by which a fuel assembly comes to be in the status of "used" and also the reasons for caring about the characteristics of the spent fuel assembly are all derived from the neutronic physics of the fuel assembly.

6.2.3 The tri-dimensionality of the physical-properties and isotopic-content vector spaces

The previous statements may have been obvious, but they are the necessary justification for this next step. Since the neutronic physics governs the relevant physics and isotopes of the spent fuel assembly, it is valid to examine an equation that describes the neutronic physics of the fuel assembly—that is, the neutron diffusion equation—to determine the dimensionality of the physical-properties vector space and of the isotopic-content vector space. The emphasis is on the state of the spent fuel assembly at the time of the NDA measurement, rather than during the burning of the fuel in the reactor. It is also assumed that the spent fuel assembly is immersed in cooling water unless otherwise stated.

The one-speed neutron-diffusion equation for the spent fuel assembly is as follows:

$$S + \left\{\frac{1}{k_{eff}}\right\}\bar{\nu}\Sigma_f\phi - \Sigma_a\phi - (-D\nabla^2\phi) = \frac{1}{v}\frac{\partial\phi}{\partial t} \qquad \text{Equation 57}$$

(This equation is basically the same as Equation 3.) The symbols have their usual nuclear-engineering meanings [74, 289]. Note that the $1/k_{eff}$ coefficient should be included only when criticality is being examined, by setting S and $\partial\phi/\partial t$ to zero. Also, delayed neutrons are not included separately in this equation, for simplicity of argument. The first two terms on the left-hand side of Equation 57 represent the production of neutrons: the first one by primary-neutron sources and the second one by induced fission. The last two terms on the left-hand side represent the loss of neutrons: the first one by absorption and the second one by diffusion (i.e., leakage). The term on the right-hand side represents the change in the neutron flux during a transient. Of course, each term changes with position inside the fuel assembly.

The fact that the physical-properties vector space is basically three dimensional can be seen by recognizing that although there are five terms in this equation, two of them are constant or known. Relative to the magnitude of the neutron flux, the diffusion term stays

almost constant with the burning of the fuel, because both the geometry of the fuel assembly and the diffusion coefficient at each location within the fuel assembly stay constant regardless of the burning of the fuel [209]. (Nauchi et al. [209] also determined that the leakage probability is constant, too; see Section 6.2.5 below.) Nauchi et al. explained this constancy of the diffusion coefficient by recognizing that the neutron diffusion is dominated by elastic scattering in water, and the water in and around the fuel assembly obviously does not change with burnup. An additional argument, not mentioned by Nauchi et al. [209], is that the inelastic scattering in the fuel also does not change greatly with burnup, because the quantity of the most prevalent heavy isotope in the fuel (^{238}U for LEU; ^{235}U for very enriched HEU) remains nearly constant over typical ranges of burnup. As for the time-dependent term, this term either is zero, for a steady-state NDA measurement, or is a known output (measured quantity), for a time-dependent NDA measurement such as neutron coincidence counting or a differential die-away (DDA) measurement. That is, the term either is zero or is represented by τ, a characteristic die-away time. This recognition is also supported by the fact that the term contains no material-related variables. It is seen then that only three terms in the neutron-diffusion equation vary with the burning of the fuel, and since the neutronic physics governs the physical properties of the spent fuel assembly, the vector space of the physical properties must therefore be basically three dimensional.

The dimensionality of the isotopic-content vector space can likewise be determined by examining this equation. Since Σ_a, by definition, includes both absorption that leads to fission and absorption that just captures the neutron, it is helpful to separate first these two kinds of absorption and to rearrange the equation accordingly:

$$S + \left(\left\{\frac{1}{k_{eff}}\right\}\bar{\nu} - 1\right)\Sigma_f\phi - \Sigma_{a,capture}\phi - (-D\nabla^2\phi) = \frac{1}{v}\frac{\partial\phi}{\partial t} \qquad \text{Equation 58 (same as Equation 3)}$$

The second term now is the net neutron production from fission. In this equation, the first three terms correspond to the three kinds of isotopes that affect the neutron physics of the fuel assembly: the primary neutron sources (corresponding to S), the fissile isotopes (corresponding to Σ_f), and the neutron-capturing isotopes (corresponding to $\Sigma_{a,capture}$). Again, the last two terms are constant or known. Therefore, the isotopic-content vector space is also three-dimensional, consisting of three groups of isotopes.

A criticism of these conclusions might be that Equations 57 and 58 are only one-speed and so do not account for the physics of the neutron energy spectrum. Neutron energy should therefore be considered as another dimension, perhaps. However, the neutron energy spectrum is determined by neutron scattering, which remains constant with the burning of the fuel, as has already been explained. (It must be reiterated that the energy spectrum *at the time of the NDA measurement* is what is in view here.) Therefore, neutron energy is indeed a secondary property, and its influence can be treated as a minor uncertainty in the values of the other, more important properties.

The fact that some NDA techniques specifically analyze the neutron energy spectrum may seem to contradict this simplification. Such techniques include neutron resonance transmission analysis (NRTA), neutron resonance capture analysis (NRCA) [12], lead slowing-down spectroscopy (LSDS), and self-interrogation neutron resonance densitometry

(SINRD). These techniques operate by analyzing the resonances of specific isotopes, though, rather than the energy spectrum of the fuel assembly as a whole. (In its most practical configuration that uses only ^{235}U fission chambers, SINRD analyzes the 0.3 eV resonances of all three fissile isotopes together as a group.) In other words, these NDA measurements are more or less direct measurements of individual isotopes, rather than measurements of a physical property of the fuel assembly. Therefore, the quantity of the isotope of interest, not neutron scattering and moderation, governs the measurement. The neutron-energy characteristics of the fuel assembly as a whole merely limit the applicability of such NDA techniques.[6]

Though the argument has already been made that the neutronic physics governs the physical properties and isotopes, it is nevertheless appropriate to show explicitly how the gamma-ray physics and associated isotopes do follow the neutronics, in fact. The delayed gamma (DG) NDA technique follows the neutronics because the delayed gamma-rays come from induced fission, primarily or totally in the fissile isotopes (according to the instrument's design) [48]. Prompt-gamma activation analysis (PGAA) is based on neutron capture in the neutron absorbers [11]. Passive gamma-ray measurements, whether energy-independent (total, TG) or energy-dependent (PG), rely on gamma-rays emitted by the radioactive decay of fission products [53, 75]. Admittedly, there is not a direct connection between the isotopes that produce these passive gamma-rays and the neutronic physics of the fuel assembly at the time of the NDA measurement, since these isotopes do not play a significant role in fission, neutron capture, or neutron scattering. An indirect link does exist, though, because these isotopes were created through the induced fission that occurred in the nuclear reactor. The induced-fission term of Equations 57 and 58 at the time of the NDA measurement must obviously be connected with the induced-fission term of Equations 57 and 58 during the burning of the fuel assembly in the reactor. From another perspective, the passive gamma-rays are clearly linked to BU; and since BU is linked, in turn, to the neutronic physical properties and isotopes at the time of the NDA measurement (as will be proven in Section 6.3), the passive gamma-rays must likewise be linked to them as well. Therefore, the gamma-ray physics is tied to the neutronic physics, in general.

6.2.4 The NDA techniques that are less dependent upon the BIC set

It was mentioned in the previous subsection that the NRTA, NRCA, LSDS, and SINRD NDA techniques analyze the characteristic neutron-energy resonances of specific isotopes. Similarly, the nuclear resonance fluorescence (NRF) technique analyzes the characteristic gamma-ray resonances of specific isotopes [357], and the X-ray fluorescence (XRF) technique analyzes the characteristic X-rays of specific elements [62, 75]. By the arguments made above, such NDA techniques should not depend upon the BIC set significantly or at all. (SINRD does have some dependence on the BIC set (Figure 52) because it is not based purely on the analysis of resonances.) On the other hand, all these techniques except NRF are

[6] One might say that the very difficult problem of self-shielding in the LSDS technique is a symptom of a partial failure of these arguments for that technique. Although LSDS does try to analyze a unique, resonance-based signal from each fissile isotope, the phenomenon of self-shielding is actually a property of the fuel assembly as a whole. LSDS requires the absence of water in the fuel assembly; and without water in between the pins, the neutron-energy characteristics of the fuel assembly become much more significant.

moderately to severely limited by the attenuation of the characteristic signal through the intervening material between the point of generation of the signal and the location of the detector. Such attenuation prevents the NDA techniques from detecting any significant signal from the inner fuel pins of a spent fuel assembly. This lack of information is unacceptable for safeguards, since inner pins could be removed (i.e., a partial defect) without the loss being detected. For this reason, it is presumed in this paper that such NDA techniques must be used in a complementary way with NDA techniques that are able to detect the inner pins and yet are dependent upon the BIC set.

6.2.5 The composition of the physical-properties and isotopic-content vector spaces

The discussion of Equations 57 and 58 has already indicated some of the various physical properties and groups of isotopes that can be included in the respective vector spaces. Nevertheless, it is necessary to list both the main properties and isotopes that can be included and those that cannot, and to provide justification for these listings. In the various extant and proposed NDA techniques, many physical properties are examined, and many different isotopes are considered. These facts do not contradict the tri-dimensionality of each space, because the many physical properties are not all independent of each other and because the isotopes must be grouped appropriately.

The first term, *S*, in Equations 57 and 58 corresponds to the quantity or production rate of primary neutrons in the spent fuel assembly. This quantity (or rate) will henceforth be designated by the symbol N_{PRI}. Primary neutrons are created chiefly by the spontaneous fission of ^{242}Cm, ^{244}Cm, and ^{240}Pu but also by (α,n) reactions and by photofission, to a much lesser extent [75]. Because the spontaneous fission of these three isotopes dominates the production of primary neutrons, these isotopes can be considered collectively as one of the variables in the isotopic-content vector space.

The second and third terms in Equation 57 correspond to neutron multiplication. There are many ways to represent neutron multiplication, but this paper will represent it by the leakage multiplication, M_L. It is to be understood that M_L can be translated into the other representations for both active and passive measurements, at least in theory [165-169, 413]. M_L is the number of neutrons that leak out of the fuel assembly per initial neutron [75]. For passive neutron measurements, M_L has a simple yet powerful relationship with both N_{PRI} and the measured neutron count rate outside the fuel assembly (Equation 14.1 of Reilly et al. [75], and Equation 17 of Henzl et al. [23]):

$$\text{Total Neutron Count Rate} = \varepsilon M_L N_{PRI} \qquad \text{Equation 59}$$

(This equation is the same as Equation 7 except that the ARR has been incorporated into M_L for simplicity of discussion.) Here, ε is the efficiency with which the neutron detector can detect neutrons that are *outside* the fuel assembly, in contrast to some other definitions. It must be emphasized that although the primary neutrons multiply differently than do neutrons introduced into the fuel assembly from an external source, the various representations of such multiplication are all connected and are not independent.

The second term in Equation 58 corresponds to the fissile isotopes. The safeguards community defines an effective ^{239}Pu content ($^{239}Pu_{eff}$) that is a weighted sum of all three

fissile isotopes—^{235}U, ^{239}Pu, and ^{241}Pu. (See Section 3.3.2.) The weighting of the isotopes depends on the particular NDA technique being considered, but this distinction will be ignored until Section 6.4.

The third term in Equation 58 corresponds to the neutron absorbers. Only those isotopes that change significantly with burning are relevant for NDA; neutron capture in ^{238}U in used LEU fuel assemblies is irrelevant for this reason, for instance. Therefore, the neutron absorbers can be divided into transuranic isotopes and fission products (which include those isotopes made by neutron capture in the direct fission products). All of the transuranic isotopes on the ^{242}Cm and ^{244}Cm nucleosynthesis pathways (Figure 5) can be considered as neutron absorbers, because all of them (including ^{239}Pu and ^{241}Pu) have thermal and epithermal neutron-capture cross sections that are larger than those of ^{238}U [125, 414]. The ^{241}Am is noteworthy because it has the largest capture cross section of all the long-lived isotopes on the nucleosynthesis pathways to ^{244}Cm and ^{242}Cm (Figure 5). As for the fission products, a mere 16 fission products (plus ^{155}Eu) are responsible for about 80% of the neutron capturing in fission products; see Section 3.3.3. In short, the neutron-absorbing isotopes are one group, consisting of two subgroups of transuranic and fission-product isotopes.

The third term in Equation 58 can sometimes also be identified explicitly with the physical property of neutron capture, such as through the NDA technique of prompt gamma-ray activation analysis (PGAA) [11]. Usually, though, the intense passive gamma-ray activity of the spent fuel assembly makes it impossible to distinguish such neutron-capture gamma-rays. Therefore, neutron capture is usually incorporated into the physical property of neutron multiplication, instead.

The fifth term in Equation 58—the "$\partial\phi/\partial t$" term—corresponds to a characteristic die-away time, τ, for a pulse of neutrons in the fuel assembly to dissipate, as was previously mentioned. The die-away time is not actually a separate and independent physical property, though. Instead, it represents the net effect of all the other physical properties on the neutron flux. Henzl et al. [22, 23] have shown that τ changes proportionally with changes in M_L for external-source neutrons; see Section 4.1.5.3. Therefore, it can be said that τ and M_L represent the same physical property.

Besides the four physical properties discussed so far, there is another way to represent the physics in Equation 58: namely, through the neutron fate probabilities [75, 415]. The last three terms on the left-hand side of Equation 58 correspond respectively to the only three ways that neutrons can be removed from the fuel assembly: by being absorbed and inducing fission, by being captured, and by permanently escaping out of the fuel ("leakage"). The three probabilities that correspond to these three fates (designated by p_f, p_c, and p_l, respectively) are thus fundamental neutronic properties of every fuel assembly. Since the fates are mutually exclusive, the fate probabilities sum to one ($p_f + p_c + p_l = 1$).

Nevertheless, only the fission and capture probabilities are relevant for characterizing an LEU or HEU fuel assembly, since the leakage probability corresponds to the diffusion term, which stays practically constant. Nauchi et al. [209] have demonstrated that the leakage probability for a given type of LEU fuel assembly (e.g., PWR vs. boiling-water-reactor (BWR)) in water does not change with BU. There are two ways to view this fact: (1) the constancy of the neutron diffusion (p_l = constant) and (2) the compensating changes in p_f and

p_c ($1 - p_l = p_f + p_c = \text{constant}$). The first viewpoint has already been justified; the second viewpoint is justified next.

Nauchi et al. [209] found that the decline in the macroscopic fission cross section of the ^{235}U in the fuel assembly because of burnup is compensated by increases in the macroscopic absorption cross sections of the fission products and the transuranic isotopes that are produced. Even the burnout of Gd burnable poison has a compensating mechanism, through changes in the neutron energy spectrum. The Gd hardens the spectrum in the fresh fuel, which decreases the effective microscopic absorption cross of the ^{235}U but also increases the production of plutonium isotopes through capture in ^{238}U. The result is that the decrease in the macroscopic cross section of the Gd during burning is compensated by increases in the ^{235}U effective microscopic cross section and in the transuranic isotopes' macroscopic cross sections. Furthermore, although they did not specifically study or mention it, their results also indicate that p_l should be practically constant with IE and CT, too. (See the arguments in the original paper [210].) Therefore, the leakage probability cannot be relevant to characterization, except in the gross sense of distinguishing one type of fuel assembly from another (e.g., PWR from BWR) [209].

As for gamma-rays (including X-rays), they are unlike neutrons and neither perpetuate themselves in a chain reaction nor multiply, in general. There are therefore only two fates for gamma-rays: capture (p_c) and leakage (p_l). The capture of gamma-rays is better known as attenuation, particularly in three-dimensional geometry in which scattering is not considered a fate (in contrast with one-dimensional, beam attenuation). Gamma-rays are attenuated by coulombic interactions with both the nuclei and the electrons of the surrounding material [74]. The material composition of a fuel assembly stays roughly constant during burning and cooling, though: heavy-metal oxide, structural metals, and water between the pins. Since the attenuation does not change with changes in the physical properties and isotopes, it cannot be relevant to the characterization of the fuel assembly, except to limit the ability to measure the gamma-rays. The only gamma-ray physical property that does change with burning, then, is the production of gamma-rays, either passively (such as through radioactive decay) or actively (such as through fluorescence or fission); and this activity is, of course, a direct function of the quantities of the gamma-ray emitting isotopes in the fuel assembly.

6.3 Results: The independence of the BIC variables with respect to the physical properties and the isotopic content

The previous section (Section 6.2) argued that the physical-properties and isotopic-content vector spaces exist, are three-dimensional, and are ruled by the neutronic physics. It also specified what physical properties and groups of isotopes are included in the respective vector spaces. This section now demonstrates the independence of the BIC variables with respect to the physical properties and the isotopes, by examining how the BIC variables affect them *at the time of the NDA measurements*.

Table 17 summarizes the arguments of the publication [210] and shows how the BIC set affects the relevant physical properties and isotopes. From this table, it is clear that the different properties vary in different ways with the BIC set: not just in magnitude but even in direction. If the logic is inverted (Figure 82), it is also clear that the three BIC variables must

be independent functions of the physical properties and of the isotopic content (see Figure 83 for an example). This deduction plus the earlier recognition of the tri-dimensionality of the vector spaces of the physical properties and isotopic content (Section 6.2) are the main results. They explain why the BIC set characterizes spent fuel assemblies as well as it does, as quantified by Burr et al. [135] (Section 6.1).

Table 17: The dependence of relevant physical properties and isotopes in used LEU and HEU fuel assemblies on the BIC variables. As BU, IE, or CT ***increases***, the table indicates whether each quantity increases (up) or decreases (down). Each table entry assumes that the other BIC variables are being held constant. The bold-faced, capitalized entries represent the variables that predominantly affect the quantity. Reprinted from [210] with permission from Elsevier.

Quantity	BU	IE	CT
Neutronic Properties			
N_{PRI}	**UP**	**DOWN**	down
M_L	**DOWN**	**UP**	down
τ	**DOWN**	**UP**	down
p_l	—	—	—
p_f	**DOWN**	**UP**	down
p_c	**UP**	**DOWN**	up
Gamma-ray Properties			
$C_{\gamma,\ total}$	**UP**	**—**	**DOWN**
$C_{\gamma,\ Cs\text{-}137}$	**UP**	**—**	**DOWN**
$C_{\gamma,\ Cs\text{-}133}$	**UP**	down	**DOWN**
$C_{\gamma,\ Eu\text{-}154}$	**UP**	down	**DOWN**
$\Sigma_{resonance}$	Corresponds to the individual isotopes.		
Specific Isotopes			
^{244}Cm & ^{240}Pu	**UP**	**DOWN**	down
^{235}U	**DOWN**	**UP**	**—**
^{239}Pu	**UP**	first down then up	**—**
^{241}Pu	**UP**	first down then up	down
^{155}Eu	**UP**	down	**DOWN**
16 Fission Products‡	**UP**	down	up

† Natural and depleted uranium fuels are excluded from this analysis.
‡ These are the set of the 16 most important fission products for neutron capture. See Sections 3.3.3 and 6.2.5.

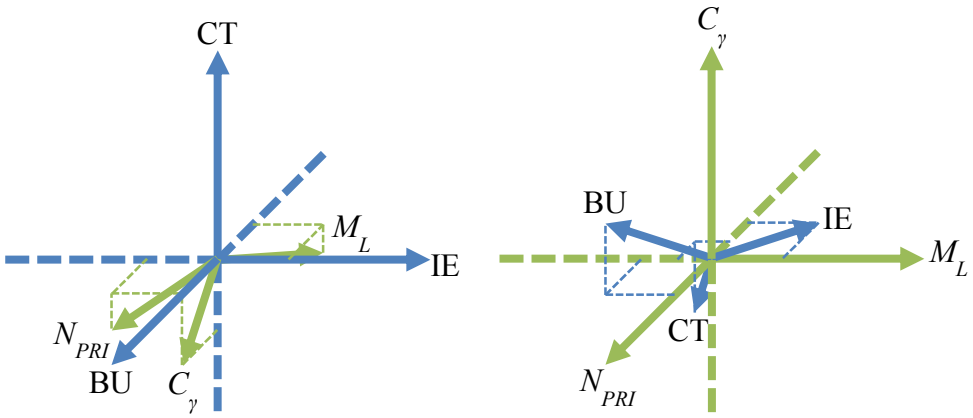

Figure 83: Illustration of how the BIC set can be a basis for an example vector of physical properties (N_{PRI}, M_L, C_γ) (left schematic) and vice versa (right schematic). The non-orthogonal vectors in each schematic are pointing in the corresponding directions of maximum increase with respect to the orthogonal vectors, in accordance with Table 17. Reprinted from [210] with permission from Elsevier.

The BIC set can fail to characterize a spent fuel assembly whenever additional variables become significant. The three main variables that can be expected to cause problems are (1) time in the reactor (i.e., irradiation history), (2) neutron energy in the reactor, and (3) geometry of the fuel assembly in the reactor, by itself, and within each fuel pin. The chemical form of the fuel and the environment of the measurement can also be complicating factors.

These failure modes can be partially mitigated, at least. The problem of irradiation history can be significantly reduced by waiting for three years after a fuel assembly has been discharged from the reactor before making an NDA measurement on it. Slight changes in the neutron energy spectrum during burning can be handled through IE and by measuring the axial burnup profile. Gross differences in the neutron energy spectrum—such as between LWRs and HWRs—can be handled by the appropriate application of the correct correlations with the BIC set for that type of fuel assembly. Similarly, separate correlations with the BIC set must be used for different types of fuel assemblies having different geometries. The position of the fuel assembly in the reactor during burning can be taken into account somewhat by measuring all sides of the fuel assembly. Different chemical forms of the fuel and different NDA measurement environments also require separate BIC-set correlations. Therefore, the BIC set is a sufficient basis for characterizing spent fuel assemblies in many cases and/or to first order. (For further arguments to this point, see the publication [210].)

6.4 Discussion: The main implication of the improved paradigm for NDA practice

The most important implication of the foregoing analysis is that three, independent NDA measurements, at minimum, are generally necessary to accurately determine a used LEU or HEU fuel assembly's isotopic content (for safeguards) and contribution to the reactivity of a collection of fuel assemblies (for burnup credit), if no other information, such as from the reactor operator, is used. Since all of the vector spaces in Figure 82 other than the measured-quantities vector space are three-dimensional (for LEU and HEU fuel), it is mathematically and physically impossible to obtain an accurate determination of any quantity from any of

those vector spaces unless the vector space of measured quantities is also three-dimensional. This rule is essentially the same rule from linear algebra, that the number of simultaneous equations must equal the number of unknowns in order to achieve a unique solution. With fewer equations, the solution is indeterminate. In the case of NDA, the forms of the simultaneous equations may be unknown and may need to be found empirically through Monte Carlo simulations, but the fundamental fact that there must be at least three of them has been proven by the foregoing analysis.

The combination of a sufficient number of independent NDA measurements enables the resolution of the multivariate problem exhibited by most of the NDA techniques. Based on the quantitative analysis by Burr et al. [135] that was discussed in Section 6.1, the expected improvement in the accuracy of the determination of the fissile content (for safeguards) or the residual reactivity (for burnup-credit) is from the 15% RESD of a single NDA measurement to the 3% or less RESD of the knowledge of the full BIC set. (See Burr's Tables I and II.) This expected improvement is based on the more conservative numbers in Burr's paper, so the actual improvement may be even greater. Thus, the common question among NDA practitioners about a given NDA technique—"What is its accuracy?"—has been shown to be a poorly posed question for NDA of spent fuel assemblies. The proper question is, "What is the accuracy of this particular combination of three NDA techniques?" Furthermore and of equal or greater importance than the improved accuracy, the determination of the fissile content or residual reactivity by a combination of three independent NDA measurements can be completely independent of any information provided by the reactor operator—i.e., totally derived from measurements. Such an ability is of essential value to the safeguards community.

There is at least one example in the literature of researchers inadvertently following this principle of combining three independent NDA measurements of a spent fuel assembly, and they achieved good results that are commensurate with the numbers of Burr et al. and the predictions of the foregoing analysis. In their recently published paper, Henzl et al. [23] have proposed combining two neutron NDA measurements: a passive, total measurement and an active, differential-die-away measurement. The neutron detectors of the differential-die-away instrument also serve to make the passive measurement. The passive measurement provides one equation for the two variables, N_{PRI} and M_L (Equation 59), and the active measurement determines a die-away time, τ, that corresponds to M_L. (See Table 17.) A third NDA measurement was not proposed, but Henzl et al. assumed that CT is known *a priori*, and they included it explicitly in their analysis through Figure 5 and Equation 20 of their paper. Their simulations indicate that with these three independent pieces of information, the total Pu content of a spent fuel assembly can be determined to an accuracy of 2% or better, which corresponds to the numbers of Burr et al. The above, logical arguments have shown that such a good result is not primarily a property of the differential-die-away NDA technique itself but rather a consequence of the combination of three independent NDA quantities.

The independence that is required of the measurements is an independence in terms of the physical properties of the fuel assembly at the time of the NDA measurement (Figure 82). The analysis of Section 6.3 proved that the BIC variables are independent in terms of these physical properties, in terms of the isotopic content, and in terms of the physical properties of the fuel assembly in a collection of fuel assemblies. Therefore, it is necessary and sufficient to

show that the NDA measurements are measuring either three different physical properties (the measurements are orthogonal) or three different combinations of three different physical properties (they are not orthogonal, but they are independent). Table 17 can be used as a guide for this purpose, since it lists the major physical properties of the fuel assembly, as derived from a consideration of Equation 58.

It must be mentioned explicitly that the point is that *a minimum* of three independent NDA measurements are necessary. If one or more other variables cause the BIC set to fail to adequately characterize a fuel assembly, then additional measurements must be made. The analyses of Section 6.3 can thus be viewed in this way: Table 17 establishes that three measurements are a necessary condition for an accurate characterization, while the paragraphs following the table indicate that three measurements are a sufficient condition in many cases but not always.

The fact of this implication has not been fully realized until now. Although the integration of NDA techniques has been suggested before [5, 73], the basis of the integration has not been these fundamental physical principles. Rather, it has been an attempt to distinguish the three fissile isotopes (by three independent equations; Section 3.3.2) and a recognition that since BU, IE, and CT all affect the assay result, it is desirable to choose NDA techniques that can determine these variables. Therefore, the realization here of the requirement for a minimum of three independent measurements and of the fundamental reasons for this requirement constitutes a significant advancement in the paradigm of NDA of spent fuel assemblies.

The aforementioned attempt to distinguish the three fissile isotopes by integrating NDA techniques [5, 73] can also be examined critically in light of this first implication. (See item number 4 in Section 2.4, above, and Section 3.3.2.) According to the theoretical treatment developed in Section 6.2, the three fissile isotopes act together as a single group with regard to the physical properties (Equations 57 and 58). Yet, the three isotopes vary differently with respect to the BIC variables (Table 17). These two facts mean that an analytical separation of the fissile isotopes by multiple NDA techniques does not proceed directly on the basis of the isotopes' unique contributions to the physical properties of the spent fuel assembly at the time of the NDA measurement, but rather it proceeds indirectly on the basis of the unique way that these isotopes are created and destroyed through enrichment, burning, and cooling (the BIC set). This fact has heretofore been hidden in the correlations. Therefore, the primary basis for integrating NDA techniques needs to be their independence with regard to the overall physical properties and the BIC variables (Figure 82), not their independence with regard to the fissile isotopes. In other words, if the recommendation of this first implication is followed, so that the NDA techniques are combined on the basis of their independence with respect to the overall physical properties and to the BIC set, then a significant separation of the fissile isotopes should proceed naturally from the correlation from the BIC set to the isotopic content—not because the isotopic-content vector space contains more than three dimensions but because the BIC set characterizes the spent fuel assembly to first order. Further refinement of the separation can then be made by adding one or more isotope-specific NDA techniques (Section 6.2.4) to the combination, as anticipated by Tables 2 and 3 in the review by Charlton and Humphrey [5].

Although the discussion of the NDA of spent MOX fuel assemblies has been omitted from this summary of the original publication [210], one important concept from that discussion does need to be repeated here. This concept comes from the fact that the three-dimensional BIC set may not completely represent all of the processes that can change the physics and isotopic composition of the fuel assembly. In the case of MOX fuel, one such process is the loading of non-fissile plutonium isotopes into the fresh fuel. Such isotopes increase the amount of ^{244}Cm and primary neutrons in the spent fuel, but none of the three BIC variables represents such initial loading of these isotopes. Therefore, a fourth variable must be added to the BIC set for MOX fuel, making the set to be four dimensional (abbreviated as the "BICC" set). Nevertheless, the physics of spent fuel assemblies at the time of the NDA measurements remains three-dimensional even for MOX fuel assemblies, because the same neutron diffusion or transport equation applies to all fuel assemblies regardless of their composition. The correlations from a four-dimensional BICC set to the three-dimensional physical-properties and isotopic-content vector spaces thus become surjective but not injective. In order to use such a four-dimensional BICC set in the NDA logic (Figure 82), it becomes necessary to have four measurements to obtain an injective correlation to the BIC set, yet because the physical-properties vector space remains three-dimensional, the fourth measurement *must not depend on the physical properties of the fuel assembly*! A fourth measurement of the physical properties of the fuel assembly would not provide information that would be substantially independent from the information already provided by the other three NDA measurements. Instead, the fourth measurement must exploit the characteristic energy resonances of specific isotopes in the fuel assembly to provide some direct quantification of them (Section 6.2.4). Such information would be independent of the physical properties of the fuel assembly.

With regard to the NDA of enriched-uranium assemblies specifically, this concept means that adding more NDA techniques beyond the first three will not lead to dramatic gains in NDA accuracy. The fourth and subsequent NDA techniques will merely be over-constraining the three-dimensional mathematical problem, so that in general, they can improve the assay result only by increasing the accuracy of the values of the three physical properties that have already been determined by the first three techniques. Of course, to whatever extent the BIC set is not precisely three dimensional, the fourth and subsequent NDA techniques can also improve the accuracy of the correlations themselves if the techniques have some sensitivity to characteristic energies of isotopes, as exemplified by the case of MOX fuel described above.

A final deduction that pertains to other large objects besides spent fuel assemblies can be made from the arguments in Sections 6.2.4 and 6.3 [416]. What is specifically in view here is large objects that contain large amounts of fissile and moderating material, just as spent fuel assemblies do. From these two sections, it can be observed that almost all NDA techniques either (1) require a three-dimensional correlation through the BIC set in accordance with Figure 82 or (2) are prevented, by attenuation, from assaying the inner portions of the assembly or object. In the case of spent fuel assemblies, the fact that the geometry of the assembly is known and constant with the BIC set means that a three-dimensional correlation through the BIC set is possible. Thus, the accurate NDA of spent fuel assemblies is theoretically possible. In the case of other large objects with unknown and variable geometry, though, such a 3-D correlation is theoretically impossible, since the diffusion term in the

neutron-diffusion equation (Equations 3, 57, and 58) is no longer constant or known. Furthermore, since attenuation prevents a direct assay without a correlation, the accurate assay of such large objects is fundamentally impossible—with *almost* all NDA techniques.

The only NDA techniques that are able to assay large objects with unknown, variable geometry are those that do not require a 3-D correlation and that can accurately account for the attenuation of the signal. Such techniques are those that analyze characteristic resonance signals that are imparted to a one-dimensional beam of radiation as it is transmitted through the object. The characteristic resonances make such techniques independent of the 3-D correlation, and calibration measurements without the object in the beam allow the attenuation of the signal by the object to be determined accurately as long as at least some of the signal is able to pass all the way through the object. The neutron NDA technique that meets these requirements is NRTA, and the corresponding gamma-ray NDA technique is NRF. Thus, only these two NDA techniques have the capability to assay accurately large objects with unknown, variable geometry. This conclusion is illustrated by Table 18, which uses the above rationale to evaluate the sixteen NDA techniques (Table 1). Since NRTA is limited to assaying fuel assemblies that are dry and that have at most 12 pins in the beam [30], NRF, which has neither limitation, is the superior NDA technique.

Table 18: Evaluation of sixteen NDA techniques regarding their ability to assay large objects with unknown and variable geometry (N = no; Y = yes) [416]

The 14 NGSI NDA Techniques	Does it directly measure a characteristic signal?	Does it account for attenuation?	Therefore, can it assay large items with unknown geometry?
Total Neutron (TN)	N	–	N
Passive Neutron Albedo Reactivity analysis (PNAR)	N	–	N
^{252}Cf Interrogation with Prompt Neutron detection (CIPN)	N	–	N
Differential Die-Away analysis (DDA)	N	–	N
Assembly Interrogation with Prompt Neutron detection (AIPN)	N	–	N
Delayed Neutron counting (DN)	N	–	N
Neutron Multiplicity (NM)	N	–	N
Differential Die-away Self-Interrogation (DDSI)	N	–	N
Total Gamma-ray counting (TG)	N	–	N
Passive Gamma-ray spectroscopy (PG)	Y	N	N
Delayed Gamma-ray (DG)	N	N	N
Self-Interrogation Neutron Resonance Densitometry (SINRD)	Maybe	N	N
X-Ray Fluorescence (XRF)	Y	N	N
Lead Slowing-Down Spectroscopy (LSDS)	Y	N (self-shielding)	N
Neutron Resonance Transmission Analysis (NRTA)	Y	Y	**Y**
Nuclear Resonance Fluorescence (NRF)	Y	Y	**Y**

6.5 Conclusion of this section

This section has summarized the most important concepts and results of the original publication [210]. It has explained the physical reasons for why the BIC set characterizes spent fuel assemblies to first order. It thereby has also explained why the lack of knowledge of one or more of the BIC variables produces significant uncertainty in the NDA result—that is, the uncertainty that was examined by Burr et al. [135]. These reasons are rooted in the fundamentally multidimensional nature of the NDA measurements and of the isotopic content, physical properties, and burning, enrichment, and cooling history of a spent fuel assembly. Section 6.2 of this report has laid out the relationships among these four vector spaces and has shown, by reference to basic nuclear engineering, that the isotopic-content and physical-property vector spaces are basically tri-dimensional. The burning, enrichment, and cooling history for LEU and HEU fuel is also tri-dimensional, at minimum, and can be represented by the BIC set.

By examining the physics and effects of the burning, enrichment, and cooling of nuclear fuel (Section 6.3), it has been proven that the three BIC variables are independent with respect to the physical properties and the isotopic content of a spent fuel assembly. This fact has established that the determination of the full BIC set is a necessary condition for accurate NDA results. Therefore, a minimum of three independent NDA measurements is generally necessary to properly characterize used LEU and HEU fuel assemblies and thereby achieve accurate results that are independent of information provided by the reactor operator. Correspondingly, the addition of more NDA measurements beyond the first three is not expected to produce similarly dramatic gains in accuracy.

A final conclusion recognizes that a correlation through the BIC set works only if the geometry of the sample stays constant, as it does for spent fuel assemblies. For large objects with unknown and variable geometry, only transmission NDA techniques seem to be capable of achieving accurate assays, since (1) they rely on measuring characteristic resonance energies and not on a correlation through the BIC set and (2) they account for attenuation of the radiation signals.

7. Evaluation of the NGSI's approaches in the Spent Fuel NDA Project and of their proposed NDA combinations

This section applies the knowledge of the sixteen NDA techniques (fourteen advanced techniques plus two simple techniques) and the new NDA paradigm that was presented in the previous section, to evaluate the NGSI's approaches in the Spent Fuel NDA Project and their proposed NDA combinations. This evaluation emphasizes the ability to provide consistent and reasonably accurate assays, rather than being concerned with such pragmatic issues as portability and equipment cost, which have been primary concerns in previous evaluations [5, 6, 73]. This different choice of emphasis is appropriate, because whereas previous NDA practice, including that by the NGSI, contained an element of trial and error, the new paradigm provides rational grounds for the confident expectation of superior assay results by combining NDA techniques according to a well-defined and physically based methodology. The rather mediocre NDA results that have been heretofore obtainable worldwide have not warranted significant investment of cost and effort in NDA of spent fuel assemblies [142], which understandably has forced NDA practitioners, including the NGSI, to prioritize reducing the cost and effort. With the promise of NDA results of truly useful accuracy because of the new paradigm, the achievement of such results necessarily rises once again to the foreground of the discussion, since they likely will justify greater investment for both traditional and new safeguards applications.

The heart of the new paradigm is that the NDA of spent fuel assemblies is fundamentally a three-dimensional problem, with the three dimensions being (1) the generation of primary neutrons, (2) the generation of secondary neutrons, and (3) the capture of neutrons. These dimensions come from the neutron diffusion or transport equation. The NGSI's proposed combinations of NDA techniques can thus be judged according to whether or not they produce three independent, measured quantities that satisfy this three-dimensional problem; see Figure 82. Additional NDA techniques beyond the first three can be expected to improve accuracy significantly only if they exhibit dependency on the characteristic resonance energies of specific, important isotopes.

Equally importantly, the evaluation criteria of the new paradigm supersede previous criteria, in particular the use of three NDA measurements to solve for the quantities of the three fissile isotopes by means of the three techniques' unique equations for effective ^{239}Pu (Section 3.3.2). As discussed in Section 6.4, the NGSI's apparent successes in combining NDA techniques according to this criterion (such as the integration of DN with DDA) are actually a consequence of the techniques' independent representations of the unique way that BU, IE, and CT alter the three-dimensional physical and isotopic characteristics of the fuel assembly. Since the NGSI, following common NDA practice, almost never calculated absolute values for the physical properties of the fuel assemblies nor evaluated their NDA techniques on fuel-assembly models other than those created by burnup simulations, there was practically no way for them to uncover the truth that both the NDA measurement results and the quantities of the fissile isotopes are consequences of the BIC set, rather than the NDA measurement results being a consequence primarily of the quantities of the individual fissile

isotopes, as they had assumed.[7] To have uncovered this truth, they would have had to have created another library of fuel-assembly models with the quantities of the fissile isotopes having been changed arbitrarily while having kept the other two dimensions—primary neutron generation and neutron capture—constant, and then they would have had to have tested several NDA instruments on this alternate library of fuel-assembly models. Such an ambitious effort would have been hard to justify within the scope of the Spent Fuel NDA Project without having known beforehand what the outcome would be.

With the criteria of the new paradigm firmly in mind, the NGSI's proposed combinations of NDA techniques can be rigorously evaluated. Table 19 lists the independent physical properties that govern each of the NDA techniques in the proposed combinations, and it also indicates the isotopes to which the techniques are sensitive because they measure their characteristic energy resonances. The table shows that all of the combinations contain more than enough independent measurements to satisfy the three-dimensional criterion. Also, note that since the TN technique is inherently part of one of the other NDA techniques in each combination, it will not be discussed separately.

As explained in Section 4.1.3.3 (the analysis of CIPN data), the combination with CIPN (No. 2) produces better data than the combination with PNAR (No. 1). The knowledge of the strength of the interrogating neutron source in CIPN allows the NDA practitioner to separate the generation rate of primary neutrons (N_{PRI}) from the multiplication of those neutrons by induced fission (M_L). Such separation is impossible in the PNAR technique because the strength of the interrogating neutron source in that technique, namely, the number of reflected neutrons, is itself a function of the unknown product of N_{PRI} and M_L. The benefit of having a clear separation between these two quantities is that they are each associated with a particular term of the neutron-diffusion equation (Equation 3) and with the corresponding group of isotopes. N_{PRI} is associated with the first term of the equation and with the primary-neutron-generating isotopes (especially ^{244}Cm), and M_L is associated with the second and third terms and with the secondary-neutron-generating isotopes (especially the fissile isotopes) and neutron absorbers, respectively. These associations make the interpretation of the three-dimensional correlation from the physical properties through the BIC set to the isotopic content much easier to follow (Figure 82). Furthermore, some other NDA techniques, such as DDA and DDSI, can produce values for the neutron leakage multiplication by itself (M_L, via τ). These values can be compared directly with the value measured by the CIPN combination but not with the product of N_{PRI} and M_L produced by the PNAR combination. The price to pay for the better data from CIPN is the expense and hassle of the ^{252}Cf source, of course.

The combination with SINRD (No. 3) is similar to the combinations with PNAR (No. 1) and with DDSI (No. 5) in several respects. All three of these techniques are passive, and all three are sensitive primarily to the induced fission events that occur in the outer rows of fuel pins. SINRD analyzes the 0.3 eV resonance chasm that is created to induce those outer fission events and analyzes the fast neutrons from those events, too; PNAR analyzes the neutron multiplication that those fission events produce ($M_{L,refl}\bar{\nu}p_{f,emit}$); and DDSI analyzes the time

[7] Of course, the three fissile isotopes do have slightly different effects on the NDA measurements; this fact is not in question here. The point is that they affect the NDA results much less than the BIC variables affect the results, and furthermore, the quantities of the three fissile isotopes in spent fuel are themselves governed by the BIC set.

coincidence of both those fission events and their multiplied neutrons. Unlike the signals from PNAR and DDSI, though, SINRD's signal is very susceptible to even a small amount of intervening moderating material, since it is an energy-based signal. Therefore, even though each of these three techniques can satisfy the three-dimensional NDA criterion when in combination with TG (and including TN, of course), the SINRD combination (No. 3) might be expected to have the worst accuracy of the three. This speculation still remains to be verified through field trials, of course, since there are many other factors involved.

The fourth combination is basically a collection of all the NDA signals that one can obtain from using a pulsed neutron generator of moderate strength and small size. The new paradigm's criteria provide the means to see how all of the signals relate to each other and to the overall assay. The main NDA technique of the combination is DDA, certainly in part because of the promising results of Henzl et al. [22, 23]. As explained above in Section 6.4, the good results are largely a consequence of a proper integration of DDA, TN, and an *a priori* knowledge of the cooling time, which could also come from including a TG measurement. Nevertheless, the DDA technique itself does give a good value for the neutron leakage multiplication through its measurement of the die-away time, and M_L can be considered as one of the fundamental physical properties of spent fuel assemblies (Table 17), even though it is the net result of both induced fission and neutron capture.

The new paradigm can then be used to show how the remaining two dimensions are satisfied by the other techniques. The TN measurement, which is made with the DDA neutron detectors while the neutron generator is turned off, provides a dependency on the number of primary neutrons, N_{PRI}, though it is still mixed with M_L. A TG measurement could provide the third dimension, and in this case, the DDA+TN+TG combination would be very similar to the CIPN+TN+TG combination, with DDA and CIPN providing the measure of M_L. The NGSI have not chosen this route, however, because they want to use this fourth combination to obtain the maximum possible amount of detailed information about the spent fuel assembly [5], and TN and TG are the opposite of detailed techniques. The third dimension is therefore provided primarily by the DN measurement. As explained in Section 4.1.6.1, the combination of DDA and DN is useful because DN significantly isolates the induced-fission term from the neutron-capture term in the neutron diffusion equation, whereas DDA's measurement of M_L includes the neutron-capture term. The trio of DDA, DN, and TN thus covers the three-dimensional NDA criterion by their dependencies on M_L, induced fission, and N_{PRI}, respectively, so the remaining NDA techniques in the combination—DG and PG—merely refine the accuracy.

For the purpose of refining the assay accuracy, DG and PG should be very good choices, since both of them analyze characteristic resonance energies of specific isotopes (Section 6.4). The PG technique is, of course, simply the making of a gamma-ray measurement with the DG detectors without any neutron interrogation. Regarding the DG measurement, if the DN measurement would not be included in the combination, an absolute DG measurement could provide a similar isolation of the induced fission term to satisfy the three-dimensional criterion; but since DN is included, a relative DG measurement should suffice (Section 5.1.1.3). In the total combination, then, the set of neutron techniques, DDA+DN+TN, serves as the base to satisfy the three-dimensional criterion, and the set of gamma-ray techniques,

DG+PG, serves to refine those results. The accuracy of this fourth combination of NDA techniques should therefore be very good.

The combination with DDSI (No. 5) is particularly interesting because of the theoretical possibility that DDSI by itself may be able to determine three independent quantities to satisfy the three-dimensional criterion, as discussed in Section 4.2.2.3 and as Table 19 indicates. It is not yet clear, though, if DDSI can determine the three quantities with sufficient accuracy for this purpose, not only because of difficulty in obtaining good statistics in the coincidence counts but also because the three quantities are only somewhat independent. For this reason, the combination of TG with DDSI is a good idea, because it ensures that enough independent information is obtained to satisfy the three-dimensional criterion. Together, the two NDA techniques can be expected to over-constrain the three-dimensional problem, leading to a more accurate assay.

Table 19: Evaluation of the NGSI combinations of NDA techniques according to the new paradigm (refer to Tables 2 and 17)

NGSI Combos (Table 2)	NDA Technique and Measurement		Physical Quantities Measured	Functional Relationships of the Measured Physical Quantities (f and g indicate functions)	Independent Physical Properties that Govern	Isotopes to which the Technique is Sensitive because of Resonances
1	PNAR No-Reflection		$M_L N_{PRI}$	—	N_{PRI}, M_L	None
	PNAR With-Reflection = TN		$ARR \cdot M_L N_{PRI}$	$ARR = f(M_{L,refl}\, \bar{\nu}p_{f,emit})$; $M_{L,refl} = f(M_L)$; $\bar{\nu}p_{f,emit} = f(M_L N_{PRI})$	N_{PRI}, M_L	None
	TG		C_γ	—	C_γ	None
2	CIPN Passive = TN		$ARR \cdot M_L N_{PRI}$	ARR: See above	N_{PRI}, M_L	None
	CIPN Active		$ARR \cdot (M_L N_{PRI} + M_{L,ext} N_{EXT})$	ARR: See above; $M_{L,ext} = f(M_L)$	N_{PRI}, M_L	None
	TG		C_γ	—	C_γ	None
3	SINRD Bare = TN		$ARR \cdot M_L N_{PRI}$	ARR: See above	N_{PRI}, M_L	None
	SINRD (Resonance and Fast Measurements)		Induced fissions, especially at the 0.3 eV resonance	$M_L = f\begin{pmatrix}\text{Induced fissions,}\\ \text{Neutron capture}\end{pmatrix}$	Induced fissions (part of M_L)	The three fissile isotopes as a group
	TG		C_γ	—	C_γ	None
4	DDA Passive = TN		$ARR \cdot M_L N_{PRI}$	ARR: See above	N_{PRI}, M_L	None
	DDA Active		τ	$\tau = f(M_{L,ext}) = f(g(M_L))$	M_L	None
	DN		$ARR \cdot (M_L N_{PRI} + M_{L,DN} N_{DN} \left[\int_{irr} \Sigma_f \phi_{irr} dt'\right])$	ARR: See above; $M_{L,DN} = f(M_L)$; $\int_{irr} \Sigma_f \phi_{irr} dt' = f(\text{Ind. fiss.})$	N_{PRI}, M_L, Induced fissions (part of M_L)	None
	DG		Delayed-γ activity	Del.-γ activity $\propto \int_{irr} \Sigma_f \phi_{irr} dt'$; $\int_{irr} \Sigma_f \phi_{irr} dt' = f(\text{Ind. fiss.})$	Induced fissions (part of M_L)	Short-lived fission products
	PG		C_γ ; $C_{\gamma,\,Cs\text{-}134}$; $C_{\gamma,\,Cs\text{-}137}$; $C_{\gamma,\,Eu\text{-}154}$	—	C_γ	^{134}Cs, ^{137}Cs, ^{154}Eu
5	DDSI	Singles = TN	$ARR \cdot M_L N_{PRI}$	ARR: See above	N_{PRI}, M_L	None
		Slow Doubles	τ_{slow}	$\tau_{slow} = f(\text{Induced Fissions})$	Induced fissions	None
		Fast Doubles	τ_{fast}	$\tau_{fast} = f\begin{pmatrix}\text{Spontaneous +}\\ \text{Induced fissions}\end{pmatrix}$; $N_{PRI} = f(\text{Spontaneous fissions})$	N_{PRI}, Induced fissions	None
	TG		C_γ	—	C_γ	None

8. Conclusion

This report has surveyed the fourteen advanced techniques of the NGSI's Spent Fuel Nondestructive Assay Project, plus two current NDA techniques. It has described how each technique operates; the designs of instruments that employ the technique, whether the NGSI's design or otherwise; the way in which the data provide information about the fissile or plutonium content; and the limitations of the technique. This report has also critiqued the current practice of NDA of spent fuel assemblies, including the NGSI's approach, and has created a new paradigm for this practice. This paradigm is built on the neutron diffusion equation, by which it highlights the salient features of each NDA technique and shows how to combine them effectively. The paradigm enhances and extends the good work already conducted by the NGSI.

The critique has shown that NDA techniques cannot be considered in isolation—that instead, three independent NDA measurements must be made to achieve a bijective correlation to the fissile and plutonium content. Therefore, the question should not be, "What is the accuracy of this NDA technique?" but rather should be, "What is the accuracy of this combination of three NDA techniques?" The resolution of this uncertainty that is caused by an indeterminacy of solution promises to reduce the total uncertainty of NDA of spent fuel assemblies by a significant amount, potentially even below the threshold of 5% uncertainty that burnup simulations have. Thus, by combining these advanced NDA techniques in appropriate sets of three, the NDA of spent fuel assemblies for safeguards verification and material accountancy should be even more successful than has been hitherto anticipated. The NDA combination instruments that the NGSI has proposed all contain enough independent measurements to satisfy this three-dimensional criterion, so it is hoped that good results will be obtained from their field trials.

Acknowledgements

The authors thank the following people for various technical discussions and assistance:

From JAEA: Ryoichi Hajima, Takehito Hayakawa, Toshiyuki Shizuma, Christopher Angell, Masatoshi Kureta, Hideo Harada, Tsuchiya Harufumi, Mitsuo Koizumi, Taketeru Nagatani, Akihiro Kitamura

From CRIEPI: Yasushi Nauchi

From the Tokyo Institute of Technology: Hiroshi Sagara

From LANL: Steve Tobin, Howard Menlove, Adrienne LaFleur, Vlad Henzl, Daniela Henzlova, Andrea Favalli, Holly Trellue, Martyn Swinhoe

From LBL and LLNL: Bernhard Ludewigt, Brian Quiter, Vladimir Mozin

From ORNL: Jianwei Hu, Stephen Croft

From PNNL: Glen Warren, Jonathan Kulisek, Douglas Rodriguez, Cynthia Heinberg

From INL: David Chichester

From Texas A&M University: Julia Eigenbrodt, William Charlton, Braden Goddard

From the University of Michigan: Alexis Kaplan

From Chalmers University: Imre Pázsit, Dina Chernikova

From JRC-IRMM: Peter Schillebeeckx

From NRCN: Chen Dubi

References

[1] IAEA, "IAEA Safeguards Glossary, 2001 Edition", IAEA/NVS/3/CD, International Atomic Energy Agency, (2002).

[2] Bevard, B. B. et al., “Review of information for spent nuclear fuel burnup confirmation”, NUREG/CR-6998, U.S. Nuclear Regulatory Commission, (2009).

[3] Veal, Kevin D. et al., "NGSI Program to Investigate Techniques for the Direct Measurement of Plutonium in Spent LWR Fuels by Non-destructive Assay", 51st Annual Meeting of the Institute of Nuclear Materials Management, (2010).

[4] Tobin, Stephen J. et al., "Update on the Next Generation Safeguard Initiative Project to Determine Pu Mass in Spent Fuel Assemblies", 53rd Annual Meeting of the Institute of Nuclear Materials Management, (2012).

[5] Charlton, William S. and Humphrey, Marc A., "External Review of the Next Generation Safeguards Initiative’s Spent Fuel Nondestructive Assay Project", JNMM, 40 (2012), pp.12-17.

[6] Humphrey, Marc A. et al., "The Next Generation Safeguards Initiative's spent fuel nondestructive assay project", JNMM, 40 (2012), pp.6-11.

[7] IAEA, "Safeguards Techniques and Equipment: 2011 Edition", IAEA/NVS/1/2011 (Rev. 2), International Atomic Energy Agency, (2011).

[8] Croft, S. et al., "A Technical Review of Non-Destructive Assay Research for the Characterization of Spent Nuclear Fuel Assemblies Being Conducted Under the US DOE NGSI", #11544, WM2011, WM Symposia (2011).

[9] Rinard, Phillip M. and Bosler, G. E., "Safeguarding LWR spent fuel with the Fork detector", LA-11096-MS, Los Alamos National Laboratory, (1988).

[10] Borella, A., "The Fork detector for spent fuel measurements: measurements and simulations", 53rd Annual Meeting of the Institute of Nuclear Materials Management, (2012).

[11] Falley, M. P. et al., "Neutron-capture prompt γ-ray activation analysis for multielement determination in complex shapes", Anal. Chem., 51 (1979), pp.2209-2221.

[12] Postma, H. and Schillebeeckx, P., "Neutron Resonance Capture and Transmission Analysis", Encyclopedia of Analytical Chemistry, John Wiley & Sons, (2000).

[13] Postma, H. and Schillebeeckx, P., "Non-destructive analysis of objects using neutron resonance capture", J. Radioanal. Nucl. Chem. 265 (2005), pp.297-302.

[14] Havrilla, George J. et al., "Ultra High Energy X-ray Fluorescence Application to Characterization of Nuclear Fuel", 53rd Annual Meeting of the Institute of Nuclear Materials Management, (2012).

[15] Tobin, Stephen J. et al., "Prototype Development and Field Trials under the Next Generation Safeguards Initiative Spent Fuel Non-Destructive Assay Project", 35th Annual Meeting of the European Safeguards Research and Development Association, (2013).

[16] Conlin, Jeremy L. and Tobin, Stephen J., "Determining Fissile Content in PWR Spent Fuel Assemblies Using a Passive Neutron Albedo Reactivity with Fission Chambers Technique", 51st Annual Meeting of the Institute of Nuclear Materials Management, (2010).

[17] Conlin, Jeremy L. and Tobin, Stephen J., "Predicting Fissile Content of Spent Nuclear Fuel Assemblies with the Passive Neutron Albedo Reactivity Technique and Monte Carlo Code Emulation", International Conference on Mathematics and Computational Methods Applied to Nuclear Science and Engineering (M&C 2011), American Nuclear Society, (2011).

[18] Gerhart, Jeremy J. et al., "Passive Neutron Albedo Reactivity with Fission Chambers", JNMM, 40 (2012), pp.45-48.

[19] Hu, J. et al., "Developing the Californium Interrogation Prompt Neutron Technique to Measure Fissile Content and to Detect Diversion in Spent Nuclear Fuel Assemblies," JNMM, 40 (2012), pp.49-57.

[20] Richard, Joshua G. et al., "Determining the Pu mass in low enriched uranium spent-fuel assemblies using assembly interrogation prompt neutron (AIPN) detection", LA-UR-10-05383, Los Alamos National Laboratory, (2010).

[21] Blanc, P. et al., "An Integrated Delayed-neutron Differential-Die-away Instrument to Quantify Plutonium in Spent Nuclear Fuel", JNMM, 40 (2012), pp.70-77.

[22] Henzl, V. et al., "Measurement of the Multiplication of a Spent Fuel Assembly with the Differential Die-away Method Within the Scope of the Next Generation Safeguards Initiative Spent Fuel Project", JNMM, 40 (2012), pp.61-69.

[23] Henzl, V. et al., "Determination of the plutonium content in a spent fuel assembly by passive and active interrogation using a differential die-away instrument", Nucl. Instrum. Methods Phys. Res., Sect. A, 712 (2013), pp.83-92.

[24] Koehler, William E. et al., "Viability of Using a Californium Interrogation of Prompt Neutrons (CIPN) Instrument as a Delayed Neutron Detector", 52nd Annual Meeting of the Institute of Nuclear Materials Management, (2011).

[25] Croft, S. et al., "Feasibility of Classic Multiplicity Analysis Applied to Spent Nuclear Fuel Assemblies", 52nd Annual Meeting of the Institute of Nuclear Materials Management, (2011).

[26] Menlove, Howard O. et al., "Fissile and fertile nuclear material measurements using a new differential die-away self-interrogation technique", Nucl. Instrum. Methods Phys. Res., Sect. A, 602 (2009), pp.588-593.

[27] Schear, Melissa A. et al., "Spent Fuel Characterization Using the Differential Die-Away Self-Interrogation Technique", 52nd Annual Meeting of the Institute of Nuclear Materials Management, (2011).

[28] Belian, A. et al., "New Design of the Differential Die-away Self-interrogation Instrument for Spent Fuel Assay", JNMM, 40 (2012), pp.58-60.

[29] Sterbentz, James W. and Chichester, David L., "Neutron resonance transmission analysis (NRTA): A nondestructive assay technique for the Next Generation Safeguards Initiative's plutonium assay challenge", INL/EXT-10-20620, Idaho National Laboratory, (2010).

[30] Sterbentz, James W. and Chichester, David L., "Further Evaluation of the Neutron Resonance Transmission Analysis (NRTA) Technique for Assaying Plutonium in Spent Fuel", INL/EXT-11-23391, Idaho National Laboratory, (2011).

[31] Chichester, David L. and Sterbentz, James W., "Assessing the feasibility of using neutron resonance transmission analysis (NRTA) for assaying plutonium in spent fuel assemblies", 53rd Annual Meeting of the Institute of Nuclear Materials Management, (2012).

[32] Gavron, Avigdor et al., "Analysis of spent fuel assemblies using a lead slowing down spectrometer", Nucl. Instrum. Methods Phys. Res., Sect. A, 602 (2009), pp.581-587.

[33] Kulisek, Jonathan A. et al., "Lead slowing-down spectrometry time spectral analysis for spent fuel assay: FY11 status report", PNNL-20769, Pacific Northwest National Laboratory, (2011).

[34] Lee, Yong-Deok et al., "Design of Lead Slowing Down Spectrometer for Spent Fuel Fissile Assay", 52nd Annual Meeting of the Institute of Nuclear Materials Management, (2011).

[35] Warren, Glen A. et al., "Lead slowing-down spectrometry for spent fuel assay: FY11 status report", PNNL-20689, Pacific Northwest National Laboratory, (2011).

[36] Kulisek, Jonathan A. et al., "Status on Establishing the Feasibility of Lead Slowing Down Spectroscopy for Direct Measurement of Plutonium in Used Fuel", 53rd Annual Meeting of the Institute of Nuclear Materials Management, (2012).

[37] Hu, Jianwei et al., "The performance of self-interrogation neutron resonance densitometry in measuring spent fuel," JNMM, 40 (2012), pp.36-44.

[38] LaFleur, Adrienne M. et al., "Development of self-interrogation neutron resonance densitometry to quantify the fissile content in PWR spent LEU and MOX assemblies", Nucl. Sci. Eng., 171 (2012), pp.175-191.

[39] LaFleur, Adrienne M. et al., "Comparison of fresh fuel experimental measurements to MCNPX calculations using self-interrogation neutron resonance densitometry", Nucl. Instrum. Methods Phys. Res., Sect. A, 680 (2012), pp.168-178.

[40] Campbell, Luke W. et al., "High-energy delayed gamma spectroscopy for spent nuclear fuel assay", 50th Annual Meeting of the Institute of Nuclear Materials Management, (2009).

[41] Campbell, Luke W. and Smith, L. Eric, "Progress on High Energy Delayed Gamma Spectroscopy for Direct Assay of Pu in Spent Fuel", 51st Annual Meeting of the Institute of Nuclear Materials Management, (2010).

[42] Mozin, Vladimir V. et al., "Delayed Gamma Technique for Fissile Material Assay", 51st Annual Meeting of the Institute of Nuclear Materials Management, (2010).

[43] Campbell, Luke W. et al., "High-Energy Delayed Gamma Spectroscopy for Spent Nuclear Fuel Assay", IEEE Trans. Nucl. Sci., 58 (2011), pp.231-240.

[44] Campbell, Luke W. et al., "High Energy Delayed Gamma Spectroscopy for Plutonium Assay of Spent Reactor Fuel", 52nd Annual Meeting of the Institute of Nuclear Materials Management, (2011).

[45] Mozin, Vladimir V. et al., "Delayed Gamma Assay for Spent Nuclear Fuel Safeguards", 52nd Annual Meeting of the Institute of Nuclear Materials Management, (2011).

[46] Rodriguez, Douglas C. et al., "Prospects for Spent Fuel Measurements Using High-Rate Germanium Detectors", 53rd Annual Meeting of the Institute of Nuclear Materials Management, (2012).

[47] Kulisek, Jonathan A. et al., "Preliminary Simulations for Geometric Optimization of a High-Energy Delayed Gamma Spectrometer for Direct Assay of Pu in Spent Nuclear Fuel", 53rd Annual Meeting of the Institute of Nuclear Materials Management, (2012).

[48] Mozin, Vladimir V. et al., "Delayed Gamma-Ray Spectroscopy for Spent Nuclear Fuel Assay", JNMM, 40 (2012), pp.78-87.

[49] Mozin, Vladimir V. et al., "Assessment of Delayed Gamma-Ray Technique Parameters for Spent Nuclear Fuel Assay", 53rd Annual Meeting of the Institute of Nuclear Materials Management, (2012).

[50] Fensin, Michael L. et al., "Quantifying the passive gamma signal from spent nuclear fuel in support of determining the plutonium content in spent nuclear fuel with nondestructive assay", 50th Annual Meeting of the Institute of Nuclear Materials Management, (2009).

[51] Galloway, Jack D. et al., "The role of Monte Carlo burnup calculations in quantifying plutonium mass in spent fuel assemblies with non-destructive assay", 33rd Annual Meeting of the European Safeguards Research and Development Association, (2011).

[52] Favalli, Andrea et al., "Determination of initial enrichment, burnup, cooling time of PWR spent fuel assemblies by analysis of passive gamma spectra and neutron count rate", 53rd Annual Meeting of the Institute of Nuclear Materials Management, (2012).

[53] Galloway, Jack D. et al., "Design and Description of the NGSI Spent Fuel Library with Emphasis on the Passive Gamma Signal", JNMM, 40 (2012), pp.25-35.

[54] Quiter, Brian J. et al., "Nondestructive spent fuel assay using nuclear resonance fluorescence", 50th Annual Meeting of the Institute of Nuclear Materials Management, (2009).

[55] Ludewigt, Bernhard A. et al., "Using Nuclear Resonance Fluorescence for Nondestructive Isotopic Analysis", 51st Annual Meeting of the Institute of Nuclear Materials Management, (2010).

[56] Ludewigt, Bernhard A.et al., "Nuclear resonance fluorescence to measure plutonium mass in spent nuclear fuel", NGSI Phase I report, September 2011 revision, Lawrence Berkeley National Laboratory, (2011).

[57] Quiter, Brian J. et al., "Assessment of Nuclear Resonance Fluorescence for Spent Nuclear Fuel Assay", 52nd Annual Meeting of the Institute of Nuclear Materials Management, (2011).

[58] Charlton, William S. et al.: "The Use of Self-Induced XRF to Quantify the Pu Content in PWR Spent Nuclear Fuel," 31st Annual Meeting of the European Safeguards Research and Development Association, (2009).

[59] Hoover, Andrew S. et al., "Measurement of plutonium in spent nuclear fuel by self-induced X-ray fluorescence", 50th Annual Meeting of the Institute of Nuclear Materials Management, (2009).

[60] Rajasingum, Akshayan et al., "Modeling of X-Ray Fluorescence using MCNPX and Geant4", 50th Annual Meeting of the Institute of Nuclear Materials Management, (2009).

[61] Stafford, Alissa S. et al., "Spent Nuclear Fuel Self-Induced X-ray Fluorescence Simulations for North Anna and TMI", 50th Annual Meeting of the Institute of Nuclear Materials Management, (2009).

[62] Freeman, Corey R. et al., "Feasibility of X-Ray Fluorescence for Spent Fuel Safeguards", 51st Annual Meeting of the Institute of Nuclear Materials Management, (2010).

[63] Solodov, Alexander A. et al., "The Use of Self-induced XRF to Quantify the Pu Content in MOX Spent Nuclear Fuel", 51st Annual Meeting of the Institute of Nuclear Materials Management, (2010).

[64] Stafford, Alissa S. et al., "Exploration of X-Ray Fluorescence Spent Nuclear Fuel Source Term," 51st Annual Meeting of the Institute of Nuclear Materials Management, (2010).

[65] Stafford, Alissa S., "Spent nuclear fuel self-induced XRF to predict Pu to U content", M.S. Thesis, Department of Nuclear Engineering, Texas A&M University, (2010).

[66] White, Julia et al., "Applications of X-Ray Fluorescence Fission Product Correlations for Nuclear Forensics", 51st Annual Meeting of the Institute of Nuclear Materials Management, (2010).

[67] Freeman, Corey R. et al., "X-ray fluorescence for safeguards of spent fuel assemblies", LA-UR-11-02843, 33rd Annual Meeting of the European Safeguards Research and Development Association, (2011).

[68] Freeman, Corey R. et al., "Using X-ray fluorescence for quantifying plutonium mass in spent fuel assemblies", NGSI Phase I report, October 2011 Draft revision of LA-UR 11-00513, Los Alamos National Laboratory, (2011).

[69] Conlin, Jeremy Lloyd and Tobin, Stephen J., "Spent Fuel Library Report", LA-UR-10-07894, Los Alamos National Laboratory, (2010).

[70] LANL, "NGSI Spent Fuel Libraries", LA-UR-10-08244, Los Alamos National Laboratory, (2012).

[71] Trellue, Holly R. et al., "Advances in spent fuel libraries", 54th Annual Meeting of the Institute of Nuclear Materials Management, (2013).

[72] Fensin, Michael L. et al., "The enhancements and testing for the MCNPX 2.6.0 depletion capability", Nucl. Technol., 170 (2010), pp.68-79.

[73] Tobin, Stephen J. et al., "Technical Cross-cutting Issues for the Next Generation Safeguards Initiative's Spent Fuel Nondestructive Assay Project", JNMM, 40 (2012), pp.18-24.

[74] Lamarsh, John R. and Baratta, Anthony J., "Introduction to Nuclear Engineering" Prentice Hall, Upper Saddle River, New Jersey, (2001).

[75] Reilly, T. Douglas et al., "Passive Nondestructive Assay of Nuclear Materials", U.S. Nuclear Regulatory Commission, (1991).

[76] Reilly, T. Douglas et al., "Passive Nondestructive Assay of Nuclear Materials: 2007 Addendum", Los Alamos National Laboratory, (2007).

[77] Global Nuclear Fuel: Sales Literature for the GNF2 BWR Fuel Assembly, Global Nuclear Fuel, (2012).

[78] Tiitta, Antero et al., "Spent BWR fuel characterisation combining a fork detector with gamma spectrometry", STUK-YTO-TR 175, STUK, (2001).

[79] Tiitta, Antero and Hautamäki, Johanna, "Spent VVER fuel characterisation combining a fork detector with gamma spectrometry", STUK-YTO-TR 181, STUK, (2001).

[80] Nakahara, Yoshinori et al., "Nuclide Composition Benchmark Data Set for Verifying Burnup Codes on Spent Light Water Reactor Fuels", Nucl. Technol., 137 (2002), pp.111-126.

[81] Ham, Young S. and Sitaraman, Shivakumar, "Partial Defect Tester: A Novel Approach to Detect Partial Defects in Pressurized Water Reactor Spent Fuel", Nucl. Technol., 175 (2011), pp.401-418.

[82] Rossa, Riccardo et al., "Application of the PDET detector to BWR fuel assemblies: gross defect testing using the spatial distribution of neutron and photon flux", 35th Annual Meeting of the European Safeguards Research and Development Association, (2013).

[83] Tanskanen, Aapo, "Assessment of the neutron and gamma sources of the spent BWR fuel", STUK-YTO-TR 170, STUK, (2000).

[84] U.S. DOE, "Integrated Data Base Report—996: U.S. Spent Nuclear Fuel and Radioactive Waste Inventories, Projections, and Characteristics", DOE/RW-0006, Rev. 13, U.S. Department of Energy, (1997).

[85] U.S. DOE, "Final Environmental Impact Statement for a Geologic Repository for the Disposal of Spent Nuclear Fuel and High-Level Radioactive Waste at Yucca Mountain, Nye County, Nevada", DOE/EIS-0250, U.S. Department of Energy, (2002).

[86] Bodansky, David, "Nuclear Energy: Principles, Practices, and Prospects", Springer-Verlag, (2004).

[87] LaFleur, Adrienne M., "Development of Self-Interrogation Neutron Resonance Densitometry (SINRD) to Measure the Fissile Content in Nuclear Fuel", Ph.D. Dissertation, Department of Nuclear Engineering, Texas A&M University, (2011).

[88] U.S. MARAD, “Technical Press Information for the *N.S. Savannah*”, U.S. Maritime Administration, (1959).

[89] Parks, Cecil V. et al., "Review and Prioritization of Technical Issues Related to Burnup Credit for LWR Fuel", ORNL/TM-1999/303 and NUREG/CR-6665, Oak Ridge National Laboratory, (2000).

[90] Wagner, John C. and DeHart, M. D., "Review of Axial Burnup Distribution Considerations for Burnup Credit Calculations", ORNL/TM-1999/246, Oak Ridge National Laboratory, (2000).

[91] Ezure, Hideo, "Evaluation of Depletion and Production of Uranium, Plutonium, Transplutoniums and Fission Products in Full-Core Fuel Assemblies of Japan Power Demonstration Reactor-1", J. Nucl. Sci. Technol., 27 (1990), pp.461-472.

[92] Bosler, G. E. et al., "Production of actinide isotopes in simulated PWR fuel and their influence on inherent neutron emission", LA-9343, Los Alamos National Laboratory, (1982).

[93] Nodvik, R. J. and Jedruch, J., "Experimentally determined burnup and spent fuel composition of Yankee Core I", WCAP-6071, UC-80, TID 4500, U.S. Atomic Energy Commission, (1965).

[94] Lacey, P. G. and Radcliffe, R. E., "Diffusion-theory depletion analysis of the Yankee core", WCAP-6077, UC-80, U.S. Atomic Energy Commission, (1966).

[95] Nodvik, R. J., "Evaluation of mass spectrometric and radiochemical analyses of Yankee Core I spent fuel", WCAP-6068, UC-80, U.S. Atomic Energy Commission, (1966).

[96] Nodvik, R. J. et al., "Supplementary report on evaluation of mass spectrometric and radiochemical analyses of Yankee Core I spent fuel, including isotopes of elements thorium through curium", WCAP-6086, UC-80, TID 4500, U.S. Atomic Energy Commission, (1969).

[97] Kraemer, R. and Beyrich W., "Joint Integral Safeguards Experiment (JEX 70) at the Eurochemic Reprocessing Plant, Mol, Belgium: January 1970 - July 1971", EUR 4576e; KFK 1100, Commission of the European Communities, General Directorate for Dissemination of Knowledge, Centre for Information and Documentation (CID), Luxembourg, (1971).

[98] Ariemma, A. et al., "Experimental and theoretical determination of burnup and heavy isotope content in a fuel assembly irradiated in the Garigliano boiling water reactor", EUR-4638e, EURATOM (1971).

[99] Crain, H. H., "Saxton Plutonium Project Quarterly Progress Report for the Period Ending Sept. 30, 1973", WCAP-3385-37, Westinghouse Electric Corporation, (1973).

[100] Thomas, Jr. C. C., et al., "Spent-fuel composition: a comparison of predicted and measured data", LA-8764-MS, Los Alamos National Laboratory, (1981).

[101] Natsume, Haruo et al., "Gamma-Ray Spectrometry and Chemical Analysis Data of JPDR-I Spent Fuel", J. Nucl. Sci. Technol., 14 (1977), pp.745-761.

[102] Suzaki, Takenori et al., "Non-Destructive and Destructive Measurements on Burnup Characteristics of Japan Power Demonstration Reactor-I Full-Core Fuel Assemblies", J. Nucl. Sci. Technol., 23 (1986), pp.53-72.

[103] Murphy, Brian D., "Characteristics of Spent Fuel from Plutonium Disposition Reactors. Vol. 1: The Combustion Engineering System 80+ Pressurized-Water-Reactor Design", ORNL/TM-13170/V1, Oak Ridge National Laboratory, (1996).

[104] Murphy, Brian D., "Characteristics of Spent Fuel from Plutonium Disposition Reactors. Vol. 3: A Westinghouse Pressurized-Water Reactor Design", ORNL/TM-13170/V3, Oak Ridge National Laboratory, (1997).

[105] Murphy, Brian D., "Characteristics of Spent Fuel from Plutonium Disposition Reactors. Vol. 4: Westinghouse Pressurized-Water-Reactor Fuel Cycle Without Integral Absorber", ORNL/TM-13170/V4, Oak Ridge National Laboratory, (1998).

[106] Ryman, J. C. and Hermann, O. W., "Characteristics of Spent Fuel from Plutonium Disposition Reactors. Vol. 2: A General Electric Boiling-Water-Reactor Design", ORNL/TM-13170/V2, Oak Ridge National Laboratory, (1998).

[107] Ando, Yoshihira and Takano, Hideki, "Estimation of LWR Spent Fuel Composition" JAERI-Research 99-004, (1999), 270p.

[108] Ando, Yoshihira et al., "Estimation of Spent Fuel Compositions from Light Water Reactors", J. Nucl. Sci. Technol., 37 (2000), pp.924-933.

[109] OECD-NEA Working Party on Nuclear Criticality Safety: Website for the Expert Group on Burn-up Credit Criticality Safety (BUC), Organisation for Economic Co-operation and Development, Nuclear Energy Agency, (2011).

[110] Takano, Makoto, "Result of Phase-1A", OECD/NEA Burnup Credit Criticality Benchmark, NEA/NSC/DOC(93)22 and JAERI-M 94-003, (1994), 145p.

[111] DeHart, M. D. et al., "Phase I-B Results", OECD/NEA Burnup Credit Criticality Benchmark, NEA/NSC/DOC(96)06 and ORNL-6901, Oak Ridge National Laboratory, (1996).

[112] Takano, Makoto and Okuno, Hiroshi, "Result of Phase IIA", OECD/NEA Burnup Credit Criticality Benchmark, NEA/NSC/DOC(96)01 and JAERI-Research 96-003, (1996), 170p.

[113] Neuber, Jens Christian, "Phase II-C: Impact of the Asymmetry of PWR Axial Burnup Profiles on the End Effect", OECD/NEA Burnup Credit Criticality Benchmark, draft, AREVA, Framatome-ANP GmbH, (2008).

[114] Barreau, Anne, "Phase II-D: PWR-UO2 Assembly Study of Control Rod Effects on Spent Fuel Composition", OECD/NEA Burnup Credit Criticality Benchmark, NEA No. 6227 and ISBN 92-64-02316-X, Commissariat à l'énergie atomique, (2006).

[115] Okuno, Hiroshi et al., "Phase IIIA: Criticality Calculations of BWR Spent Fuel Assemblies in Storage and Transport," OECD/NEA Burnup Credit Criticality Benchmark, NEA/NSC/DOC(2000)12 and JAERI-Research 2000-041, (2000), 179p.

[116] Okuno, Hiroshi et al., "Phase IIIB: Burnup Calculations of BWR Fuel Assemblies for Storage and Transport", OECD/NEA Burnup Credit Criticality Benchmark, NEA/NSC/DOC(2002)2 and JAERI-Research 2002-001, (2002), 181p.

[117] O'Connor, Gregory J. et al.: "Phase IV-A: Reactivity Prediction Calculations for Infinite Arrays of PWR MOX Fuel Pin Cells", NEA/NSC/DOC(2003)3 , OECD/NEA Burnup Credit Criticality Benchmark, Organisation for Economic Co-operation and Development, Nuclear Energy Agency, (2003).

[118] O'Connor, Gregory J. and Liem, P., "Phase IV-B: Results and Analysis of MOX Fuel Depletion Calculations", OECD/NEA Burnup Credit Criticality Benchmark, NEA/NSC/DOC(2003)4 and ISBN 92-64-02124-8, Organisation for Economic Co-operation and Development, Nuclear Energy Agency, (2003).

[119] Radulescu, G. and Wagner, John C., "UO_2 Fuel: Study of Spent Fuel Compositions for Long-Term Disposal", OECD/NEA Burnup Credit Criticality Benchmark, NEA No. 6998 and ISBN 978-92-64-99172-9, Organisation for Economic Co-operation and Development, Nuclear Energy Agency, (2012).

[120] OECD-NEA Working Party on Nuclear Criticality Safety, "Spent Fuel Isotopic Composition Database (SFCOMPO)", Organisation for Economic Co-operation and Development, Nuclear Energy Agency, (2011).

[121] Richard, Joshua G. et al., "Characterization of the Neutron Source Term and Multiplicity of a Spent Fuel Assembly in Support of NDA Safeguards of Spent Nuclear Fuel", 51st Annual Meeting of the Institute of Nuclear Materials Management, (2010).

[122] Perry, R. T. and Wilson, William B., "Neutron Production from (αn) Reactions and Spontaneous Fission in ThO_2, UO_2, and $(U,Pu)O_2$ Fuels", LA-8869-MS, Los Alamos National Laboratory, (1981).

[123] Jacobs, G. J. H. and Liskien, H., "Energy spectra of neutrons produced by αparticles in thick targets of light elements", Ann. Nucl. Energy, 10 (1983), pp.541-552.

[124] Sonzogni, A., "Chart of the Nuclides", National Nuclear Data Center, Brookhaven National Laboratory (BNL), (2013).

[125] Chadwick, M. B. et al., "ENDF/B-VII.1 Nuclear Data for Science and Technology: Cross Sections, Covariances, Fission Product Yields and Decay Data", Nucl. Data Sheets, 112 (2011), pp.2887-2996.

[126] Hsue, S. T. et al., "Passive Neutron Assay of Irradiated Nuclear Fuels", LA-7645-MS, Los Alamos National Laboratory, (1979).

[127] Phillips, John R. et al., "Application of nondestructive gamma-ray and neutron techniques for the safeguarding of irradiated fuel materials", LA-8212, Los Alamos National Laboratory, (1980).

[128] Sasahara, A. et al., "Neutron and Gamma Ray Source Evaluation of LWR High Burn-up UO2 and MOX Spent Fuels", J. Nucl. Sci. Technol., 41 (2004), pp.448-456.

[129] Whitney, Scott M. et al., "Analyzing nuclear fuel cycles from isotopic ratios of waste products applicable to measurement by accelerator mass spectrometry", Nucl. Sci. Eng., 157 (2007), pp.200-209.

[130] Bolind, Alan M. and Seya, M., "A collection and distillation of the important physics for understanding, interpreting, and evaluating neutron-based non-destructive assay techniques for nuclear fuel", 53rd Annual Meeting of the Institute of Nuclear Materials Management, (2012).

[131] Ryzhov, Sergei B. et al., "VVER-Type Reactors of Russian Design" in “Handbook of Nuclear Engineering” Vol. 5, Dan Gabriel Cacuci, editor, Springer (2010), pp.2249-2320.

[132] Reilly, T. Douglas, "The Measurement of Leached Hulls" LA-7784-MS (ISPO-63), Los Alamos National Laboratory, (1979).

[133] Roque, B. et al., "Burnup credit calculation route for PWR MOX assemblies and experimental validation in Minerve R1-MOX and SLB1 P.I.E.", Practices and developments in spent fuel burnup credit applications, 22-26 April, 2002, Madrid, Spain, IAEA-TECDOC-1378, International Atomic Energy Agency, (2003), pp.424-439.

[134] Caldwell, John T. et al., "Apparatus and method for quantitative assay of generic transuranic wastes from nuclear reactors", U.S. Patent No. 4483816 (1984).

[135] Burr, T. et al., "Uncertainty Quantification for New Approaches to Spent Fuel Assay", Nucl. Sci. Eng., 172 (2012), pp.180-192.

[136] Toubon, H. et al., "Burnup credit methodology for UO2 and MOX fuel assemblies in AREVA/COGEMA", Practices and developments in spent fuel burnup credit applications, 22-26 April 2002, Madrid, Spain, IAEA-TECDOC-1378, International Atomic Energy Agency, (2003), pp. 395-401.

[137] U.S. DOE, "Nuclear Physics and Reactor Theory", DOE Fundamentals Handbook, Vol. 1, DOE-HDBK-1019/1-93, U.S. Department of Energy, (1993).

[138] U.S. DOE, "Nuclear Physics and Reactor Theory" DOE Fundamentals Handbook, Vol. 2, DOE-HDBK-1019/2-93, U.S. Department of Energy, (1993).

[139] Canadian Nuclear Safety Commission, "Module One: Science & Engineering Fundamentals; Concepts of Reactivity and Criticality", Fundamentals of Power Reactors Training Course, Vol. 1, CANTEACH Project, CANDU Owners Group, Toronto, (1993).

[140] Smith, Darryl B. and Jaramillo, Genara R., "Safeguards and Security Progress Report: January--December 1989" LA-11914-PR, Los Alamos National Laboratory, (1990).

[141] Evans, Louise G. et al., "^{3}He Replacement for Nuclear Safeguards Applications Part I: Test Program and Experimental Results", 52nd Annual Meeting of the Institute of Nuclear Materials Management, (2011).

[142] E.R. Johnson Associates, "The incentives and feasibility for direct measurement of spent nuclear fuel characteristics in the Federal Waste Management System", ORNL/Sub/86-SA094/3, JAI-296, Oak Ridge National Laboratory, (1989).

[143] Bosler, G. E. and Rinard, Phillip M., "Burnup measurements with the Los Alamos Fork detector", LA-UR-91-2508, 32nd Annual Meeting of the Institute of Nuclear Materials Management, (1991).

[144] Bignan, G. andMartin-Deidier, L., "Evaluation of the U-Pu residual mass from spent fuel assemblies with passive and active neutronic methods", 13th Annual Meeting of the European Safeguards Research and Development Association, (1991).

[145] Ewing, Ronald I., "Burnup verification measurements with the FORK measurement system--implementation for burnup credit", 35th Annual Meeting of the Institute of Nuclear Materials Management, (1994).

[146] Lebrun, A. et al., "SMOPY: a new NDA tool for safeguards of LEU and MOX spent fuel", Symposium on International Safeguards – Verification and Nuclear Material Security, 29 October – 2 November, 2001, Vienna, Austria, IAEA-SM-367/14/03, International Atomic Energy Agency, (2001).

[147] Phillips, John R. et al., "Apparatus for in situ determination of burnup, cooling time and fissile content of an irradiated nuclear fuel assembly in a fuel storage pond", U.S. Patent No. 4510117 (1985).

[148] Ewing, Ronald I., "Burnup verification measurements on spent fuel assemblies at Arkansas Nuclear One", 36th Annual Meeting of the Institute of Nuclear Materials Management, (1995).

[149] Conlin, Jeremy L. et al., "On Using Code Emulators and Monte Carlo Estimation to Predict Assembly Attributes of Spent Fuel Assemblies for Safeguards Applications", Nucl. Sci. Eng., 169 (2011), pp.314-328.

[150] Ulrich II, Timothy J. et al., "Simulated Performance of the Integrated Passive Neutron Albedo Reactivity and Self-Interrogation Neutron Resonance Densitometry Detector Designed for Spent Fuel Measurement at the Fugen Reactor in Japan", 53rd Annual Meeting of the Institute of Nuclear Materials Management, (2012).

[151] Eigenbrodt, Julia M. et al., "Simulations and Preparation for PNAR Measurements of Fugen Fuel", 35th Annual Meeting of the European Safeguards Research and Development Association (2013).

[152] Lee, D. M. and Lindquist L. O., "Self-interrogation of spent fuel", LA-9494-MS, Los Alamos National Laboratory, (1982).

[153] Menlove, Howard O. and Beddingfield, David H.,: "Passive neutron reactivity measurement technique", LA-UR-97-2651, Los Alamos National Laboratory, (1997).

[154] Evans, Louise G. et al., "Non-destructive Assay of Spent Nuclear Fuel Using Passive Neutron Albedo Reactivity", 51st Annual Meeting of the Institute of Nuclear Materials Management, (2010).

[155] Lee, S. et al., "Development of a passive neutron albedo reactivity counter for a Korean advanced pyroprocessing facility", 49th Annual Meeting of the Institute of Nuclear Materials Management, (2008).

[156] Lee, T. et al., "Passive Neutron Albedo Reactivity Technique for Non-Destructive Assay of U/TRU Product of Pyroprocessing", 52nd Annual Meeting of the Institute of Nuclear Materials Management, (2011).

[157] Lee, T. et al., "Determination of Pu Content of U/TRU Ingot of Pyroprocessing Using the Passive Neutron Albedo Reactivity Technique", 53rd Annual Meeting of the Institute of Nuclear Materials Management, (2012).

[158] Ebara, N. et al., "The JAEA part of the Joint JAEA-U.S. DOE Project for Pu Measurement of Fugen Spent Fuel Assemblies by Integrated PNAR and SINRD", 53rd Annual Meeting of the Institute of Nuclear Materials Management, (2012).

[159] Hayashi, K. et al., "Rehearsal and Actual Measurement of Fugen Spent Fuel Assemblies by Integrated PNAR and SINRD under the JAEA-USDOE Collaboration Program", 54th Annual Meeting of the Institute of Nuclear Materials Management, (2013).

[160] Bolind, Alan M., "Development of an analytical theory to describe the PNAR and CIPN nondestructive assay techniques" Ann. Nucl. Energy, 66 (2014), pp.167-176.

[161] Menlove, Howard O. et al., "Verification of Plutonium Content in Spent Fuel Assemblies Using Neutron Self-Interrogation", 50th Annual Meeting of the Institute of Nuclear Materials Management, (2009).

[162] Hu, J. et al., "Determining Plutonium Mass in Spent Fuel Using Cf-252 Interrogation with Prompt Neutron Detection", 51st Annual Meeting of the Institute of Nuclear Materials Management, (2010).

[163] Hu, J. et al., "Quantifying fissile content in spent nuclear fuel assemblies using ^{252}Cf interrogation with prompt neutron detection", 356978, GLOBAL 2011, 11-16 December, 2011, Makuhari Messe, Chiba, Japan (2011).

[164] Hu, J. et al., "Customized Design and Simulated Performance of the ^{252}Cf Interrogation with Prompt Neutron Detector for Spent Fuel Measurement at the Post Irradiation Examination Facility in the Republic of Korea", 53rd Annual Meeting of the Institute of Nuclear Materials Management, (2012).

[165] Schulze, G. et al., "Neutron assay plus isotopic correlations: a method for determining Pu and burnup in spent LWR fuel assemblies", 2nd Annual Meeting of the European Safeguards Research and Development Association, (1980), pp.396-403.

[166] Würz, H. et al., "A Nondestructive Method for Light Water Reactor Fuel Assembly Identification", Nucl. Technol., 90 (1990), pp.191-204.

[167] Suzaki, T., "Subcriticality Determination of Low-Enriched UO2 Lattices in Water by Exponential Experiment", J. Nucl. Sci. Technol., 28 (1991), pp.1067-1077.

[168] Ueda, M. et al., "Active Neutron Multiplication Method for Fuel Lattices in Water", Nucl. Technol., 97 (1992), pp.131-142.

[169] Ueda, M. et al., "Basic Studies on Neutron Emission-Rate Method for Burnup Measurement of Spent Light-Water-Reactor Fuel Bundle", J. Nucl. Sci. Technol., 30 (1993), pp.48-59.

[170] Lee, T. et al., "Differential Die-Away Technique for Determination of the Fissile Contents in Spent Fuel Assembly" 51st Annual Meeting of the Institute of Nuclear Materials Management, (2010).

[171] Lee, T. et al., "Monte Carlo simulations of differential die-away instrument for determination of fissile content in spent fuel assemblies", Nucl. Instrum. Methods Phys. Res., Sect. A, 652 (2011), pp.103-107.

[172] Henzl, V. et al., "Quantifying the Plutonium Mass in Spent Fuel with an Integrated Prompt Plus Delayed Neutron Detector", 52nd Annual Meeting of the Institute of Nuclear Materials Management, (2011).

[173] Blanc, P. et al., "Optimization of the Combined Delayed Neutron and Differential Die-Away Prompt Neutron Signal Detection for Characterization of Spent Nuclear Fuel Assemblies", #11419, WM2011, WM Symposia (2011).

[174] Henzl, V. et al., "Determination of total plutonium content in a spent fuel assembly by measuring passive neutron count rate and multiplication with the differential die-away instrument", 53rd Annual Meeting of the Institute of Nuclear Materials Management, (2012).

[175] Henzl, V. et al., "Direct measurement of initial enrichment and burn-up of spent fuel assembly with a differential die-away technique based instrument", 53rd Annual Meeting of the Institute of Nuclear Materials Management, (2012).

[176] Caldwell, John T. et al., "The Los Alamos Second-Generation System for Passive and Active Neutron Assays of Drum-Size Containers", LA-10774-MS, Los Alamos National Laboratory, (1986).

[177] Jordan, Kelly A. and Gozani, T., "Pulsed neutron differential die away analysis for detection of nuclear materials" Nucl. Instrum. Methods Phys. Res., Sect. B, 261 (2007), pp.365-368.

[178] Jordan, Kelly A. and Gozani, T., "Detection of 235U in hydrogenous cargo with Differential Die-Away Analysis and optimized neutron detectors", Nucl. Instrum. Methods Phys. Res., Sect. A, 579 (2007), pp.388-390.

[179] Jordan, Kelly A. et al., "Differential die-away analysis system response modeling and detector design", Nucl. Instrum. Methods Phys. Res., Sect. A, 589 (2008), pp.436-444.

[180] Pázsit, Imre and Pál, Lénárd, "A Stochastic Model of the Differential Die-away Analysis (DDAA) Method", 51st Annual Meeting of the Institute of Nuclear Materials Management, (2010).

[181] Chabod, Sébastien P., "Neutron slowing-down time in matter", Nucl. Instrum. Methods Phys. Res., Sect. A, 669 (2012), pp.32-46.

[182] IAEA, "Neutron Generators for Analytical Purposes", STI/PUB/1535 and ISBN 978-92-0-125110-7, International Atomic Energy Agency, (2012).

[183] Rinard, Phillip M., "Application Guide to Shufflers", LA-13819-MS, Los Alamos National Laboratory, (2001).

[184] Blanc, P. et al., "Delayed Neutron Detection with an Integrated Differential Die-Away and a Delayed Neutron Instrument", 51st Annual Meeting of the Institute of Nuclear Materials Management, (2010).

[185] Rinard, Phillip M., "Shuffler instruments for the nondestructive assay of fissile materials", LA-12105, Los Alamos National Laboratory, (1991).

[186] Cox, Samson A., "Delayed neutron data - review and evaluation", ANL/NDM-5, Argonne National Laboratory, (1974).

[187] Tuli, Jagdish K., "Nuclear Wallet Cards" National Nuclear Data Center, Brookhaven National Laboratory, (2011).

[188] Waldo, R. W. et al., "Delayed neutron yields: Time dependent measurements and a predictive model", Phys. Rev. C: Nucl. Phys., 23 (1981), pp.1113-1127.

[189] MacMurdo, K. W. and Bowman, W. W., "Assay of fissile materials by a cyclic method of neutron activation and delayed-neutron counting", Nucl. Instrum. Methods, 141 (1977), pp.299-306.

[190] Menlove, Howard O. and Crane, Thomas W., "A ^{252}Cf based nondestructive assay system for fissile material", Nucl. Instrum. Methods, 152 (1978), pp.549-557.

[191] Pázsit. I. and Yamane, Y., "The variance-to-mean ratio in subcritical systems driven by a spallation source", Ann. Nucl. Energy, 25 (1998), pp.667-676.

[192] Baeten, P., "Heuristic derivation of the Rossi-alpha formula for a pulsed neutron source", Ann. Nucl. Energy, 31 (2004), pp.43-53.

[193] Mihalczo, J. T., "Use of Californium-252 as a Randomly Pulsed Neutron Source for Prompt Neutron Decay Measurements", Nucl. Sci. Eng., 41 (1970), p.296.

[194] Mihalczo, J. T. et al., "Cf-source-driven neutron-noise measurements of subcriticality for a 4.95 wt% ^{235}U-enriched uranyl fluoride solution cylinder" Ann. Nucl. Energy, 13 (1986), pp.351-362.

[195] Perez, R. B. et al., "Determination of the multiplication factor and its bias by the ^{252}Cf-source technique: a method for code benchmarking with subcritical configurations", Joint international Conference on Mathematical Methods and Supercomputing for Nuclear Applications, Saratoga Springs, New York, October 6-10, 1997, CONF-971005--18, Oak Ridge National Laboratory, (1997).

[196] Baeten, P. et al., "Determination of the subcriticality level using the ^{252}Cf source-detector method", Ann. Nucl. Energy, 37 (2010), pp.740-752.

[197] Pacilio, N., "Reactor-Noise Analysis in the Time Domain", TID-24512, AEC Critical Review Series, U.S. Atomic Energy Commission, (1969).

[198] Ensslin, N. et al., "Application Guide to Neutron Multiplicity Counting", LA-13422-M, Los Alamos National Laboratory, (1998).

[199] Böhnel. K., "Die Plutoniumbestimmung in Kernbrennstoffen mit der Neutronenkoinzidenzmethode", KFK2203, Kernforschungszentrum Karlsruhe, (1975).

[200] Böhnel,K., "Determination of plutonium in nuclear fuels using the neutron coincidence method", AWRE translation No. 70 (54/4252) of KFK 2203. ISBN 0-85518121-4. H.M. Stationery Office, London (1978).

[201] Böhnel,K., "The effect of multiplication on the quantitative determination of spontaneously fissioning isotopes by neutron correlation analysis", Nucl. Sci. Eng., 90 (1985), pp.75-82.

[202] Bruggeman, M. et al., "Neutron coincidence counting based on time interval analysis with one- and two-dimensional Rossi-alpha distributions: an application for passive neutron waste assay", Nucl. Instrum. Methods Phys. Res., Sect. A, 382 (1996), pp.511-518.

[203] Baeten, P. et al., "Single- and multi-deadtime parameter corrections of one- and two-dimensional Rossi-alpha distributions for time interval analysis in neutron coincidence counting", Nucl. Instrum. Methods Phys. Res., Sect. A, 390 (1997), pp.345-358.

[204] Baeten, P. et al., "Validation aspects of multiplicity counting: a new approach by time interval analysis", 20th Annual Meeting of the European Safeguards Research and Development Association, (1998).

[205] Bruggeman, M. et al., "Neutron Coincidence Counting with Time Interval Correlation Spectroscopy, luxury or necessity?", 20th Annual Meeting of the European Safeguards Research and Development Association, (1998).

[206] Bolind, Alan M., "Categorization of the Main Techniques of Neutron Coincidence/ Multiplicity Analysis", 35th Annual Meeting of the European Safeguards Research and Development Association, (2013).

[207] Dierckx,R. and Hage, W., "Neutron Signal Multiplet Analysis for the Mass Determination of Spontaneous Fission Isotopes", Nucl. Sci. Eng., 85 (1983), pp.325-338.

[208] Pázsit, I. et al., "A note on the multiplicity expressions in nuclear safeguards", Nucl. Instrum. Methods Phys. Res., Sect. A, 603 (2009), pp.541-544.

[209] Nauchi, Y., Kameyama, T. and Sasahara,A., "Numerical simulations of neutrons transport in spent LWR fuel assemblies for burn-up credit application techniques", Track 1-27, International Conference on Nuclear Criticality (ICNC2011), 19-23 September, 2011, Edinburgh, Scotland, IBC Energy / Informa Energy, (2011).

[210] Bolind, Alan M., "The use of the BIC set to characterize used nuclear fuel assemblies for the purpose of non-destructive assay", Ann. Nucl. Energy, 66 (2014), pp.31-50.

[211] Schear, Melissa A. et al., "Fissile Material Measurements Using the Differential Die-away Self Interrogation Technique", 51st Annual Meeting of the Institute of Nuclear Materials Management, (2010).

[212] Kaplan, Alexis C. et al., "Simulation of Spent Fuel Isotopic Content Measurement with the Differential Die-Away Self-Interrogation System", 54th Annual Meeting of the Institute of Nuclear Materials Management, (2013).

[213] Pál, L. and Pázsit I., "A special branching process with two particle types" Eur. Phys. J. Plus, 126 (2011), p.26.

[214] Anderson, J. et al., "Two-point theory for the differential self-interrogation Feynman-alpha method", Eur. Phys. J. Plus, 127 (2012), p.90.

[215] Anderson, J. et al., "Derivation and quantitative analysis of the differential self-interrogation Feynman-alpha method", Eur. Phys. J. Plus, 127(2012), p.6.

[216] Chichester, David L. and Sterbentz, James W., "Neutron resonance transmission analysis (NRTA): initial studies of a method for assaying plutonium in spent fuel", 33rd Annual Meeting of the European Safeguards Research and Development Association, INL/CON-10-20684, Idaho National Laboratory, (2011).

[217] Chichester, David L. and Sterbentz, James W., "A second look at neutron resonance transmission analysis as a spent fuel NDA technique", 52nd Annual Meeting of the Institute of Nuclear Materials Management, (2011).

[218] Priesmeyer, H. G. and Harz, U., "Isotopic content determination in irradiated fuel by neutron transmission analysis", Atomkernenergie, 25 (1975), pp.109-113.

[219] Schrack, Roald A. et al., "Resonance neutron radiography using an electron linac", IEEE Trans. Nucl. Sci., NS-28 (1981), pp.1640-1643.

[220] Bowman, C. D. et al., "Neutron resonance transmission analysis of reactor spent fuel assemblies" in “Neutron Radiography: Proceedings of the First World Conference, San Diego, California, U.S.A., December 7-10, 1981”, John P. Barton and Peter von der Hardt, editors, D. Reidel Publishing Company, Dordrecht, Holland, ISBN 90-277-1528-9 (1983), pp.503-511.

[221] Behrens, James W. et al., "Neutron resonance transmission analysis of reactor fuel samples", Nucl. Technol., 67 (1984), pp.162-168.

[222] Noguere, G. et al., "Non-destructive analysis of materials by neutron resonance transmission", Nucl. Instrum. Methods Phys. Res., Sect. A, 575 (2007), pp.476-488.

[223] Koizumi, M. et al., "Proposal of neutron resonance densitometry for particle like debris of melted fuel using NRTA and NRCA", 53rd Annual Meeting of the Institute of Nuclear Materials Management, (2012).

[224] Becker, B. et al., "Particle size inhomogeneity effect on neutron resonance densitometry" 35th Annual Meeting of the European Safeguards Research and Development Association, (2013).

[225] Schillebeeckx, P. et al., "Contribution of the JRC to the development of neutron resonance densitometry to characterize melted fuel from severe accidents", 54th Annual Meeting of the Institute of Nuclear Materials Management, (2013).

[226] Tsuchiya, H. et al., "Sample thickness effect on nuclear material quantification with NRTA for particle like debris of melted fuel", 54th Annual Meeting of the Institute of Nuclear Materials Management, (2013).

[227] Harada, H. et al., "Recent Progress in Research and Development on the Neutron Resonance Densitometry for Particle-Like Debris of Melted Fuel", 54th Annual Meeting of the Institute of Nuclear Materials Management, (2013).

[228] Harada, H. et al., "Proposal of Neutron Resonance Densitometry for Particle-Like Debris of Melted Fuel using NRTA and NRCA" 35th Annual Meeting of the European Safeguards Research and Development Association, (2013).

[229] Zerkin, V., "Multi-platform EXFOR-CINDA-ENDF project", National Nuclear Data Center, Brookhaven National Laboratory and International Atomic Energy Agency, (2012).

[230] Evans, Louise G. et al., "Nuclear Safeguards ^{3}He Replacement Requirements", JNMM, 40 (2012), pp.88-96.

[231] Schillebeeckx, P. et al.: "Neutron resonance spectroscopy for the characterization of materials and objects" JINST, 7, C03009 (2012).

[232] U.S. NRC, "Fact Sheet on Dry Cask Storage of Spent Nuclear Fuel", U.S. Nuclear Regulatory Commission, (2011).

[233] Smith, L. Eric et al., "Time-spectral analysis algorithms for lead slowing-down spectroscopy of spent fuel", 50th Annual Meeting of the Institute of Nuclear Materials Management, (2009).

[234] Smith, L. Eric et al., "Recent progress in the development of lead slowing-down spectroscopy for direct measurement of Pu in spent fuel", 50th Annual Meeting of the Institute of Nuclear Materials Management, (2009).

[235] Smith, L. Eric et al., "Advancements in Time-Spectra Analysis Methods for Lead Slowing-Down Spectroscopy" 51st Annual Meeting of the Institute of Nuclear Materials Management, (2010).

[236] Smith, L. Eric et al., "Time-spectral analysis methods for spent fuel assay using lead slowing-down spectroscopy", IEEE Trans. Nucl. Sci., 57 (2010), pp.2230-2238.

[237] Kulisek, Jonathan A. et al., "Progress on Establishing the Feasibility of Lead Slowing Down Spectroscopy for Direct Measurement of Plutonium in Used Fuel", 52nd Annual Meeting of the Institute of Nuclear Materials Management, (2011).

[238] Warren, Glen A. et al., "Characterization of a New Lead Slowing Down Spectrometer" 52nd Annual Meeting of the Institute of Nuclear Materials Management, (2011).

[239] Warren, Glen A. et al., "Lead slowing-down spectrometry status report" PNNL-21457, Pacific Northwest National Laboratory, (2012).

[240] Kulisek, Jonathan A.et al., "Update on Establishing the Feasibility of Lead Slowing Down Spectroscopy for Direct Measurement of Plutonium in Used Fuel", 54th Annual Meeting of the Institute of Nuclear Materials Management, (2013).

[241] Bergman, A. A. et al., "A neutron spectrometer based on measuring the slowing-down time of neutrons in lead", Proceedings of the (First) International Conference on the Peaceful Uses of Atomic Energy, 8-20 August, 1955, Geneva, Switzerland, United Nations, (1956), pp.135-146.

[242] Cohen, E. Richard, "The neutron velocity spectrum in a heavy moderator", Nucl. Sci. Eng., 2 (1957), pp.227-245.

[243] Kazarnovskii, M.V., "A calculation of the neutron energy spectrum produced by a pulsed source in a heavy moderator, assuming a constant mean free path", J. Nucl. Energy, Part B, 9 (1959), pp.293-303.

[244] Krinninger, H. et al., "Pulsed neutron method for non-destructive and simultaneous determination of the ^{235}U and ^{239}Pu contents of irradiated and non-irradiated reactor fuel elements", Nucl. Instrum. Methods, 73 (1969), pp.13-33.

[245] Wakabayashi, H. et al., "Some New Applications of Neutron Slowing Down Time Spectrometry", J. Nucl. Sci. Technol. 7 (1970), pp.487-499.

[246] Conn, Robert W. and Sawan, M., "Time-dependent phenomena in neutron slowing down theory", Nucl. Sci. Eng., 48 (1972), pp.361-366.

[247] Krinninger, H. et al., "Operational experience with the automatic lead-spectrometer facility for nuclear safeguards", Nucl. Instrum. Methods, 117 (1974), pp.61-84.

[248] Sawan, M. and Conn, Robert W.,"Neutron pulses slowing down in heavy media: analysis with applications of the lead spectrometer", Nucl. Sci. Eng., 54, No. 2 (1974), pp.127-142.

[249] Cramer, D. S. et al., "Lead spectrometer for non-destructive nuclear fuel assay", KAPL-M-7449, Knolls Atomic Power Laboratory, (1976).

[250] Bornt, Jr., F. W. et al., "Fissile Assay Measurements of 235U in a Lead Slowing Down Time Spectrometer", Trans. Am. Nucl. Soc., 39 (1981), pp.344-345.

[251] Little, R. C. et al., "Monte Carlo modeling of the neutronics of a lead slowing down time assay device", Trans. Am. Nucl. Soc., 43 (1982), pp.119-121.

[252] Harris, Donald R. et al., "Measurement of uranium and plutonium content in a fuel assembly using the RPI spent-fuel assay device", Trans. Am. Nucl. Soc., 61 (1990), pp.73-74.

[253] Vanterpool, Ernesto C. et al., "Fuel assembly assay by neutron interrogation in a lead slowing-down-time spectrometer", Nucl. Sci. Eng., 110 (1992), pp.186-194.

[254] Abdurrahman, Naeem M. et al., "Spent-fuel assay performance and Monte Carlo analysis of the Rensselaer slowing-down-time spectrometer", Nucl. Sci. Eng., 115 (1993), pp.279-296.

[255] Rubbia, Carlo, "Relation between Time and Kinetic Energy in a Constant Lethargy System", CERN-AT-ET-Internal Note 95-010, European Organization for Nuclear Research (CERN), (1995).

[256] Hawari, Ayman I. et al., "Compact new-technology neutron generators for nondestructive assay of nuclear materials using slowing-down-time spectrometry", Trans. Am. Nucl. Soc., 76 (1997), pp.143-144.

[257] Kobayashi, K. et al., "Characteristics of the Kyoto University Lead Slowing-down Spectrometer (KULS) coupled to an electron linac", Nucl. Instrum. Methods Phys. Res., Sect. A, 385 (1997), pp.145-156.

[258] Przytula, M. et al., "Lead slowing-down neutron spectrometer at Łódź University", Acta Universitatis Lodziensis, Folia Physica, 21 (1998), pp.3-9.

[259] Lee, Y. et al., "Design of a spent-fuel assay device using a lead spectrometer", Nucl. Sci. Eng., 131 (1999), pp.45-61.

[260] Lee, Y. et al., "Neutron tomographic fissile assay in spent fuel using the lead slowing down time spectrometer", Nucl. Instrum. Methods Phys. Res., Sect. A, 459 (2001), pp.365-376.

[261] Abánades, A. et al., "Results from the TARC experiment: spallation neutron phenomenology in lead and neutron-driven nuclear transmutation by adiabatic resonance crossing", Nucl. Instrum. Methods Phys. Res., Sect. A, 478 (2002), pp.577-730.

[262] Smith, L. Eric and Abdurrahman, Naeem M., "Neutron spectrometry for the assay of high fissile content spent fuel", Nucl. Technol., 140 (2002), pp.328-349.

[263] Rochman, D. et al., "Characteristics of a lead slowing-down spectrometer coupled to the LANSCE accelerator", Nucl. Instrum. Methods Phys. Res., Sect. A, 550 (2005), pp.397-413.

[264] Romodanov, Vadim L. et al., "A method to decrease the load on scintillation channels in fissile material detection and control devices with pulsed neutron sources", 47th Annual Meeting of the Institute of Nuclear Materials Management, (2006).

[265] Ressler, Jennifer J. et al., "Lead slowing down spectroscopy for direct Pu mass measurements", #70, 8th International Conference on Facility Operations – Safeguards Interface, March 30 – April 4, 2008, Portland, Oregon, American Nuclear Society, (2008).

[266] Lee, Y. et al., "Status of Lead Slowing Down Spectrometer Development for Nuclear Fissile Assay", 51st Annual Meeting of the Institute of Nuclear Materials Management, (2010).

[267] Pál, Lénárd and Pázsit, Imre, "Stochastic aspects of neutron slowing down processes", Phys. Scr., 82, 015005 (2010).

[268] Romodanov, Vadim L. et al., "Testing of data libraries for lead, based on the analysis of time and energy distributions of neutrons", Current Problems in Nuclear Physics and Atomic Energy (NPAE) 3, June 7-12, 2010, Kyiv, Ukraine, Institute for Nuclear Research of the National Academy of Sciences of Ukraine (KINR), (2010), pp.496-500.

[269] Romodanov, Vadim L. et al., "Evaluation of ^{235}U and ^{239}Pu content in fuel assembly by using neutrons slowing-down time in lead", Current Problems in Nuclear Physics and Atomic Energy (NPAE) 3, June 7-12, 2010, Kyiv, Ukraine, Institute for Nuclear Research of the National Academy of Sciences of Ukraine (KINR), (2010), pp.492-495.

[270] Chernikova, Dina N. et al., "Time Intervals Matrix Analysis of ^{235}U and ^{239}Pu Content in a Spent Fuel Assembly Using Lead Slowing Down Spectrometer", 52nd Annual Meeting of the Institute of Nuclear Materials Management, (2011).

[271] Danon, Y. et al., "Fission Physics and Cross Section Measurements with a Lead Slowing down Spectrometer", Journal of the Korean Physical Society, 59 (2011), pp.1649-1653.

[272] Chernikova, Dina N. et al., "Analysis of ^{235}U, ^{239}Pu, and ^{241}Pu content in a spent fuel assembly using lead slowing down spectrometer and time intervals matrix", JNMM, 40 (2012), pp.9-18.

[273] Lee, Y. et al., "LSDS System Development for Isotopic Fissile Assay", 53rd Annual Meeting of the Institute of Nuclear Materials Management, (2012).

[274] Becker, B. et al., "Nondestructive Assay Measurements Using the RPI Lead Slowing-Down Spectrometer", Nucl. Sci. Eng., 175 (2013), pp.124-134.

[275] Williams, M. M. R., "The Slowing Down and Thermalization of Neutrons", North-Holland, (1966).

[276] Lamarsh, John R., "Introduction to Nuclear Reactor Theory", 2002 reprint, ISBN 0-89448-040-5, American Nuclear Society, (1966).

[277] Lakosi, Lázló et al., "Quantitative non-destructive assay of PuBe neutron sources", Nucl. Instrum. Methods Phys. Res., Sect. B, 243 (2006), pp.385-391.

[278] Gozani, T., "Active Nondestructive Assay of Nuclear Materials: Principles and Applications", NUREG/CR-0602, U.S. Nuclear Regulatory Commission, (1981).

[279] LaFleur, Adrienne M. et al., "Nondestructive measurements of fissile material using self-indication neutron resonance absorption densitometry (SINRAD)", LA-UR-08-1804, Los Alamos National Laboratory, (2008).

[280] LaFleur, Adrienne M. et al., "Comparison of Using Self-Interrogation Neutron Resonance Densitometry (SINRD) versus the Fork Detector (FDET) to Measure Partial Defects in Spent Fuel Assemblies", Trans. Am. Nucl. Soc., 101 (2009), pp.235-236.

[281] LaFleur, Adrienne M. et al., "Development of self-interrogation neutron resonance densitometry (SINRD) to measure the U-235 and Pu-239 content in a PWR spent fuel assembly", 31st Annual Meeting of the European Safeguards Research and Development Association, (2009), pp.1-15.

[282] LaFleur, Adrienne M. et al., "Development of Self-Interrogation Neutron Resonance Densitometry (SINRD) to Measure the Fissile Content in Nuclear Fuel", LA-UR-09-08178, Los Alamos National Laboratory, (2009).

[283] LaFleur, Adrienne M. et al., "Experimental Benchmark of MCNPX Calculations Against Self-Interrogation Neutron Resonance Densitometry (SINRD) Fresh Fuel Measurements", 51st Annual Meeting of the Institute of Nuclear Materials Management, (2010).

[284] Hu, J.et al., "Assessment of the self-interrogation neutron resonance densitometry technique for the Next Generation Safeguards Initiative spent fuel research effort", LA-UR-11-06177, Los Alamos National Laboratory, (2011).

[285] LaFleur, Adrienne M. et al., "Use of Self-Interrogation Neutron Resonance Densitometry to Measure the Fissile Content in a BWR 9x9 Spent Fuel Assembly", LA-UR-11-02843, 33rd Annual Meeting of the European Safeguards Research and Development Association, (2011).

[286] Rauch, Eric B. et al., "Combining PNAR-FC and SINRD to Determine Plutonium Content in Spent Nuclear Fuel", LA-UR-11-02592, 33rd Annual Meeting of the European Safeguards Research and Development Association, (2011).

[287] LaFleur, Adrienne M. et al., "Assessment of the self-interrogation neutron resonance densitometry technique for the Next Generation Safeguards Initiative spent fuel research effort", LA-UR-11-00516, Los Alamos National Laboratory, (2010).

[288] Menlove, Howard O. et al., "A resonance self-indication technique for isotopic assay of fissile materials", Safeguards Papers from ANS/AIF Winter Meeting, November 1968, WASH-1149, U.S. Atomic Energy Commission, (1970), pp.89-160.

[289] Duderstadt, James J. and Hamilton, Louis J., "Nuclear Reactor Analysis", ISBN 0-471-22363-8, John Wiley & Sons, Inc., (1976).

[290] Knoll, Glenn Frederick, "Radiation Detection and Measurement", 4th edition, ISBN 978-0-470-13148-0, John Wiley & Sons, Inc., (2010).

[291] ORTEC, "The Best Choice of High Purity Germanium (HPGe) Detector", ORTEC, Advanced Measurement Technology (AMETEK), (2007).

[292] ORTEC, "Lanthanum Bromide Scintillation Detectors", ORTEC, Advanced Measurement Technology (AMETEK), (2013).

[293] Löher, B. et al., "High count rate spectroscopy with $LaBr_3$:Ce scintillation detectors", Nucl. Instrum. Methods Phys. Res., Sect. A, 686 (2012), pp.1-6.

[294] Mantel, M. et al., "Isotopic analysis of uranium by neutron activation and high resolution gamma ray spectrometry", J. Radioanal. Chem., 2 (1969), pp.395-407.

[295] Beddingfield, David H. and Cecil, F. E., "Identification of fissile materials from fission product gamma-ray spectra", Nucl. Instrum. Methods Phys. Res., Sect. A, 417 (1998), pp.405-412.

[296] Norman, Eric B. et al., "Signatures of fissile materials: high-energy γ-rays following fission", Nucl. Instrum. Methods Phys. Res., Sect. A, 521 (2004), pp.608-610.

[297] Firestone, R. B. et al., "Analysis of fissile materials by high-energy neutron-induced fission decay gamma-rays", J. Radioanal. Nucl. Chem., 265 (2005), pp.241-245.

[298] Marrs, R. E. et al., "Fission-product gamma-ray line pairs sensitive to fissile material and neutron energy", Nucl. Instrum. Methods Phys. Res., Sect. A, 592 (2008), pp.463-471.

[299] Kröhnert, H. et al., "Freshly induced short-lived gamma-ray activity as a measure of fission rates in lightly re-irradiated spent fuel", Nucl. Instrum. Methods Phys. Res., Sect. A, 624 (2010), pp.101-108.

[300] Rennhofer, H. et al., "Detection of SNM by delayed gamma rays from induced fission", Nucl. Instrum. Methods Phys. Res., Sect. A, 652 (2011), pp.140-142.

[301] Kröhnert, H. et al., "Gamma-ray spectrometric measurements of fission rate ratios between fresh and burnt fuel following irradiation in a zero-power reactor", Nucl. Instrum. Methods Phys. Res., Sect. A, 698 (2013), pp.72-80.

[302] Zerkin, Viktor, "Flex-DB-Ex – Flexible Database Explorer, v-1.004, Database Version of August 13, 2013", International Atomic Energy Agency, (2013).

[303] Watt, B. E., "Energy spectrum of neutrons from thermal fission of U^{235}", Phys. Rev., 87 (1952), pp.1037-1041.

[304] Rinard, Phillip M., "A Spent-Fuel Cooling Curve for Safeguard Applications of Gross-Gamma Measurements", LA-9757-MS, Los Alamos National Laboratory, (1983).

[305] Viererbl, L. et al., "Measurement of gamma and neutron radiations inside spent fuel assemblies with passive detectors", Nucl. Instrum. Methods Phys. Res., Sect. A, 652 (2011), pp.90-93.

[306] Cobb, Donald D. et al., "Nondestructive verification and assay systems for spent fuels", LA-9041, Los Alamos National Laboratory, (1982).

[307] Hsue, S. T. et al., "Nondestructive Assay Methods for Irradiated Nuclear Fuels", LA-6923, Los Alamos Scientific Laboratory, (1978).

[308] Phillips, John R. et al., "Nondestructive Measurement of Spent Fuel Assemblies at the Tokai Reprocessing and Storage Facility", LA-8076-MS, Los Alamos National Laboratory, (1979).

[309] Sher, R. and Untermeyer, II ,S., "The Detection of Fissionable Materials by Nondestructive Means", American Nuclear Society (ANS), (1980).

[310] Tarvainen, M. et al., "Calibration of the TVO spent BWR reference fuel assembly", STUK-YTO-TR 37, STUK, (1992).

[311] Pan, Lung Kwang and Tsao, Cheng Si, "Estimation of burnup in Taiwan Research Reactor fuel pins by using nondestructive techniques", Nucl. Technol., 102 (1993), pp.313-322.

[312] Abbas, K. et al., "Use of miniature CdZnTe X/γ detector in nuclear safeguards: characterisation of spent nuclear fuel and uranium enrichment determination", Nucl. Instrum. Methods Phys. Res., Sect. A, 405 (1998), pp.153-158.

[313] Min, D. K. et al., "Determination of burnup, cooling time, and initial enrichment of PWR spent fuel by use of gamma-ray activity ratios" in “Storage of spent fuel from power reactors”, Crijns, M. J., editor, IAEA-TECDOC-1089, International Atomic Energy Agency, (1999), pp.421-426.

[314] Tiitta, Antero et al., "Enhanced Fork detector for partial defect verification of BWR fuel assemblies", Symposium on International Safeguards – Verification and Nuclear Material Security, 29 October – 2 November, 2001, Vienna, Austria, IAEA-SM-367/14/02, International Atomic Energy Agency, (2001).

[315] Mortreau, Patricia and Berndt, Reinhard, "Characterisation of cadmium zinc telluride detector spectra –application to the analysis of spent fuel spectra", Nucl. Instrum. Methods Phys. Res., Sect. A, 458 (2001), pp.183-188.

[316] Lebrun, Alain and Bignan, Gilles, "Nondestructive assay of nuclear low-enriched uranium spent fuels for burnup credit application", Nucl. Technol., 135 (2001), pp.216-229.

[317] Willman, Christofer et al., "Nondestructive assay of spent nuclear fuel with gamma-ray spectroscopy", Ann. Nucl. Energy, 33 (2006), pp.427-438.

[318] Berndt, Reinhard and Mortreau, Patricia, "Spent-fuel characterization with small CZT detectors", Nucl. Instrum. Methods Phys. Res., Sect. A, 564 (2006), pp.290-294.

[319] Gauld, Ian C. and Francis, Matthew, "Investigation of Passive Gamma Spectroscopy to Verify Spent Nuclear Fuel Content", 51st Annual Meeting of the Institute of Nuclear Materials Management, (2010).

[320] Mora, Mariano Vela et al., "Nondestructive burnup measurements by gamma-ray spectroscopy on spent fuel elements of the RP-10 research reactor", Prog. Nucl. Energy, 53 (2011), pp.344-353.

[321] Berndt, Reinhard and Mortreau, Patricia, "Experimental determination of the self-absorption factor for MTR plates by passive gamma spectrometric measurement", Nucl. Instrum. Methods Phys. Res., Sect. A, 644 (2011), pp.27-32.

[322] Bender, Sarah et al., "Experimental Gamma Ray Burnup Analysis of Penn State TRIGA Reactor Spent Fuel Rods", 54th Annual Meeting of the Institute of Nuclear Materials Management, (2013).

[323] Pivovaroff, Michael J. et al., "Gamma-ray Mirrors for Direct Measurement of Spent Nuclear Fuel", 54th Annual Meeting of the Institute of Nuclear Materials Management, (2013).

[324] Borella, Alessandro et al., "Towards an Improved Burnup Measurement Equipment for Spent Fuel Assemblies in Belgian Nuclear Power Plants", 54th Annual Meeting of the Institute of Nuclear Materials Management, (2013).

[325] Lévai, Ferenc et al., "Use of an underwater multidetector system for gamma emission tomography of spent fuel assemblies", 15th Annual Meeting of the European Safeguards Research and Development Association, (1993), pp.387-392.

[326] Hautamäki, Johanna and Tiitta, Antero, "Spent Fuel Verification Options for Final Repository Safeguards in Finland", STUK-YTO-TR 173, STUK, (2000).

[327] Lévai, Ferenc et al., "An exercise for partial defect testing of a PWR assembly by underwater tomography", Symposium on International Safeguards – Verification and Nuclear Material Security, 29 October – 2 November, 2001, Vienna, Austria, IAEA-SM-367/14/06, International Atomic Energy Agency, (2001).

[328] Jacobsson, Staffan, "Safeguard Analysis of Tomographic Data from a Measurement on a PWR Nuclear Fuel Assembly", STUK-YTO-TR 189-Annex, STUK and Uppsala University, (2002).

[329] Jansson, Peter, "Studies of nuclear fuel by means of nuclear spectroscopic methods", ISSN 1104-232X, ISBN 91-554-5315-5, Ph.D. Dissertation, Department of Nuclear and Particle Physics, Uppsala University, (2002).

[330] Lévai, Ferenc et al., "Feasibility of Gamma Emission Tomography for Partial Defect Verification of Spent LWR Fuel Assemblies", STUK-YTO-TR 189, STUK, (2002).

[331] Jansson, Peter et al., "A Device for Nondestructive Experimental Determination of the Power Distribution in a Nuclear Fuel Assembly", Nucl. Sci. Eng., 152 (2006), pp.76-86.

[332] Jansson, Peter et al., "A laboratory device for developing analysis tools and methods for gamma emission tomography of nuclear fuel", 35th Annual Meeting of the European Safeguards Research and Development Association (2013).

[333] Phillips, John R. and Bosler, G. E., "Calculated response contributions of gamma rays emitted from fuel pins in an irradiated PWR fuel assembly", LA-9837-MS, Los Alamos National Laboratory, (1983).

[334] Metzger, Franz R., "Resonance Fluorescence in Nuclei", in "Progress in Nuclear Physics", Vol. 7, O. R. Frisch, editor, Pergamon Press, (1959), pp.53-88.

[335] Booth, E. C. et al., "Nuclear resonance fluorescence from light and medium weight nuclei", Nuclear Physics, 57 (1964), pp.403-420.

[336] Skorka, S. J., "Nuclear Resonance Fluorescence", Chapter 8 in "The Electromagnetic Interaction in Nuclear Spectroscopy", W. D. Hamilton, editor, American Elsevier, (1975), pp.283-310.

[337] Schumacher, M. et al., "The energy dependence of Delbrück scattering investigated at Z = 73, 82 and 92", Nucl. Phys. A, 346 (1980), pp.418-430.

[338] Rullhusen, P. et al., "Coulomb Correction Effect in Delbrück Scattering and Nuclear Resonance Fluorescence of 2 to 10 MeV Photons on ^{238}U", Nucl. Phys. A, 382 (1982), pp.79-96.

[339] Ohgaki, H. et al.: "Linearly polarized photons from Compton backscattering of laser light for nuclear resonance fluorescence experiments", Nucl. Instrum. Methods Phys. Res., Sect. A, 353 (1994), pp.384-388.

[340] Kneissl, U. et al., "Investigation of nuclear structure by resonance fluorescence scattering", Progress in Particle and Nuclear Physics, 37 (1996), pp.349-433.

[341] Pietralla, N. et al., "Parity Measurements of Nuclear Levels Using a Free-Electron-Laser Generated γ-ray Beam", Physical Review Letters, 88, 012502 (2001).

[342] Enders, J. et al., "Nuclear resonance fluorescence experiments on ^{204,206,207,208}Pb up to 6.75 MeV", Nucl. Phys. A, 724 (2003), pp.243-273.

[343] Weller, Henry R. and Ahmed, Mohammad W., "The HIγS Facility: A Free-Electron Laser Generated Gamma-Ray Beam for Research in Nuclear Physics", Mod. Phys. Lett. A, 18 (2003), pp.1569-1590.

[344] Tonchev, A. P. et al., "The high intensity γ-ray source (HIγS) and recent results", Nucl. Instrum. Methods Phys. Res., Sect. B, 241 (2005), pp.170-175.

[345] Bertozzi, William and Ledoux, Robert J., "Nuclear resonance fluorescence imaging in non-intrusive cargo inspection", Nucl. Instrum. Methods Phys. Res., Sect. B, 241 (2005), pp.820-825.

[346] Pruet, J. et al., "Detecting clandestine material with nuclear resonance fluorescence", J. Appl. Phys., 99, 123102 (2006).

[347] Johnson, Micah S. and McNabb, Dennis P., "Comparison of techniques to reduce bremsstrahlung background radiation from monoenergetic photon beams", UCRL-TR-222530, Lawrence Livermore National Laboratory, (2006).

[348] Hagmann, Christian A. and Pruet, J., "Photon production through multi-step processes important in nuclear resonance fluorescence experiments", Nucl. Instrum. Methods Phys. Res., Sect. B, 259 (2007), pp.895-908.

[349] Bertozzi, William et al., "Nuclear resonance fluorescence and effective Z determination applied to detection and imaging of special nuclear material, explosives, toxic substances and contraband", Nucl. Instrum. Methods Phys. Res., Sect. B, 261 (2007), pp.331-336.

[350] Bertozzi, William et al., "Nuclear resonance fluorescence excitations near 2 MeV in ^{235}U and ^{239}Pu", Phys. Rev. C: Nucl. Phys., 78, 041601(R) (2008).

[351] Hajima, Ryoichi et al., "Proposal of Nondestructive Radionuclide Assay Using a High-Flux Gamma-Ray Source and Nuclear Resonance Fluorescence", J. Nucl. Sci. Technol. 45 (2008), pp.441-451.

[352] Hagmann, Christian A. et al., "Transmission-based detection of nuclides with nuclear resonance fluorescence using a quasimonoenergetic photon source", J. Appl. Phys., 106, 084901 (2009).

[353] Sun, C. et al., "End-to-end spectrum reconstruction method for analyzing Compton gamma-ray beams", Nucl. Instrum. Methods Phys. Res., Sect. A, 605 (2009), pp.312-317.

[354] Hajima, Ryoichi et al., "Detection of radioactive isotopes by using laser Compton scattered γ-ray beams", Nucl. Instrum. Methods Phys. Res., Sect. A, 608 (2009), pp.S57-S61.

[355] Kikuzawa, Nobuhiro et al., "Nondestructive Detection of Heavily Shielded Materials by Using Nuclear Resonance Fluorescence with a Laser-Compton Scattering γ-ray Source", Appl. Phys. Express, 2, 036502-036502-03 (2009).

[356] Angell, Christopher T. et al., "Nuclear resonance fluorescence of ^{237}Np", Physical Review C, 82, 054310 (2010).

[357] Hayakawa, Takehito et al., "Nondestructive assay of plutonium and minor actinide in spent fuel using nuclear resonance fluorescence with laser Compton scattering", Nucl. Instrum. Methods Phys. Res., Sect. A, 621(2010), pp.695-700.

[358] Bertozzi, William et al., "Non-intrusive Isotope Detection with Nuclear Resonance Fluorescence", 51st Annual Meeting of the Institute of Nuclear Materials Management, (2010).

[359] Hayakawa, Takehito et al., "Nondestructive Assay of Plutonium in Spent Nuclear Fuel Assembly in Water Pool", 51st Annual Meeting of the Institute of Nuclear Materials Management, (2010).

[360] Johnson, Micah S. et al., "Using Nuclear Resonance Fluorescence to Probe Nuclear Materials", 51st Annual Meeting of the Institute of Nuclear Materials Management, (2010).

[361] Walsh, William J. et al., "Analysis of the Uncertainty of Nuclear Resonance Fluorescence Cross Sections", 51st Annual Meeting of the Institute of Nuclear Materials Management, (2010).

[362] Hartemann, Frederic V. et al., "VELOCIRAPTOR: LLNL's precision Compton scattering light source", THPB05, 32nd International Free Electron Laser Conference (FEL2010), August 23-27, 2010, Malmö, Sweden, The Joint Accelerator Conferences Website, CERN, (2010).

[363] Hendricks, John S. and Quiter, Brian J., "MCNP/X Form Factor Upgrade for Improved Photon Transport", Nucl. Technol., 175 (2011), pp.150-161.

[364] Quiter, Brian J. et al., "Transmission nuclear resonance fluorescence measurements of ^{238}U in thick targets", Nucl. Instrum. Methods Phys. Res., Sect. B, 269 (2011), pp.1130-1139.

[365] Johnson, Micah S.et al., "Preliminary study of the efficacy of using nuclear resonance fluorescence with quasi-monoenergetic gamma-ray sources for nuclear safeguards assay", LLNL-TR-483851, Lawrence Livermore National Laboratory, (2011).

[366] Albert, Felicie et al., "NRF-based Isotope Material Detection Experiments with the LLNL T-REX MEGa-ray Machine", 52nd Annual Meeting of the Institute of Nuclear Materials Management, (2011).

[367] Ambers, Scott D. et al., "Importance of Elastic, Non-Resonant Scattering in the Assessment of NRF for NDA", 52nd Annual Meeting of the Institute of Nuclear Materials Management, (2011).

[368] Anderson, Scott G. et al., "Compact linear accelerator sources for gamma-ray generation", 52nd Annual Meeting of the Institute of Nuclear Materials Management, Palm Desert, California (2011).

[369] Angell, Christopher T., "Nuclear Resonance Fluorescence as an Educational Tool for the Next Generation of Safeguards Specialists", 52nd Annual Meeting of the Institute of Nuclear Materials Management, (2011).

[370] Barty, Christopher P. J. et al., "Overview of MEGa-ray-based Nuclear Materials Management Activities at the Lawrence Livermore National Laboratory", 52nd Annual Meeting of the Institute of Nuclear Materials Management, (2011).

[371] Bertozzi, William et al., "Nuclear Resonance Fluorescence Technologies for Nuclear Materials Management", 52nd Annual Meeting of the Institute of Nuclear Materials Management, (2011).

[372] Hajima, Ryoichi et al., "Research and Development Program on Nondestructive Measurement of Isotopes by Using Laser Compton Scattered Gamma-rays", 52nd Annual Meeting of the Institute of Nuclear Materials Management, (2011).

[373] Hall, James M. et al., "Numerical Simulation of Nuclear Materials Detection, Imaging and Assay with MEGa-rays", 52nd Annual Meeting of the Institute of Nuclear Materials Management, (2011).

[374] Hartemann, Frederic V. et al., "Optimization of Compton Scattering for NRF-based Nuclear Materials Management with MEGa-rays", 52nd Annual Meeting of the Institute of Nuclear Materials Management, (2011).

[375] Hayakawa, Takehito et al., "Development of Simulation Code for NDA Using Nuclear Resonance Fluorescence with Laser Compton Scattering Gamma-rays", 52nd Annual Meeting of the Institute of Nuclear Materials Management, (2011).

[376] Hayakawa, Takehito et al., "Basic Study for Nondestructive Assay of Plutonium in Spent Nuclear Fuel with Nuclear Resonance Fluorescence", 52nd Annual Meeting of the Institute of Nuclear Materials Management, (2011).

[377] Hicks, Curtis L. et al., "Introduction to Nuclear Resonance Fluorescence as a Tool for Nuclear Materials Management", 52nd Annual Meeting of the Institute of Nuclear Materials Management, (2011).

[378] Johnson, Micah S. et al., "Using Nuclear Resonance Fluorescence to Determine Pu Content in Spent Nuclear Fuel", 52nd Annual Meeting of the Institute of Nuclear Materials Management, (2011).

[379] Simakov, S. P. et al., "Experimental Data for Nuclear Resonance Fluorescence", 52nd Annual Meeting of the Institute of Nuclear Materials Management, (2011).

[380] Walsh, William J. et al., "Nuclear Resonance Fluorescence Simulation Techniques Using MCNP", 52nd Annual Meeting of the Institute of Nuclear Materials Management, (2011).

[381] Warren Glen A. and Detwiler, Rebecca S., "Nuclear Resonance Fluorescence for Material Verification in Dismantlement", 52nd Annual Meeting of the Institute of Nuclear Materials Management, (2011).

[382] Runkle, Robert C. et al., "Rattling nucleons: New developments in active interrogation of special nuclear material", Nucl. Instrum. Methods Phys. Res., Sect. A, 663 (2012), pp.75-95.

[383] Johnson, Micah S. et al., "Searching for illicit materials using nuclear resonance fluorescence stimulated by narrow-band photon sources", Nucl. Instrum. Methods Phys. Res., Sect. B, 285 (2012), pp.72-85.

[384] Quiter, Brian J. et al., "Nuclear resonance fluorescence in ^{240}Pu", Physical Review C, 86, 034307 (2012).

[385] Hammond, Samantha L., "Dipole response of ^{238}U to polarized photons below the neutron-separation energy", Ph.D. Dissertation, Department of Physics and Astronomy, University of North Carolina at Chapel Hill, (2012).

[386] Angell, Christopher T. et al., "Significant improvement of nuclear resonance fluorescence non-destructive assay by using the average resonance technique and photofission", 53rd Annual Meeting of the Institute of Nuclear Materials Management, (2012).

[387] Hajima, Ryoichi et al., "Status of JAEA Development Program of gamma-ray Nondestructive Assay for Melted Nuclear Fuel", 54th Annual Meeting of the Institute of Nuclear Materials Management, (2013).

[388] Hayakawa, Takehito et al., "Measurement technique of plutonium using nuclear resonance fluorescence with laser Compton scattering gamma-rays", 35th Annual Meeting of the European Safeguards Research and Development Association, (2013).

[389] Hayakawa, Takehito et al., "Measurement technique of plutonium and minor actinides using nuclear resonance fluorescence with laser Compton scattering gamma-rays" 53rd Annual Meeting of the Institute of Nuclear Materials Management, (2012).

[390] Quiter, Brian J.et al., "Examining ^{239}Pu and ^{240}Pu Nuclear Resonance Fluorescence Measurements on Spent Fuel for Nuclear Safeguards", 53rd Annual Meeting of the Institute of Nuclear Materials Management, (2012).

[391] Angell, Christopher T. et al., "Demonstration of the Nuclear Resonance Fluorescence Integral Resonance Transmission Method for NDA of debris of melted nuclear fuel", 54th Annual Meeting of the Institute of Nuclear Materials Management, (2013).

[392] Pope Thomas C. and Croft, Stephen, "Benchmarking NRF simulation in MCNPX", 54th Annual Meeting of the Institute of Nuclear Materials Management, (2013).

[393] Quiter, Brian J. et al., "Plutonium nuclear resonance fluorescence measurements using narrow energy-spread photon sources" 54th Annual Meeting of the Institute of Nuclear Materials Management, (2013).

[394] Seya, Michio et al., "Development of Basic NDA Technologies for Nuclear Material Accountancy of Debris of Melted Fuel Formed in Severe Accidents", 54th Annual Meeting of the Institute of Nuclear Materials Management, (2013).

[395] Shizuma, Toshiyuki et al., "Improvement of Precision of NRF-Based NDA using Monochromatic Gamma-Ray Beam for Nuclear Materials in Debris of Melted Fuel" 35th Annual Meeting of the European Safeguards Research and Development Association, (2013).

[396] Shizuma, Toshiyuki et al., "Statistical uncertainties of nondestructive assay for spent nuclear fuel by using nuclear resonance fluorescence", Nucl. Instrum. Methods Phys. Res., Sect. A, 737 (2014), pp.170-175.

[397] Seya, Michio et al., "JAEA development programs of advanced technologies of measurement and detection of nuclear material for safeguards and security", 52nd Annual Meeting of the Institute of Nuclear Materials Management, (2011).

[398] Berant, Z. et al., "Nuclear Thomson scattering of 5.5–7.2 MeV photons", Physics Letters B, 69 (1977), pp.281-283.

[399] Roy, S. C. et al., "Elastic scattering of photons", Radiat. Phys. Chem., 56 (1999), pp.3-26.

[400] Kwan, E. et al., "Discrete deexcitations in ^{235}U below 3 MeV from nuclear resonance fluorescence", Physical Review C, 83, 041601(R) (2011).

[401] Schumacher, Martin, "Delbrück scattering", Radiat. Phys. Chem., 56 (1999), pp.101-111.

[402] Mills, D. M. et al., "Report of the Working Group on Synchrotron Radiation Nomenclature - brightness, spectral brightness or brilliance?", J. Synchrotron Radiat., 12 (2005), p.385.

[403] Vretena,r M., "Radio frequency for particle accelerators: evolution and anatomy of a technology", contribution to the CAS - CERN Accelerator School: Specialised Course on RF for Accelerators/ 8 - 17 Jun 2010, Ebeltoft, Denmark, CERN Yellow Report CERN-2011-007, CERN, (2012).

[404] Bushuev, A. V. et al., "A nondestructive method of determining the Pu/U ratio in fast reactor fuel elements, based on X-ray spectrometry", Atomic Energy, 53 (1982), pp.776-778.

[405] Ahmed, Iqbal et al., "Utilization of fluorescent uranium X-rays as verification tool for irradiated CANDU fuel bundles", Symposium on International Safeguards – Verification and Nuclear Material Security, 29 October – 2 November, 2001, Vienna, Austria, IAEA-SM-367/14/01, International Atomic Energy Agency, (2001).

[406] Rudy, Cliff et al., "Determination of Pu in Spent Fuel Assemblies by X-Ray Fluorescence", 46th Annual Meeting of the Institute of Nuclear Materials Management, (2005).

[407] Goodsell, Alison V. and Charlton, William S., "Bent-crystal spectrometer analyzing plutonium K X-rays for applications in nuclear forensics", 52nd Annual Meeting of the Institute of Nuclear Materials Management, (2011).

[408] Goodsell, Alison V. and Charlton, William S., "Optimization of a quartz-crystal spectrometer design for analyzing K X-rays from Pu and U", 53rd Annual Meeting of the Institute of Nuclear Materials Management, (2012).

[409] Havrilla, George J.et al., "Ultra High Energy X-ray Fluorescence: A New Paradigm for Actinide Characterization of Spent Fuel", 52nd Annual Meeting of the Institute of Nuclear Materials Management, (2011).

[410] JNCDI, "Advanced Thermal Reactor Fugen: R&D and Operational Performance Achievements", INC TN3410 2002-005, March 2003, Japan Nuclear Cycle Development Institute, (2003).

[411] Zhao, K. et al., "International Target Values 2010 for Measurement Uncertainties in Safeguarding Nuclear Materials", STR-368, Rev. 6, International Atomic Energy Agency, (2010).

[412] Bernstein, Adam et al., "Monitoring the thermal power of nuclear reactors with a prototype cubic meter antineutrino detector", J. Appl. Phys., 103 (2008), pp.074905-074910.

[413] Tsuji, Masashi et al., "Subcriticality Measurement by Neutron Source Multiplication Method with a Fundamental Mode Extraction", J. Nucl. Sci. Technol., 40 (2003), pp.158-169.

[414] Brown, David A. et al., "Evaluated Nuclear Data File (ENDF) website", National Nuclear Data Center, Brookhaven National Laboratory, (2013).

[415] Croft, Stephen et al., "Feynman variance-to-mean in the context of passive neutron coincidence counting", Nucl. Instrum. Methods Phys. Res., Sect. A, 686 (2012), pp.136-144.

[416] Bolind, Alan Michael, "A paradigm for the nondestructive assay of spent fuel assemblies and similar large objects, with emphasis on the role of photon-based techniques", "Nuclear Physics and Gamma-ray sources for Nuclear Security and Nonproliferation, Proceedings of the International Symposium Nuclear Physics and Gamma-ray sources for Nuclear Security and Nonproliferation", January 28-30, 2014, Ricotti, Tokai-mura, Ibaraki, Japan, World Scientific, Singapore, (2015).

This is a blank page.

国際単位系（SI）

表１．SI 基本単位

基本量	SI 基本単位	
	名称	記号
長さ	メートル	m
質量	キログラム	kg
時間	秒	s
電流	アンペア	A
熱力学温度	ケルビン	K
物質量	モル	mol
光度	カンデラ	cd

表２．基本単位を用いて表されるSI組立単位の例

組立量	SI 組立単位	
	名称	記号
面積	平方メートル	m^2
体積	立方メートル	m^3
速さ，速度	メートル毎秒	m/s
加速度	メートル毎秒毎秒	m/s^2
波数	毎メートル	m^{-1}
密度，質量密度	キログラム毎立方メートル	kg/m^3
面積密度	キログラム毎平方メートル	kg/m^2
比体積	立方メートル毎キログラム	m^3/kg
電流密度	アンペア毎平方メートル	A/m^2
磁界の強さ	アンペア毎メートル	A/m
量濃度(a)，濃度	モル毎立方メートル	mol/m^3
質量濃度	キログラム毎立方メートル	kg/m^3
輝度	カンデラ毎平方メートル	cd/m^2
屈折率(b)	（数字の） 1	1
比透磁率(b)	（数字の） 1	1

(a) 量濃度（amount concentration）は臨床化学の分野では物質濃度（substance concentration）ともよばれる。
(b) これらは無次元量あるいは次元１をもつ量であるが、そのことを表す単位記号である数字の１は通常は表記しない。

表３．固有の名称と記号で表されるSI組立単位

組立量	SI 組立単位			
	名称	記号	他のSI単位による表し方	SI基本単位による表し方
平面角	ラジアン(b)	rad	1 (b)	m/m
立体角	ステラジアン(b)	sr(c)	1 (b)	m^2/m^2
周波数	ヘルツ(d)	Hz		s^{-1}
力	ニュートン	N		m kg s^{-2}
圧力，応力	パスカル	Pa	N/m^2	m^{-1} kg s^{-2}
エネルギー，仕事，熱量	ジュール	J	N m	m^2 kg s^{-2}
仕事率，工率，放射束	ワット	W	J/s	m^2 kg s^{-3}
電荷，電気量	クーロン	C		s A
電位差（電圧），起電力	ボルト	V	W/A	m^2 kg s^{-3} A^{-1}
静電容量	ファラド	F	C/V	m^{-2} kg^{-1} s^4 A^2
電気抵抗	オーム	Ω	V/A	m^2 kg s^{-3} A^{-2}
コンダクタンス	ジーメンス	S	A/V	m^{-2} kg^{-1} s^3 A^2
磁束	ウエーバ	Wb	Vs	m^2 kg s^{-2} A^{-1}
磁束密度	テスラ	T	Wb/m^2	kg s^{-2} A^{-1}
インダクタンス	ヘンリー	H	Wb/A	m^2 kg s^{-2} A^{-2}
セルシウス温度	セルシウス度(e)	℃		K
光束	ルーメン	lm	cd sr(c)	cd
照度	ルクス	lx	lm/m^2	m^{-2} cd
放射性核種の放射能(f)	ベクレル(d)	Bq		s^{-1}
吸収線量，比エネルギー分与，カーマ	グレイ	Gy	J/kg	m^2 s^{-2}
線量当量，周辺線量当量，方向性線量当量，個人線量当量	シーベルト(g)	Sv	J/kg	m^2 s^{-2}
酸素活性	カタール	kat		s^{-1} mol

(a)SI接頭語は固有の名称と記号を持つ組立単位と組み合わせても使用できる。しかし接頭語を付した単位はもはやコヒーレントではない。
(b)ラジアンとステラジアンは数字の１に対する単位の特別な名称で、量についての情報をつたえるために使われる。実際には、使用する時には記号radおよびsrが用いられるが、習慣として組立単位としての記号である数字の１は明示されない。
(c)測光学ではステラジアンという名称と記号srを単位の表し方の中に、そのまま維持している。
(d)ヘルツは周期現象についてのみ、ベクレルは放射性核種の統計的過程についてのみ使用される。
(e)セルシウス度はケルビンの特別な名称で、セルシウス温度を表すために使用される。セルシウス度とケルビンの単位の大きさは同一である。したがって、温度差や温度間隔を表す数値はどちらの単位で表しても同じである。
(f)放射性核種の放射能（activity referred to a radionuclide）は、しばしば誤った用語で"radioactivity"と記される。
(g)単位シーベルト（PV,2002,70,205）についてはCIPM勧告2（CI-2002）を参照。

表４．単位の中に固有の名称と記号を含むSI組立単位の例

組立量	SI 組立単位		
	名称	記号	SI 基本単位による表し方
粘度	パスカル秒	Pa s	m^{-1} kg s^{-1}
力のモーメント	ニュートンメートル	N m	m^2 kg s^{-2}
表面張力	ニュートン毎メートル	N/m	kg s^{-2}
角速度	ラジアン毎秒	rad/s	m m^{-1} s^{-1}=s^{-1}
角加速度	ラジアン毎秒毎秒	rad/s^2	m m^{-1} s^{-2}=s^{-2}
熱流密度，放射照度	ワット毎平方メートル	W/m^2	kg s^{-3}
熱容量，エントロピー	ジュール毎ケルビン	J/K	m^2 kg s^{-2} K^{-1}
比熱容量，比エントロピー	ジュール毎キログラム毎ケルビン	J/(kg K)	m^2 s^{-2} K^{-1}
比エネルギー	ジュール毎キログラム	J/kg	m^2 s^{-2}
熱伝導率	ワット毎メートル毎ケルビン	W/(m K)	m kg s^{-3} K^{-1}
体積エネルギー	ジュール毎立方メートル	J/m^3	m^{-1} kg s^{-2}
電界の強さ	ボルト毎メートル	V/m	m kg s^{-3} A^{-1}
電荷密度	クーロン毎立方メートル	C/m^3	m^{-3} s A
表面電荷	クーロン毎平方メートル	C/m^2	m^{-2} s A
電束密度，電気変位	クーロン毎平方メートル	C/m^2	m^{-2} s A
誘電率	ファラド毎メートル	F/m	m^{-3} kg^{-1} s^4 A^2
透磁率	ヘンリー毎メートル	H/m	m kg s^{-2} A^{-2}
モルエネルギー	ジュール毎モル	J/mol	m^2 kg s^{-2} mol^{-1}
モルエントロピー，モル熱容量	ジュール毎モル毎ケルビン	J/(mol K)	m^2 kg s^{-2} K^{-1} mol^{-1}
照射線量（X線及びγ線）	クーロン毎キログラム	C/kg	kg^{-1} s A
吸収線量率	グレイ毎秒	Gy/s	m^2 s^{-3}
放射強度	ワット毎ステラジアン	W/sr	m^4 m^{-2} kg s^{-3}=m^2 kg s^{-3}
放射輝度	ワット毎平方メートル毎ステラジアン	$W/(m^2$ sr)	m^2 m^{-2} kg s^{-3}=kg s^{-3}
酵素活性濃度	カタール毎立方メートル	kat/m^3	m^{-3} s^{-1} mol

表５．SI 接頭語

乗数	名称	記号	乗数	名称	記号
10^{24}	ヨタ	Y	10^{-1}	デシ	d
10^{21}	ゼタ	Z	10^{-2}	センチ	c
10^{18}	エクサ	E	10^{-3}	ミリ	m
10^{15}	ペタ	P	10^{-6}	マイクロ	μ
10^{12}	テラ	T	10^{-9}	ナノ	n
10^{9}	ギガ	G	10^{-12}	ピコ	p
10^{6}	メガ	M	10^{-15}	フェムト	f
10^{3}	キロ	k	10^{-18}	アト	a
10^{2}	ヘクト	h	10^{-21}	ゼプト	z
10^{1}	デカ	da	10^{-24}	ヨクト	y

表６．SIに属さないが、SIと併用される単位

名称	記号	SI 単位による値
分	min	1 min=60 s
時	h	1 h =60 min=3600 s
日	d	1 d=24 h=86 400 s
度	°	1°=(π/180) rad
分	’	1’=(1/60)°=(π/10 800) rad
秒	”	1”=(1/60)’=(π/648 000) rad
ヘクタール	ha	1 ha=1 hm^2=10^4m^2
リットル	L, l	1 L=1 l=1 dm^3=10^3cm^3=$10^{-3}m^3$
トン	t	1 t=10^3 kg

表７．SIに属さないが、SIと併用される単位で、SI単位で表される数値が実験的に得られるもの

名称	記号	SI 単位で表される数値
電子ボルト	eV	1 eV=1.602 176 53(14)×10^{-19}J
ダルトン	Da	1 Da=1.660 538 86(28)×10^{-27}kg
統一原子質量単位	u	1 u=1 Da
天文単位	ua	1 ua=1.495 978 706 91(6)×10^{11}m

表８．SIに属さないが、SIと併用されるその他の単位

名称	記号	SI 単位で表される数値
バール	bar	1 bar=0.1MPa=100 kPa=10^5Pa
水銀柱ミリメートル	mmHg	1 mmHg≈133.322Pa
オングストローム	Å	1 Å=0.1nm=100pm=10^{-10}m
海里	M	1 M=1852m
バーン	b	1 b=100fm^2=(10^{-12}cm)^2=$10^{-28}m^2$
ノット	kn	1 kn=(1852/3600)m/s
ネーパ	Np	SI単位との数値的な関係は、対数量の定義に依存。
ベル	B	
デシベル	dB	

表９．固有の名称をもつCGS組立単位

名称	記号	SI 単位で表される数値
エルグ	erg	1 erg=10^{-7} J
ダイン	dyn	1 dyn=10^{-5}N
ポアズ	P	1 P=1 dyn s cm^{-2}=0.1Pa s
ストークス	St	1 St =1cm^2 s^{-1}=$10^{-4}m^2$ s^{-1}
スチルブ	sb	1 sb =1cd cm^{-2}=10^4cd m^{-2}
フォト	ph	1 ph=1cd sr cm^{-2} =10^4lx
ガル	Gal	1 Gal =1cm s^{-2}=$10^{-2}ms^{-2}$
マクスウエル	Mx	1 Mx = 1G cm^2=10^{-8}Wb
ガウス	G	1 G =1Mx cm^{-2} =10^{-4}T
エルステッド(a)	Oe	1 Oe ≙ (10^3/4π)A m^{-1}

(a) ３元系のCGS単位系とSIでは直接比較できないため、等号「 ≙ 」は対応関係を示すものである。

表10．SIに属さないその他の単位の例

名称	記号	SI 単位で表される数値
キュリー	Ci	1 Ci=3.7×10^{10}Bq
レントゲン	R	1 R = 2.58×10^{-4}C/kg
ラド	rad	1 rad=1cGy=10^{-2}Gy
レム	rem	1 rem=1 cSv=10^{-2}Sv
ガンマ	γ	1 γ=1 nT=10^{-9}T
フェルミ		1 フェルミ=1 fm=10^{-15}m
メートル系カラット		1 メートル系カラット= 0.2 g = 2×10^{-4}kg
トル	Torr	1 Torr = (101 325/760) Pa
標準大気圧	atm	1 atm = 101 325 Pa
カロリー	cal	1 cal=4.1858J（「15℃」カロリー），4.1868J（「IT」カロリー），4.184J（「熱化学」カロリー）
ミクロン	μ	1 μ =1μm=10^{-6}m

（第8版，2006年）